Doctoral Dissertations 1896 - February 2014

1-1-1993

Synthesis, structure and phase behavior of liquid crystalline polyurethanes/

Fotios, Papadimitrakopoulos
University of Massachusetts Amherst

Recommended Citation

Papadimitrakopoulos, Fotios,, "Synthesis, structure and phase behavior of liquid crystalline polyurethanes/" (1993). *Doctoral Dissertations 1896 - February 2014*. 813.

https://scholarworks.umass.edu/dissertations_1/813

SYNTHESIS, STRUCTURE AND PHASE BEHAVIOR
OF LIQUID CRYSTALLINE POLYURETHANES

A Dissertation Presented

by

FOTIOS PAPADIMITRAKOPOULOS

Submitted to the Graduate School of the
University of Massachusetts in partial fulfillment
of the requirements for the degree of

DOCTOR OF PHILOSOPHY

February 1993
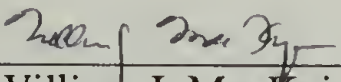
Polymer Science and Engineering

SYNTHESIS, STRUCTURE AND PHASE BEHAVIOR
OF LIQUID CRYSTALLINE POLYURETHANES
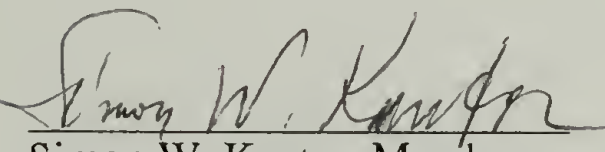
A Dissertation Presented

by

FOTIOS PAPADIMITRAKOPOULOS
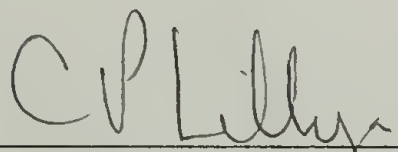
Approved as to the style and content by:
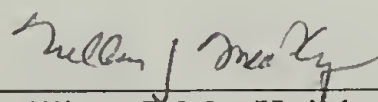
_____
William J. MacKnight, Chair

_____
Simon W. Kantor, Member

_____
C. Peter Lillya, Member

_____
William J. MacKnight, Department Head
Polymer Science & Engineering

'Tis a lesson you should heed
Try, try, try again.
If at first you don't succeed,
Try, try, try again.
Then your courage should appear,
For if you will persevere
You will conquer, never fear.
Try, try, try again.

Hickson

Dedicated to my parents, LUCY and PETER.
The seed you planted and nourished with so much love and sacrifice
has finally flourished.

ACKNOWLEDGEMENTS

ABSTRACT

SYNTHESIS, STRUCTURE AND PHASE BEHAVIOR
OF LIQUID CRYSTALLINE POLYURETHANES

FEBRUARY 1993

FOTIOS PAPADIMITRAKOPOULOS, B.S., UNIVERSITY OF ATHENS, GREECE

M.S., UNIVERSITY OF MASSACHUSETTS

Ph. D., UNIVERSITY OF MASSACHUSETTS

Directed by: Professor William J. MacKnight

This dissertation describes the synthesis, structure and phase behavior of

polyurethanes based on the mesogenic biphenol 4,4'-bis(6-hydroxyhexoxy)biphenyl

(BHHBP) and meta substituted tolylene / phenylene diisocyanates. The structure-

property relationships were determined as a function of hydrogen-bonding, the position

of the methyl group in the tolylene diisocyanate moiety (TDI) and the biphenol moiety.

The liquid crystalline phase (mesophase) and crystalline phase were investigated

primarily with differential scanning calorimetry (DSC), wide angle X-ray scattering

(WAXS) and infrared spectroscopy. From this combination of characterization

techniques, a more detailed description emerges about the thermodynamic stability and

kinetic accessibility of each phase.

Previous investigation of the (2,4-TDI/BHHBP) mesogenic polyurethane, 2,4-

LCPU-6, has shown that this polymer is a monotropic liquid crystal. The influence of

H-bonding on the structure and phase behavior of 2,4-LCPU-6 was determined by the

synthesis of high molecular wight N-Methyl 2,4-LCPU-6, using a novel high

temperature polymerization of a biscarbamoyl chloride with the BHHBP mesogenic diol. The comparison of the structure and physical properties of these two polymers revealed that H-bonding does not affect the mesophase morphology although its absence disrupts crystallinity and results in an enantiotropic liquid crystal. In addition, it was found that the effect of H-bonding on the mesophase-isotropic transition is enthalpic in nature.

In contrast to the "regular" (α,ω-hexane diol) based polyurethanes (PUs), BHHBP derived polyurethanes (LCPUs) crystallize rapidly from their melts. This is due to the strong nucleating power of their thermodynamically unstable mesophases (monotropic L.C.) Hexafluoroisopropanol fast solvent-evaporation casting or rapid cooling from the melt resulted in thin films or bulk samples with a glassy mesophase morphology. During the subsequent heating scan, the mesophase to crystal transition takes place. Considerable amount of effort was expended to understand the nature of this transition. With the combination of vibrational spectroscopy which provides a measure of the localized structure, along with DSC and WAXS (which examine the long range order) we established the microstructural changes occurring in the different phases.

Applying the results of previously mentioned analysis (kinetic control and phase perfection), highly oriented fibers were obtained for the mesogenic polyurethanes. Atomistic molecular simulations coupled with X-ray intensity refinement allowed us to determine the crystalline chain conformation and packing characteristics for the 2,6-LCPU-6 and 1,3-LCPU-6 (2,6-TDI and 1,3-Phenylene Diisocyanate (1,3-PDI) derived LCPUs). On the basis of structural similarity and well resolved WAXS powder patterns we extended the similar analysis to the "regular" polyurethanes as well (2,6-PU-6 and 1,3-PU-6). The good correlation between H-bonding distance and melting temperature for these four polymers suggests that melting is primarily controlled by the dissociation of H-bonds in the ordered domains.

TABLE OF CONTENTS

Chapter

LIST OF TABLES

xii

LIST OF FIGURES

LIST OF SCHEMES

CHAPTER 1

INTRODUCTION

Polyurethane products historically have proven to be among the most versatile plastic materials available. The wide range of physical properties from supersoft flexible foam to tough elastomers, and to long wearing coatings has resulted in many end use applications.[1] Polyurethane elastomers derive their elastomeric properties from phase separation of the hard and soft, "blocky" type copolymer segments. The hard (urethane) segment domains serve as cross links between the amorphous soft segment domains, which are usually polyesters or polyethers.[1-3] The wide industrial demand for high modulus elastomers resulted in reinforced polyurethane elastomers (using milled glass fibers,[4] fillers,[5] and ceramics [6]), sacrificing processability and recycling capability.

The inherent ability of liquid crystalline polymers to form easily elongated superstructures under shear fields [7-9] has motivated our laboratory to synthesize and study extensively biphenol containing mesogenic polyurethanes.[10-13] The well-known decomposition temperatures of polyurethanes [14,15] (~ 200 °C) along with the elevated transitions due to H-bonding impose serious restrictions in designing liquid crystal polyurethanes. The placement of urethane groups (H-bonding) with respect to the mesogen greatly influences the transition temperatures. On the basis of this placement, one can classify the literature reported main-chain mesogen containing polyurethanes [10,16-23] in two groups (see Scheme 1.1): Scheme 1.2 illustrates the chemical structures of the first group where the urethane moieties are attached to the mesogen. This arrangement stiffens the structure and increases the melting (T_m) and isotropization (T_i) temperatures to significantly higher than 200 °C. In order to obtain transition temperatures lower than 200

°C, Iimura et al.[16] had to use a twelve methylene spacer (T_m = 174 °C, T_i = 186 °C) or mixture of 6 and 10 methylene spacers (30% and 50% of the HO-$(CH_2)_6$-OH). The separation of the urethane moiety from the mesogen by a spacer lowers considerably the transition temperatures in the second group (see Scheme 1.3). The longer the spacer between these two groups, the lower the transitions occur.[10,19-22] The mesogenic polyurethanes based on 4,4'-bis(6-hydroxyhexoxy)biphenyl (BHHBP) (Scheme 1.3, 3rd-mesogen with x=6) and meta-substituted toluene diisocyanates have attracted considerable attention due to their low melting point (170-200 °C), and fast crystallization from their melt.[10,12,13,24]

In recent years the mesomorphic state (liquid crystalline phase) has come increasingly to the forefront of science and technology. The conditions for realizing the mesomorphic state can be readily expressed in terms of the relative thermodynamic stability of the crystalline (C), liquid crystalline or mesophase (M), and liquid phases (L).[25,26] The Gibbs free energy (G) of each phase can be expressed by the following thermodynamic equation where S is the entropy, V is the volume, p is the pressure and T is the

$$dG = V \, dp - S \, dT$$

temperature. At constant pressure (dp = 0) the free energies of the crystal (G_C), liquid crystal (G_M), and liquid (G_L) decrease with increasing temperature (see Figure 1.1). The decrease of G_L is steeper than G_M and G_C, since

$$S_L > S_M > S_C$$

If, for a moment, we assume that these curves are straight lines, their intercepts can be expressed in terms of enthalpy and their slopes in terms of entropy. For the simplest case, where only one mesophase and one crystalline phase is present, the relative position of each curve with respect to the others produces three types of mesophases.

Enantiotropic Mesophase: This mesophase is observed upon both heating and cooling. It thus appears as a thermodynamically stable phase between the T_{C-M} and T_{M-L} (see Figure 1.1A).

Virtual Mesophase: This refers to a mesophase that is potentially possible, however, is thermodynamically less stable than the crystalline phase at the same temperature. It is unrealizable upon both heating and cooling due to the great difference between T_{C-L} and T_{M-L} (see Figure 1.1B).

Monotropic Mesophase: This refers to a mesophase that is thermodynamically metastable with respect to the crystalline phase. It is a particular case of the virtual mesophase and can be observed under certain kinetic conditions such as fast cooling. This is due to the small difference between T_{C-L} and T_{M-L}, where a high enough cooling rate can surpass crystallization and bring the sample into the mesophase (see Figure 1.1B).

Too often in polymer science the relationship between microstructure and macroscopic properties has been obscured by poor structure understanding and by complex processing conditions leading to non-equilibrium microstructures. Simultaneously occurring processes, such as H-bond association and mesogenic group alignment, can result in complex phase behavior and poor structure understanding.[24] For the case of strong intermolecularly interacting polymers like polyurethanes and polyamides, the existence of a thermotropic liquid crystalline phase and its thermodynamic stability is still a matter of debate.[10,24] In addition, factors such as molecular weight, polydispersity, molecular regularity of the repeat, strength of the intermolecular interactions, packing capability, etc., play a dominant role on the thermodynamic stability of each phase, and contribute to the complexity of this class of materials.[24] Since most of the liquid crystalline polyurethane literature is dominated by synthetically oriented publications, it is wise to be cautious about the reported T_m's and T_i's of the polymers of Scheme 1.2 and 1.3. As will become clearer during the course of this dissertation, in the case that a polymers is a monotropic liquid crystal, the order of the transitions has to be reversed (see Figure 1.1).

3

Undoubtedly, a more detailed characterization is required for each particular system in order to address this argument unequivocally.

Previous investigation of the mesogenic polyurethane, 2,4-LCPU-6, based on the mesogenic biphenol 4,4'-bis(6-hydroxyhexoxy)biphenyl (BHHBP) and 2,4-toluene diisocyanate (2,4-TDI), has shown that this polymer is a monotropic liquid crystal. The inherent complexities of this system such as H-bonding, asymmetric position of the methyl group in the TDI moiety, biphenol moiety, etc., make the task of determining property-structure relationships difficult. This dissertation describes a comprehensive study of the pure hard-phase (BHHBP) based mesogenic polyurethanes (LCPUs). Answers are sought to the following three sets of questions:

1) What is the effect of H-bonding upon the structure and phase behavior of liquid crystal polyurethanes? Will the elimination of H-bonding result in a liquid crystalline system, and of what kind, monotropic or enantiotropic? What is the extent and perfection of H-bonding in the individual phases.

2) Why do BHHBP based mesogenic polyurethanes crystallize so readily from their melts, while the α,ω-hexane diol based "regular" polyurethanes don't? How much is the mesophase involved in this process? Can a frozen mesophase nucleate crystallization and if so, in what temperature range?

3) What is the molecular architecture and conformational characteristics of TDI based, "regular" and liquid crystal polyurethanes, as a function of the TDI's methyl group position? How does this methyl group affect the packing in the liquid crystal and crystal states? How much does the H-bonding participate in the formation as well as the destruction of the ordered phases?

These expansive questions pervade the entire dissertation. Chapters 2 and 4 focus on the first question and attack it with two completely different approaches. Chapter 2 utilizes a chemical modification which eliminates the H-bonding. It details the synthesis, structure and phase characterization of the N-Methyl analogue 2,4-LCPU-6. The

comparison between the original and the N-Methyl analogue elucidates the effect of H-bonding upon the structure and phase behavior of LCPUs.

Chapter 3 describes the thermal, optical microscopy and wide angle X-ray scattering (WAXS) characterization of biphenol containing LCPUs, as well as 1,6-hexanediol based regular polyurethanes (PUs). It demonstrates the influence of the biphenol and TDI moieties on the crystallization characteristics for this class of materials. In addition, it provides specific processing conditions (thermal treatments, elongational fields and solvent-polymer interactions) that maximize the liquid crystalline and crystalline phase content. These processing conditions will facilitate a comprehensive structural characterization of each phase (in Chapter 4) and establish the extent of H-bonding in the individual phases. Future applications can be readily envisioned in terms of the prime goal of the project; to maximize the degree of crystallinity and anisotropic character of the hard domains in polyurethane based thermoplastic elastomers. The key component of this system is the liquid crystalline state, which can be employed in the first stage to elongate the hard domains and in the second stage to nucleate crystallization.

Chapter 4 applies infrared (IR) spectroscopy to characterize LCPUs around the underlying phase transitions. It focuses on the highly localized mode of the amide I region (carbonyl stretching), which is sensitive to conformation through dipole-dipole interactions.

The conformation characteristics and crystal packing of TDI based, "regular" and liquid crystal polyurethanes, as a function of the TDI's methyl group positioning are discussed in Chapter 5. With the help of well resolved WAXS fiber patterns and atomistic molecular modeling simulations we aim to deduce a detailed structure for the symmetric LCPUs. A similar analysis will be extended to the "regular" polyurethanes on the basis of structural similarities and well resolved WAXS powder patterns.

The conclusions of the dissertation are presented in Chapter 6 within the context of the general questions given above. The last chapter also includes suggestions for future work.

Chapters 2, 3, 4 and 5 are written as separate entities to facilitate submission for individual journal publication. The text, references, tables, schemes and figures for each chapter are presented sequentially to maintain the flow of the manuscript.

Mesogen Containing Polyurethanes can be classified in two groups

A. Mesogen Containing Polyurethanes with the Urethane Groups (H-bonding) attached to the Mesogen
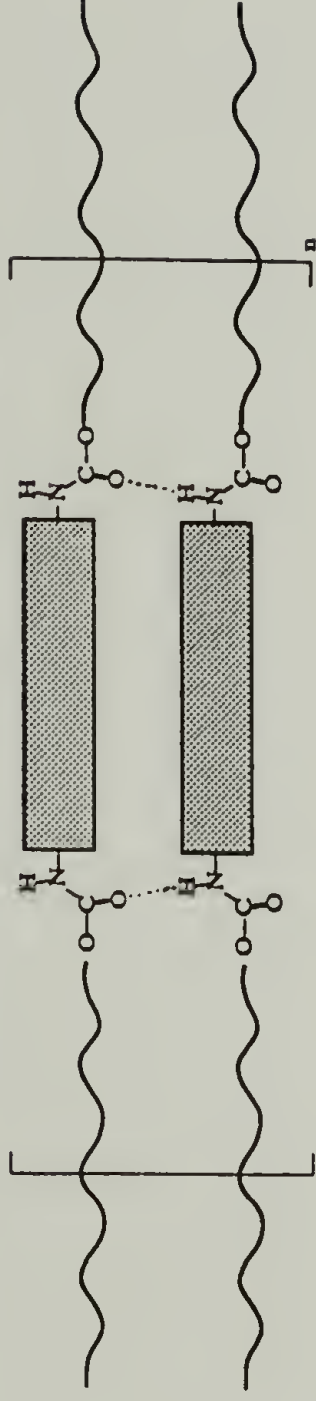
B. Mesogen Containing Polyurethanes with the Urethane Groups (H-bonding) Separated from the Mesogen with a Spacer
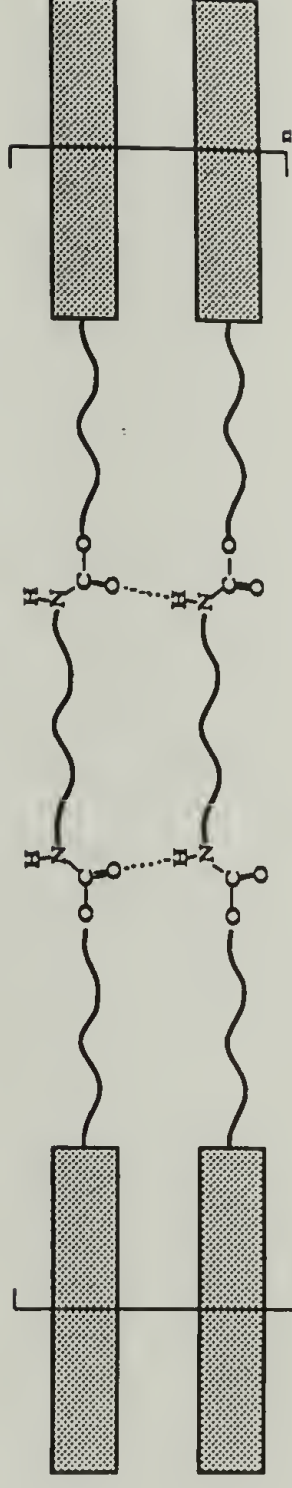
Scheme 1.1 Classification of mesogen containing polyurethanes according to the placement of the urethane group (H-bonding) with respect to the mesogen.

7

A. Mesogen Containing Polyurethanes with the Urethane Groups (H-bonding) attached to the Mesogen

$R = \begin{cases} -(CH_2)_x-, \ x = 2,3,4,5,6,8,10,12 \\ -(CH_2)_x-, \ -(CH_2)_y-; \ x = 6, \ y = 10 \\ -(CH_2)_2-O-(CH_2)_2- \\ -[(CH_2)_2-O_2-(CH_2)_2- \\ -[(CH_2)_2-O_3-(CH_2)_2- \end{cases}$ L.C. / 30%x & 50% x* / amorphous
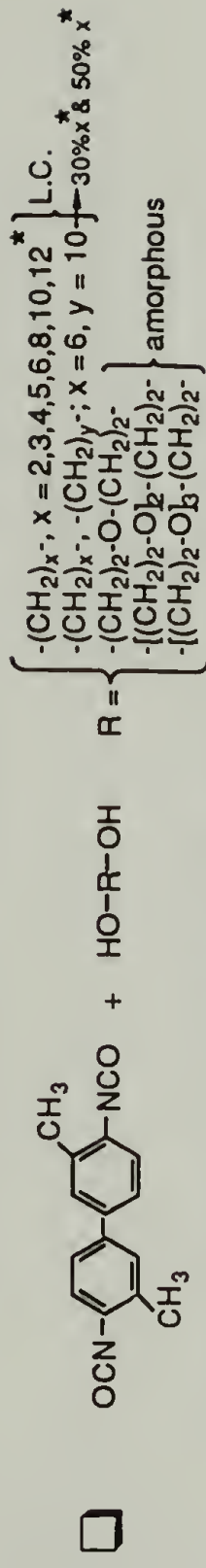
K. Iimura; N. Koiede; H. Tanabe; M. Takeda, *Macromol. Chem.*, **182** , 2569 (1981)

$R = \begin{cases} -(CH_2)_x-, \ x = 4,5,10 \\ -(CH_2)_2-O-(CH_2)_2- \\ -[(CH_2)_2-O_2-(CH_2)_2- \\ -(CH_2)_2-CH(CH_3)-(CH_2)_2- \\ -CH_2-C(CH_3)_2-CH_2- \end{cases}$
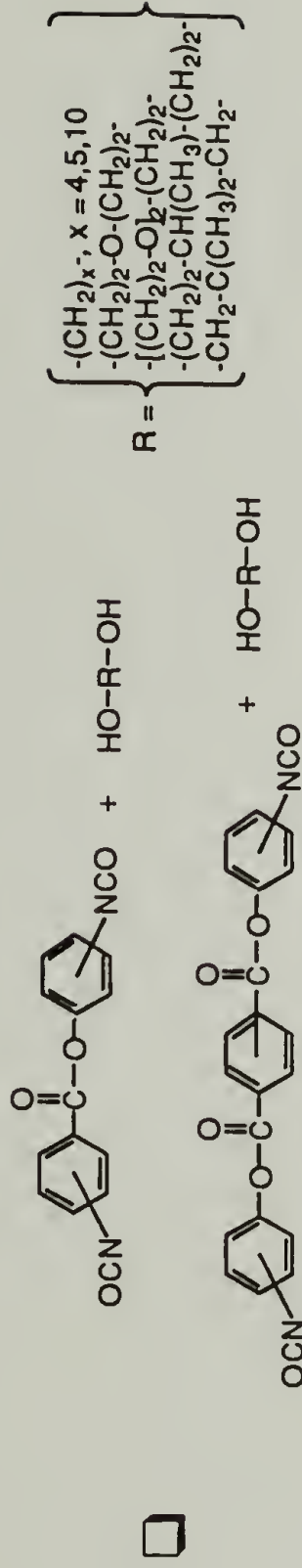
W. Mormann; M. Brahm, *Macromol. Chem.*, **190** , 631 (1989)

$R_1, R_2, R_3 = H, CH_3$

$R = -(CH_2)_2-CH(CH_3)-(CH_2)_2-$ } Monotropic L.C.

$R = \begin{cases} -[(CH_2)_2-O_2-(CH_2)_2- \\ -(CH_2)_4- \end{cases}$ } Crystalline
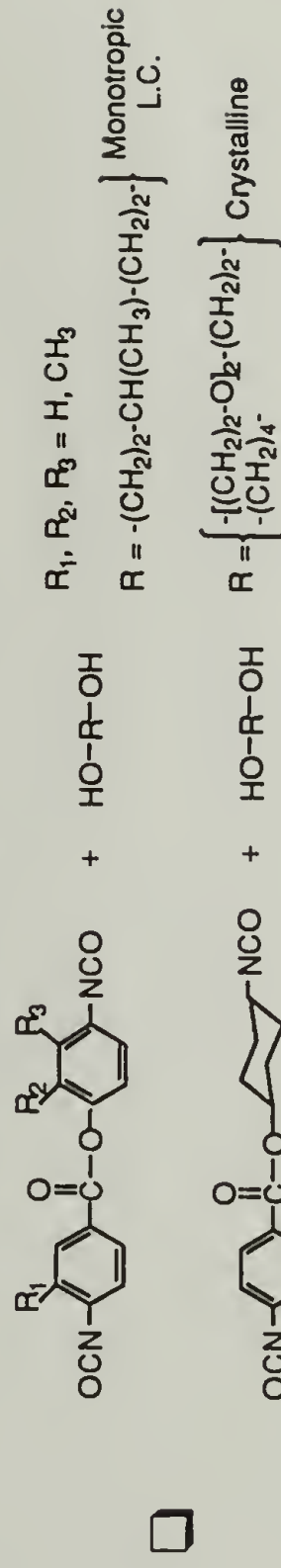
W. Mormann; M. Brahm, *Macromolecules*, **1991** , 24, 1096

---

* Melting Temperature (T_m) and Isotropization Temperature (T_I) less than 200 °C

Scheme 1.2 Mesogen containing polyurethanes with the urethane group (H-bonding) attached to the mesogen.

B. Mesogen Containing Polyurethanes with the Urethane Groups (H-bonding) Separated from the Mesogen with a Spacer

☐ HOCH₂CH₂—[ring]—N=CH—[ring]—CH=N—[ring]—CH₂CH₂OH

$$HOCH_2CH_2-N=CH-CH=N-CH_2CH_2OH$$

+ OCN–R–NCO

$$R = \begin{cases} -(CH_2)_6- & T_m=206; T_i=230 \\ H_{12}MDI & T_m=160; T_i=216 \\ H_6XDI & T_m=186; T_i=226 \\ 3,5\text{-}TDI & T_m=144; T_i=204 \\ MDI & T_m=272; T_i= \text{-} \\ 1,4\text{-}PDI & T_m= \text{-} ; T_i= \text{-} \end{cases}$$
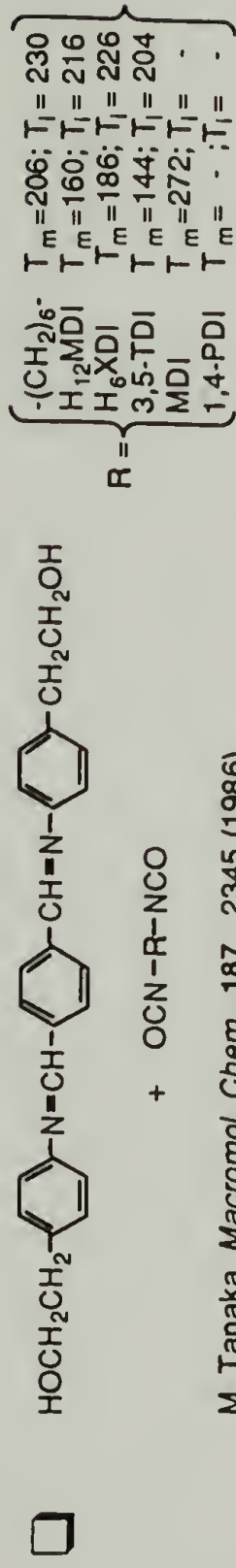
M. Tanaka, *Macromol. Chem.*, **187**, 2345 (1986)

☐ HOCH₂—[ring]—O—C(=O)—[ring]—C(=O)—O—[ring]—CH₂OH

$$HOCH_2-O-\overset{O}{C}-\overset{O}{C}-O-CH_2OH$$

+ OCN–R–NCO

$$R = \begin{cases} -(CH_2)_6- & T_m=243; T_i=291 \\ H_{12}MDI & T_m=214; T_i=250 \\ H_6XDI & T_m=172; T_i=229 \\ 3,5\text{-}TDI & T_m=185; T_i=234 \\ MDI & T_m= \text{-} ; T_i= \text{-} \\ 1,4\text{-}PDI & T_m= \text{-} ; T_i= \text{-} \end{cases}$$
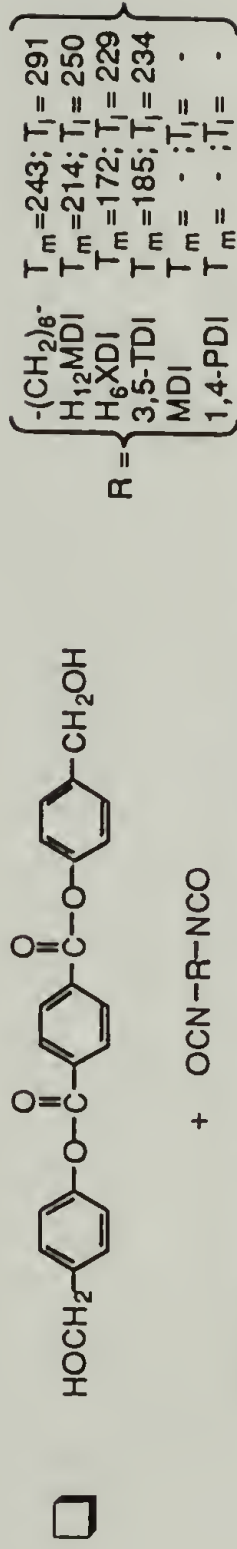
M. Tanaka; T. Nakaya, *J. Macromol. Sci.-Chem.*, **A24** (7), 777 (1987)

☐ HO-(CH₂)ₓ-O—[ring]—[ring]—O-(CH₂)ₓ-OH

$$HO-(CH_2)_x-O-O-(CH_2)_x-OH$$

+ OCN–R–NCO

$$\begin{cases} X=2 ; R = -(CH_2)_6-, -(CH_2)_{10}-, TDI, MDI \\ X=6 ; R = -(CH_2)_6^*-, -(CH_2)_{10}^*-, TDI, MDI \end{cases} \begin{matrix} \text{Monotropic} \\ \text{L.C.} \end{matrix}$$
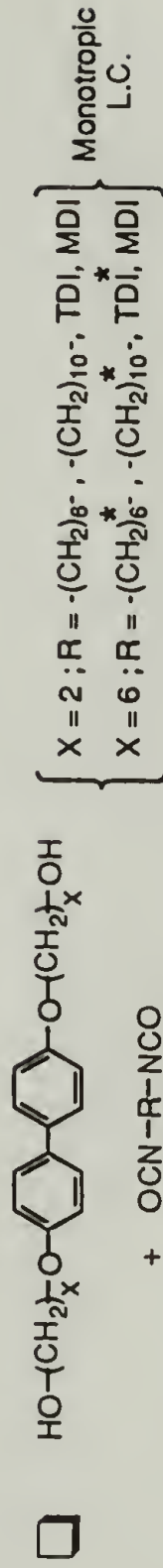
J. Y. Jadhav; S. W. Kantor, *Personal Communication*, 7/8/86

---

* Melting Temperature (T_m) and Isotropization Temperature (T_i) less than 200 °C

Scheme 1.3 Mesogen containing polyurethanes with the urethane group (H-bonding) separated from the mesogen with a spacer.

9
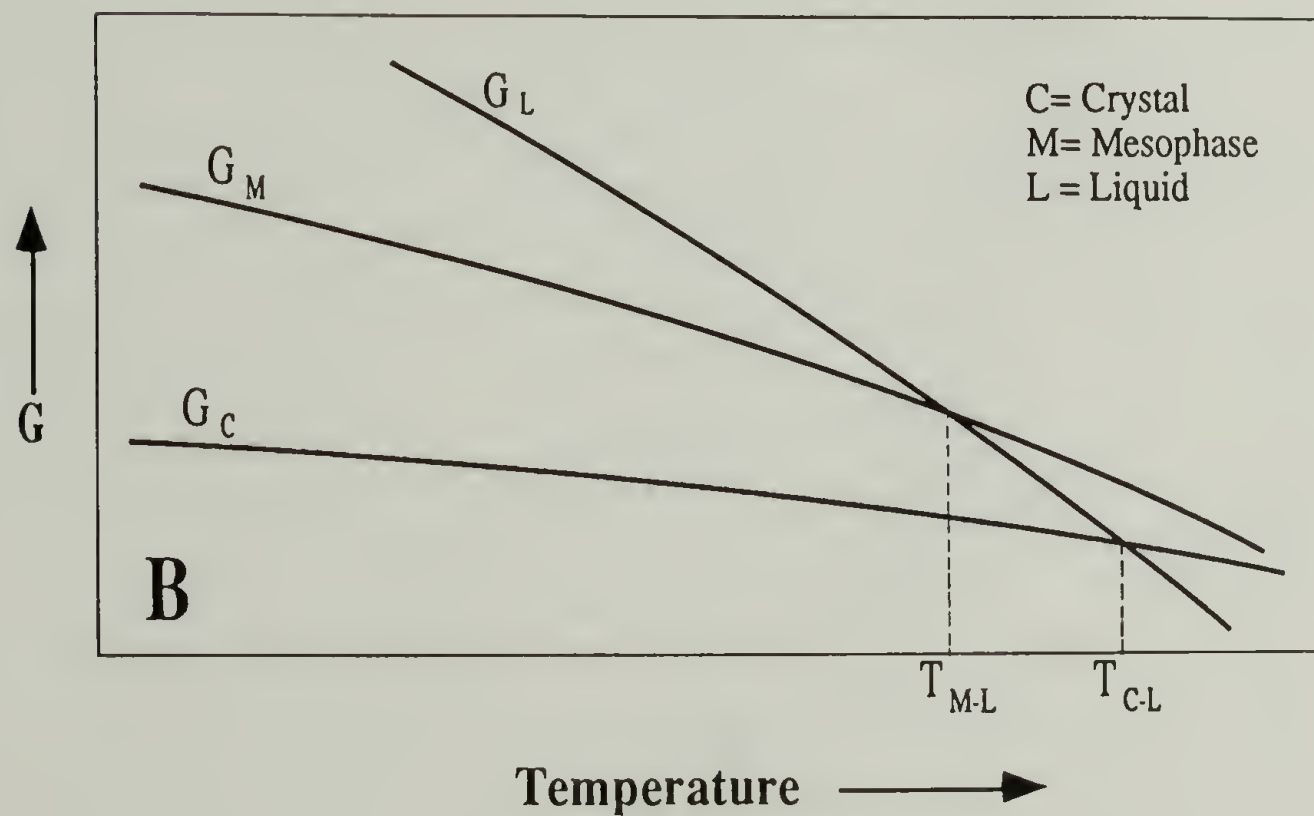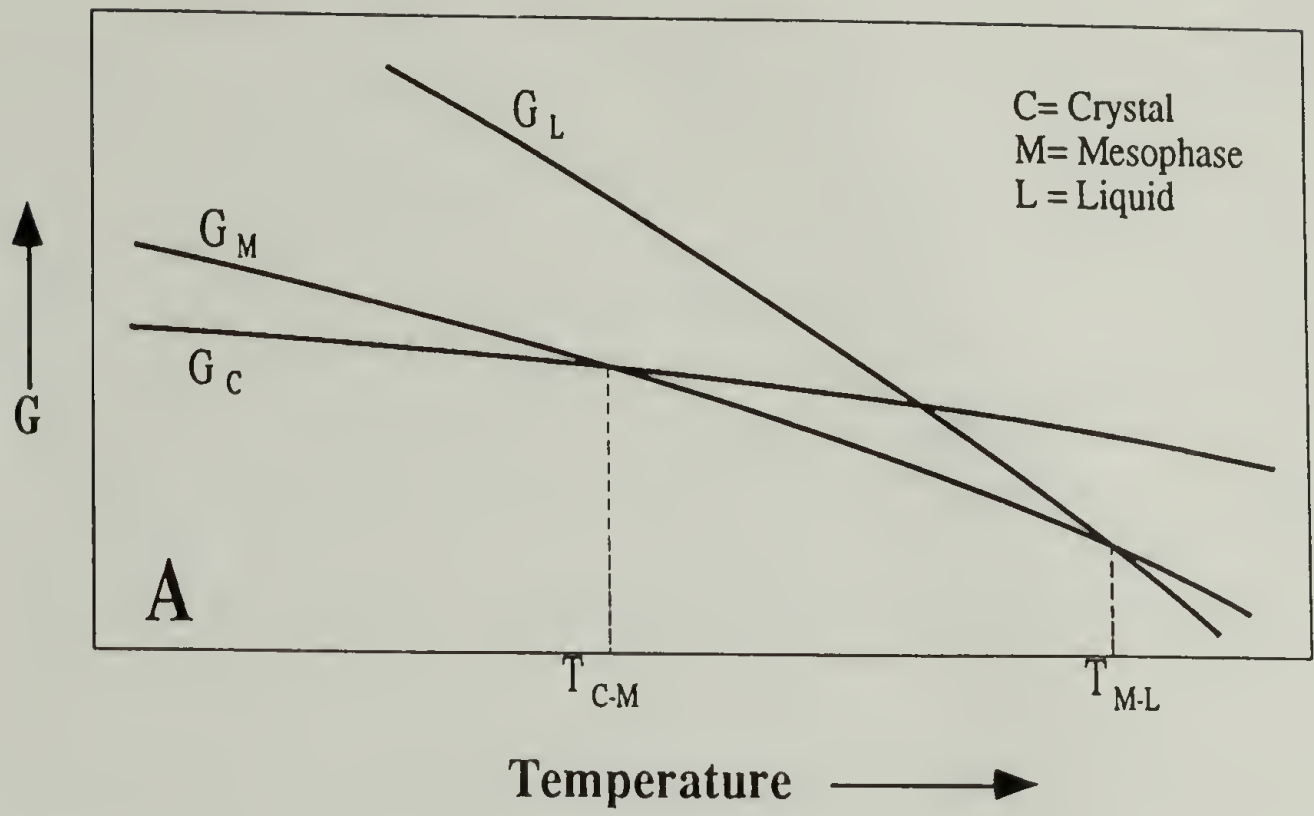
Figure 1.1 Schematic temperature dependence of Gibbs free energy (G) for:
A) representative enantiotropic mesophase and
B) representative virtual mesophase when (T_{C-L} - T_{M-L}) is large or
monotropic mesophase when (T_{C-L} - T_{M-L}) is small.

References

(1) Edwards, K. N. *Urethane Chemistry and Applications*; ACS: Washington, D.C, 1981; Vol. 172.

(2) Hager, S. L.; Rury, T. B. M.; Gerkin, R. M.; Gritchfield, F. E. In *Urethane Chemistry and Applications*; K. N. Edwards, Ed.; ACS: Washington, D.C, 1981; Vol. 172; pp 149-166.

(3) O'shea, F. X. In *Urethane Chemistry and Applications*; K. N. Edwards, Ed.; ACS: Washington, D.C, 1981; Vol. 172; pp 243-257.

(4) Melzger, S. H.; Jr. In *Urethane Chemistry and Applications*; K. N. Edwards, Ed.; ACS: Washington, D.C, 1981; Vol. 172; pp 69-86.

(5) Leis, D. G. In *Urethane Chemistry and Applications*; K. N. Edwards, Ed.; ACS: Washington, D.C, 1981; Vol. 172; pp 33-48.

(6) Pottick, L. A., Personal Communication.

(7) Chapoy, L. L. *Recent Advances in Liquid Crystalline Polymers*; Elsevier Appl. Sci. Publ.: 1985.

(8) Blumstein, A. *Liquid Crystalline Order in Polymers*; Academic Press: N.Y., 1978.

(9) Cifferri, A.; Krigbaum, W. R.; Meyer, R. B. *Polymer Liquid Crystals*; Academic Press: N.Y., 1982.

(10) Stenhouse, P. J.; Valles, E. M.; Kantor, S. W.; MacKnight, W. J. *Macromolecules* **1989**, *22*, 1467.

(11) Smyth, G.; Pollack, S. K.; MacKnight, W. J.; Hsu, S. L. *Liquid Crystals* **1990**, *7*, 839.

(12) Pollack, S. K.; Shen, D. Y.; Hsu, S. L.; Wang, Q.; Stidham, H. D. *Macromolecules* **1989**, *22*, 551.

(13) Shen, D. Y.; Pollack, S. K.; Hsu, S. L. *Macromolecules* **1989**, *22*, 2564.

(14) Yang, W. P.; Macosko, C. W.; Wellinghoff, S. T. *Polymer* **1986**, *27*, 1235.

(15) Dyer, E.; Hammond, R. J. *Journal of Polymer Science: Part A* **1964**, *2*, 1.

(16) Iimura, K.; Koide, N.; Tanabe, H.; Takeda, M. *Makromol. Chem.* **1981**, *182*, 2569.

(17) Mormann, W.; Brahm, M. *Makromol. Chem.* **1989**, *190*, 631.

(18) Mormann, W.; Brahm, M. *Macromolecules* **1991**, *24*, 1096.

(19) Tanaka, M.; Nakaya, T. *Makromol. Chem.* **1986**, *187*, 2345.

(20) Tanaka, M.; Nakaya, T. *J. Macromol. Sci. - Chem.*, **1987**, *A24*, 777.

(21) Jadhav, J. Y.; Kantor, S. W. To be published.

(22) Sato, M.; Komatsu, F.; Takeno, N.; Mukaida, K. *Makromol. Chem., Rapid Commun.* **1991**, *12*, 167.

(23) Lorenz, R.; Els, M.; Haulena, F.; Schmitz, A.; Lorenz, O. *Angew.Makrom.Chem.* **1990**, *180*, 51.

(24) Smyth, G.; Valles, E. M.; Pollack, S. K.; Grebowicz, J.; Stenhouse, P. J.; Hsu, S. L.; MacKnight, W. J. *Macromolecules* **1990**, *23*, 3389.

(25) Keller, A.; Ungar, G., To be published.

(26) Percec, V.; Keller, A. *Macromolecules* **1990**, *23*, 4347.

CHAPTER 2

SYNTHESIS OF MESOGENIC N-METHYL POLYURETHANES AND DEMONSTRATION OF THE EFFECT OF H-BONDING ON POLYURETHANE LIQUID CRYSTALLINE PROPERTIES

Introduction

A great number of mesogen containing polymers like polyesters, polyethers, polycarbonates, etc., exhibit thermotropic liquid crystalline phases and strongly ordered structures in the solid state.[1] Unlike the above polymers, mesogen containing polyurethanes are strongly interacting through their hydrogen-bonds. A large body of work details the effect of specific hydrogen-bonding interactions in polyurethane systems.[2-7] The fact that the existence of a liquid crystalline phase and its thermodynamic stability is still a matter of debate for the mesogenic polyurethanes, has been attributed to the strong specific interactions of H-bonding.[8-11] The primary focus of this chapter is to elucidate the effect of H-bonding upon the structure and phase behavior of liquid crystal polyurethanes.

The polyurethane designated 2,4-LCPU-6 has been shown to exhibit monotropic liquid crystalline (LC) behavior.[8]

2,4-LCPU-6

13
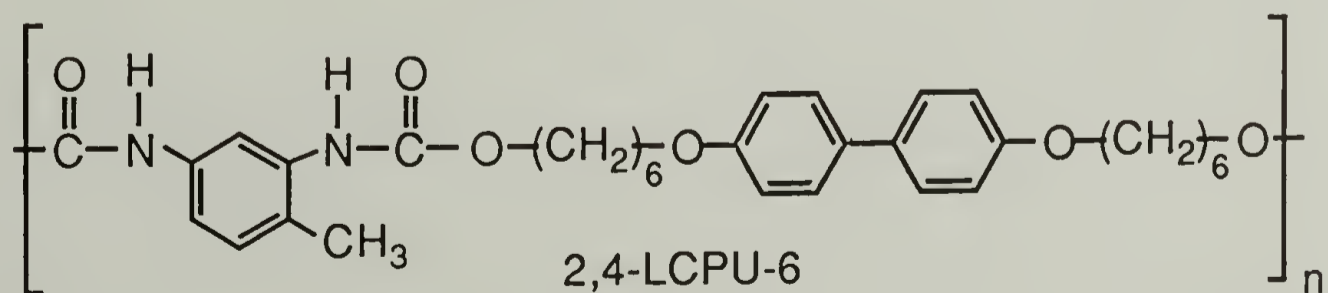
Systematic studies of the structural elements of this system, (H-bonding, asymmetric position of the methyl group in the 2,4-TDI moiety, copolymer effects, etc.) and their effects on the phase behavior are lacking due to synthetic difficulties and thermal instabilities. It is of fundamental interest of this dissertation to understand the property - structure relationships of 2,4-LCPU-6 and its family of related mesogenic containing polyurethanes. The mesogen of choice is based on biphenol. The six methylene units on both sides of the biphenol provide the appropriate amount of flexibility[12,13] without diluting the mesogen too much. The resulting molecule, 4,4'-bis(6-hydroxyhexoxy)biphenyl (BHHBP) exhibits a highly ordered, stable, smectic mesophase.[8]

$$HO\text{-}(CH_2)_6\text{-}O\text{-}\langle\rangle\text{-}\langle\rangle\text{-}O\text{-}(CH_2)_6\text{-}OH$$
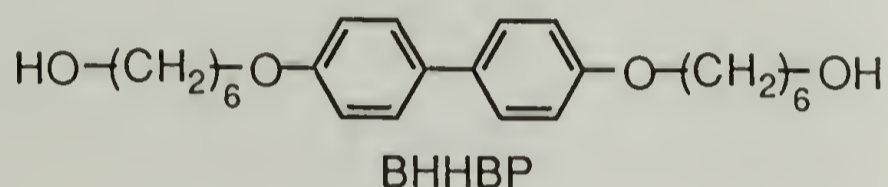
BHHBP

The introduction of BHHBP into various polymers, like polyesters[14-16] and polycarbonates[17-19] has resulted in mostly smectic A or C mesophases. The incorporation of BHHBP into polyurethanes based on 2,4-TDI has also been reported to result in smectic A or C mesophases.[8,9,11] This fact is an indication that the strong intermolecular interactions introduced by hydrogen-bonding do not govern the mesophase morphology. The present chapter of this dissertation confirms this hypothesis by examining the phase behavior of a polymer similar in structure to 2,4-LCPU-6 but without the hydrogen-bonding.

N-substituted polyurethanes (polycarbamates) have been synthesized in the past, mainly from the condensation of N-substituted diamines with bischloroformates.[20,21] However the N-methyl analog of 2,4- LCPU-6 is difficult to prepare in this way due to the highly unstable nature of the 2,4-TMA diamine (see Scheme 2.1). The synthesis of high molecular weight N-Methyl 2,4-LCPU-6 (hereafter referred to as NM-2,4-LCPU-6) was accomplished using a novel high temperature polymerization of a biscarbamoyl chloride with the BHHBP mesogenic diol (see Scheme 2.2). This novel high temperature

14

polymerization is closely related to polyester high temperature polymerization from acid chlorides and alcohols, and manifests most of the advantages of such reactions. Bilibin et al.[22-25] as well as other researchers[26] reported that this polymerization provides high molecular weight polyesters with excellent molecular weight control utilizing monomer stoichiometry. In contrast, normal polyurethane polymerization from the condensation of diisocyanates and alcohols results in moderate molecular weight polymers with poor molecular weight control.[27]

This chapter details the thermal and morphological characterization of NM-2,4-LCPU-6. The results obtained for NM-2,4-LCPU-6 are directly compared with those for 2,4-LCPU-6 previously obtained from our laboratory, as well as some new ones. The thermodynamic effects of hydrogen-bonding on the mesophase are clearly demonstrated on the basis of the observed entropy and enthalpy of fusion,[13,28] as well as X-ray diffraction data. Schematic temperature dependencies of the Gibbs free energy[29,30] for 2,4-LCPU-6 and NM-2,4-LCPU-6, rationalize the monotropic-enantiotropic behavior as a function of H-bond content. In addition to that, some interesting behavior of the NM-2,4-LCPU-6 near its glass transition temperature will be also discussed.

Experimental

Materials. All chemicals were obtained from Aldrich except for 2,4-tolylene diisocyanate (2,4-TDI) which was obtained from Fluka. The reaction solvents were dried and distilled before their use and recrystallization solvents were stored previously over activated 3-4 Å molecular sieves. Prepurified Ar and N_2 inert gases were previously passed over BTS catalyst (O_2 scavenger)[31] and $CaCl_2$ desiccant.

Synthesis of NM-2,4-LCPU-6. (Scheme 2.1 & 2.2) Synthesis of BHHBP: In a 500 ml three neck round-bottom flask fitted with a condenser, pressure equalizing dropping funnel, inert gas inlet and magnetic stirrer, was added 250 ml absolute ethanol and 16.0 g (0.4 mole) NaOH. Purified Ar was bubbled through the solution for 15 minutes.

Subsequently 18.6 g (0.1 mole) 4,4'-dihydroxy biphenyl was added maintaining the bubbling of Ar for 15 more minutes at ambient temperature to prevent oxidation of the dianion of biphenol to diphenoquinone (purple color). The resulting slurry is heated to reflux, and 61.1 g (0.44 mole) 6-chlorohexanol previously purged with Ar, is added slowly. The reaction mixture is refluxed for 24 hours, cooled to room temperature and poured into 1 liter of distilled ice water. The crude solid was washed twice with distilled water, acidified to pH = 5 - 6 with HCl and filtered. The solid product was washed with distilled water to pH = 7, dried and recrystallized twice from dioxane - activated charcoal. High purity BHHBP can be obtained by final recrystallization from ethyl acetate - charcoal and drying under vacuum at 100 °C for a day, m.p. = 179 °C, yield 70%. Elemental analysis; Calculated for $C_{24}H_{34}O_4$: C, 74.57% ; H, 8.87%. Found : C, 74.52% ; H, 8.86%.

Synthesis of 2,4-TMA:[32-34] A two liter flask was charged with 470 ml of a 1.0 M diethyl ether dispersion of $LiAlH_4$ and 35.0 g (0.201 mole) of freshly distilled 2,4-TDI diluted with 150 ml diethyl ether was added slowly with stirring. The reaction mixture was refluxed for 3 hours before the excess $LiAlH_4$ was decomposed with water. The reaction complex, $LiAl[NR(CH_3)]_4$,[32] was hydrolyzed with 500 ml of a 30% NaOH solution. After the ether was distilled, the resulting mixture was refluxed for 2 hours. The brown oil was extracted with ether, dried with CaH_2 and vacuum distilled over CaH_2 to give 19.9 g (66% yield) of a colorless liquid (b.p. = 117 - 118 °C at 0.7 mmHg). This compound turns yellow after 5 minutes under vacuum. The more stable hydrochloride salt decomposes above 200 °C prior to melting. *Elemental analysis* ; Calculated for $C_9H_{16}N_2Cl_{l2}$: C, 48.44% ; H, 7.23% ; N, 12.56% ; Cl, 31.78%. Found : C, 48.62% ; H, 7.22% ; N, 12.41% ; Cl, 31.64%.

Synthesis of 2,4-TCC:[34-36] A 1000 ml flask was charged with 300 ml dry, O_2 free ethyl acetate, 37.2 g (0.125 mole) of triphosgene[36] and 7.1 g (0.047 mole) of freshly distilled 2,4-TMA was added at 25 °C, forming immediately a white precipitate (I).

Overnight reflux at 55 °C resulted in a clear solution which was distilled to dryness. The residue was recrystallized three times from a mixed solvent [CCl$_4$/hexane 3:1, with charcoal] to yield 7.1 g of 2,4-TCC (55% yield), m.p. = 116.5 °C. *Elemental analysis* ; Calculated for C$_{11}$H$_{12}$N$_2$O$_2$Cl$_2$: C, 48.02% ; H, 4.40% ; N, 10.18% ; Cl, 25.77%. Found: C, 47.98% ; H, 4.30% ; N, 10.12% ; Cl, 25.49%.

Polymerization: A dry Schlenk tube with condenser was charged with 0.50000 g (1.8173 mmole) 2,4-TCC, 0.70167 g (1.8154 mmole) BHHBP (0.1% excess TCC) and 12.0 ml orthodichlorobenzene, freshly distilled over CaH$_2$. The reaction mixture was maintained between 175-180 °C under a slow stream of dry, O$_2$ free Ar for 96 hours and precipitated in MeOH. The solid was re dissolved in CH$_2$Cl$_2$ and reprecipitated twice with MeOH, Soxhlet extracted in hot MeOH and vacuum dried to give 0.930 g NM-2,4-LCPU-6 (yield 87.0%). Its inherent viscosity in CH$_2$Cl$_2$ at 30.0 °C was 0.82 dL/g. *Elemental analysis* ; calculated for C$_{35}$H$_{44}$N$_2$O$_6$ repeat unit : C, 71.40% ; H, 7.53% ; N, 4.76% ; Cl, 0.00% Found : C, 71.38% ; H, 7.51% ; N, 4.68% ; Cl, 0.18%.

The synthesis and characterization of 2,4-LCPU-6 is described elsewhere.[11]

Characterization Techniques. Inherent viscosity. Inherent viscosities for NM-2,4-LCPU-6 were determined at 30.0 °C in CH$_2$Cl$_2$, using a Cannon-Ubbelohde viscometer. The NM-2,4-LCPU-6 polymers referred as low and as high molecular weight were determined to have an inherent viscosity [η]$_{inh}$ = 0.48 dL/g and [η]$_{inh}$ = 0.82 dL/g respectively.

Solution NMR. Solution ^{1}H NMR spectra of NM-2,4-LCPU-6 and 2,4-LCPU-6 polymers were recorded on a Varian XL-200 operating at 200 MHz in deuterated solvents. All spectra were referenced relative to the solvent chemical shift.

Optical Microscopy. Optical microscopy was performed on a Carl Zeiss Ultraphoto II polarizing microscope equipped with a Linkham Scientific Instruments TMS 90 temperature controller and a TMH 600 hot stage. The hot stage temperature was calibrated with vanillin and potassium nitrate melting point standards.

Thermal Analysis. DSC measurements were conducted with a Perkin-Elmer DSC-7 employing a 20 mL/min flow of dry nitrogen as purge gas for the sample and reference cells. The coolant was ice-water bath except for the case of NM-2,4-LCPU-6 polymer where chopped dry-ice was employed. The temperature and power ordinates of the DSC were calibrated with respect to the known melting point and heat of fusion of a high purity indium standard. For exothermic and endothermic processes the peak temperatures were taken as the transition temperature, while for the glass transition the midpoint of the heat capacity step was taken as the transition temperature. Long term annealing was performed under nitrogen or vacuum to ensure the absence of thermal degradation.

X-Ray Diffraction. Room temperature WAXS patterns were obtained with a Statton X-ray camera using Ni filtered Cu Kα radiation.

Results and Discussion

Scheme 2.1 illustrates the synthesis of the monomers needed to achieve the synthesis of the NM-2,4-LCPU-6 illustrated in Scheme 2.2. The present polymerization Scheme was adopted due to the peculiarities of this system which cause several problems with previously reported methylation techniques. Although it was possible to synthesize the α,ω-bis-chloroformate of BHHBP,[20,34,37] the highly unstable nature of the 2,4-tolylene-dimethylamime (2,4-TMA) (Scheme 2.1) inhibited the formation of high molecular weight NM-2,4-LCPU-6 using either interfacial or homogeneous polymerization in CH_2Cl_2. In addition the metallation methods of Cooper et al.[38-40] using NaH - CH_3I in dry DMF, resulted in severe molecular weight degradation[40] and only partial methylation, as indicated from solution ^{1}H-NMR.

Since the salts of 2,4-TMA are more stable than the free amine, they were utilized to improve the yield in the synthesis of the 2,4-tolylene-di(N-methylcarbamoylchloride) (2,4-TCC). When the freshly distilled 2,4-TMA was added to the ethyl acetate-triphosgene solution, a white precipitate (I)[41] was formed instantaneously and protected the 2,4-TMA

from further degradation. The 2,4-TCC is a very stable compound and easy to purify to high purity levels. Although the synthesis of the NM-2,4-LCPU-6 (Scheme 2.2) resembles polyester polymerization[22-26] from acid chlorides and alcohols, it requires special conditions to take place quantitatively and to result in high molecular weight polymer. The fact that no polymer was obtained from solution polymerization carried out at 90 °C, using bases such as pyridine as an acid acceptor, is attributed to the stability of carbamoyl chloride/base salts [34,41] similar to (I). This salt equilibrates with the hydrochloric/base salt altering the stoichiometry and the efficient removal of the by-product HCl. In addition, reaction temperatures higher than 110 °C resulted in severe discoloration of the reaction solution probably due to pyridine side reactions. The absence of base was proven necessary in order to obtain high molecular weight polymer. The reaction without an acid acceptor starts around 160 °C and was monitored by the evolution of gaseous hydrogen chloride. The optimum reaction temperature was around 180 °C where the reaction proceeded moderately. A slow stream of dry, O_2 free argon gas was used to remove the by-product HCl, in order to drive the reaction to completion. Higher temperatures resulted in lower molecular weight due to the instability of the urethane bond[42,43] above 195 °C. Solution polymerization in high boiling solvents resulted in higher molecular weights than melt polymerization. The inherent viscosities, solvent type and experimental conditions for the melt and solution polymerization are summarized in Table 2.1. The melt polymerization required much greater control over the polymerization conditions mainly due to the high viscosity of the melt, poor stirring and particularly the loss of 2,4-TCC due to sublimation. For this purpose we added a much greater excess of 2,4-TCC compared to the solution polymerization, and lowered the reaction temperature. A small excess of 2,4-TCC (0.1 mole %) proved to be the optimum for the solution polymerization. This polymerization scheme seems to give excellent molecular weight control based on monomer stoichiometry (see Table 2.1). Thus, the reaction of carbamoyl chloride with an alcohol proceeds quantitatively[44] under these conditions. The only

disadvantage of this polymerization scheme is the low reaction rate, because the carbonyl electrophilicity of carbamoyl chlorides is much less than that of acid chlorides, due to the +R resonance effect of the adjacent nitrogen atom. Additionally the low reaction rate is exacerbated by the narrow temperature window available (160 °C reaction begins - 195 °C urethane degradation begins). The polyester of isophthaloyl dichloride and BHHBP with similar inherent viscosity to the high molecular weight NM-2,4-LCPU-6, was obtained in 8 hours compared to 4 days for the latter. Nevertheless, the molecular weights that can be achieved (at long times) with this method for N-substituted polyurethanes are much higher than those reported for conventional polyurethanes as well as for N-substituted polyurethanes.

The solution ^{1}H NMR spectra of NM-2,4-LCPU-6 and 2,4-LCPU-6 are shown in Figure 2.1. The molecular weight of both polymers was the highest obtained and the sample concentration was 5% w/v. The high spectral resolution of both samples indicated a relatively stiff backbone chain. In agreement with the structures, both downfield peaks of N-H protons of 2,4-LCPU-6 (at 9.29 and 8.52 ppm) have been removed and two new peaks are present in the spectra of NM-2,4-LCPU-6 (at 3.16 and 3.25 ppm) due to the N-CH$_3$. The rest of the spectra[11] for both samples is virtually the same.

Representative 10 °C/min DSC heating and cooling scans of the NM-2,4-LCPU-6 are presented in Figure 2.2. The curve (A) is usually observed upon heating a sample which was left at room temperature for more than five minutes. The first peak at 45.6 °C is associated with the enthalpic relaxation[45-47] at the glass transition temperature. The second endotherm around 56 °C is weaker and much broader than the first one, and is associated with the melting of a mesophase. Curve (C) is the representative cooling scan which shows a very broad exothermic region associated with the formation of this mesophase which is interrupted by the glass transition. The enthalpy relaxation peak is enhanced because room temperature is 10 to 15 °C below the T_g and this is the optimum range for physical aging. In order to avoid the enthalpy relaxation which interferes with the second

endotherm, the samples were maintained at temperatures below -20 °C after the cooling cycle and the heating cycle was started from -30 °C. In this case, curve (B) was obtained showing a sharp glass transition at 38.6 °C and a broad region of endothermic behavior associated with the isotropization of the mesophase. The molecular weight seems to have very little effect on the transition temperatures and enthalpies for both NM-2,4-LCPU-6 samples. Annealing at 50 °C, which is in the middle of the narrow temperature window between solidification and isotropization, increased the amount of the mesophase as well as perfecting it, as shown in Figure 2.3.

In order to understand the temperature-phase behavior of NM-2,4-LCPU-6 better and to provide a basis for the interpretation of the effect of hydrogen-bonding in the LCPU systems, the optical textures obtained by cooling samples of high and low molecular weight from the melt to the annealing temperature of 50 °C were studied by polarized light microscopy. The results are shown in Figure 2.4. Rapid cooling from the melt to temperatures below the T_g resulted in a "glassy" appearing material with no texture. On the other hand, cooling rates of 10 °C/min and lower generated around 52-55 °C a very fine texture (white region on the right and left of Figure 2.4A). It was observed that long before this fine texture formed, the sample could not be sheared because of high viscosity, due to the close proximity of the glass transition. Annealing at 50 °C resulted in a threaded texture formed around air bubbles or dust particles shown clearly in Figure 2.4A, indicating a nucleation type of growth. Further annealing spread and enhanced the threaded textures (Figure 2.4B & 2.4C) which are more akin to that reported for a variety of liquid crystalline polymers.[1,48] Additional annealing did not change the texture and no evidence of banded spherulitic textures appeared. On heating, these perfected mesophases melted around 60-65 °C. The molecular weight affects the coarsening rate of the threaded structure and since all this happens near T_g, the low molecular weight sample developed the morphology more quickly.

The observations of differential scanning calorimetry and polarized light microscopy suggest the presence of an enantiotropic mesophase very close to the T_g of the sample. WAXS was employed in order to establish the nature of this mesophase. Fibers of the high and low molecular weight NM-2,4-LCPU-6 were drawn from the melt and quenched in air. The X-ray diffraction pattern for a single fiber of the high molecular weight sample is shown in Figure 2.5A. The pattern exhibits diffuse equatorial reflections corresponding to a spacing of about 4.5 Å. In addition one can observe four weak off-meridional reflections at smaller scattering angles. These types of patterns have been observed for a number of liquid crystalline polymers and low molecular weight compounds.[49-52] They have been attributed to the so-called "Cybotactic" nematic structure, a morphology intermediate between nematic and smectic C phases. The off-meridional reflections corresponds to a spacing of approximately 15 Å. The fiber, upon annealing at 50 °C, develops a smectic C phase[53-55] imbedded in the residual nematic phase (Figure 2.5B). The pattern exhibits again the diffuse equatorial reflections corresponding to a spacing of about 4.5 Å, while the diffuse off-meridional reflections have increased in number as well as sharpening considerably. The tilt angle is $\beta_t = 20° \pm 1°$ with repeat length $l = 58.9 \pm 0.6$ Å $(l = 001)^\dagger$, and meridional layer spacing $d = 58.9 \pm 0.6$ Å $(d = l \cdot \cos\beta_t)$. The molecular weight seems to have no effect on the spacing distances and tilt angle, although the higher molecular weight resulted in fibers with higher orientation.

Having established the basic phase-temperature behavior of the NM-2,4-LCPU-6, differential scanning calorimetry was used to provide more detailed information about the effects of thermal history. It is noteworthy that since the isotropic to mesophase transition occurs so close to the T_g lengthy annealing has to be employed in order to achieve an equilibrium morphology. Figure 2.3 displays the 10 °C/min DSC heating traces of the low molecular weight sample previously annealed at 50.0 °C for various annealing times. The measurements from Figure 2.3 of the glass transition temperature T_g, change in the heat

---

† The layer line spacings were assigned to 002, 004 (strong), and 006 (weak) and 008 (diffuse) reflections. For more details see Chapter 3 and 5.

capacity Δc_p at T_g and the isotropization temperature T_i versus mesophase-isotropic melting enthalpy ($\Delta H_{m,i}$) are shown in Figure 2.6. The increase of the melting enthalpy as well as the clearing temperature with the annealing time indicate that the initial mesophase is very disordered and an appreciable fraction of the polymer is amorphous. This material is located either in disordered regions between mesophase domains or in the various defects within the mesophase domains.[12] The fact that a completely amorphous material is not obtained, no matter how fast the quench was, indicates that the isotropic-mesophase transition occurs instantaneously[56] with a cooperative mechanism involving aligning of the mesogenic units. This mechanism leads to a very fine dispersion of the mesophase with a large quantity of grain boundaries and defects.[57] A secondary mechanism of the mesophase perfection is observed similar to the crystal perfection during annealing resulting in higher melting enthalpy and melting temperature.

As has been previously reported[12,58] low order mesophases such as nematic and smectic A and C exhibit glass transitions due to their inherent disorder. There is an increasing interest in the behavior of the glass transition as a function of phase disorder. Wunderlich et al.[58-60] have addressed this problem from both a theoretical and experimental point of view. The dependence of glass transition temperature and change in heat capacity of thermotropic nematic liquid crystal azoxy polyesters on their spacer length and molecular weight has been reported recently by Blumstein et al.[61-63] and Percec et al.[30,64]. Zachmann et al.[65,66], investigating thermotropic liquid crystal copolyesters of ethyleneterephtalate (ET), ethylenenaphthalene-2,6-dicarboxylate (EN) and oxybenzoate (HB), observed by DSC and DMTA different glass transition temperatures for the liquid-crystalline phase (T_g^{LC}) and amorphous phase (T_g^i). Characteristically, for the copolyester of ET/EN/HB (35/35/30) the T_g^{LC} was about 40 °C lower than the T_g^i and the relative amounts of the two phases was governed by the annealing temperature which produced the mesophase. The free volume of the chains in the isotropic state, below or above the T_g^i, will always be higher than their free volume in the mesophase, below or above the T_g^{LC}

respectively, due to the loss of two translational modes in the mesophase. Zachmann's interpretation was based on the relative difference of the volumes of the glass transition ΔV_c ($\Delta V_c = V_c^i - V_c^{LC}$) versus the change in volume at the mesophase-isotropic transition ΔV_t ($\Delta V_t = V_t^i - V_t^{LC}$) (see Figure 2.7). This approach explains both possible cases, for T_g^i higher or lower than T_g^{LC}. The criteria for $T_g^{LC} < T_g^i$ is $\Delta V_t < \Delta V_c$ (Figure 2.7A) while for $T_g^{LC} > T_g^i$ is $\Delta V_t > \Delta V_c$ (Figure 2.7B). The magnitude of ΔV_t corresponds to the mesophase order, while the ΔV_c is related to the difference in the free volume between the isotropic phase at its glass transition and the mesophase at the glass transition temperature.

The fact that the glass transition temperature of the NM-2,4-LCPU-6 is only 20 °C below the mesophase - isotropic transition affords the possibility to vary systematically the fraction of mesophase present. In addition, because the mesophase transition occurs so fast and so close to the T_g, phenomena like "cold crystallization" of the mesophase from the amorphous phase immediately above T_g, do not interfere with its determination the way they do in Zachmann's system. The increase of the T_g with the mesophase melting enthalpy (mesophase perfection) of Figure 2.6 shows that the mesophase has a higher glass transition (T_g^{LC}) than the amorphous (T_g^i). It is noteworthy that $\Delta H_{m,i}$ less than 4 J/g was not obtainable due to the fast rate of the mesophase formation. The increase of T_g is linear with $\Delta H_{m,i}$ and on the basis of extrapolation the T_g^{LC} seems to be about 6 °C higher than the T_g^i. This can be easily explained with Zachmann's model, assuming that the $\Delta V_t > \Delta V_c$. The above assumption is reasonable since Zachmann's copolyesters exhibit less ordered nematic mesophases when compared to the more ordered smectic mesophase of NM-2,4-LCPU-6.

If the increase of isotropization temperature T_i, with the mesophase melting enthalpy (Figure 2.6) is due to an increase of the mesophase order, then the following explanation is proposed. Assuming ΔV_c remains more or less constant, then ΔV_t is the

only variable. The ΔV_t increases with the mesophase order, leading to a linear increase of T_g (Figure 2.8), in accordance with the Zachmann's model.

In addition to the linear increase of T_g a subtle increase in the change of the heat capacity Δc_p, within the experimental error, is also observed (Figure 2.6). Presently we can not propose a model to explain this phenomenon which will imply knowledge of the differences of the translational, vibrational, and rotational modes[60] of the present system in its mesophase and amorphous phase.

Comparison of 2,4-LCPU-6 and NM-2,4-LCPU-6

Utilizing previously published data[8] from our laboratory, we will attempt to draw conclusions about the effect of the hydrogen bonding on the 2,4-LCPU-6 liquid crystalline properties based on data comparison with the methylated version, NM-2,4-LCPU-6. Representative 10 °C/min, normalized DSC heating and cooling scans of the two polymers are presented in Figure 2.9. For the low molecular weight ([η]=0.46 dL/g) 2,4-LCPU-6, upon heating the glass transition is observed at approximately 85 °C. This is followed by a region of "cold crystallization" peaking at about 110 °C but continuing until the onset of melting as characterized by the endothermic peaks at 158 and 170 °C. Since the polymer has been identified as monotropic,[8] these two endotherms are associated with crystal melting transitions. Upon cooling, two exotherms at 142 and 138 °C are observed. The high temperature exotherm is associated with the isotropic-mesophase transition while its lower temperature counterpart is associated with the mesophase-imperfect crystal transition. These crystals are associated with the 158 °C endotherm of the heating cycle. In order to allow a direct comparison of the polarized optical micrographs of the two polymers, we reprint* in Figure 2.10A and 2.10B the mesophase and crystalline phase textures of the of 2,4-LCPU-6 [η]=0.46 dL/g respectively. The texture of Figure 2.10A has been obtained

---

* After permission of Smyth et al.[8].

from the melt after shearing and annealing at 130 °C. On the other hand, samples annealed at 150 °C from the melt give banded spherulitic textures such as the one shown in Figure 2.10B. The bluish hue is a result of the mercury lamb used for these particular micrographs. Tungsten lamp has been employed throughout the rest of the optical micrographs of this dissertation.

More concisive results about the mesophase order of 2,4-LCPU-6 can be obtained by WAXS. Figure 2.11A portrays the WAXS pattern of a 2,4-LCPU-6 [η]=0.60 dL/g fiber drawn from the melt. It displays the familiar "Cybotactic" structure shown also in MN-2,4-LCPU-6 with diffuse equatorial reflections at about 4.5 Å, and inner off-meridional reflections at about 14 Å. Utilizing a specific solvent treatment, which will be explained in detail in Chapter 3 (Soxhlet extraction in hot MeOH), we can perfect the thermodynamically unstable mesophase of 2,4-LCPU-6. Figure 2.11B illustrate the WAXS fiber pattern of the same fiber after soxhlet extraction in hot MeOH for 5 days. The pattern exhibits again the diffuse equatorial reflections corresponding to a spacing of about 4.5 Å, while the diffuse off-meridional reflections have sharpened considerably. The tilt angle is $\beta_t = 32° \pm 1°$ with repeat length $l = 59.9 \pm 0.6$ Å $(l = 001)$**, and meridional layer spacing $d = 51 \pm 1$ Å $(d = l \cdot \cos\beta_t)$. The repeat length of the 2,4-LCPU-6 in the smectic C mesophase is slightly longer than in the NM-2,4-LCPU-6, indicating that although the hydrogen-bonding does not affect the mesophase morphology, it results in a more extended chain conformation, (see Table 2.2). Heat treatment of the Figure 2.11B fiber results into the highly oriented crystalline pattern of Figure 2.11C. The crystallographic analysis of the Figure 2.11C pattern is limited only to the inner most reflections associated with the long repeat of the structure. The tilt angle is $\beta_t = 28° \pm 1°$ with repeat length $l = 50.8 \pm 0.1$ Å $(l = 001)$*** and meridional layer spacing $d = 46.0 \pm 0.2$ Å $(d = l \cdot \cos\beta_t)$. Undoubtedly,

---

** The layer line spacings were assigned to 002, 004 (strong) reflections. For more details see Chapter 3 and 5.
*** The layer line spacings were assigned to 001, 002, 004 (strong), 006, and 008 reflections. For more details see Chapter 3 and 5.

crystal packing results into a c axis shrinkage which has also been observed with the 1,3-LCPU-6 as well (see Chapter 5).

Utilizing DSC annealing data from both polymers and the familiar relationship ($T_m = \Delta H_m / \Delta S_m$), the calculated mesophase-isotropic change in entropy for NM-2,4-LCPU-6 is $\Delta S_{m,i} = 0.16$ J/g,$^\circ$C. In the case of the monotropic 2,4-LCPU-6[67] the calculated isotropic-mesophase change in entropy is $\Delta S_{i,m} = 0.15$ J/g,$^\circ$C while the calculated crystal-isotropic change in entropy is $\Delta S_{c,i} = 0.24$ J/g,$^\circ$C. Comparing the $\Delta S_{m,i}$ for the NM-2,4-LCPU-6 with the $\Delta S_{i,m}$ of the 2,4-LCPU-6, and assuming the same degree of disorder for both the molten phases, confirms the conclusion that hydrogen-bonding has little effect on the mesophase morphology, Table 2.2. In other words, in these systems the main effect of H-bonding on the mesophase-isotropic transition is primarily enthalpic in nature[68] and can be easily visualized in Figure 2.9. The transitions in the 2,4-LCPU-6 are much larger than in the NM-2,4-LCPU-6, but the mesophase-isotropic ΔS is almost the same. On the other hand the $\Delta S_{c,i}$ of the 2,4-LCPU-6 is almost 1.5 times greater than the $\Delta S_{i,m}$, once again indicating the monotropic nature of the sample (see Table 2.2).

In order to better elucidate the monotropic-enantiotropic character of both samples, the schematic temperature dependence of the Gibbs free energy is presented in Figure 2.12.[29,30] The phases are represented as solid lines while below the glass transition where equilibrium cannot be attained, the lines are broken. The above ΔS values correspond to the slope changes between phases at the transition. In the case of 2,4-LCPU-6 the mesophase is less stable than the crystalline phase mainly due to the strong, highly directional H-bonds in the crystal lattice. Upon cooling from the melt, the material supercools along the liquid phase line until it meets the mesophase. The spontaneous transition to the mesophase provides the necessary nuclei for crystallization and a transformation takes place to the stable crystal phase. Upon heating the crystal phase free energy is always less than the mesophase and it melts before it transforms to a mesophase.

In the case of NM-2,4-LCPU-6 the mesophase is stable relative to the crystalline phase because H-bonding is lacking. Unfortunately the glass transition temperature lies so close to the mesophase-isotropic transition that it is impossible to observe a crystal phase in NM-2.4-LCPU-6, if it exists. Although Figure 2.12 carries no quantitative information, it is quite helpful for a qualitative comparison of the two polymers. The y-axis position of each curve corresponds to the enthalpy of the individual phase. With the knowledge of the transition temperatures and entropies, the relative positions of the various phases can be positioned with a limited amount of freedom. Keeping the curvatures more or less constant, we observe that the y-axis difference between the liquid phases (l´ - l) is smaller than the mesophase phases (m´ -m) and the "fictional" crystal phases as well. This is an additional evidence of the enthalpic contribution of H-bonding since the phase order is directly related with its strength and perfection.

The absence of hydrogen-bonding results also in the enhancement of the solubility of NM-2,4-LCPU-6 in most organic solvents, except saturated hydrocarbons and alcohols. On the other hand 2,4-LCPU-6 is soluble only in polar aprotic solvents like DMF, DMAC, DMP, DMSO, HMPA, etc..

Conclusions

(1)   Scheme 2.2 illustrates a novel general route for the preparation of N-substituted polyurethanes with high molecular weights and excellent molecular weight control.

(2)   2,4-LCPU-6 and NM-2,4-LCPU-6 exhibit similar mesophase morphologies, showing that the presence or absence of H-bonding is not important in determining the nature of the mesophase, Table 2.2.

(3)   H-bonding affects the temperatures of the various transitions, primarily through an enthalpic effect, Table 2.2.

(4) The NM-2,4-LCPU-6 is an excellent model to provide understanding of the glass transition temperature as a function of mesophase perfection. The T_g of the mesophase is estimated to be 6 °C higher than the amorphous phase T_g, on the basis of extrapolation to zero fraction of mesophase.

Table 2.1

Polymerization of NM-2,4-LCPU-6 at various polymerization conditions.

Solvent	Polymerization Time (hrs) *	Temperature ($^\circ$C)	$\dfrac{[N(CH_3)COCl]}{[OH]}$ †	Inherent Viscosity (dL/g)
1,2-dichlorobenzene	96	175-180	1.0020	0.48
1,2-dichlorobenzene	96	175-180	1.0010	0.82
1,2-dichlorobenzene	96	175-180	1.0001	0.57
1,2-dichlorobenzene	72	175-180	1.0010	0.65
1-chloronapthalene	72	180-190	1.0010	0.55
1-chloronapthalene	24	205-215	1.0010	0.32
Diphenyl-ether	40	190-210	1.0010	0.29
Melt	8 - 8	170-175	1.0200	0.17
Melt	8 - 12	170-175	1.0100	0.38

* At the melt polymerization the first number indicates the polymerization time with the Ar flow on, while the second number indicates the time that a vacuum of 5mmHg was applied.

† Molar ratio.

Table 2.2

Comparison of 2,4-LCPU-6 and NM-2,4-LCPU-6.

Property *	2,4-LCPU-6 $[\eta] = 0.46$ dL/g †	NM-2,4-LCPU-6 $[\eta]_{inh} = 0.48$ dL/g
T_g	85 °C	39 °C
T_m	158 °C, 170 °C	----
$T_{m,i}$	----	56 °C
$T_{i,m}$	142 °C	53 °C
$\Delta S_{c,i}$	0.24 J/g,°C †	----
$\Delta S_{m,i}$	----	0.16 J/g,°C
$\Delta S_{i,m}$	0.15 J/g,°C †	----
Mesophase type	S_c	S_c
Repeat Length, l	59.9 ± 0.6 Å	58.9 ± 0.6 Å
Tilt Angle, β_t	32°±1°	20°±1°

* The transition temperatures correspond to 10 °C/min heating or cooling scans, while the transition entropies were calculated from annealing experiments using the plateau ΔH values.

† From ref. [8].

SYNTHESIS OF MONOMERS

A.   Synthesis of BHHBP

HO—⟨benzene⟩—⟨benzene⟩—OH   +   Excess   Cl—(CH$_2$)$_6$—OH

↓ NaOH

HO—(CH$_2$)$_6$—O—⟨benzene⟩—⟨benzene⟩—O—(CH$_2$)$_6$—OH
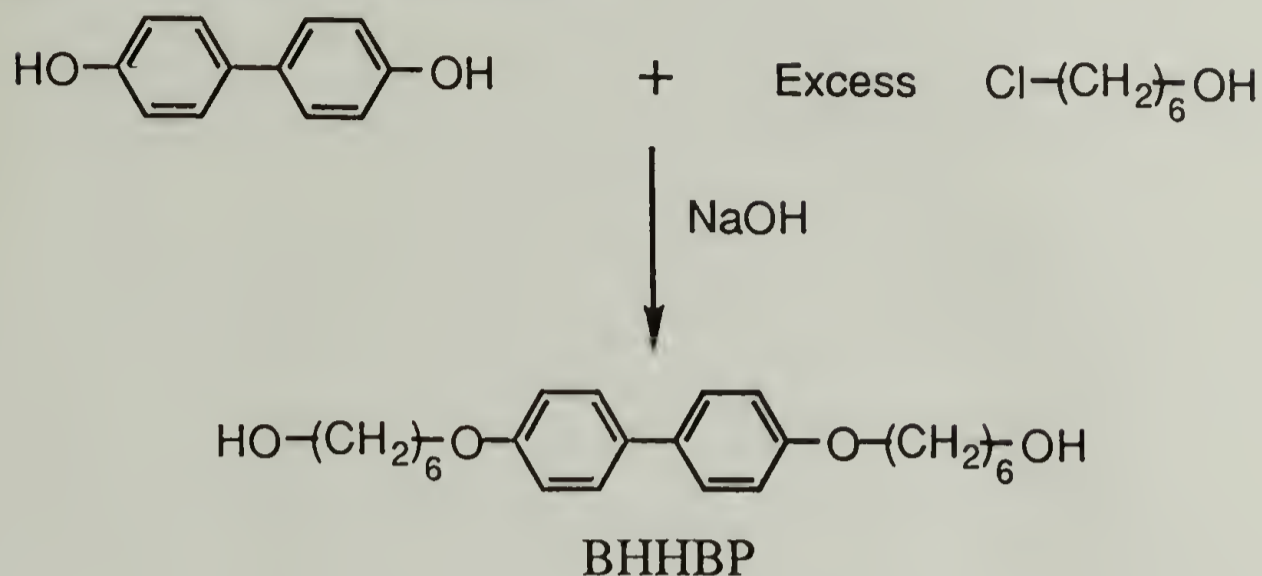
BHHBP

B. Synthesis of 2,4-TMA and 2,4-TCC

OCN—⟨benzene⟩—NCO, CH$_3$ →[1) LiAlH$_4$][2) aq. NaOH]   H—N(CH$_3$)—⟨benzene⟩—N(H$_3$C)—H, CH$_3$

2,4-TDI   2,4-TMA

+
Excess
COCl$_2$
↓

Cl—C(=O)—N(CH$_3$)—⟨benzene⟩—N(H$_3$C)—C(=O)—Cl, CH$_3$ ←[Heat][- 2 HCl]   [Cl—C(=O)—N$^+$(CH$_3$)(H)—⟨benzene⟩—N$^+$(H$_3$C)(H)—C(=O)—Cl, CH$_3$] 2 Cl$^-$
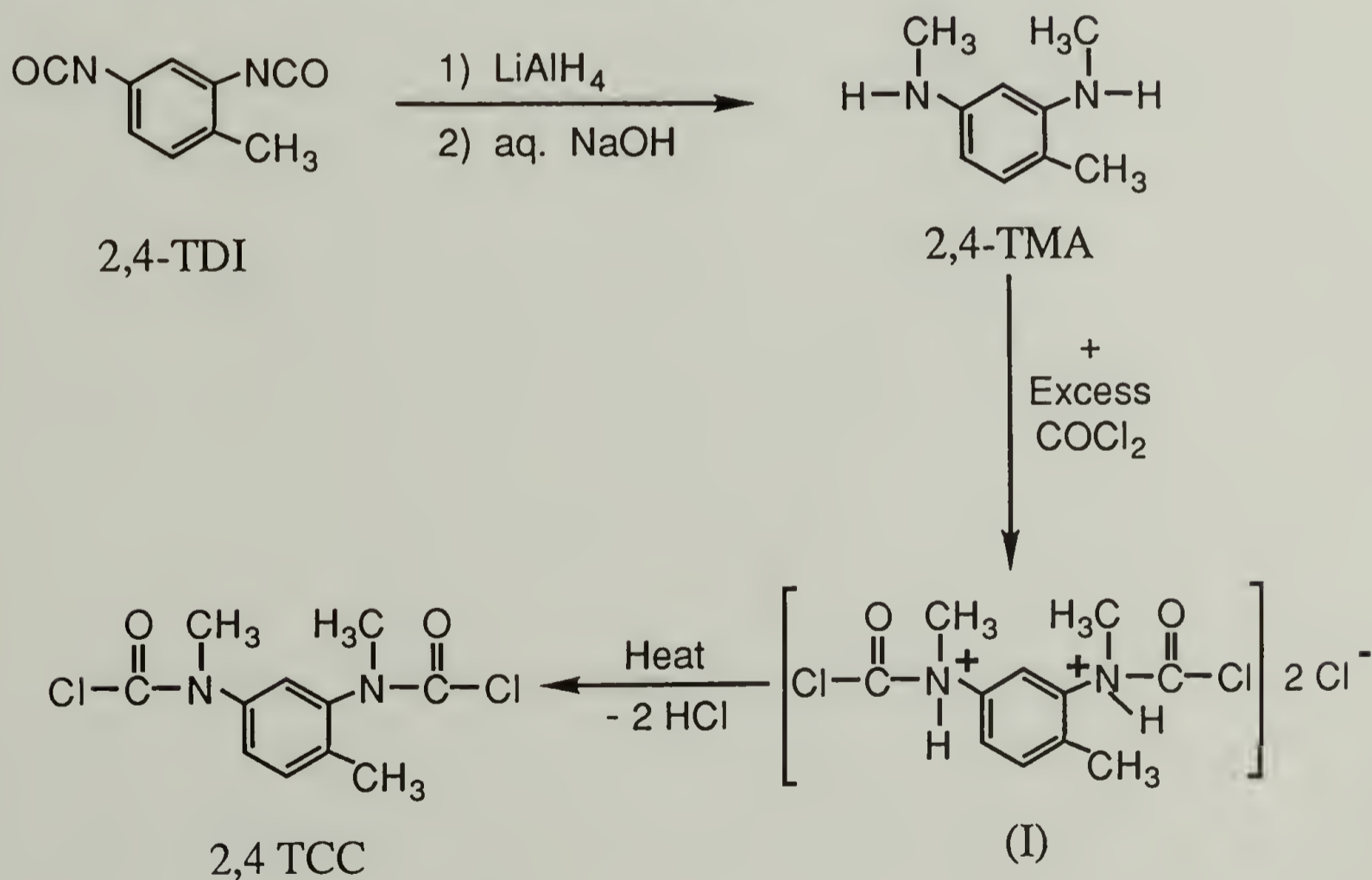
2,4 TCC   (I)

Scheme 2.1   Synthesis of monomers (BHHBP, 2,4-TMA and 2,4-TCC).

POLYMERIZATION

BHHBP

2,4 TCC

180 °C, 96 hrs, Ar flow
High boiling point solvent
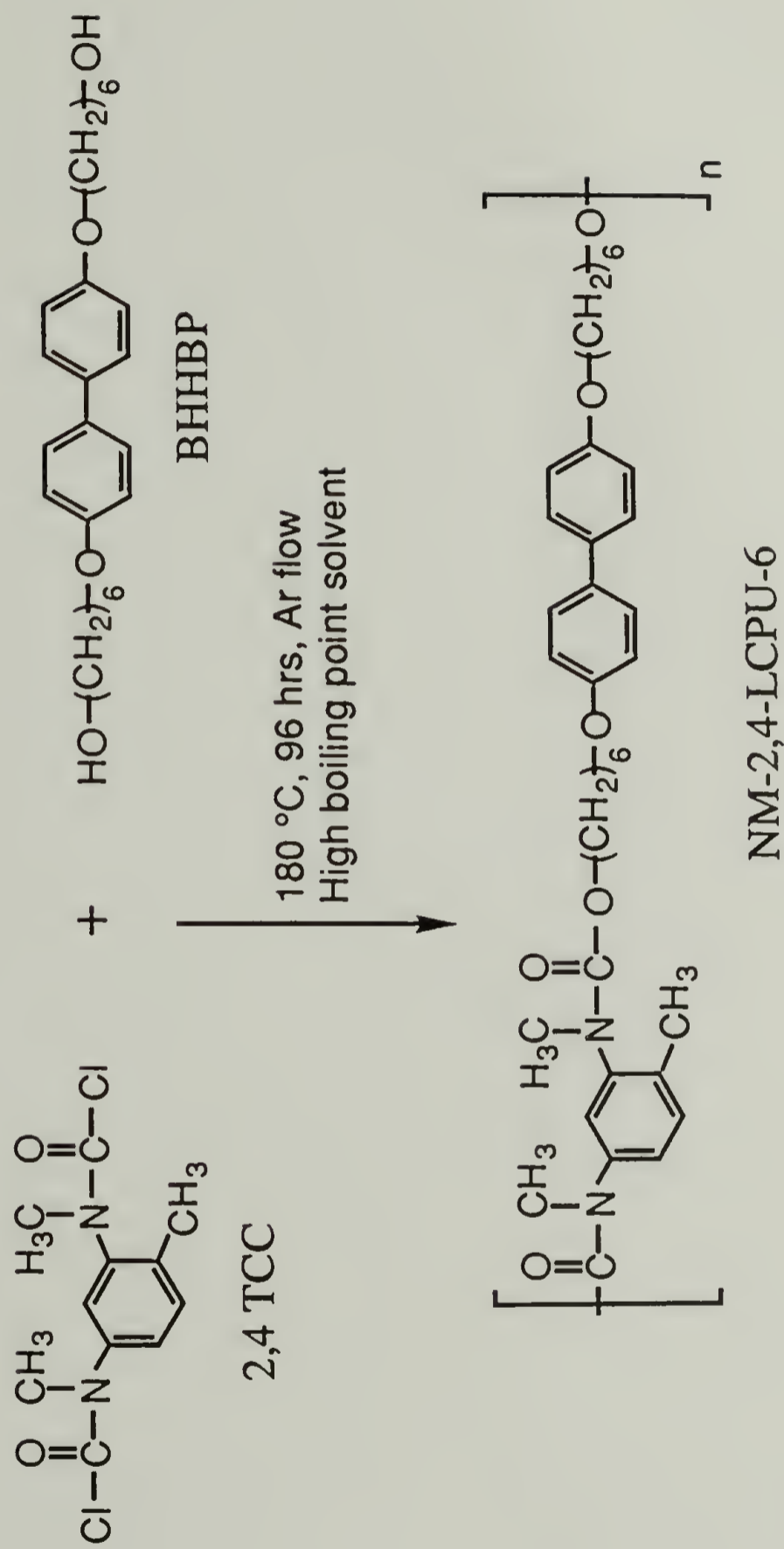
NM-2,4-LCPU-6

Scheme 2.2 Polymerization of NM-2,4-LCPU-6.

33
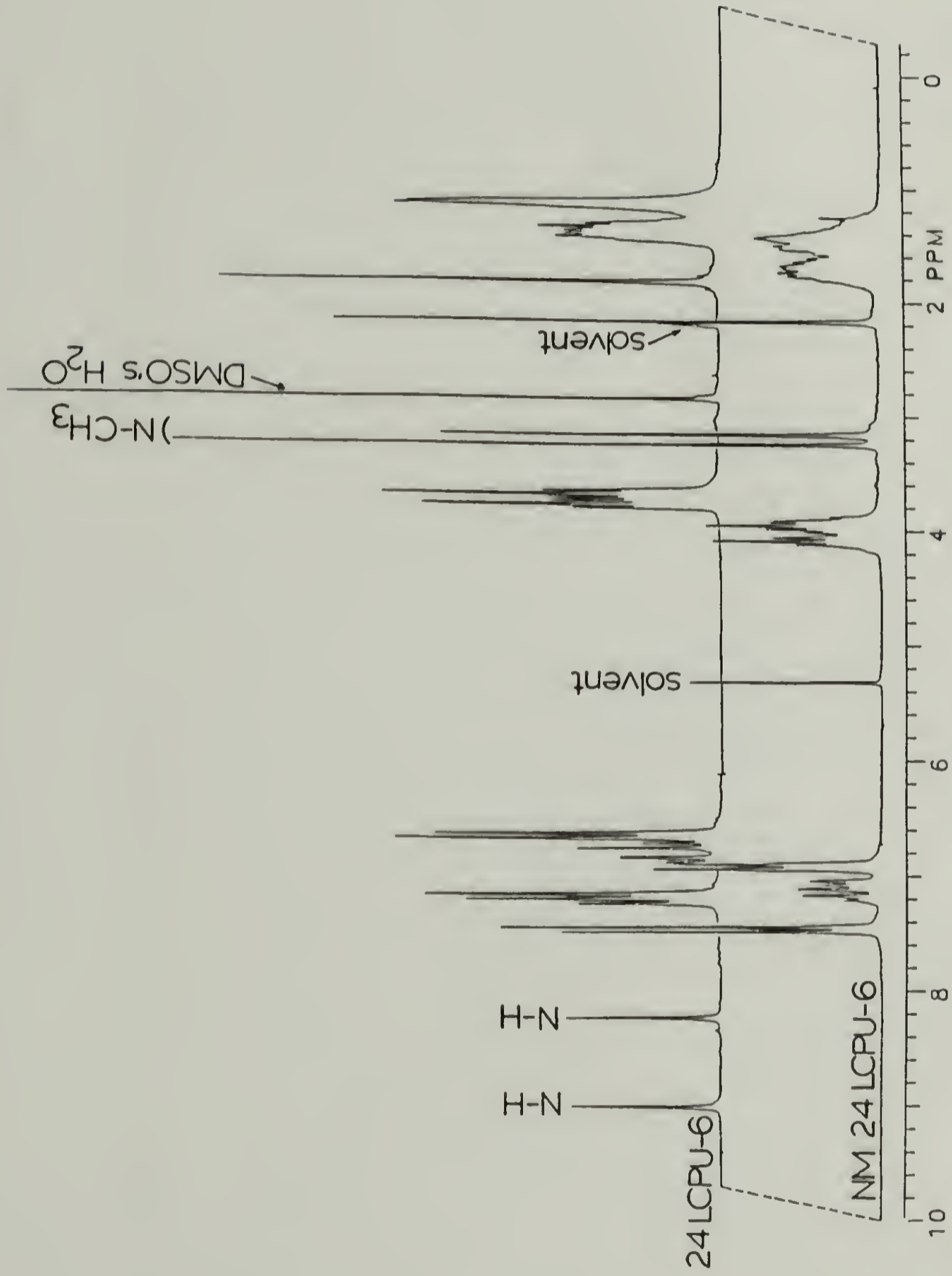
Figure 2.1 ^{1}H NMR spectra of a 5% solution of 2,4-LCPU-6 $[\eta]$=0.60 dL/g [11] in d_6-DMSO and NM-24-LCPU-6 $[\eta]_{inh}$=0.82 dL/g in CD_2Cl_2 at room temperature.
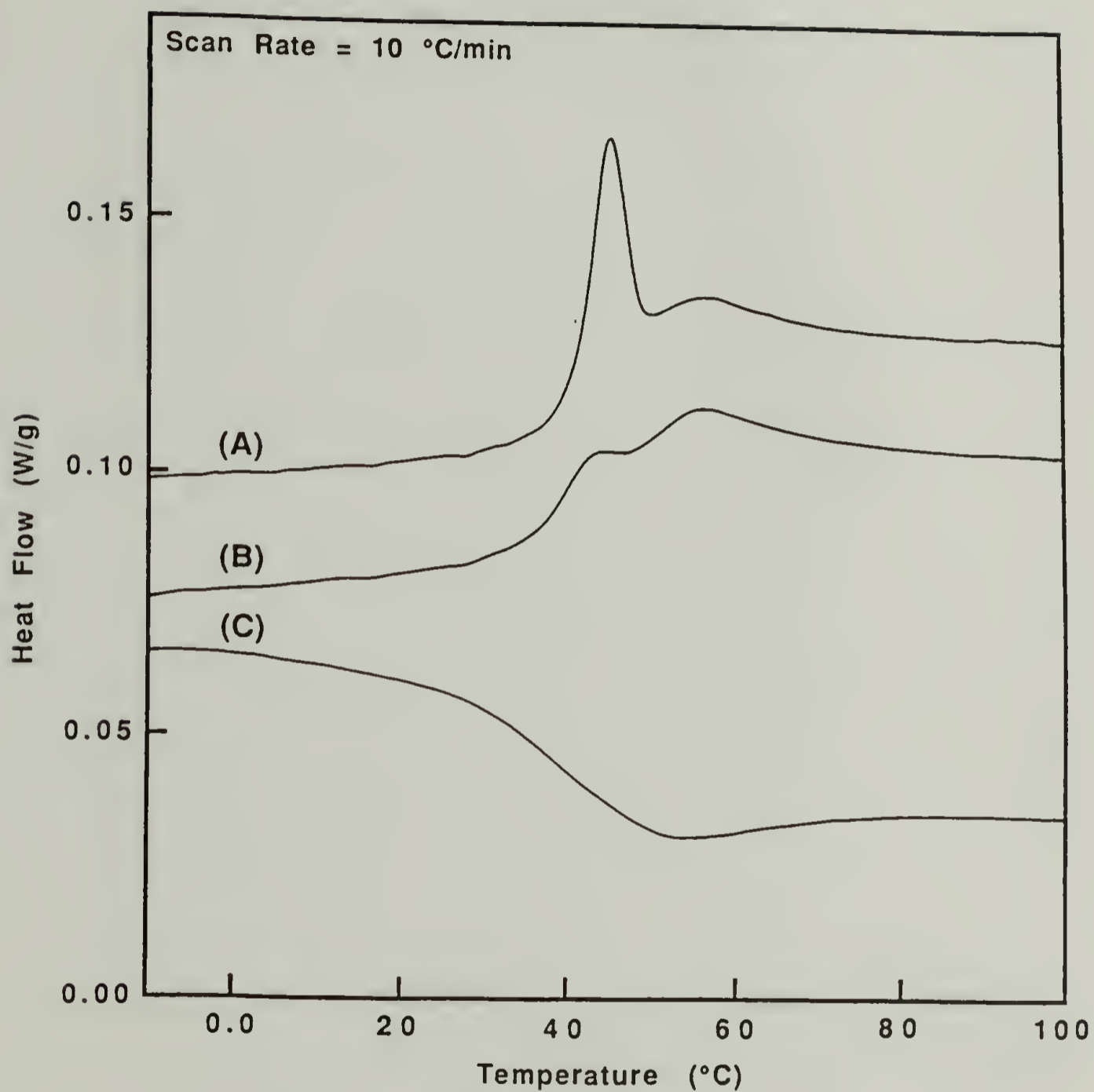
Figure 2.2 10 °C/min DSC heating (A) & (B) and cooling (C) traces of NM-24-LCPU-6 [η]inh=0.48 dL/g. (A) heating trace of a sample cooled 10 °C/min from the melt and aged around 15 minutes at room temperature, (B) heating trace of a sample cooled 10 °C/min from the melt, and maintained at -20 °C before the heating scan. See text for details.
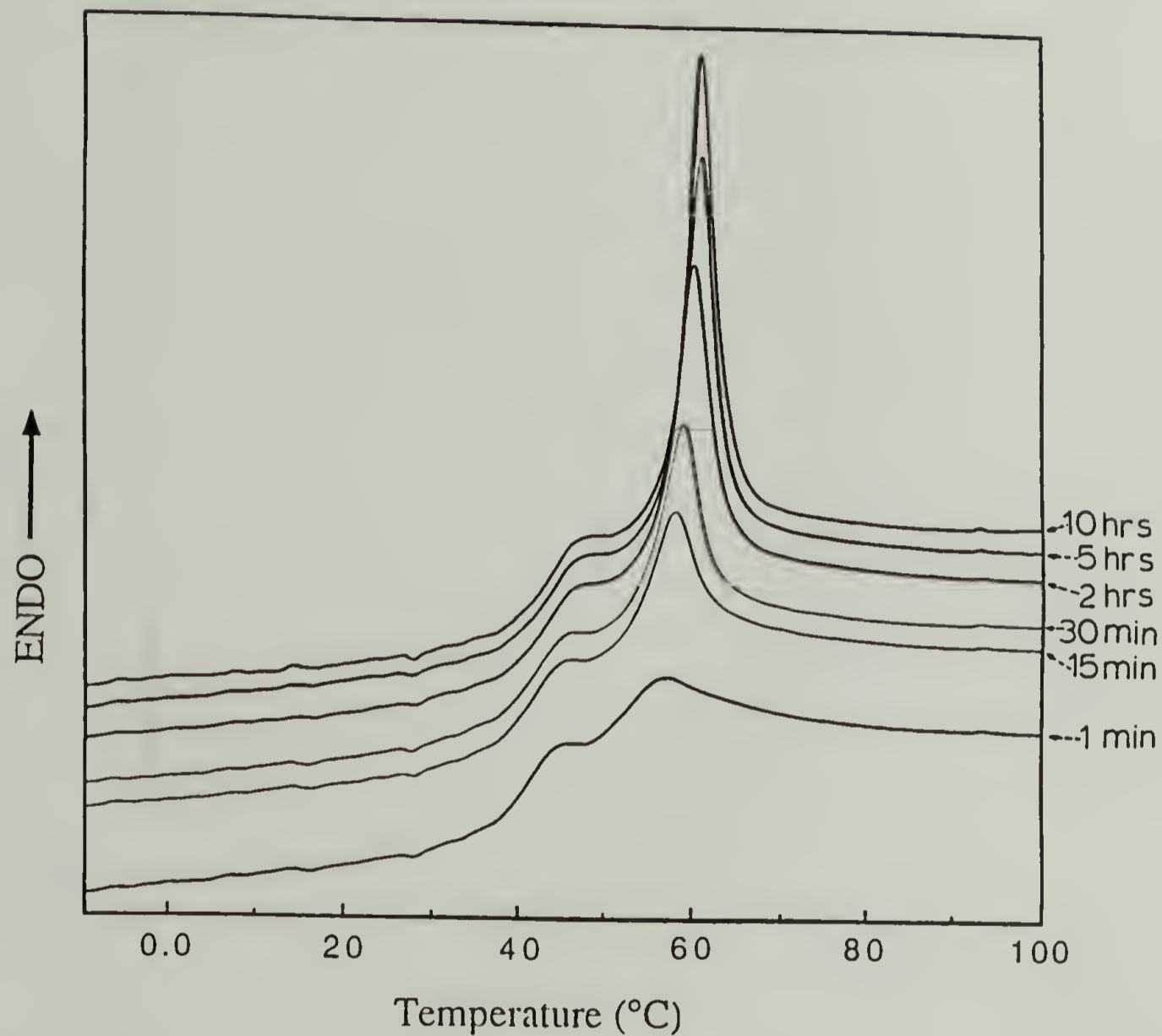
Figure 2.3 10 °C/min DSC heating traces of NM-2,4-LCPU-6 [η]inh=0.48 dL/g previously annealed at 50.0 °C for various annealing times.
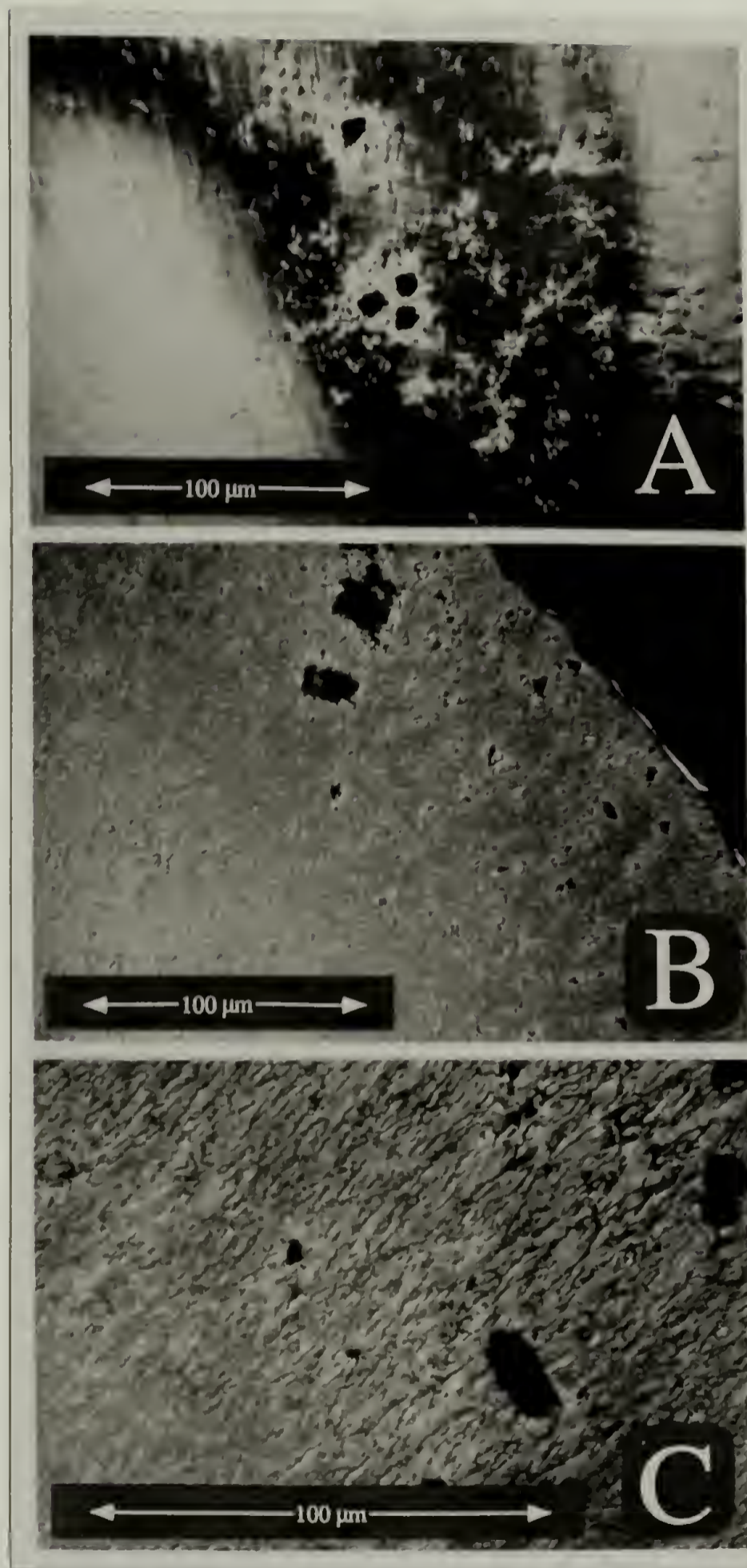
Figure 2.4 Polarized optical micrographs of NM-2,4-LCPU-6 [η]inh=0.48 dL/g displaying the evolution of a mesophase upon annealing at 50 °C. (A) after 10 minutes, (B) after 2 hours, (C) after 6 hours.
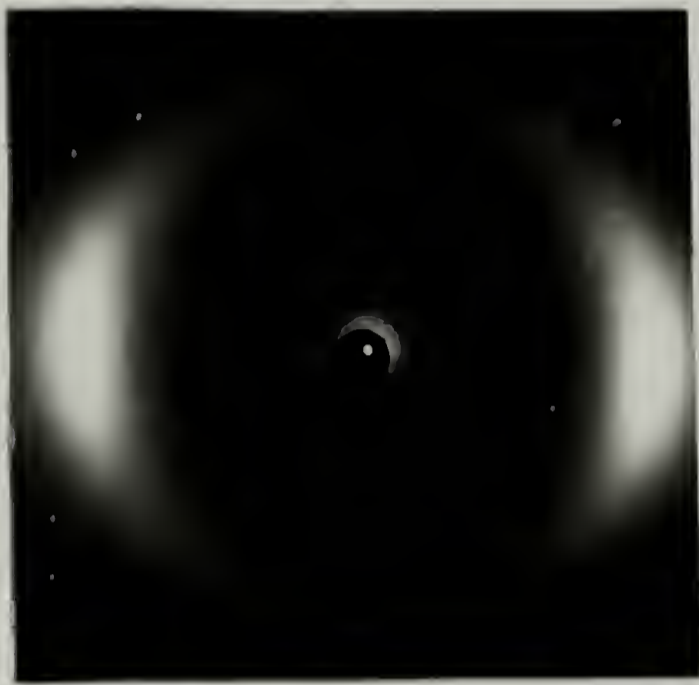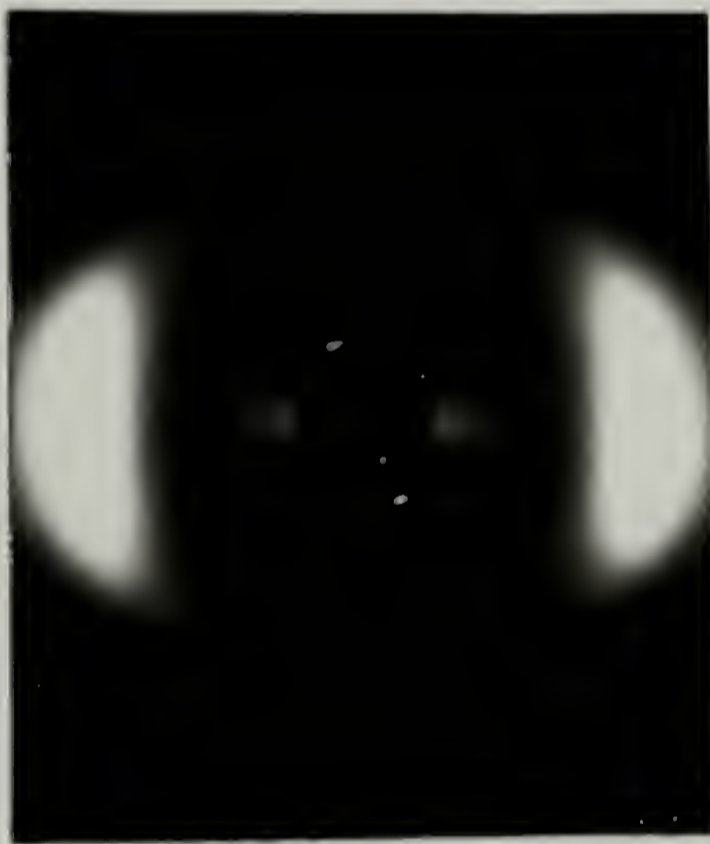
Figure 2.5 WAXS patterns of a fiber of NM-2,4-LCPU-6 $[\eta]_{inh}$=0.82 dL/g, (A) drawn from the melt and (B) annealed 2 days at 50 °C. Fiber axis is oriented vertically.
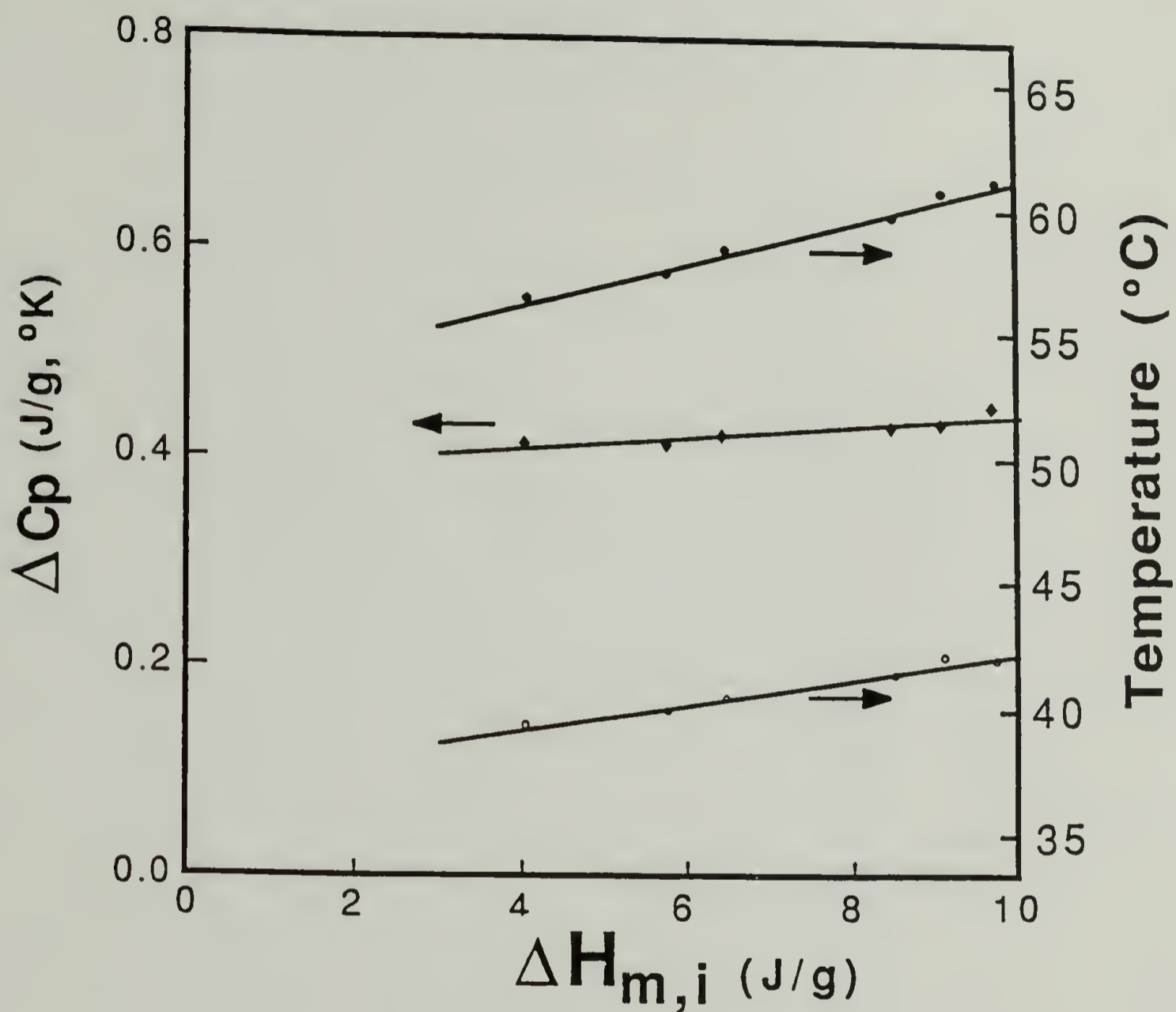
Figure 2.6 Heat capacity Δc_p (♦), clearing temperature T_i (•), and glass transition temperature T_g (o) vs mesophase-isotropic melting enthalpy ($\Delta H_{m,i}$) of NM-2,4-LCPU-6 $[\eta]_{inh}=0.48$ dL/g. Data from Figure 2.3.
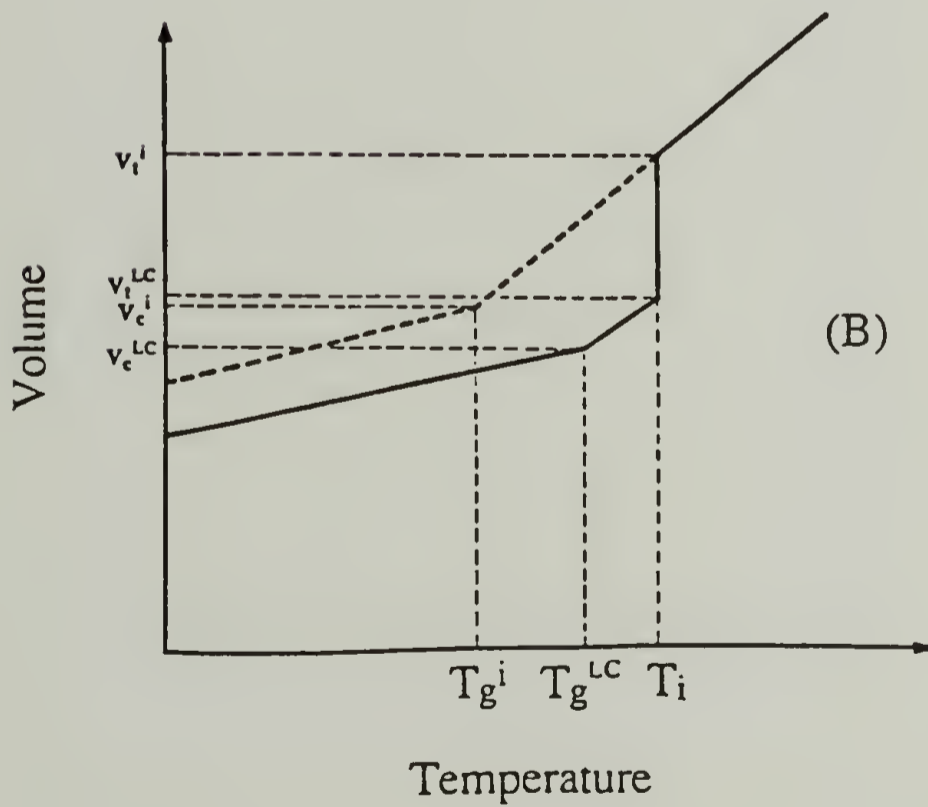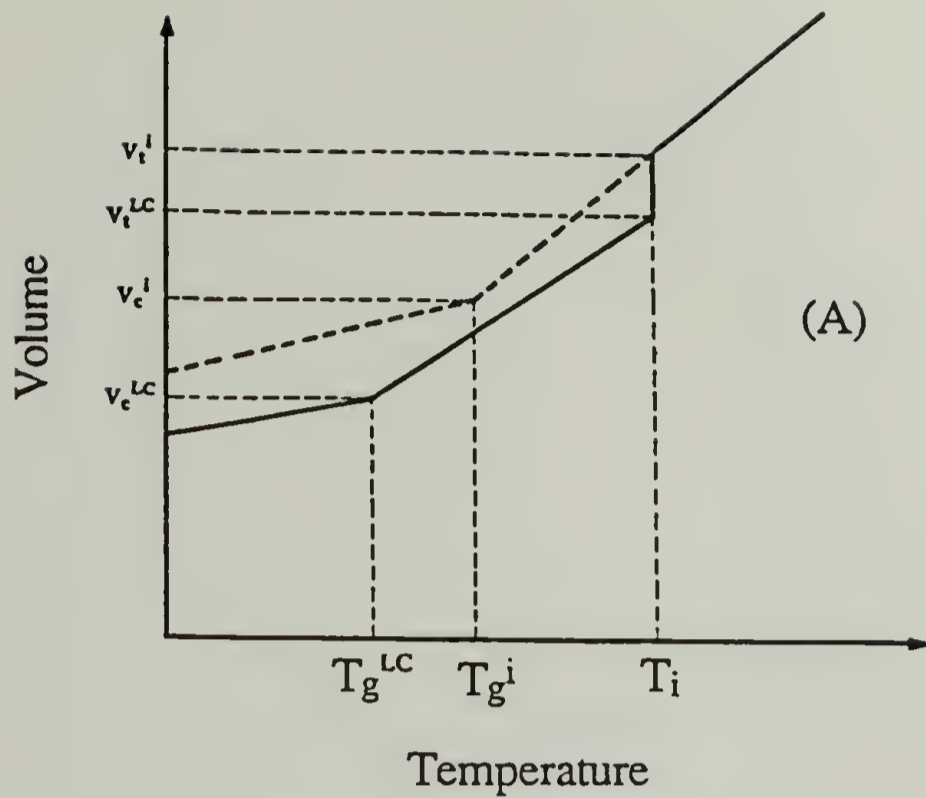
Figure 2.7 Schematic volume dependence as a function of temperature for $T_g^{LC} < T_g^i$ (A) and for $T_g^{LC} > T_g^i$ (B). See text for details.
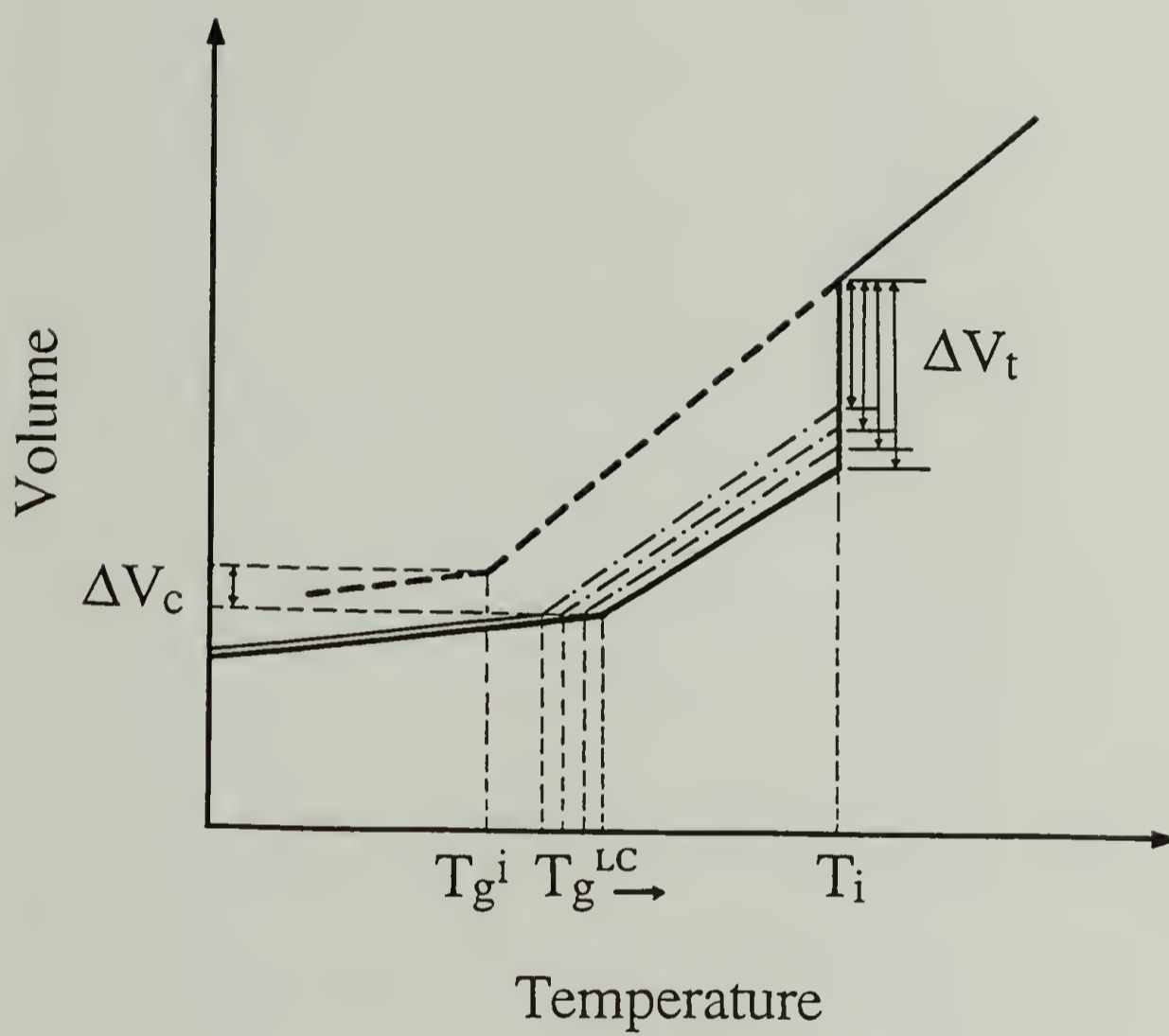
Figure 2.8   Schematic volume dependence as a function of temperature for NM-2,4-LCPU-6. See text for details.
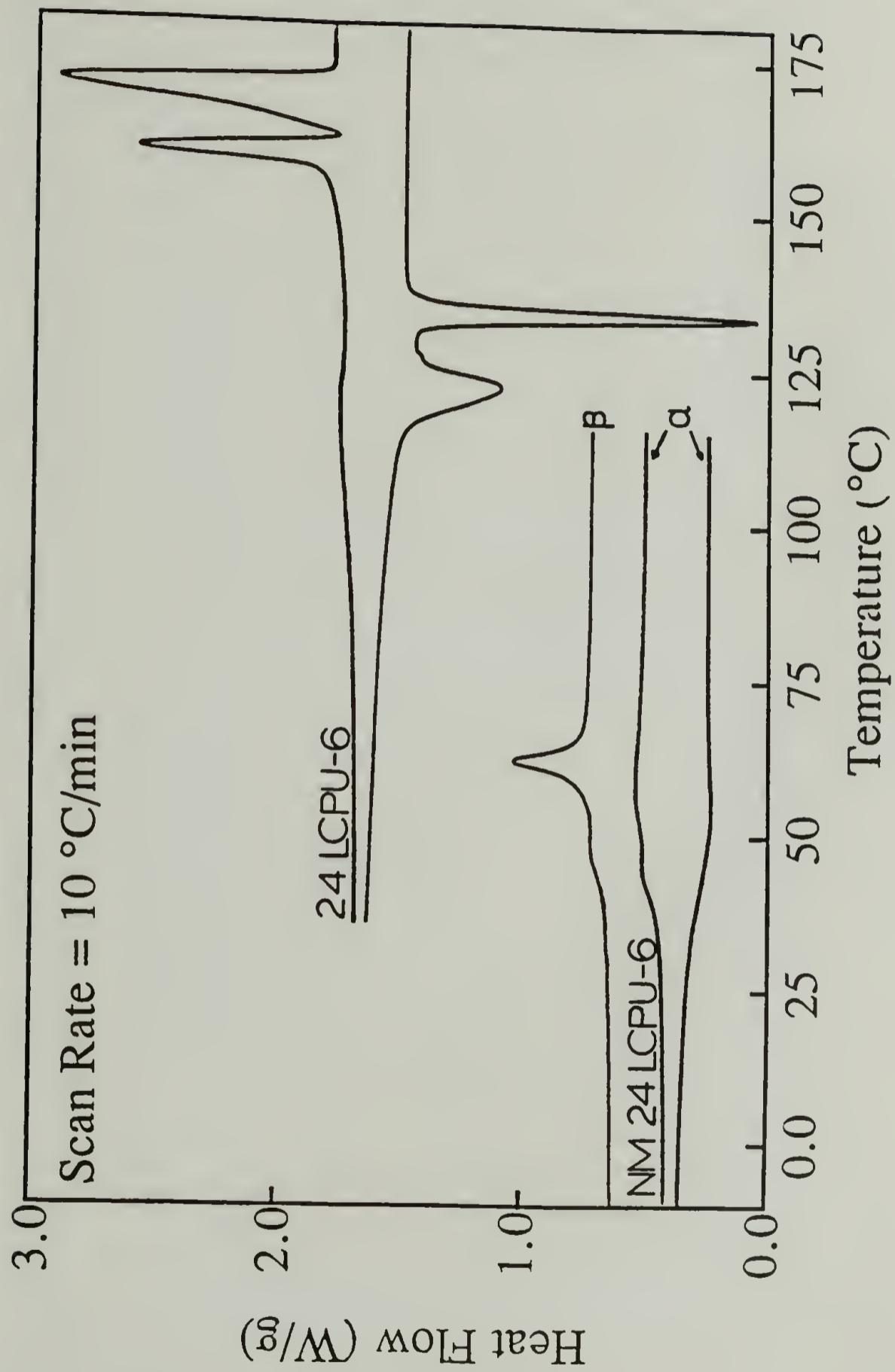
Figure 2.9 Normalized DSC heating and cooling traces of 2,4-LCPU-6 [η]=0.46 dL/g [8] and NM-2,4-LCPU-6 [η]inh=0.48 dL/g. (α) normal cyclic scan, (β) after 10 hours annealing at 50.0 °C.
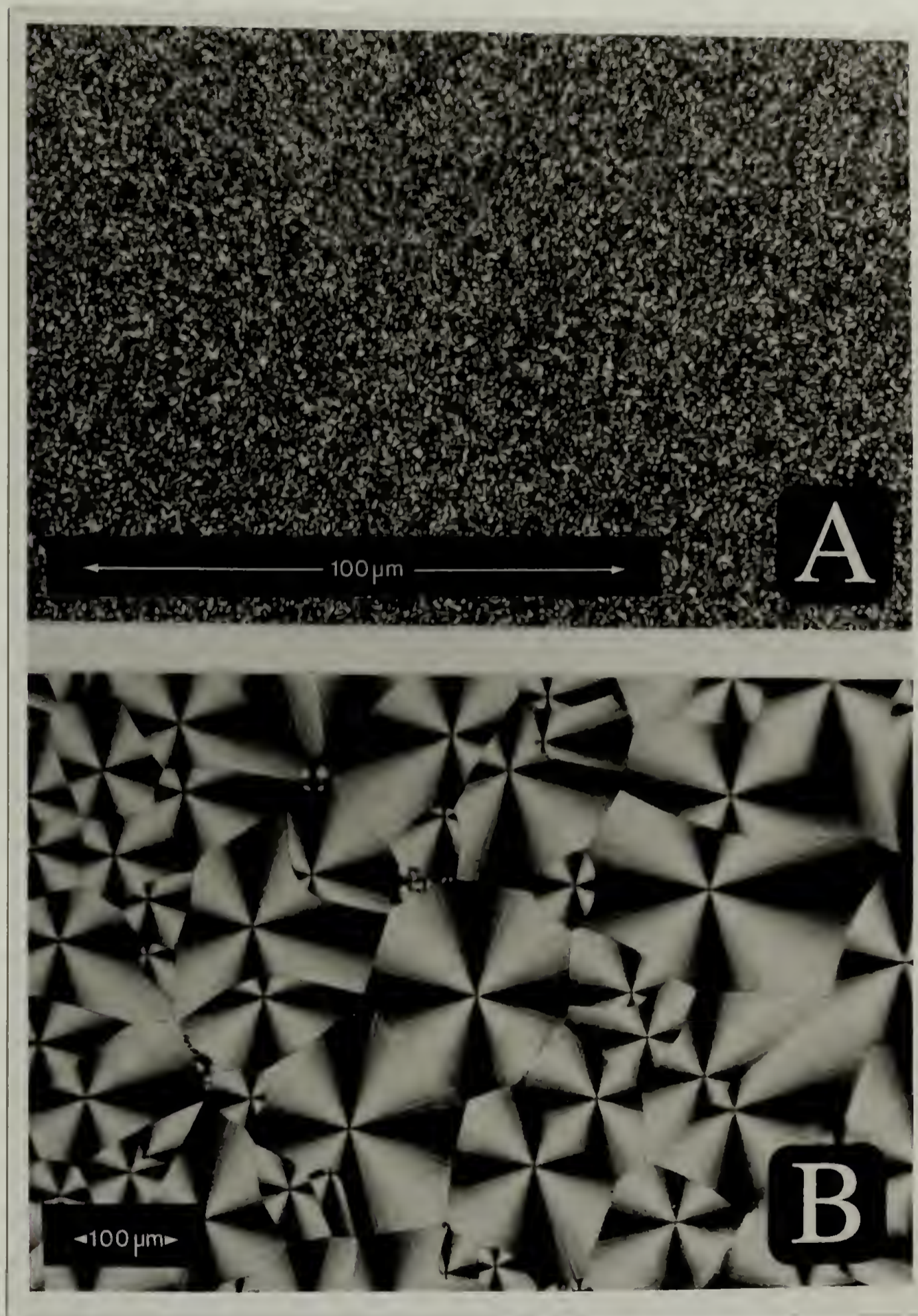
Figure 2.10   Polarized optical micrographs of 2,4-LCPU-6 [η]=0.46 dL/g displaying the threaded texture of the mesophase (A), and a highly perfected spherulitic texture of the crystalline phase (B). See text for details. Reprinted after permission of Smyth et al.[8]
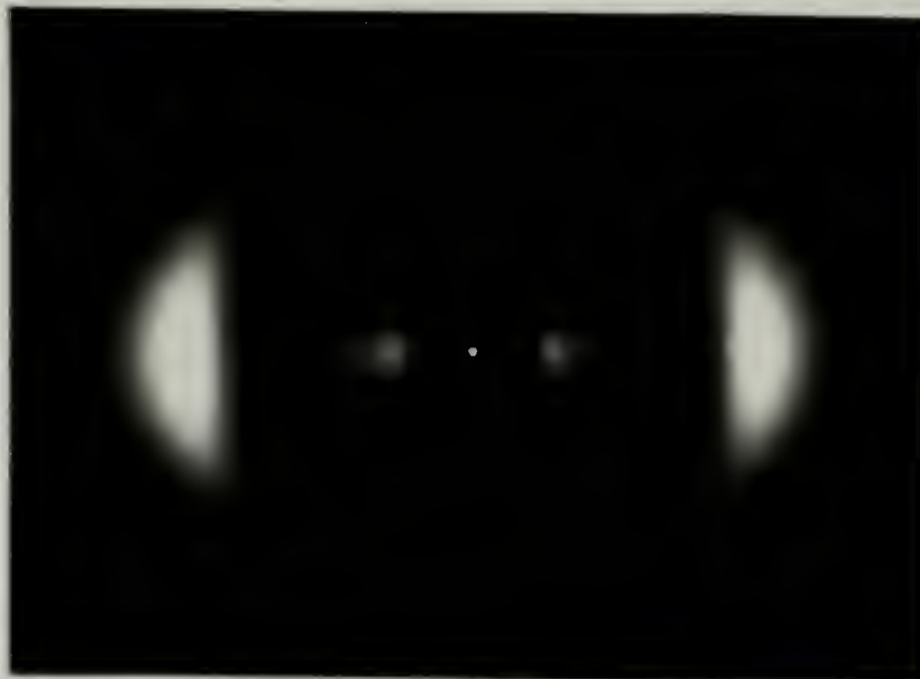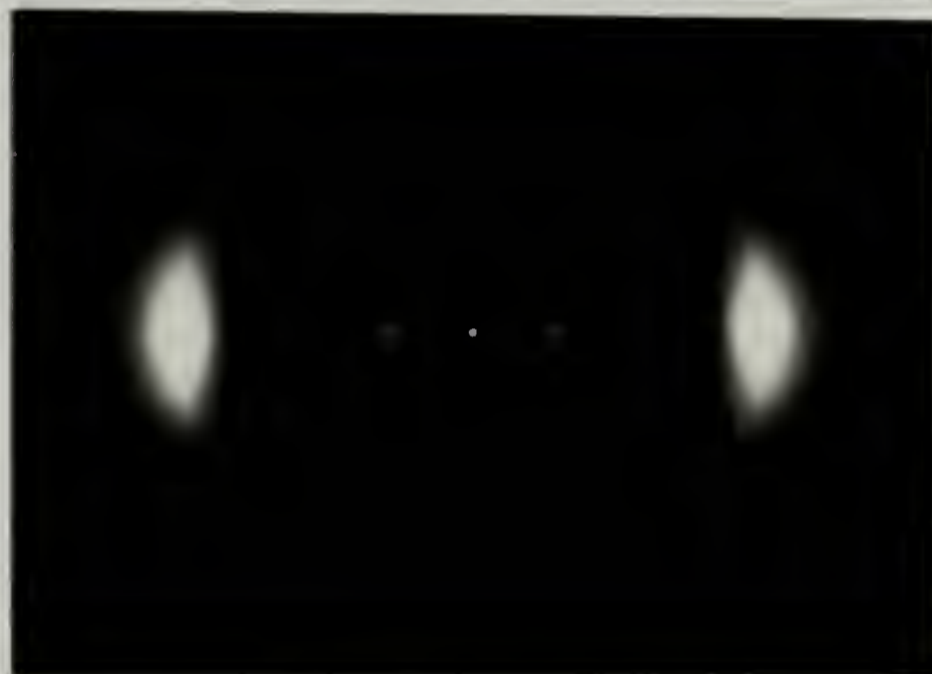
Figure 2.11 WAXS patterns of a 2,4-LCPU-6 [η]=0.60 dL/g fiber, drawn from the melt (A), soxhlet extracted in hot MeOH for 5 days (B), and annealed at 165 °C for 5 more days (C). Fiber axis is oriented vertically.

45
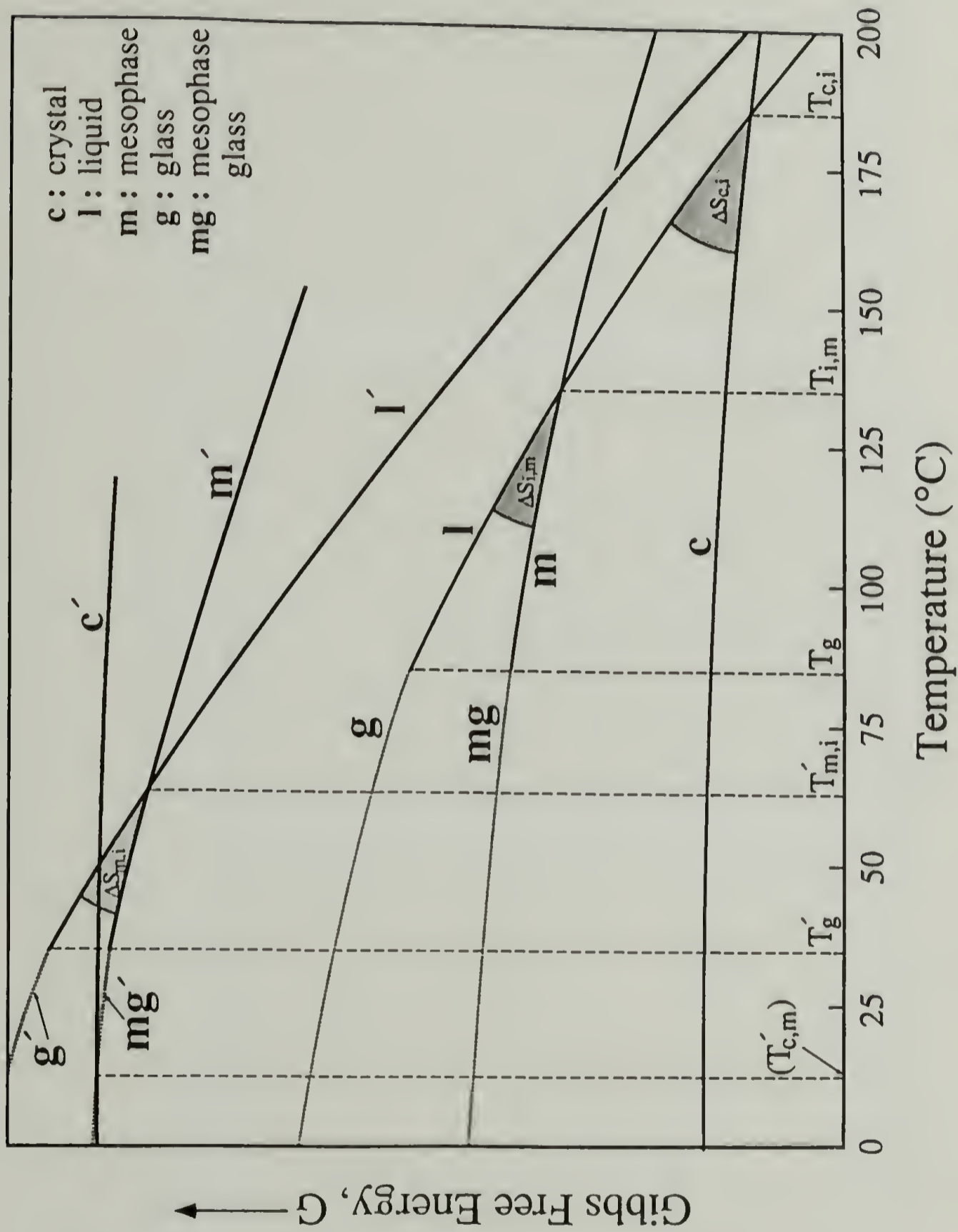
Figure 2.12   Schematic temperature dependence of Gibbs free energy for 2,4-LCPU-6 and for NM-2,4-LCPU-6 (primed). See text for details.

References

(1) Chapoy, L. L. *Recent Advances in Liquid Crystalline Polymers*; Elsevier Appl. Sci. Publ.: 1985.

(2) Brunette, C. M.; Hsu, S. L.; MacKnight, W. J. *Macromolecules* **1982**, *15*, 71.

(3) West, J. C.; Cooper, S. L. *Journal of Polymer Science* **1977**, *Polymer Symposium 60*, 127.

(4) Seymour, R. W.; Estes, G. M.; Cooper, S. L. *Macromolecules* **1970**, *3*, 579.

(5) Christenson, C. P.; Harthcock, M. A.; Meadows, M. D.; Spell, H. L.; Hpward, W. L.; Crestwick, M. W.; Guerra, R. E.; Turner, R. B. *J. Polym. Sci., Polym. Phys.* **1986**, *24*, 1401.

(6) Koberstein, J. T.; Gancarz, I.; Clark, T. C. *J. Polym. Sci., Polym. Phys.* **1986**, *24*, 2487.

(7) Coleman, M. M.; Lee, K. H.; Skrovanek, D. J.; Painter, P. C. *Macromolecules* **1986**, *19*, 2149.

(8) Smyth, G.; Valles, E. M.; Pollack, S. K.; Grebowicz, J.; Stenhouse, P. J.; Hsu, S. L.; MacKnight, W. J. *Macromolecules* **1990**, *23*, 3389.

(9) Pollack, S. K.; Shen, D. Y.; Hsu, S. L.; Wang, Q.; Stidham, H. D. *Macromolecules* **1989**, *22*, 551.

(10) Shen, D. Y.; Pollack, S. K.; Hsu, S. L. *Macromolecules* **1989**, *22*, 2564.

(11) Stenhouse, P. J.; Valles, E. M.; Kantor, S. W.; MacKnight, W. J. *Macromolecules* **1989**, *22*, 1467.

(12) Blumstein, R. B.; Blumstein, A. *Mol. Cryst. Liq. Cryst.* **1988**, *165*, 361.

(13) MacKnight, W. J.; Yang, M. *Journal of Polymer Science, Symposium Series* **1973**, *42*, 817.

(14) Reck, B.; Ringsdorf, H. *Makromol. Chem., Rapid Commun.* **1985**, *6*, 291.

(15) Zentel, R.; Reckert, G. *MaKromol. Chem.* **1986**, *187*, 1915.

(16) Bualek, S.; Zentel, R. *Makromol. Chem.* **1988**, *189*, 791.

(17) Sato, M.; Nakatsuchi, K.; Ohatatsu, Y. *Makromol. Chem., Rapid Commun.* **1986**, *7*, 231.

(18) Sato, M.; Nakatsuchi, K.; Ohatatsu, Y. *Makromol. Chem., Rapid Commun.* **1987**, *8*, 383.

(19) Sato, M.; Kurosawa, K.; Nakatsuchi, K.; Ohkatsu, Y. *Journal of Polymer Science: Part A: Polymer Chemistry* **1988**, *26*, 3077.

(20) Harrell, L. L. *J. Macromolecules* **1969**, *2*, 607.

(21) Sorenson, W. R.; Campbell, T. W. *Preparative methods in polymer chemistry, 2nd ed.*; New York Interscience Pub.: .

(22) Bilibin, A. Y.; Ten'kovtsev, A. V.; Piraner, O. N.; Skorokhodov, S. S. *Polymer Science U.S.S.R.* **1984**, *26*, 2882.

(23) Bilibin, A. Y.; Pashkovsky, E. E.; Tenkovtsev, A. V.; Skorokhodov, S. S. *Makromol. Chem., Rapid Commun.* **1985**, *6*, 545.

(24) Bilibin, A. Y.; Zuev, V. V.; Skorokhodov, S. S. *Makromol. Chem., Rapid Commun.* **1985**, *6*, 601.

(25) Skorokhodov, S. S.; Bilibin, A. Y. *Makromol. Chem., Makromol. Chem.* **1989**, *26*, 9.

(26) Melendez, E.; Navarro, F.; Pinol, M.; Rodriguez, J. L.; Serrano, J. L. *Mol. Cryst. Liq. Cryst.* **1988**, *155*, 83.

(27) Sato, M.; Komatsu, F.; Takeno, N.; Mukaida, K. *Makromol. Chem., Rapid Commun.* **1991**, *12*, 167.

(28) Bechtoldt, H.; Wendorff, J. H.; Zimmermann, H. J. *Makromol. Chem.* **1987**, *188*, 651.

(29) Keller, A.; Ungar, G., To be published.

(30) Percec, V.; keller, A. *Macromolecules* **1990**, *23*, 4347.

(31) Shriver, D. F.; Drezdzon, M. A. *The Manipulation of Air-Sensitive Compounds;* 2nd ed.; Wiley-Interscience Pub.: 1986.

(32) Finholt, A. E.; Anderson, C. D.; Agre, C. L. *J. Org. Chem.* **1953**, *18*, 1338.

(33) Ellzey, J., S. E.; Mack, C. H. *J. Org. Chem.* **1962**, *28*, 1600.

(34) Smith, P. A. S. *The Chemistry of Open-Chain Organic Nitrogen Compounds*; W. A. Benjamin Inc.: New York, 1965; Vol. 1.

(35) Weygand, F.; Mitgau, R. B. *Beilstein* **1955**, *88*, 301.

(36) Eckert, H.; Forster, B. *Angew. Chem. Int. Ed. Engl.* **1987**, *26*, 894.

(37) Saotome, K.; Komoto, H. *Journal of Polymer Science: Part A-1* **1967**, *5*, 107.

(38) Hwang, K. K. S.; Speckhard, T. A.; Cooper, S. L. *J. Macromol. Sci.-Phys.* **1984**, *B 23*, 153.

(39) Srichatrapimuk, V. W.; Cooper, S. L. *Journal of Macromolecular Science & Physics* **1978**, *B15*, 267.

(40) Adibi, K.; George, M. H.; Barrie, J. A. *Polymer* **1979**, *20*, 483.

(41) Babad, H.; Zeiler, A. G. *Chemical Reviews* **1973**, *73*, 75.

(42) Dyer, E.; Hammond, R. J. *Journal of Polymer Science: Part A* **1964**, *2*, 1.

(43) Yang, W. P.; Macosko, C. W.; Wellinghoff, S. T. *Polymer* **1986**, *27*, 1235.

(44) Odian, G. *Principles of Polymerization*; Wiley-Intersience Pub.: 1981.

(45) Struick, L. C. E. *Physical Aging in Amorphous Polymers and Others Materials*; Elsevier Scientific Pub. Co.: New York, 1978.

(46) Bosma, M.; Brinke, G. T.; Ellis, T. S. *Macromolecules* **1988**, *21*, 1465.

(47) Tsitsilianis, C.; Staikos, G. *Macromolecules* **1992**, *25*, 910.

(48) Demus, D.; Richter, L. *Textures of Liquid Crystals*; Verlag Chemie: Weihheim, 1978.

(49) Vries, A. D. *Journal of Molecular Liquids* **1986**, *31*, 193.

(50) Azaroff, L. V.; Schuman, C. A. *Mol. Cryst. Liq. Cryst.* **1985**, *122*, 309.

(51) Safinya, C. R.; Martinez-Miranda, L. J.; Kaplan, M.; Litster, J. D.; Birgeneau, R. J. *Phys. Rev. Lett.* **1983**, *50*, 56.

(52) McMillan, W. L. *Phys. Rev. A* **1973**, *8*, 328.

(53) Gray, G. W.; Goodby, J. W. G. *Smectic Liquid Crystals*; Leonard Hill: Philadelphia, 1984.

(54) Vries, A. D. *Mol. Cryst. Liq. Cryst.* **1985**, *131*, 131.

(55) Doucet, J. In *The Molecular Physics of Liquid Crystals*; G. R. Luckhurst and G. W. Gray, Ed.; Academic Press: 1979; pp 317-341.

(56) Cheng, S. Z. D. *Macromolecules* **1988**, *21*, 2475.

(57) Rojstaczer, S. R.; Stein, R. S. *Macromolecules* **1990**, *23*, 4863.

(58) Grebowicz, J.; Wunderlich, B. *J. Polym. Sci., Polym. Phys.* **1983**, *21*, 141.

(59) Loufakis, K.; Wunderlich, B. *J. Phys. Chem.* **1988**, *92*, 4205.

(60) Wunderlich, B. *Polymer Preprints* **1990**, *31 (1)*, 272.

(61) McGowan, C. B.; Kim, D. Y.; Blumstein, R. B. *Polymer Preprints* **1990**, *31(1)*, 261.

(62) Kim, D. Y.; Blumstein, R. B. *Polymer Preprints* **1990**, *30(2)*, 472.

(63) Blumstein, R. B.; Stickles, E. M.; Gauthier, M. M.; Blumstein, A.; Volino, F. *Macromolecules* **1984**, *17*, 177.

(64) Percec, V.; Tomazos, D.; Pugh, C. *Macromolecules* **1989**, *22*, 3259.

(65) Chen, D.; Zachmann, H. G. *Polymer*

(66) Zachmann, H. G.; Chen, D.; Nowacki, J.; Olbrich, E.; Schulze, C. In *Integration of Fundamental Polymer Science and Technology*; L. A. Kleintjents and P. J. Lemstra, Ed.; Elsevier: 1990.

(67) Smyth, G.; Pollack, S. K.; MacKnight, W. J.; Hsu, S. L. *Liquid Crystals* **1990**, *7*, 839.

(68) Van Krevelen, D. W.; Hoftyzer, P. J. *Properties of Polymers, Their Estimation and Correlation with Chemical Structure*; Elsevier Scientific Pub. Co.: Netherlands, 1976.

CHAPTER 3

PHASE BEHAVIOR DETERMINATION,

OF TDI BASED, REGULAR AND LIQUID CRYSTAL POLYURETHANES

Introduction

Thermotropic liquid crystal polyesters, polyethers, polycarbonates, etc., have been

shown to form stable liquid crystalline phases over a wide range of temperatures.

However, the liquid crystallinity of mesogen containing polyurethanes is still a subject of

debate. Previous investigation of the mesogenic polyurethane, 2,4-LCPU-6,[1] based on

2,4-LCPU-6
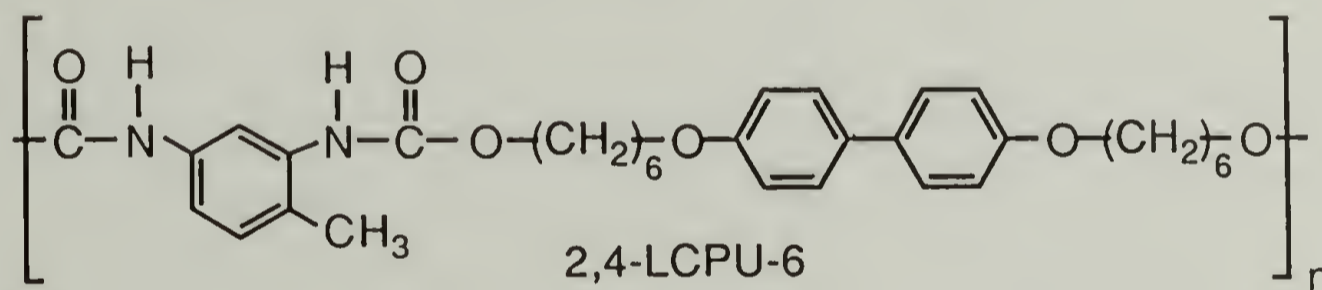
the mesogenic biphenol 4,4'-bis(6-hydroxyhexoxy)biphenyl (BHHBP) and 2,4-tolylene-

diisocyanate (2,4-TDI), has shown to be a monotropic liquid crystal.[2,3] The inherent

complexities of this system, such as H-bonding, asymmetric position of the methyl group

in the TDI moiety, biphenol moiety, etc., make the task of determining property-structure

relationships difficult. The lack of detailed structural characterization along with the

polyurethane poor thermal stability, above 200 °C,[4,5] are the principal reasons for the

uncertainties that exist.

The previous chapter of this dissertation (Chapter 2) examined in details the effect

of the H-bond on the mesophase morphology of 2,4-LCPU-6. This Chapter aims to

establish the effect of biphenol and TDI's methyl group positioning upon the structure and

phase behavior of regular and mesogenic containing polyurethanes. It describes the synthesis, thermal analysis, optical microscopy, and wide-angle X-ray scattering (WAXS) of two BHHBP based mesogenic polyurethanes designated as 2,6-LCPU-6 and

2,6-LCPU-6
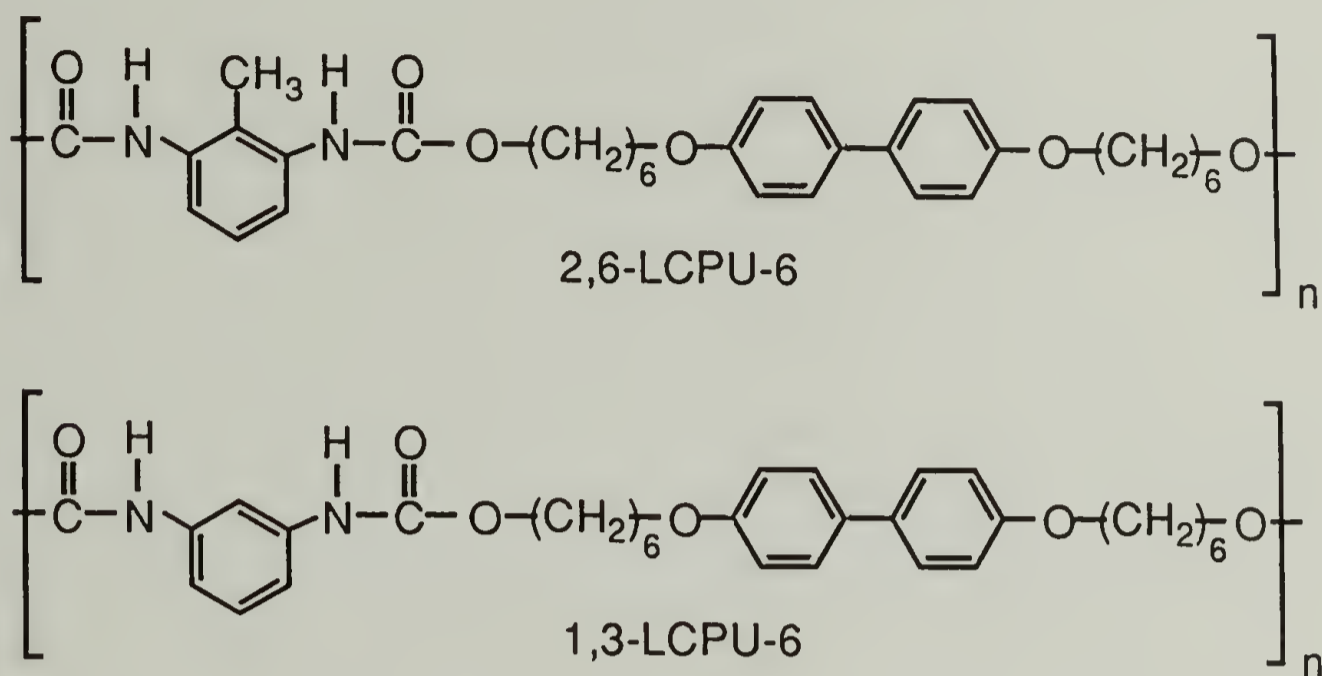
1,3-LCPU-6

1,3-LCPU-6. The symmetrically placed methyl group in the 2,6-tolylenediisocyanate (2,6-TDI) as well as the lack of the methyl group in the 1,3-phenylene diisocyanate afford a comparison between their phase behavior and that of 2,4-LCPU-6. As will become apparent in the discussion, the randomly substituted methyl group along the polymer chain of 2,4-LCPU-6 leads to a lowering of the transition temperatures and the "partial" stabilization of the mesophase relative to the crystal phase. However the asymmetrical methyl group complicates substantially the molecular modeling and crystallographic analysis. Fortunately the transition temperatures of 2,6-LCPU-6 and 1,3-LCPU-6 are within the acceptable limits of polyurethane thermal stability.[4,5]

In order to obtain a molecular understanding of the structure and phase transitions of BHHBP mesogenic polyurethanes it is necessary to assess the role of mesogen as well. For this purpose, we will also examine the phase behavior of regular type polyurethanes based on similar diisocyanate moieties and α,ω-hexanediol. These regular polyurethanes (PU) are designated as 2,6-PU-6, 1,3-PU-6, and 2,4-PU-6 (see Scheme 3.1 for their chemical structure).

Experimental

Materials. All chemicals were obtained from Aldrich, except for 2,4-TDI which was obtained from Fluka. The reaction solvents were dried and distilled before their use, and recrystallization solvents were stored previously over activated 3-4 Å molecular sieves. Prepurified Ar and N_2 inert gases were previously passed over BTS catalyst (O_2 scavenger)[6] and $CaCl_2$ desiccant. N,N-dimethylformamide (DMF) was stirred over BaO for 2 days, at room temperature, filtered with a 0.45 μm syringe filter to remove residual BaO, and vacuum distilled at ~30 mmHg and the middle portion was kept. The 2,6-TDI, 1,3-PDI, 2,4-TDI, and α,ω-hexanediol were vacuum distilled at ~0.5 mmHg and the middle portion were kept.

Synthesis of 2,6-LCPU-6 and 1,3-LCPU-6. The synthesis of the mesogenic diol 4,4'-bis(6-hydroxyhexoxy)biphenyl (BHHBP) has been reported in Chapter 2. Here we report the ^1H NMR data of BHHBP. ^1H NMR (DMF d_7) (reported as follows: chemical shift*, multiplicity, integration, assignment in Figure 3.1): δ 7.94/7.91 (d, 4 H, a), 7.40/7.37 (d, 4 H, b), 4.74 (t, 2 H, h) 4.39 (t, 4 H, g), 3.84 (t, 4H, c) 2.16 (p, 4 H, f), 1.97-1.56 (m, 12 H, e + d).

The 2,6-LCPU-6 polyurethane was synthesized by the reaction of BHHBP and 2,6 TDI (Scheme 3.2). A slight excess (0.3-0.7 mol %) of 2,6-TDI was used to compensate for side reactions involving isocyanate groups. The reaction was run on several scales, ranging from 3 to 20 g. Higher molecular weights were obtained in the larger scale polymerization, probably because the influence of impurities was decreased. The procedure described here is for the small-scale preparation whereas for the larger scale, which produced the highest molecular weight, the excess 2,6-TDI was 0.5 mol %.

Into a 250 ml flame-dried, three-neck, round-bottom flask fitted with a condenser, pressure equalizing dropping funnel, inert gas inlet, and magnetic stirrer, were added

---

* Both chemical shifts of doublets are reported, separated by a "/".
Only the middle peak, chemical shift of triplets or pentates is reported.
Chemical shifts of multiplets are reported from the higher to lower, separated by "-".

4.8035 g (12.428 mmol) of BHHBP and 50 ml freshly distilled DMF. Purified Ar was bubbled through the solution for 15 min, and its temperature was raised to 45 °C. Argon was kept flowing slowly through the top of the apparatus continually. Subsequently, 2.1709 g (12.465 mmol) of freshly distilled 2,6-TDI (0.3 mol % excess) and 30 ml of DMF were added slowly. The temperature was raised slowly to 85 °C and held there for 20 h. As the reaction proceeded, 20 ml more of DMF was added to keep the solution viscosity low enough to allow stirring. Finally the reaction temperature was raised to 95 °C, held there for an additional 12 more h and cooled to 45 °C. The warm, viscous solution was poured into cold filtered MeOH to precipitate the polymer in the form of white, fibrous material. The polymer was filtered, Soxhlet extracted in hot MeOH, and vacuum dried to give 6.6 g of 2,6-LCPU-6 (yield 94.3 %), $[\eta]=0.400$ dL/g in HFIP at 30.0 °C. ^{1}H NMR (DMSO-d$_6$) (reported in order, as follows: chemical shift, multiplicity, integration, assignment in Figure 3.1): δ 8.88 (s, 2 H, h), 7.50/7.47 (d, 4 H, a), 7.09 (s, 3 H, j + k), 6.96/6.93 (d, 4 H, b), 4.03 (t, 4 H, g), 3.95 (t, 4 H, c), 2.02 (s, 3 H, i), 1.75-1.65 (broad s, 4 H, f), 1.65-1.55 (broad s, 4 H, d), 1.5-1.3 (broad s, 8 H, e). Elemental analysis; Calculated for C$_{33}$H$_{40}$N$_2$O$_6$: C, 70.69% ; H, 7.19% ; N, 5.00%. Found: C, 70.68% ; H, 7.30% ; N, 4.95%.

The 1,3-LCPU-6 synthesis was similar to that of 2,6-LCPU-6, whereas 1,3-PDI was used instead of 2,6-TDI. A slight excess (0.3-0.7 mol %) of 1,3-PDI was also employed in order to used to compensate for side reactions involving isocyanate groups. From the polymerization of 0.95245 g (5.9480 mmol) of freshly distilled 1,3-PDI with 2.2921 g (5.9301 mmol) BHHBP (0.3 mol % excess), 3.15 g of 1,3-LCPU-6 were produced (yield 97.2 %), $[\eta]=0.402$ dL/g in DMF at 30.0 °C. Elemental analysis; Calculated for C$_{32}$H$_{38}$N$_2$O$_6$: C, 70.31% ; H, 7.01% ; N, 5.13%. Found: C, 70.19% ; H, 7.00% ; N, 5.13%.

Synthesis of 2,4-PU-6, 2,6-PU-6 and 1,3-PU-6. The syntheses of these regular polyurethanes were identical to that of 2,6-LCPU-6, described above. From the

polymerization of 35.658 g (0.1770 mol) of freshly distilled 2,4-TDI with 20.810 g (0.1761 mol) of freshly distilled α,ω-hexanediol (0.5 mol % excess), 53.8 g of 2,4-PU-6 were produced (yield 95.3 %), $[\eta]=0.462$ dL/g in DMF at 30.0 °C. Elemental analysis; Calculated for $C_{15}H_{20}N_2O_4$: C, 61.63% ; H, 6.90% ; N, 9.58%. Found: C, 61.55% ; H, 7.02% ; N, 9.55%.

From the polymerization of 5.0764 g (29.003 mmol) of freshly distilled 2,6-TDI with 3.4223 g (28.961 mmol) of freshly distilled α,ω-hexanediol (0.65 mol % excess), 8.06 g of 2,6-PU-6 were produced (yield 94.8 %), $[\eta]=0.433$ dL/g in DMF at 30.0 °C. Elemental analysis; Calculated for $C_{15}H_{20}N_2O_4$: C, 61.63% ; H, 6.90% ; N, 9.49%. Found: C, 61.55% ; H, 6.98% ; N, 9.47%.

The polymerization of 3.0331 g (18.941 mmol) of freshly distilled 1,3-PDI with 2.2272 g (18.847 mmol) of freshly distilled α,ω-hexanediol (0.5 mol % excess), yielded 4.90 g of 1,3-PU-6 (yield 93.1 %), $[\eta]=0.501$ dL/g in DMF at 30.0 °C. Elemental analysis; Calculated for $C_{14}H_{18}N_2O_4$: C, 60.42% ; H, 6.52% ; N, 10.07%. Found: C, 60.28% ; H, 6.59% ; N, 9.98%.

Characterization Techniques. In the case of 2,6-LCPU-6, intrinsic viscosities were determined in 1,1,1,3,3,3-hexafluoro-2-propanol 99+% (HFIP; Aldrich) at 30.0 °C and in DMF at 70.0 °C, using a Cannon-Ubbelohde viscometer. Elevated temperatures were employed to ensure complete solubilization. For the rest of regular and mesogenic polyurethanes, intrinsic viscosities were determined in DMF at 70.0 °C.

Solution ^{1}H NMR spectra were recorded on a Varian XL-300 operating at 300 MHz in deuterated solvents. All spectra were referenced relative to the solvent chemical shifts.

Optical microscopy was performed on a Carl Zeiss Ultraphoto II polarizing microscope equipped with a Linkham Scientific Instruments TMS 90 temperature controller and a TMH 600 hot stage. The hot stage temperature was calibrated with vanillin and potassium nitrate melting point standards.

Differential scanning calorimetric (DSC) measurements were conducted with a Perkin-Elmer DSC-7, employing a 20 mL/min flow of dry nitrogen as a purge gas for the sample and reference cells. The coolant was ice-water except for the case of the rapid cooling experiments where chopped dry ice was employed. The temperature and power ordinates of the DSC were calibrated with respect to the known melting point and heat of fusion of a high-purity indium standard. Long-term annealing was performed under nitrogen or vacuum to ensure the absence of oxidative thermal degradation.

Room-temperature X-ray diffraction patterns were recorded on flat films with a Statton X-ray camera using Ni filtered Cu Kα radiation. The samples, free-standing fibers, or contained in 1.5 mm Lindemann glass tubes, were mounted directly on the pinhole with the help of a double-stick tape. The X-ray camera length was calibrated with the 2.319-Å diffraction line of NaF and 3.035-Å diffraction line of $CaCO_3$ for the wide-angle range, while for the intermediate angle range, the layer diffraction lines of the monoclinic form of n-hexatriacontane, n-$C_{36}H_{74}$[7] was used. The films were measured for interplanar spacing data with a Supper circular film measuring device. Well-oriented samples were produced by drawing fibers out of the melt, with a pair of tweezers. Free-standing fibers were exposed to thermal and Soxhlet treatment in MeOH, while a weight of 0.5—3 g was attached to their ends in order to prevent shrinkage. No significant elongation was observed after the end of each treatment.

Results and Discussion

Characterization of 2,6-LCPU-6. Molecular Weight Characterization: The 2,6-LCPU-6 is soluble in polar aprotic solvents such as DMF, DMAC, DMSO, etc., only at elevated temperatures (above 70 °C). Hexafluoro-isopropanol (HFIP) was found capable of solubilizing 2,6-LCPU-6 at room temperature, without significant molecular weight degradation. Intrinsic viscosity measurements were performed in HFIP (at 30.0 °C) as well as in DMF (at 70 °C). In the present study two samples of 2,6-LCPU-6 were

employed. The polymer referred to as low molecular weight was determined to have an intrinsic viscosity of 0.400 dL/g and the polymer referred to as high molecular weight had an intrinsic viscosity of 0.882 dL/g. From the intrinsic viscosity measurements it is apparent that a reasonably high degree of polymerization has been achieved for the $[\eta] = 0.882$ dL/g sample.

Differential Scanning Calorimetry: Typical 10 °C/min heating and cooling traces of 2,6-LCPU-6 are illustrated in Figure 3.2.

For the low molecular weight polymer (Figure 3.2A), upon heating, a weak step in heat capacity corresponding to the glass transition (T_g) is observed at approximately 65-85 °C. This is followed by a broad shallow exotherm, typical of "cold crystallization", with a peak at ~160 °C. This region of exothermic behavior is typically more intense on the first heating scan than subsequently. In addition, a strong endotherm with a peak at 190 °C, followed by a weaker one with a peak at 197 °C, is also observed. The overall ΔH_m from 139 °C to 209 °C is 42.0 ± 0.5 J/g. Upon cooling, a sharp exotherm around 158 °C followed by a 25 °C exothermic "tail" is observed. The overall ΔH_c from 126 to 166 °C is 41.6 ± 0.5 J/g.

For the high molecular weight polymer (Figure 3.2B), upon heating, the T_g is observed at approximately 65-85 °C. This is also followed by a very weak cold crystallization region, with a peak at ~160 °C. Endothermic behavior similar to but slightly broader than that of the low molecular weight polymer is also observed. The strong endotherm peaks at 190 °C and the weak one at 197 °C. The overall ΔH_m from 139 °C to 209 °C is 41.4 ± 0.5 J/g. Upon cooling, the sharp exotherm is observed at 151 °C, 7 °C lower than in the low molecular weight 2,6-LCPU-6. The exothermic tail of this sharp exotherm extends for 15-20 °C, in a fashion similar to the corresponding exotherm in the low molecular weight polymer. The overall ΔH_c from 115 to 162 °C is 41.8 ± 0.5 J/g.

It is apparent that the high molecular weight sample exhibits thermal behavior which is very similar to that of the low molecular weight sample, with the exception of the sharp

exothermic peak, on the cooling scan. Particular attention was given to ensure complete isotropization of the two samples, in order to destroy residual crystallinity that might act as crystallization nuclei. This was accomplished by heating the molten samples 2 to 3 minutes at elevated temperatures (210—225 °C) before the subsequent cooling scan. In addition, moisture levels were kept very low by storing the samples in vacuum desiccators before and after successive measurements. Although the urethane bond is known to undergo a variety of reactions above 200 °C,[4,5] almost no changes were observed in the time frame of this experiment apart from a slight yellowing of the samples. Therefore the reason for this 7 °C difference in their sharp exothermic transition temperatures upon cooling must arise from the molecular weight difference which affects the mobility of the polymers and the concentration of end groups.

The monotropic liquid crystalline phase behavior of 2,4-LCPU-6 is well established.[1] The randomly substituted methyl group along the polymer chain of 2,4-LCPU-6 somewhat destabilizes the crystalline phase and makes the mesophase easier to observe. In the case of 2,6-LCPU-6, the methyl group is symmetrically placed along the polymer backbone, leading to a more stable crystal phase than in the case of 2,4-LCPU-6.[2,3] Having this model in mind, we will undertake the task of explaining most of the features of the 2,6-LCPU-6 polymer. A schematic plot of the temperature dependence of Gibbs free energy (Figure 3.3) is a convenient way to express the relative thermodynamic stability of the crystalline, liquid crystalline, and liquid phases (see Chapter 1 for details). The solid lines in Figure 3.3 represent the equilibrium temperature dependence of each phase.** Polymers in particular often exhibit marked kinetic effects in the vicinity of the equilibrium phase transitions. Supercooling is very common because of the high viscosity of such systems. In particular, polymers usually crystallize with a large degree of supercooling.[8] On the other hand, mesophase formation generally requires less supercooling.[2,3,9] Thus it is possible to observe a mesophase formation upon cooling 2,6-

---

** Note that each sample can be a composite of many individual phases.

LCPU-6 rapidly from the melt, without the occurrence of crystallinity. The accessibility of the mesophase is easily seen to be a function of the cooling rate.

Annealing at 165 °C, 5 °C higher than the peak of the shallow cold crystallization region, has proven to be an effective way to increase the crystallinity of 2,6-LCPU-6. The 10 °C/min heating traces of the high molecular weight 2,6-LCPU-6, previously annealed at 165 °C for various times, are presented in Figure 3.4. The strong endothermic peak at 190 °C is gradually transformed into a single, much sharper endotherm with a higher T_m and ΔH_m. On the other hand, the weaker endotherm at 197 °C gradually decreases in the annealing process and eventually disappears into the rising lower temperature, strong endotherm. Similar behavior is also observed for the low molecular weight sample. As will be discussed in Chapter 5, WAXS indicates the existence of only one crystal structure which is subjected to perfection and densification upon annealing. This explains the gradual shift of the 190 °C peak toward higher temperatures but does not address the nature of the 197 °C peak. Examination by means of polarizing optical microscopy reveals unambiguously the existence of two different crystalline domains with different morphologies. The two domains melt at temperatures very near to the DSC melting points and have volume ratios comparable to the DSC transition enthalpies. Previous thermal investigations[1] of 2,4-LCPU-6 also disclosed multiple endotherms on melting, which were explained similarly. The 10 °C/min DSC heating scans for two fiber samples were incorporated into Figure 3.4 to indicate the amount of crystal perfection that can be achieved by orientation and long-term annealing. The fiber annealed for 4 days shows a melting point of 208.6 °C and $\Delta H_m = 69.8$ J/g, ~1.7 times greater than the overall ΔH_m of Figure 3.2B. It is noteworthy that the 208.6 °C peak can be higher than the equilibrium melting point due to superheating phenomena.[8] Following publications will address in detail the development of crystallinity in the 2,6-LCPU-6 system.

The effect of cooling rate on the exothermic processes that occur on cooling is illustrated in Figure 3.5 for the low molecular weight 2,6-LCPU-6. Complete

isotropization was ensured by preheating the sample to 225 °C for 2 min and holding the temperature at 210 °C for an additional 1 min, before the start of the cooling scan. At the end of each cooling scan the sample was replaced with a fresh one and the old one was subjected to WAXS for further phase characterization. From Figure 3.5 it is observed that as the scanning rate is increased the main peak at 160 °C shifts to lower temperatures and broadens. In addition a smaller peak at ~133 °C is observed at the end of the exothermic tail. Table 3.1 lists the transition temperatures and enthalpies for the cooling scans of Figure 3.5. The main peak shifts to lower temperatures 3 times faster than the smaller one. From a simple deconvolution of the two peaks the enthalpy under the small peak increases at the expense of the main peak. Similar behavior has been observed for the high molecular weight 2,6-LCPU-6 as well. Before any decisive conclusion about the nature of these peaks is drawn it is necessary to take WAXS data into consideration.

X-ray Diffraction, Powder Samples: All X-ray diffraction patterns of powder samples were obtained at room temperature which is ~50 °C lower than the glass transition temperature of 2,6-LCPU-6. The desired thermal history was imposed on the samples either in a sealed DSC pan or in a temperature-controlled vacuum oven. The samples were cooled rapidly to room temperature after the heat treatment. Figure 3.6 presents the X-ray powder pattern of the low molecular weight 2,6-LCPU-6 sample, cooled at 100 °C/min from the melt to room temperature (from Figure 3.5). As will become apparent in the discussion, the eight well-defined rings of Figure 3.6 powder pattern manifest the crystalline character of this sample. Slightly better resolved X-ray powder patterns have been obtained from the other samples of Figure 3.5, which have been cooled more slowly. Similar behavior has been observed for the high molecular weight 2,6-LCPU-6 as well.

From the above DSC experiments it is obvious that these cooling rates are not sufficient to uncover the mesophase if it exists. Liquid N_2 quenching can be an effective method of providing low levels of contamination as well as cooling rates in the range of thousands of degrees per minutes. Figure 3.7 illustrates a typical 10 °C/min heating trace

59

of a high molecular weight 2,6-LCPU-6 sample quenched into liquid N_2 from the melt (225 °C). The exotherm peaking at 140 °C is the important feature in this DSC heating scan. The ΔH under this exotherm, measured from 127 to 157 °C, is 5.8 J/g, corresponding to a $\Delta S = 1.4 \times 10^{-2}$ J/g·K. In addition, the two well-separated endotherms, peaking at 189 and 197 °C, appear in the same positions as their counterparts from Figure 3.2. It is noteworthy to mention that the overall ΔH from 127 to 207 °C is 41.5 J/g, almost identical with its counterpart from Figure 3.2 (41.4 $\pm$ 0.5 J/g).

In order to characterize the 140 °C exotherm, X-ray powder patterns were taken above and below it. Figure 3.8 presents the room-temperature X-ray powder patterns of four high molecular weight 2,6-LCPU-6 DSC samples with the following thermal history. All four samples were quenched in liquid N_2 from the melt and allowed to return slowly to room temperature, where the WAXS powder pattern of sample A was obtained. Samples B and C were subjected to 10 °C/min heating scans, to 125 and 150 °C, respectively, and cooled at 100 °C/min to room temperature. Sample D was subjected to a 10 °C/min heating scan, to 165 °C, maintained isothermally at this temperature for 90 min and then cooled at 100 °C/min to room temperature. Even a brief examination of the (A) and (B) WAXS powder patterns (4—6 rings) serves to confirm their different structures as compared to those of (C) and (D) (8—12 rings). In fact the C and D patterns of Figure 3.8 are identical with the crystalline WAXS powder pattern of Figure 3.6.

The X-ray patterns of Figure 3.8A and B exhibit three inner sharp rings corresponding to the lattice spacings given in Tables 3.2 and 3.3, respectively. These three sharp reflections can be indexed, within experimental error, as even[***] orders of a 57.6 and 58.2 Å spacings respectively, indicating a strong layer ordering of biphenyls and TDI electron-rich moieties as well as a small fiber axis expansion with increase of temperature. In addition to the three sharp inner reflections, there are a few broad reflections that

---

[***] The odd order reflections are extremely weak and can be observed at highly overexposed, oriented samples. In particular, the first order reflection is the strongest of all odd order reflections and has been observed from medium small-angle X-ray scattering diffraction of fiber patterns at 54 Å.

constitute the outer part of the Figure 3.8A and B powder pattern associated with the weak intermolecular lateral ordering. The strong diffuse halo centered at a spacing of 4.5 Å followed by the well-defined outer ring at 4.0 Å indicates a higher than smectic-A or C mesophase but lower than the higher order smectics such as B, G, etc..[10]. From the powder pattern alone, we were unable to characterize the type of mesophase present. Therefore it was necessary to obtain highly oriented fiber patterns in order to assess that problem.

The slight expansion of the chain repeat (from 57.6 to 58.2 Å) and the small contraction of the well-defined outer ring (from 4.05 to 4.00 Å) implies an underlying lateral ordering process in the mesophase. The ordering is greatly enhanced above 140 °C, where the mesophase to crystal transformation occurs. This is manifested by the increase in the number of reflections at the wide angles and the smearing of the 002 and 004 as well as the disappearance of the 008 layer reflection. The crystallographic analysis[‡] of the Figure 3.8C and 3.8D powder patterns (see Tables 3.4 and 3.5) suggests that the chain repeat continues to expand at the c-axis (58.4 Å and 58.7 Å for the 3.8(C) and (D) respectively) and to contract at the a- and b-axis. After 90 min annealing at 165 °C it reaches a length 1.1 Å longer than that of the quenched mesophase.

The remarkable sharpness of the main exotherm upon cooling has drawn considerable attention during the course of this investigation (Figures 3.2 and 3.4) Even though it appears to be an isotropic to mesophase transition, X-ray analysis suggests that the final form of the sample at room temperature is crystalline. The good agreement of transition enthalpies in the 10 °C/min DSC scans of Figures 3.2, 3.5, and 3.7, along with the assumption that the same amount of 2,6-LCPU-6 is always involved in the transitions schematically depicted in Figure 3.3, can provide us with a rough understanding of the magnitude of the isotropic to mesophase transition. Figure 3.7 indicates that the mesophase to crystal transition ($\Delta H_{m-c} = 5.8$ J/g) is 12.3% relative to the crystal to

---

[‡] Discussed in detail in Chapter 5.

isotropic transition (ΔH_{c-i} = 47.3 J/g). If the above assumption is correct, the isotropic-mesophase transition must account for the remaining 87.7% (ΔH_{c-i} = 35.7 J/g), indicative of a strong order in the mesophase. We deliberately ignore the enthalpy of cold crystallization for reasons of simplicity, since its contribution is very small. These arguments along with the very small transition enthalpy under the lower temperature exotherm (~5% relative to ΔH_{c-i}, Table 3.1) contribute to the composite character of the main exotherm.

Smyth et al.[1] in their study on low molecular weight 2,4-LCPU-6, observed that the main exothermic transition shifts to higher temperatures with slower cooling rates. They presented enough arguments to support the conclusion that at low cooling rates the two-stage exothermic process (isotropic to mesophase, followed by the mesophase to crystal transition) is replaced by a single-stage exothermic process, which is remarkably sharp and narrow. Similarly in 2,6-LCPU-6, because crystallization occurs so fast and readily, a 10—50 °C/min cooling rate can be considered low. Therefore, due to its higher mobility, the low molecular weight sample crystallizes faster (7 °C higher) than the high molecular weight one. Although a single-stage exothermic process which involves crystallization of the sample explains the behavior upon cooling of the main exotherm, it fails to address the nature of the lower temperature exotherm. The stabilized mesophase from copolymers of 2,4-TDI and 2,6-TDI with BHHBP[11] indicates that the isotropic to mesophase transition occurs in the vicinity of 130 °C. With this in mind we can propose the following scenario to elucidate the lower temperature exotherm. As the cooling rate increases, there is less time left for the ordered domain to "space fill" the sample as well as to perfect itself, leaving more and more sample liquidlike. When the temperature is around 130 °C the liquidlike portions convert to mesophase.

To demonstrate even further the involvement of crystallization in the main exotherm upon cooling, we examined the 10 °C/min DSC behavior of a sample annealed at 165 °C for 4 days (Figure 3.9). Stenhouse et al.[12] observed a molecular weight dispersity of 1.42 and

1.87 for their fresh 2,4-LCPU-6 samples. Because there is very little difference in the way 2,4-LCPU-6 and 2,6-LCPU-6 were synthesized, it is reasonable to assume the polydispersity of fresh 2,6-LCPU-6 to be comparable to that of the 2,4-LCPU-6. On the other hand, the polydispersity of the sample annealed for 4 days at 165 °C is expected to be much higher than 2, due to the well-documented transurethanefication as well as other side reactions[4,5] occurring at this elevated temperature. Figure 3.9 shows, as expected, that the molecular weight distribution affects only the cooling trace (3.9b) while the second heating trace (3.9c) is virtually identical to that of Figure 3.2Bα. On the first heating we observe the sharp crystal melting endotherm at 210 °C (ΔH_m = 72.8 J/g). The first cooling trace shows a "typical" broad crystallization exotherm peaking at 150 °C (ΔH_c = 40.5 J/g), 1 °C lower than the sharp crystallization peak of Figure 3.2Bα. This "textbook" behavior of polydispersity upon crystallization[8] proves unequivocally the involvement of crystallization in the main exotherm upon cooling. On second heating, the typical cold crystallization region around 160 °C is followed by a strong endotherm peaking at 190 °C and a weaker one peaking at 197 °C ($\Delta H_{m(144-210)}$ = 40.0 J/g). This shows that very little has changed in the sample apart from the polydispersity and a 3% reduction of the crystallization transition enthalpy.

X-ray Diffraction, Oriented Samples: It is difficult to obtain well oriented samples of normal polyurethanes primarily due to their low molecular weights. Blackwell et al.[13] employed a polyurethane hard-segment-rich thermoplastic elastomer (slowly stretched in water to ~700%, and annealed for 24 h at 130 °C) in order to get the desired orientation.

The slow relaxation rate of liquid crystalline polymers is a great advantage in obtaining highly oriented samples. The maximum molecular orientation we were able to accomplish, drawing fibers of high molecular weight 2,6-LCPU-6 from the melt, is demonstrated in Figure 3.10. As shown in Figure 3.10, there are two basic features to note: (1) a series of meridional arcs, parallel with the orientation direction, that are all orders of 57.7 Å spacing; (2) a quite broad and diffuse equatorial arc, composed of two

arcs with spacing of 4.5 and 4.0 Å. These data are in qualitative agreement with the mesophasic Figure 3.8A WAXS powder pattern of 2,6-LCPU-6 quenched in liquid N_2 from the melt. Apparently the cooling rate achieved by drawing fibers from the melt and quenching them in room temperature air is fast enough to bring the sample into the mesophase. Unfortunately we can draw very few conclusions about the mesophase structure of the 2,6-LCPU-6 from this poorly oriented WAXS fiber pattern.

Frequently orientation as well as domain coarsening can be enhanced with proper thermal treatment of fibers under stress. This generally results in an increase of the phase which is stable at the annealing temperature and pressure at the expense of the other phases. The monotropic liquid crystalline nature of 2,6-LCPU-6 makes it clear that thermal treatment cannot be used to enhance the thermodynamically unstable mesophase. Obviously the task of obtaining higher orientation, with the present molecular weight sample, is equivalent to finding a way to prevent the polymer from achieving equilibrium. Plasticization with a low molecular weight compound that will provide partial mobility to allow the system to reorganize was our next attempt. Hot MeOH and room temperature 50% DMF—50% H_2O were the two systems we tried. Even though originally we were reluctant to use the above solvents due to our experience with normal polyurethanes, where they induce crystallinity, the results were unexpectedly rewarding. Soxhlet extraction (in hot methanol for 4 days) of the fibers of Figure 3.10 under 0.5—3-g tension resulted in an appreciable molecular orientation, which is shown in the WAXS fiber pattern of Figure 3.11. Similar results were also obtained from the 50% DMF—50% H_2O mixture. The removal of DMF and H_2O was ensured by washing the treated fiber in cold MeOH for 12 h and overnight vacuum drying at 60 °C. An attempt to provide a physical insight into whatever process is involved to achieve this orientation is based on the following scenario. Plasticization occurs predominantly in the small mesophase domains which are randomly oriented along the fiber due to weaker interaction with the strong elongational flow.

Deposition of the plasticized molecules on the strongly oriented larger domains thickens them, similar to crystal annealing.

Figure 3.11 exhibits the same features as Figure 3.10, but substantially more resolved. The much sharper meridional arcs are orders of 57.8 Å, only 0.1 Å larger than those of the untreated fibers. This indicates the negligible perturbation of the original structure resulting from the hot MeOH treatment. Significant resolution enhancement is observed at the wider angles. The quite broad and diffuse equatorial arc of Figure 3.10 has been split into diffuse four-point, off-equatorial wide-angle reflections centered at a spacing of 4.5 Å with intensity maxima lying between the 004 and 008 layer line spacing, and a well-defined equatorial arc centered on the 4.0 Å spacing. In addition to these wide angle reflections there is a weak and diffuse equatorial crescent, centered at 3.3 Å.

The 57.6—58.7 Å is almost twice the value reported for the chain-axis repeat (c spacing) of the related 2,4-LCPU-6.[1,12,14] This comes from the fact that previous researchers have neglected the presence of a backbone kink per monomer repeat, arising from the meta-substituted benzene ring of the 2,6-TDI, and assumed that the c spacing arises from one repeat only. Consequently the layer line spacings were assigned to 001, 002 (strong), and 004 reflections instead of to 002, 004 (strong), and 008 reflections. This explains the assignment difference of this publication relative to previous publications.[1,12,14] As will become obvious in Chapter 5, the use of a fiber repeat consisting of two monomer repeat units (dimer) related by a 2-fold screw axis is essential to obtain regular molecular sequences and packing, as well as to justify the observed reflection intensities. A centrosymmetric dimer repeat can also justify the observed intensities. Unfortunately its applicability is restricted only in the disordered mesophase rather than the ordered crystalline phase where the repulsions of TDI's methyl group (from the surrounding chains) distort the dimer repeat away from centrosymmetricity (see Chapter 5).

A dimer repeat has been repeatedly observed in the literature when the backbone of the monomer is kinked, frequently due to an odd number of atoms per monomer backbone. For example the crystalline chain-axis repeat proposed by Blackwell et al. for the 4,4'-diphenylmethane diisocyanate (MDI)—1,4-butanediol (BDO) polyurethane[15] consists of two repeat units. This arises from the odd methylene group on the center of the MDI unit which introduces a kink in its structure. Similar behavior is observed with the aromatic polyimide Kapton H (DuPont), synthesized from pyromellitic dianhydride and diaminodiphenyl ether,[16,17] where the ether oxygen introduces the kink. Polyaniline also displays similar behavior[18] with the nitrogen atom introducing the kink.

It is apparent that the mesophase under investigation is not one of the "classics" frequently encountered in liquid crystal textbooks.[10] The complex nature of the Figure 3.11 WAXS fiber pattern arises from a superposition of elements, which will be discussed extensively in Chapter 5. Currently we will present briefly the basic molecular architecture that characterizes this system. The presence of a meta substituted benzene ring (2,6-TDI) introduces a backbone distortion in the structure. Assuming a more or less extended hexamethylene spacer in BHHBP, the 57.6—58.2 Å repeat can be achieved by the introduction of a 54.0—54.5 ° tilt angle, between the planes of the TDI ring and the urethane group (see Chapter 5). This angle was determined from periodic boundary[19] energy minimization based on the Dreiding II[20] force field, conducted with the Molecular Simulations Inc., Polygraf module. The biphenol moiety orients with its plane (which contains the O···O axis) at 51° with respect to the all-trans hexamethylene plane. Based primarily on the TDI-urethane torsion angle and secondarily on the biphenyl-hexamethylene torsion angle, the fully extended 2,6-LCPU-6 dimer repeat can be over 70 Å long with only a 15% reduction in the H-bonding energy. This reduction arises primarily from the H-bonding angle (N-H···O) which for the case of 73.2 Å long repeat is ~164°. Allowing the dimer as well as its unit cell to relax, we obtain an equilibrium repeat of 57.8 Å with H-bonding angle (N-H···O) of 176°. The crystalline structure of 2,6-LCPU-6, discussed in

detail in Chapter 5, suggests the absence of gauche conformations in the hexamethylene spacer. On the basis of this result, and from the high-order mesophase structure with repeat length only 0.2—0.5 Å shorter than the crystalline repeat, the existence of gauche conformations in the "perfected" mesophase structure is unlikely but not completely ruled out.

A schematic representation of the mesophase of 2,6-LCPU-6 is illustrated in Figure 3.12. Biphenyls and 2,6-TDI moieties form alternative electron-dense layers perpendicular to the fiber axis. These layers along with the 2_1 screw axis symmetry-element, result in only the even meridional reflections (00l: l = 2n) to be observed. The strong 004 meridional reflection can be explained by a mirror reflection symmetry element perpendicular to the 2,6-TDI ring and the fact that the BHHBP portions lie in the 014 plane (see Chapter 5).[21,22] Similarly the crystal structure of MDI–BDO polyurethane reported by Blackwell et al.[15] shows only a strong 004 reflection. The alternative tilted biphenyls lie at an approximate distance of ca. 4.5 Å from each other and give rise to the four diffuse equatorial arcs of Figure 3.11. Smectic-C mesophases[23,24] demonstrate similar arrangements of the wide angle diffuse arcs. The well-defined equatorial arc at 4.0 Å, and the diffuse equatorial crescent at ca. 3.3 Å, indicate a order higher than smectic-C mesophase[25]. From the fact that these two reflections are aligned on the equator, combined with the tilted biphenyls and hexamethylene spacer, we can conclude that they arise from three-dimensional correlations of the 2,6-TDI moieties (Figure 3.12). This strong correlation arises from the restricted mobility of the 2,6-TDI moiety due to its meta-substituted benzene ring (backbone kink). Recently, for a side-chain poly(organophosphazene) in a smectic-C state, Atkins et al.[26] reported mesophase oriented patterns which look very much like that of Figure 3.11, except for the outer two reflections mentioned above. The schematic diagram they used to represent the herringbone arrangement of the side-chain liquid crystal poly(organophosphazene) looks similar to that of Figure 3.12 with the only major difference being the backbone arrangement (parallel to

smectic layers (side-chain liquid crystal) vs. perpendicular to smectic layers (main-chain liquid crystal)). According to their explanation, the lack of *hkl* reflections is due to the absent three-dimensional correlation between the smectic layers. In contrast to side-chain liquid crystals the main chain liquid crystal of 2,6-LCPU-6 retains this three-dimensional correlation due to bond connectivity and therefore is expected to demonstrate a higher order.

Heat treatment of the well-oriented fibers above 140 °C produces highly oriented crystalline fibers. Figure 3.13 shows the oriented WAXS pattern of the fiber of Figure 3.11 subjected to 5-days annealing at 165 °C. The lattice spacings of the 17 reflections of Figure 3.13 are in qualitative agreement with the spacings of Figures 3.6 and 3.8C and D, indicative of the strong order in the crystal phase. The crystallographic analysis will be discussed in detail in Chapter 5.

Optical Microscopy: Slow heating of 2,6-LCPU-6 indicates partial melting around 192 °C, followed by complete isotropization above 200 °C. Between 192 and 200 °C we observe a partial molten state which possesses adequate fluidity, with no birefringence in the fluid portion.

Upon cooling from the isotropic liquid, a fine white texture is formed ~157 °C for the low molecular weight and 150 °C for the high molecular weight. This fine white texture persists upon reheating until 194 °C, where it starts to melt slowly as described above. The sample quenched from the melt with cold air demonstrates a fine *schlieren* texture.[10] Soxhlet extraction in hot MeOH coarsens considerably this *schlieren* texture, which is presented in Figure 3.14A. In addition to this, Figure 3.14B indicates the existence of banded spherulitic textures (pointed out by white arrows) embedded in the *schlieren* texture. These spherulites were found in low quantities, gathered together in sections of the sample. Figure 3.14B shows an area of the sample where the spherulite concentration is relatively high while most of the sample has the appearance of Figure 3.14A. This is the result of a non uniform quenching which generates regions rich in crystallinity. Soxhlet

extraction in hot methanol coarsened the *schlieren* texture as well as the small crystals to result in the Figure 3.14 textures. More uniform quenching and Soxhlet extraction resulted in lower concentrations of these spherulitic textures, while slower cooling and Soxhlet extraction resulted in higher concentrations. Slow cooling rates result in complete crystallization, which is not amenable to perfection, upon Soxhlet extraction in hot MeOH. This is due to the highly insoluble nature of the crystal domains in MeOH. Upon heating, we observe no textural changes in the vicinity of 140 °C where the mesophase to crystal transition occurs. Further heating results in the melting of the *schlieren* texture at ~190 °C, followed by the melting of the spherulitic texture at ~200 °C. This is in qualitative agreement with the DSC data of Figure 3.7, where we explained the higher melting point endotherm as melting of crystalline regions with different morphology. Smyth et al.[1] reported similar morphologies for the 2,4-LCPU-6. The spherulitic morphology was produced from the isothermal melt, and possessed very high perfection, while the threaded crystalline morphology was produced from the mesophase. We attempted numerous times with DSC and polarized optical microscopy to crystallize the 2,6-LCPU-6 from its melt, over a 35 °C region, above the crystallization temperature without success. The reason for this as well as the unusual textures shown in Figure 3.14B must lie in the nature of 2,6-LCPU-6 and is not known at present.

Long term annealing of the *schlieren* texture of Figure 3.14A resulted in a substantially brighter threaded structure, which melts higher than 200 °C. This is in qualitative agreement with the annealing data of Figure 3.4, where the low temperature endotherm is amenable to perfection.

It might be argued that the phase we call mesophase might arise from the presence of small disordered crystallites. However, the polarizing optical microscopic data, coupled with the X-ray scattering data (based on the relative intensities[27,28]) of Figures 3.10 and 3.11) and the detailed DSC analysis, suggest that the term mesophase is more consistent than the alternative mentioned above.

Characterization of 1,3-LCPU-6. Molecular Weight Characterization: Intrinsic viscosity measurements of 1,3-LCPU-6 were performed in DMF at 30.0 °C. The highest intrinsic viscosity sample we managed to synthesize was 0.402 dL/g. Since DMF at 30.0 °C is a very good solvent for this polymer, its molecular weight is in the medium range.[29]

Differential Scanning Calorimetry: Figure 3.15 illustrates four consecutive cyclic DSC scans of a fresh 1,3-LCPU-6 sample. In an effort to address the large wealth of information contained in this figure we will focus our attention at the cooling traces first. The sample was isothermally annealed at the end of each heating scan for 0.5 min at 200 °C (A), 2 min at 200 °C (B), 1 min at 210 °C (C) and 1 min at 220 °C (D) respectively. Upon the first cooling (A), we observed a large endotherm peaking at 156.0°C followed by two smaller exotherms peaking at 140.6 and 137.6 °C respectively. During the second cooling scan the large exotherm shifted slightly lower at 155.5 °C while the two smaller exotherms remained at the same position. Upon the third cooling only the shoulder of the first exotherm is observed. The rest of the exothermic heat has been relocated to the previously smaller exotherms, at 140.6 and 137.6 °C respectively. For the fourth and last cooling trace, we witnessed the compete elimination of the first exotherm and only the 140.6 and 137.6 °C exotherms are present. On the basis of prior knowledge obtained from the study of 2,4-LCPU-6[1] and 2,6-LCPU-6, this behavior can be explained with the following scenario. Assuming that the 1,3-LCPU-6 is a monotropic liquid crystal, its crystal phase must be thermodynamically more stable than its mesophase (see Figure 3.3). In the case of incomplete crystal melting during the preceding heating scan, the remaining crystallites will nucleate crystallization (first exotherm at 156 °C) prior to isotropic–mesophase transition (second exotherm at 140.6 °C). The portion that did not manage to crystallize at the 156 °C exotherm, will transform into the mesomorphic state during the second exotherm, and eventually will crystallize from the mesophase during the third exotherm at 137.6 °C.[1] Annealing the sample at higher and higher temperatures (Figures 3.15C and 3.15D respectively) we managed to destroy the high melting point (T_m) crystals that act as a

nucleating agent, and to supercool the polymeric liquid past the isotropic–crystal transition. Some of the melting endotherms of these high T_m crystals are indicated with an asterisk in Figure 3.15. Additional proof is presented in Figure 3.16. In order to observe these high T_m crystals (endotherms), we maximized the sample crystallinity by drawing and annealing 1,3-LCPU-6 similarly to the 2,6-LCPU-6. Following the main melting endotherm at 202.2 °C we find a number of high melting endotherms with the 221.4 °C as the most prominent one. Upon the second heating scan we observe none of these endotherms which eliminates the possibility of baseline artifacts. The structure of these high T_m crystals will be discussed in detail in Chapter 5.

Having established the monotropic nature of 1,3-LCPU-6, the two endothermic peaks of Figure 3.15 (at ~165 and at ~180 °C) must be associated with crystal melting. Polarized optical microscopic data reveals unambiguously the existence of two different crystalline domains with different macroscopic morphologies similar to these of 2,4-LCPU-6.[1] The melting of the threaded and spherulitic crystal morphology corresponds to the lower (~165 °C) and higher (~180 °C) endotherm respectively.

X-ray Diffraction, Fiber Samples: Figure 3.17A exhibits the WAXS patterns of a fiber drawn from the melt, and Shoxhlet extracted in hot MeOH for 4 days. It displays similar structure to the 2,6-LCPU-6 (Figure 3.11) except for the lack of the well defined equatorial reflection at 4.0 Å and the weak equatorial reflection of 3.3 Å. The 002 and 004 (strong) meridional reflections correspond to a 56.5 Å repeat while the broad and diffuse of equatorial arcs (centered at 4.4 Å) indicate an alternative smectic-C structure. Annealing at 165 °C for 5 days transforms the mesophase structure of Figure 3.17A to a well oriented crystalline fiber with Figure 3.17B WAXS fiber pattern. The crystallographic analysis of this pattern will be discussed extensively in Chapter 5.

Comparison of the mesomorphic state of the 2,6-LCPU-6, 1,3-LCPU-6 and 2,4-LCPU-6. A qualitative picture of the order present in the mesophase structure of 2,6-LCPU-6, 1,3-LCPU-6, and 2,4-LCPU-6 can be obtained from Figures 3.11, 3.17A, and

2.11B respectively. The 10 °C/min heating traces of the liquid N_2 quenched samples of these polymers (Figure 3.18) can provide us the relative order of the mesophase with respect to the crystalline phase. The exothermic transition upon heating a sample with mesophase morphology will be the key element in this analysis. This transition is the characteristic signature of the monotropic liquid crystalline state, and arises from the greater thermodynamic stability of the crystalline state with respect to the mesophase. Table 3.6 tabulates the transition temperatures and enthalpies for the three polymers of Figure 3.18. The mesophase–crystal transition temperature of 2,6-LCPU-6 (140 °C) indicates the higher order of this mesophase versus the 1,3-LCPU-6 (117 °C), and 2,4-LCPU-6 (115 °C) respectively. Figure 3.18 can also provide us with a rough understanding of the magnitude of the mesophase–crystal transition for the three polymers. Table 3.6 indicates that the mesophase–crystal transitions of 2,6-LCPU-6, 1,3-LCPU-6, and 2,4-LCPU-6 are 12.3, 28.4 and 42.4 % respectively. This is indicative of the strong order in the mesophase of 2,6-LCPU-6 followed by 1,3-LCPU-6 and 2,4-LCPU-6. The fact that 2,4-LCPU-6 displays the lower amount of order can be easily explained on the basis of the random placement of the methyl substituent in the TDI moiety. For the case of 2,6-LCPU-6 and 1,3-LCPU-6 the explanation is not straight forward. Chapter 5 will attempt to elucidate some key structural elements of the two polymers that can provide some sort of explanation, though it will be far from complete.

Characterization of 2,6-PU-6, 1,3-PU-6 and 2,4-PU-6. Molecular Weight Characterization: Intrinsic viscosity measurements of the three polymers were performed in DMF at 30.0 °C. The highest intrinsic viscosity sample we managed to synthesize for the 2,4-PU-6, 2,6-PU-6, and 1,3-PU-6 was 0.462, 0.433, and 0.501 dL/g respectively. Since DMF at 30.0 °C is a very good solvent for all three regular polyurethanes, their molecular weights lie in the medium range.

Differential Scanning Calorimetry: Symmetric polyurethanes such as the 2,6-PU-6 and 1,3-PU-6 are capable of forming a crystal phase.[30] For a fresh (Soxhlet-extracted in

72

hot MeOH) sample of 2,6-PU-6, we observed upon heating (Figure 3.19A) a weak step in heat capacity associated with the T_g (~85 °C), followed by a broad endothermic region (peaking at 207 °C, $\Delta H_m = 59$ J/g) associated with crystal melting. Annealing at 165 °C, prior to crystal melting, perfects the crystalline domains and shifts the T_m up to 215 °C ($\Delta H_m = 85.5$ J/g). In the subsequent cooling trace (Figure 3.19B) as well as the second heating trace (Figure 3.19C) the 2,6-PU-6 behaves like a glass with T_g at ~73 °C ($\Delta C_p = 0.42$ J/g·°C). Long-term annealing at various temperatures between 95 and 185 °C failed to restore crystallinity, indicative of a very low crystallization rate from the melt. Plasticization with small molecular weight molecules such as MeOH readily restores the sample's crystallinity.[31] Similar phenomena have been reported in literature. A classic example is the bisphenol-A polycarbonate and poly(p-phenylene oxide) which has been attributed to lack of polymer mobility.[8]

Comparable behavior is also displayed from the 1,3-PU-6 polyurethane. Upon the first heating scan (Figure 3.20A), we observed a relatively low melting endotherm that peaks at 137 °C, $\Delta H_m = 45$ J/g. Annealing at 120 °C prior to crystal melting perfects the crystalline domains, and shifts the T_m up to 145 °C ($\Delta H_m = 59.4$ J/g). The origin of this surprisingly low T_m of 1,3-PU-6 is going to be addressed extensively in Chapter 5. Similarly to the 2,6-PU-6 polyurethane, the subsequent cooling trace (Figure 3.20B) and second heating trace (Figure 3.20C) of 1,3-PU-6 exhibits the same difficulty to crystallize from the melt ($T_g = 90$ °C, $\Delta C_p = 0.42$ J/g·°C). Long-term annealing at various temperatures between 95 and 130 °C also failed to restore crystallinity.

Figure 3.21 illustrates the 10 °C/min DSC traces of a fresh 2,4-PU-6 sample, Soxhlet-extracted in hot MeOH for 4 days. Upon the first heating scan a broad step in heat capacity, corresponding to the glass transition (T_g), is observed at ~78 °C ($\Delta C_p = 0.58$ J/g·°C). On the subsequent cooling scan the T_g occurs at ~72 °C. Additional heating scans, even after long annealing at 10 to 50 °C higher than Tg (at ~75 °C, $\Delta C_p = 0.51$

J/g·°C for Figure 3.21C), indicate the pure amorphous nature of this polymer[30] due to the random placement of the methyl substituent in the TDI moiety.

Conclusions

(1)   DSC, X-ray diffraction, and polarized optical microscopic data prove unambiguously the monotropic liquid crystalline nature of 2,6-LCPU-6 and 1,3-LCPU-6. The isotropic to mesophase transition is approximately 60—70 °C lower than the crystal melting transition. This very large temperature difference along with the fast crystallization of 2,6-LCPU-6, results in the mesophase being accessible only with very fast cooling rates. Cooling rates higher than 100 °C/min need to be employed in order to avoid homogeneous nucleation and crystallization and to bring the sample into the mesophase (Figure 3.3). In the case of 1,3-LCPU-6 the crystallization rate is slightly slower and the isotropic–mesophase can be observed upon moderate cooling (Figure 3.15).

(2)   X-ray diffraction patterns obtained from the frozen mesophases indicate higher than smectic-C order for the mesophase of 2,6-LCPU-6 and a smectic-C order for the mesophase of 1,3-LCPU-6. The zigzag structure proposed in Figure 3.12 is a result of the kink introduced by the meta-substituted benzene ring of the 2,6-TDI and 1,3-PDI moiety. DSC measurements also indicate the high order of the 2,6-LCPU-6 mesophase relative to the 1,3-LCPU-6 and 2,4-LCPU-6 mesophases (Table 3.6).

(3)   Soxhlet extraction in hot MeOH of the quenched mesophase results in considerable orientation enhancement as well as phase thickening and perfection. The value of this technique arises from its ability to perfect an unstable phase, such as the mesophase of 2,6-LCPU-6, preventing the polymer from achieving equilibrium. Using this technique, we obtained highly oriented mesophase and crystalline WAXS patterns which are the basis of the crystallographic analysis to be presented in Chapter 5.

(4)   Polarized optical microscopy studies demonstrate that 2,6-LCPU-6 and 1,3-LCPU-6 exhibit two macroscopically distinct crystal morphologies—a spherulitic morphology produced from slow cooling and a threaded crystalline morphology when they crystallize upon heating from the quenched mesophase.

Table 3.1

Differential scanning calorimetric data for the low molecular weight 2,6-LCPU-6 as a function of cooling rate

cooling rate, °C/min	transition temperature, °C		total transition enthalpy, J/g·min	Relative % transition enthalpy ‡	
	T_c'	T_c''	ΔH_c	% $\Delta H_c'$	% $\Delta H_c''$
10	160	133	42	95	5
30	153	131	41	92.5	7.5
50	147	129	40	8.9×10	1.1×10
100	132	--	39	--	--

'   main exothermic peak at Figure 3.5.
"   smaller peak at the end of the exothermic tail , indicated with an asterisk in Figure 3.5.
‡   estimated from a simple deconvolution.

Table 3.2

Observed and alculated d spacings of Figure 3.8A X-ray powder pattern,
indexed as orders of 57.6 Å

d_{obsd}, Å	Intensity	orders of 57.6 Å	d_{calcd}, Å
28.8	weak, sharp	2	28.8
14.34	very strong, sharp	4	14.40
- -	- -	6	9.60
7.20	weak, sharp	8	7.20
4.5	strong, broad		
4.05	medium, w.d.‡		
3.3	very weak, broad		

‡ Well distinguished.

Table 3.3

Observed and calculated d spacings of figure 3.8B X-ray powder pattern,
indexed as orders of 58.2 Å

d_{obsd}, Å	Intensity	orders of 58.2 Å	d_{calcd}, Å
29.0	weak, sharp	2	29.1
14.55	very strong, sharp	4	14.55
- -	- -	6	9.70
7.28	weak, sharp	8	7.28
4.5	strong, broad		
4.00	medium, w.d.‡		
3.3	very weak, broad		

‡ Well distinguished.

Table 3.4

Observed and calculated d spacings from Figure 3.8C X-ray powder pattern

unit cell params			scattering condtns, obsd.	scattering condtns, $P2_1/b$
$a = 4.79_0$ Å				
$b = 10.7_8$ Å			$00l$: $l = 2n$	$00l$: $l = 2n$
$c = 58.4$ Å			$hk0$: $k = 2n$	$hk0$: $k = 2n$
$\gamma = 103\,°$				hkl: No conditions

$\rho_{calcd} = 1.26_8$ g/cm^3

h	k	l	d_{calcd} Å	d_{obsd} Å	Intensity
0	0	2	29.2	29.1	weak, w.d.[‡]
0	0	4	14.60	14.60	strong, w.d.
0	1	1	10.34	10.33	medium, w.d.
0	1	3	9.24	9.20	faint, broad
0	1	5	7.81	7.83	very weak, broad
0	1	7	6.53	6.58	faint, broad
0	1	9	5.52	-.-	- -
0	2	2	5.17	5.15	medium, w.d.
1	0	1	4.65	4.65	strong, w.d.
1	0	4	4.45	} 4.35	med. strong, broad
0	2	8	4.26		
1	-2	2	3.92	3.91	medium, broad
1	-2	6	3.67	3.67	medium, broad
1	-2	8	3.48	- -	- -
1	-3	1	3.16	3.12	weak, broad

‡ Well distinguished.

Table 3.5

Observed and calculated d spacings from Figure 3.8D X-ray powder pattern

unit cell params			scattering condtns, obsd.	scattering condtns, P2$_1$/b
$a = 4.752$ Å				
$b = 10.70$ Å			$00l$: $l = 2n$	$00l$: $l = 2n$
$c = 58.7$ Å			$hk0$: $k = 2n$	$hk0$: $k = 2n$
$\gamma = 103$ °				hkl: No conditions

$\rho_{calcd} = 1.280$ g/cm^3

h	k	l	d_{calcd} Å	d_{obsd} Å	Intensity
0	0	2	29.4	29.2	weak, w.d.‡
0	0	4	14.68	14.68	medium, diffuse.
0	1	1	10.27	10.27	medium, w.d.
0	1	3	9.20	9.18	faint, broad
0	1	5	7.80	7.83	very weak, broad
0	1	7	6.53	6.56	faint, broad
0	1	9	5.53	-.-	- -
0	2	2	5.13	5.14	medium, w.d.
1	0	1	4.62	4.62	strong, w.d.
1	0	4	4.42	4.42	medium, w.d.
0	2	8	4.25	4.22	mead. strong, w.d.
1	-2	2	3.89	3.89	medium, diffuse
1	-2	6	3.65	3.65	medium, w.d.
1	-2	8	3.46	3.45	weak, broad
1	-3	1	3.13	3.11	weak, broad

‡ Well distinguished.

Table 3.6

Differential scanning calorimetric data of Figure 3.18 liquid N_2 quenched samples of 2,6-LCPU-6, 1,3-LCPU-6, and 2,4-LCPU-6.

Property	2,6-LCPU-6 $[\eta]$ = 0.882 dL/g	1,3-LCPU-6 $[\eta]$ = 0.402 dL/g	2,4-LCPU-6 $[\eta]$ = 0.60 dL/g
Mesophase–Crystal Transition Temp. (°C)	140	117	115
Crystal-Isotropic Transition Temp. (°C)	189 / 197 *	161 / 180 *	165‡ / 170.5 *
Mesophase–Crystal Transition Enthalpy (ΔH_{m-c}) (J/g)	- 5.8 **	- 14.4 **	- 17.7 **
Crystal–Isotropic Transition Enthalpy (ΔH_{c-i}) (J/g)	47.3 ***	50.7 ***	41.7 ***
$[(\Delta H_{m-c}) / (\Delta H_{c-i})]\cdot100\%$	12.3 %	28.4 %	42.4 %

* The first and second transition temperatures correspond to the melting of the two different crystalline domains (threaded and spherulitic macroscopic morphology crystals).

‡ Weak shoulder at the main endotherm.

** For the 2,6-LCPU-6, 1,3-LCPU-6, and 2,4-LCPU-6 the transition enthalpy was calculated from area integration between (127—157 °C), (100—145 °C), and (93—148 °C) respectively.

*** For the 2,6-LCPU-6, 1,3-LCPU-6, and 2,4-LCPU-6 the transition enthalpy was calculated from area integration between (157—207 °C), (145—216 °C), and (148—178 °C) respectively.

CHEMICAL STRUCTURES OF REGULAR POLYURETHANES
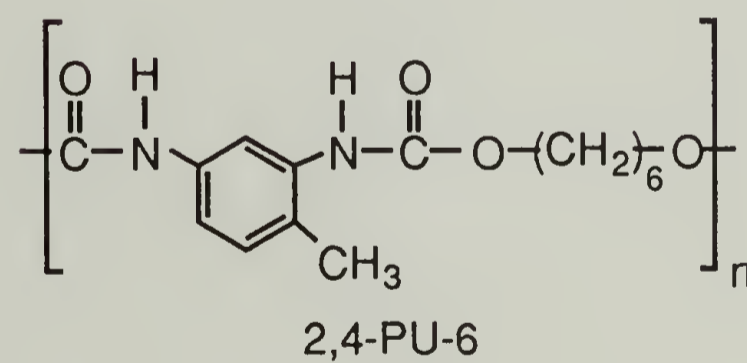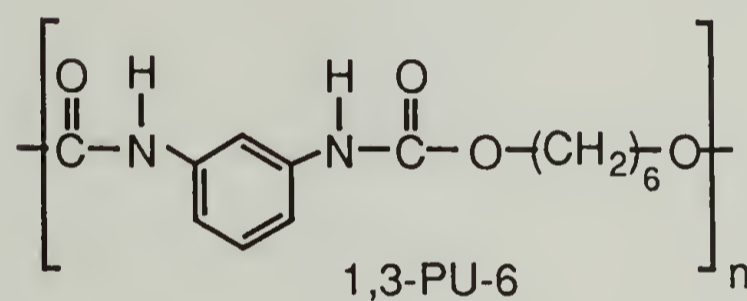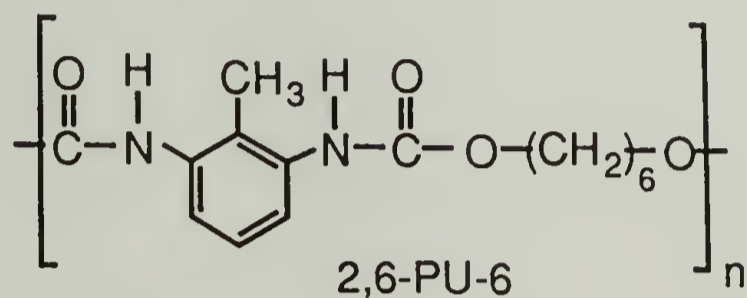
Scheme 3.1   Chemical structures of regular polyurethanes.

SYNTHESIS OF 2,6-LCPU-6
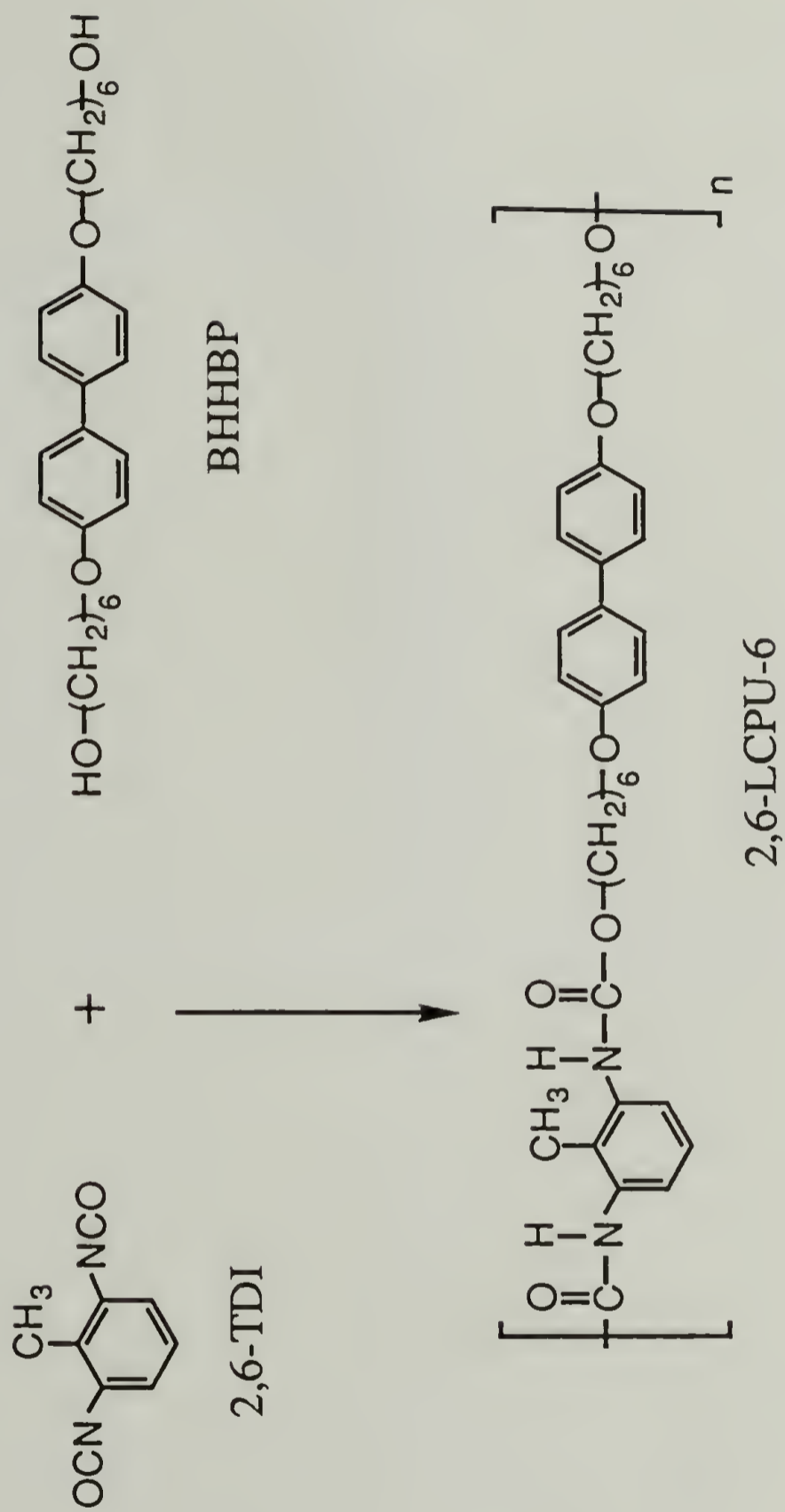
Scheme 3.2 Synthesis of 2,6-LCPU-6.

82

Figure 3.1 Structures of BHHBP and 2,6-LCPU-6. Lower case letters refer to ^{1}H NMR results (see Experimental section).

83
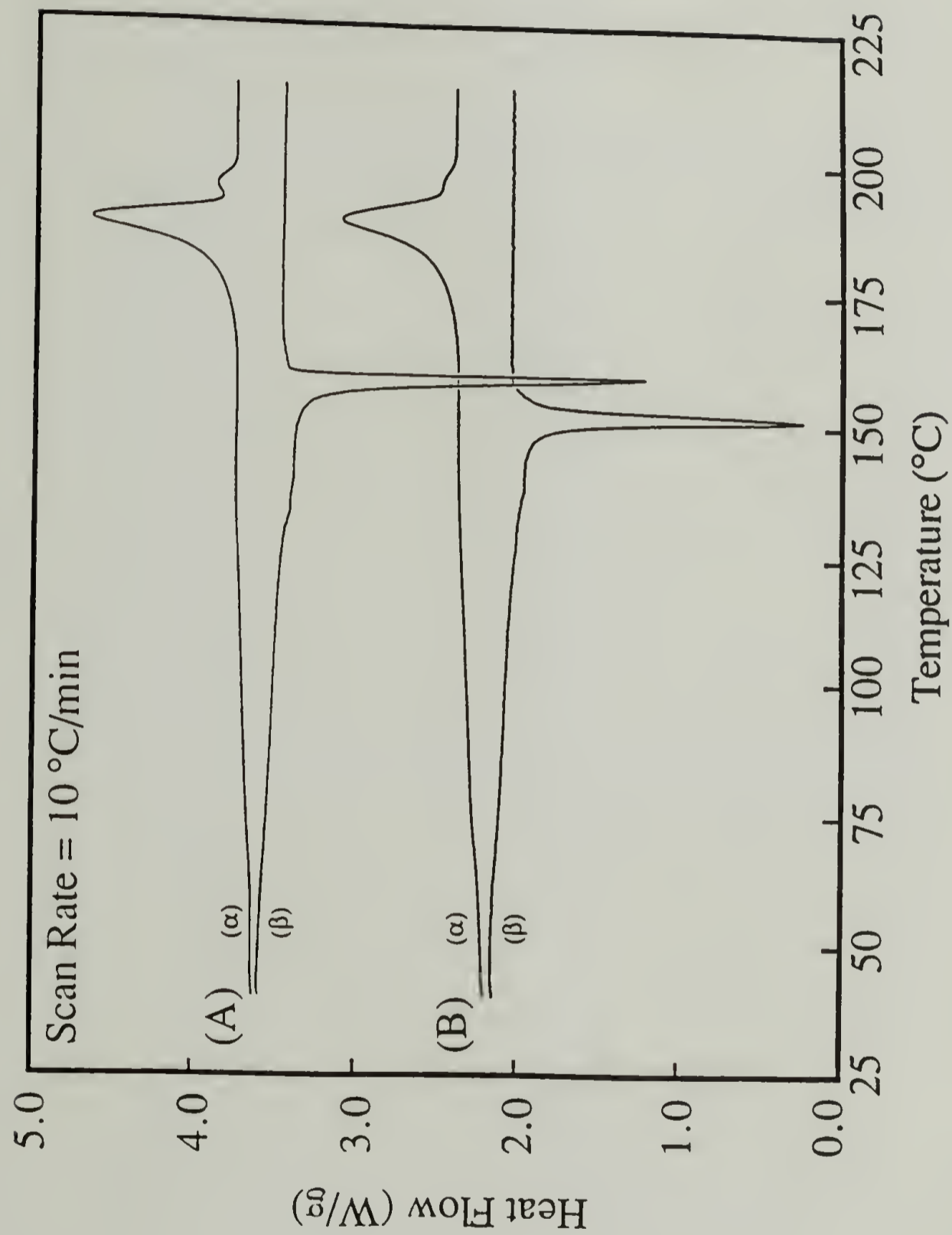
Figure 3.2 DSC traces for (A) low molecular weight 2,6-LCPU-6 and (B) high molecular weight 2,6-LCPU-6 recorded at 10 °C/min scanning rate: (α) heating; (β) cooling curves.

84
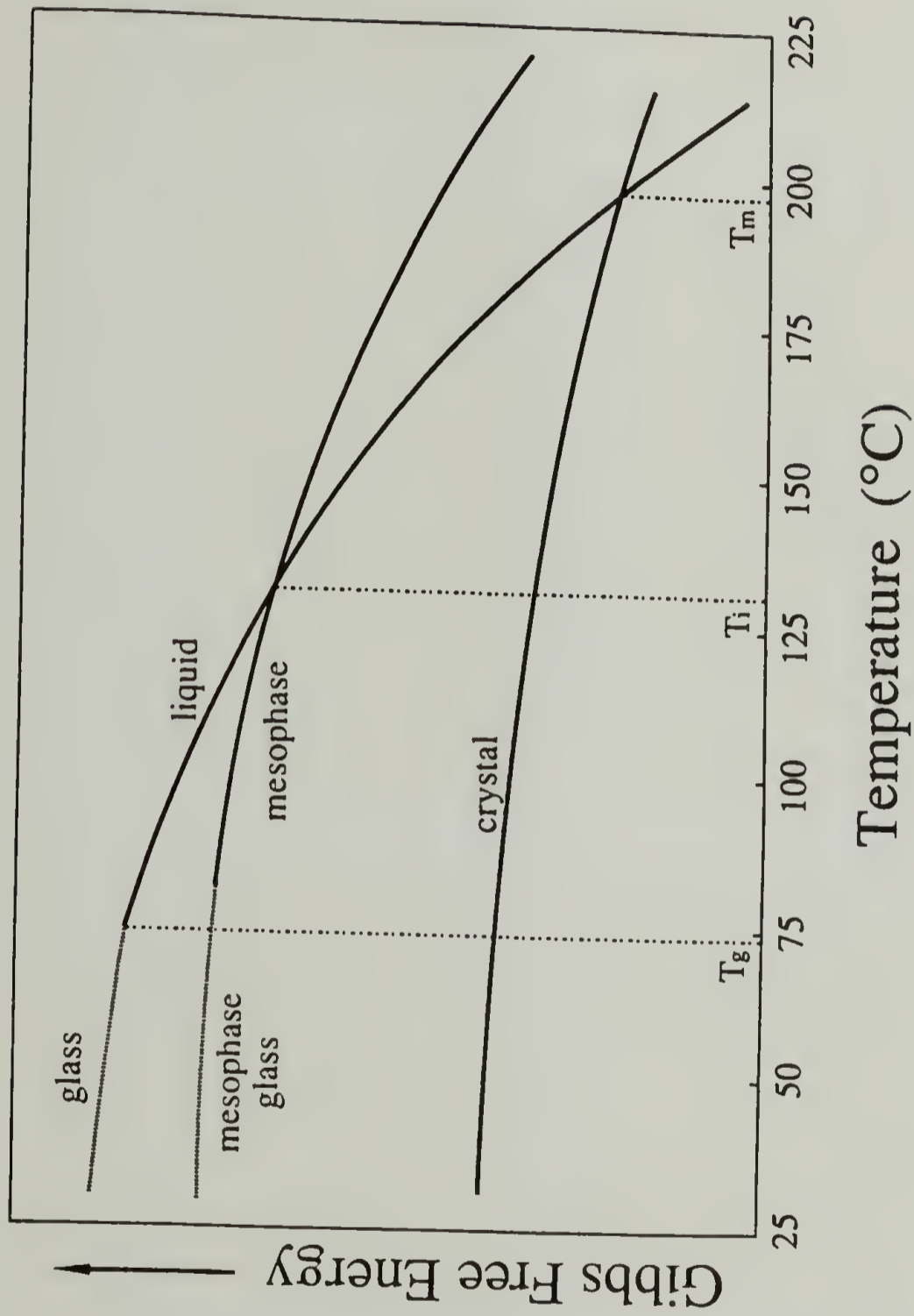
Figure 3.3 Schematic plot of temperature dependence of Gibbs free energy for 2,6-LCPU-6 (see text for details).
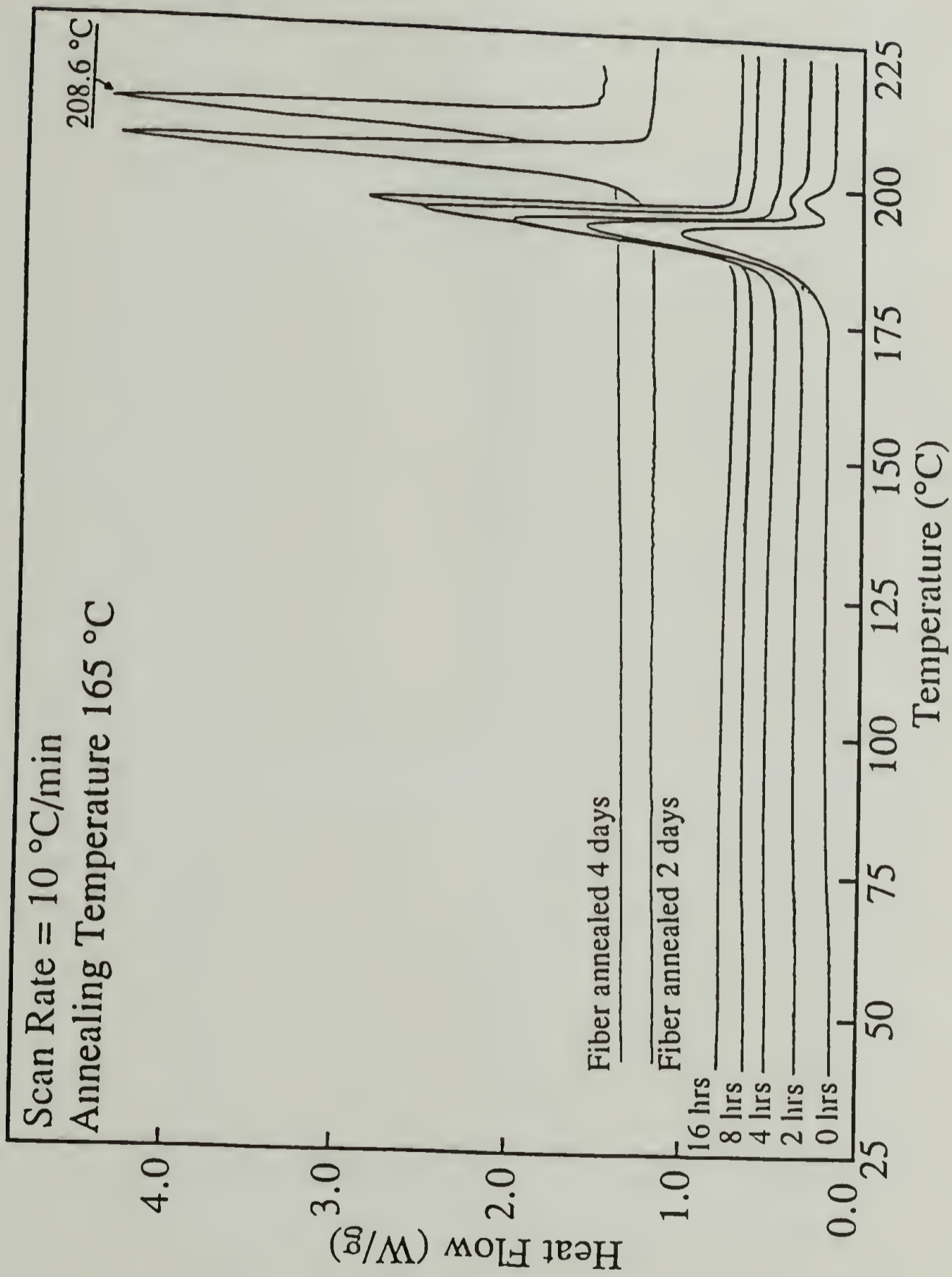
Figure 3.4 10 °C/min DSC heating traces of high molecular weight 2,6-LCPU-6 samples, previously annealed at 165 °C for various annealing times.
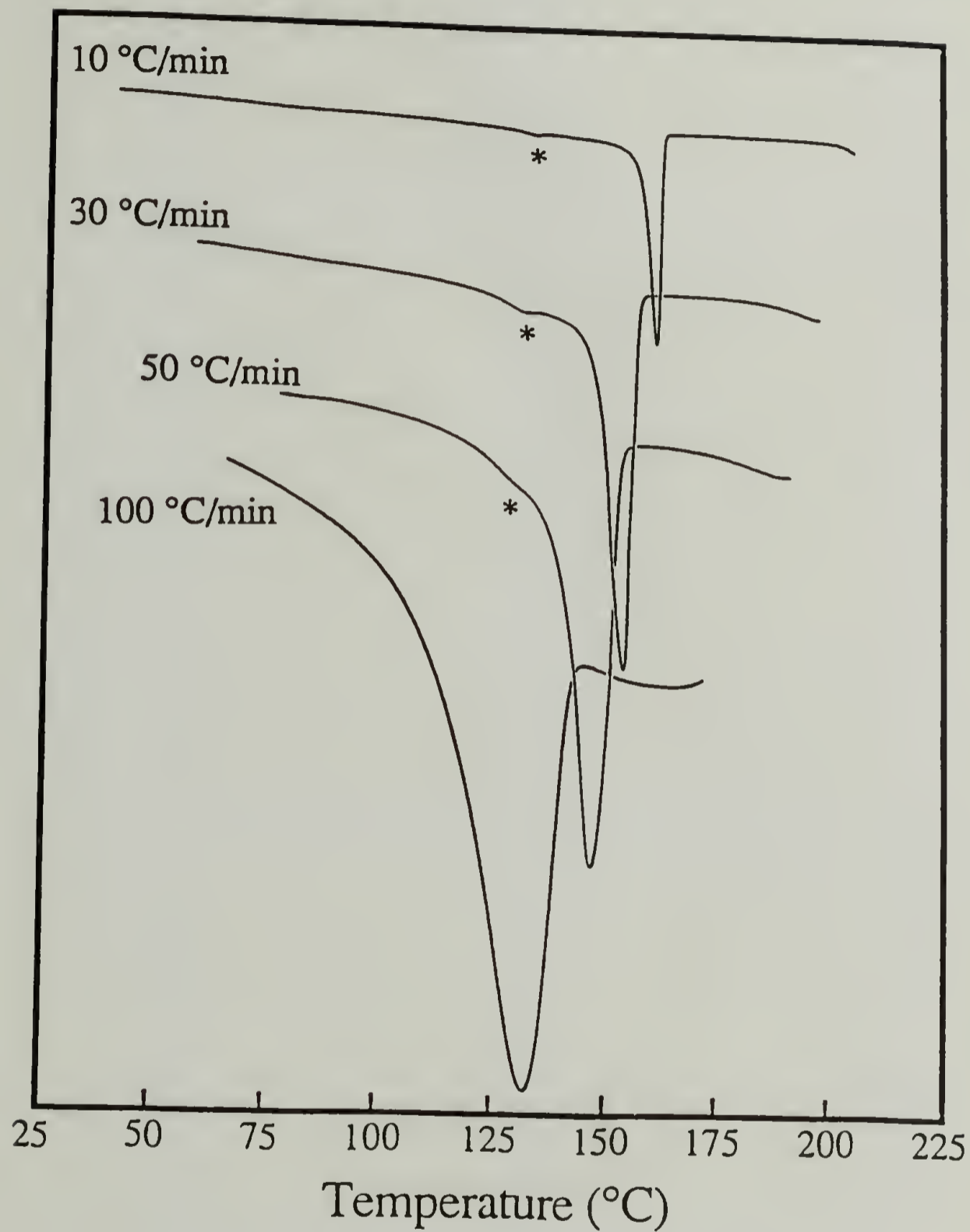
Figure 3.5 DSC cooling traces of the low molecular weight 2,6-LCPU-6 for various cooling rates.
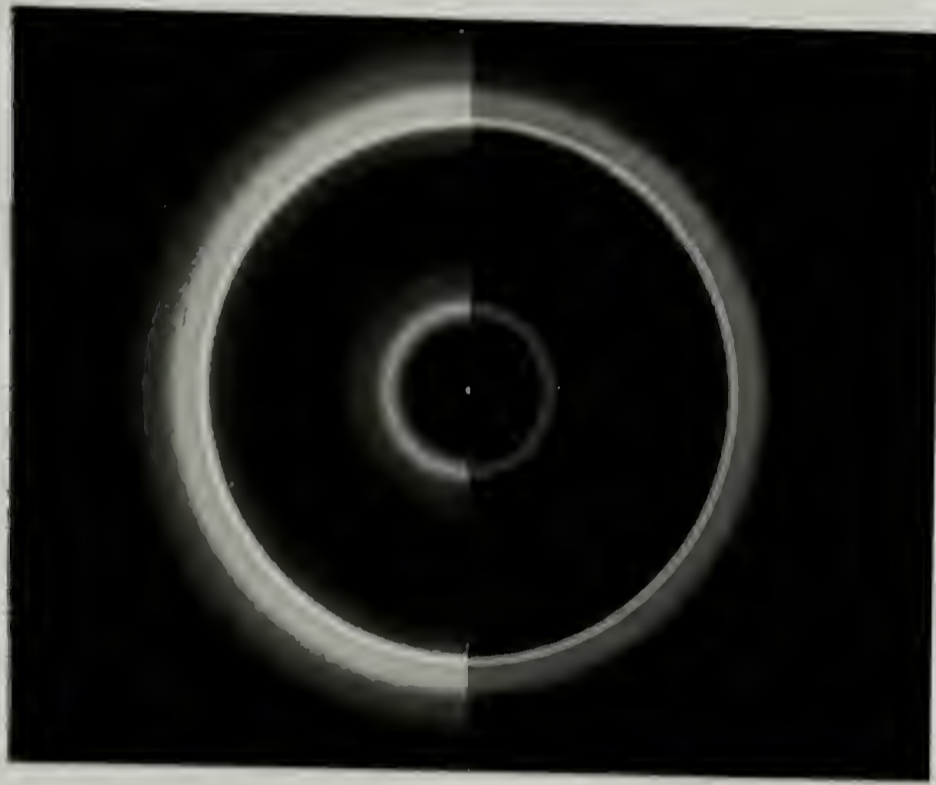
Figure 3.6 Room temperature X-ray diffraction powder pattern of a low molecular weight 2,6-LCPU-6 sample, cooled 100 °C/min from the melt to the room temperature (underexposed, left half; overexposed, right half).
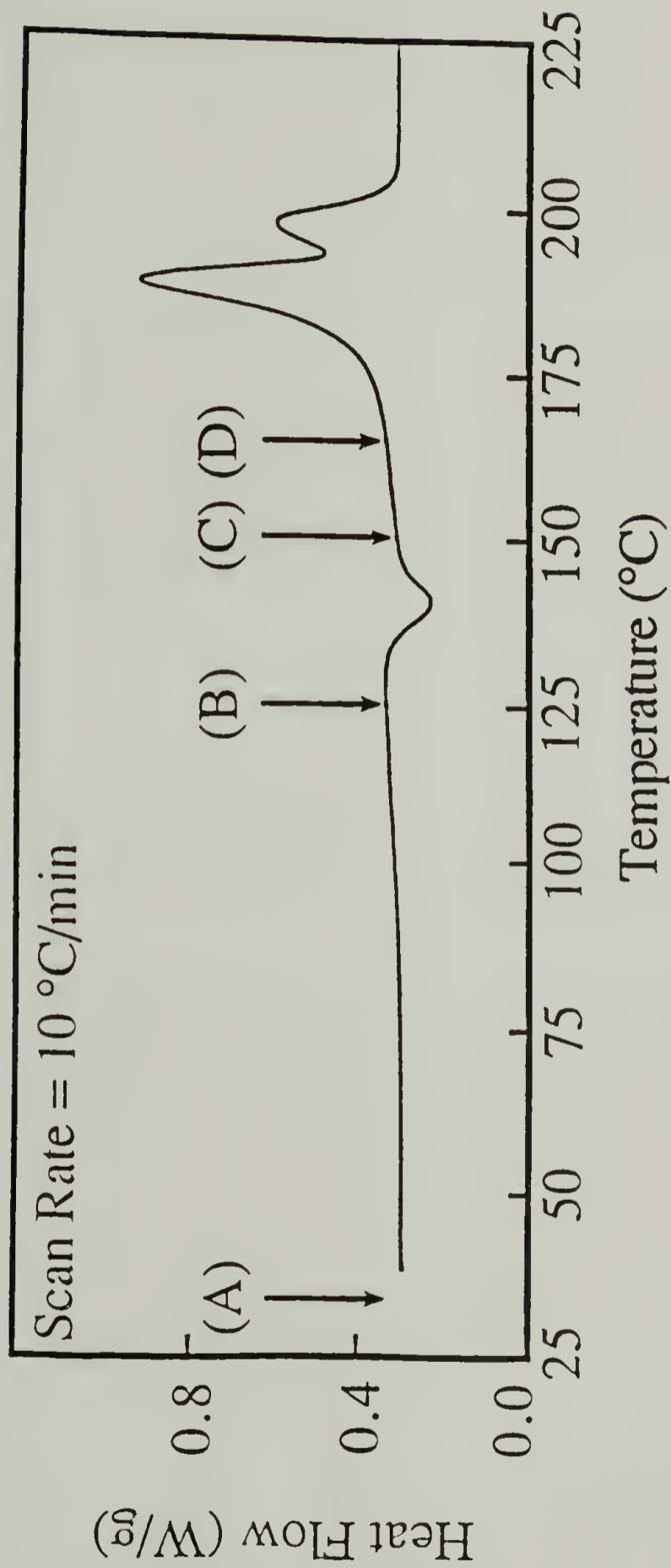
Figure 3.7 10 °C/min DSC heating trace of a high molecular weight 2,6-LCPU-6 sample quenched into liquid N_2 from the melt.
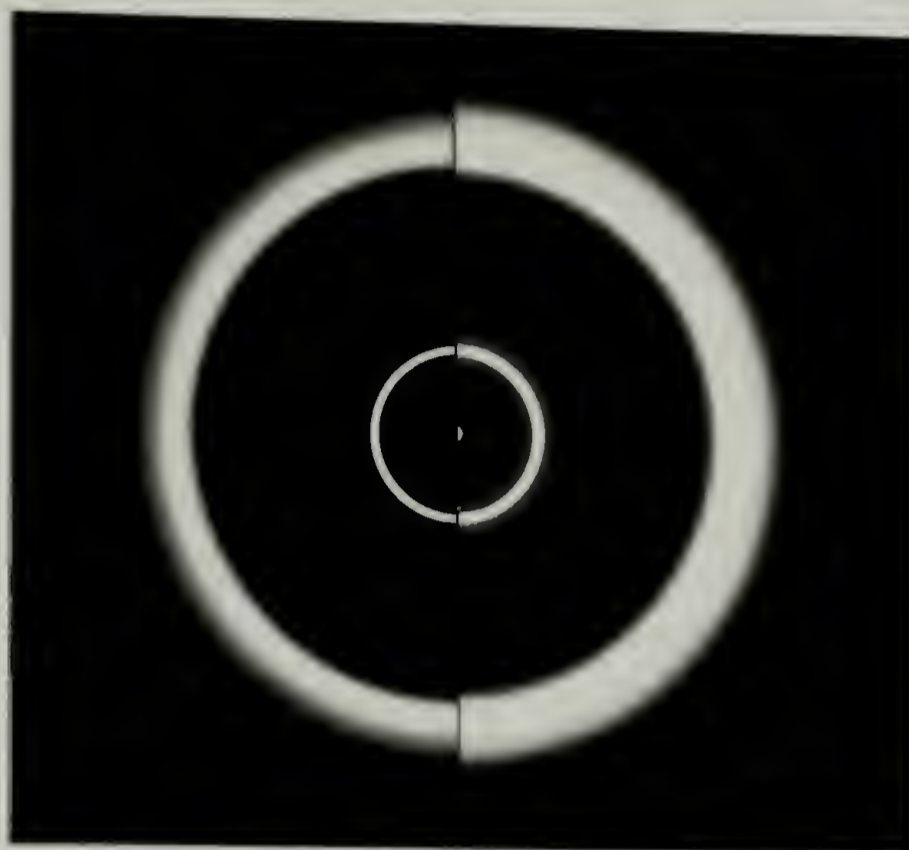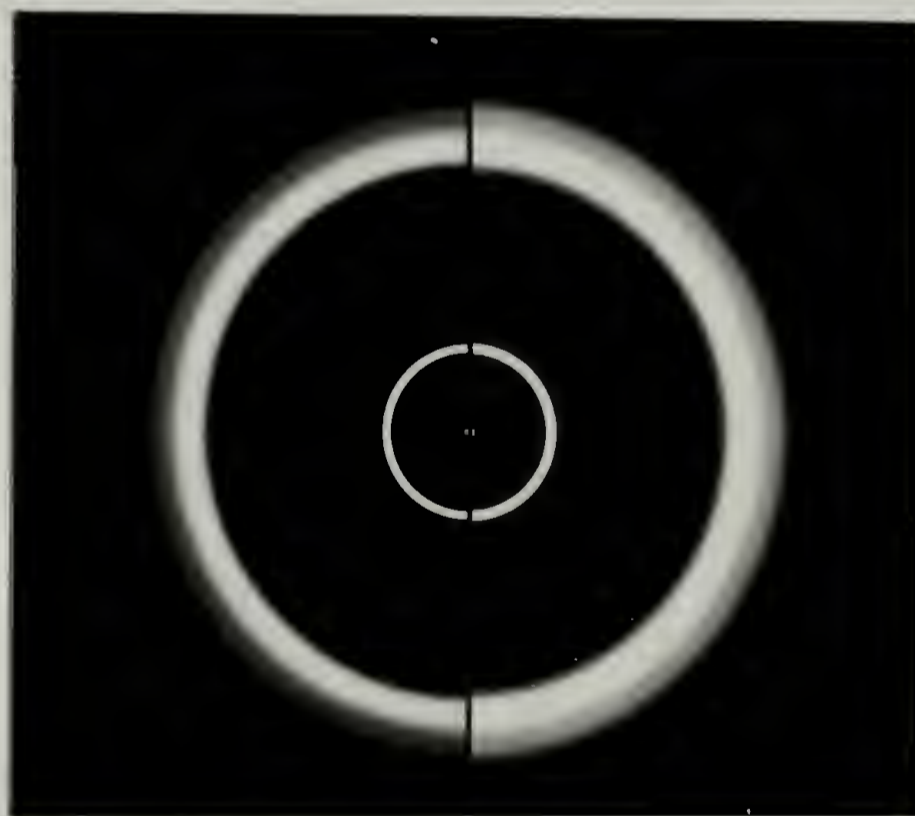
Figure 3.8 Room temperature X-ray diffraction powder patterns of high molecular weight 2,6-LCPU-6 samples which have been quenched in liquid N_2 from the melt, heated 10 °C/min to (B) 125 °C, (C) 150 °C, and (D) (165 °C and kept 90 minutes at 165 °C) (see letters in Figure 3.7), and cooled 100 °C/min to room temperature (underexposed, left half; overexposed, right half).

(C)
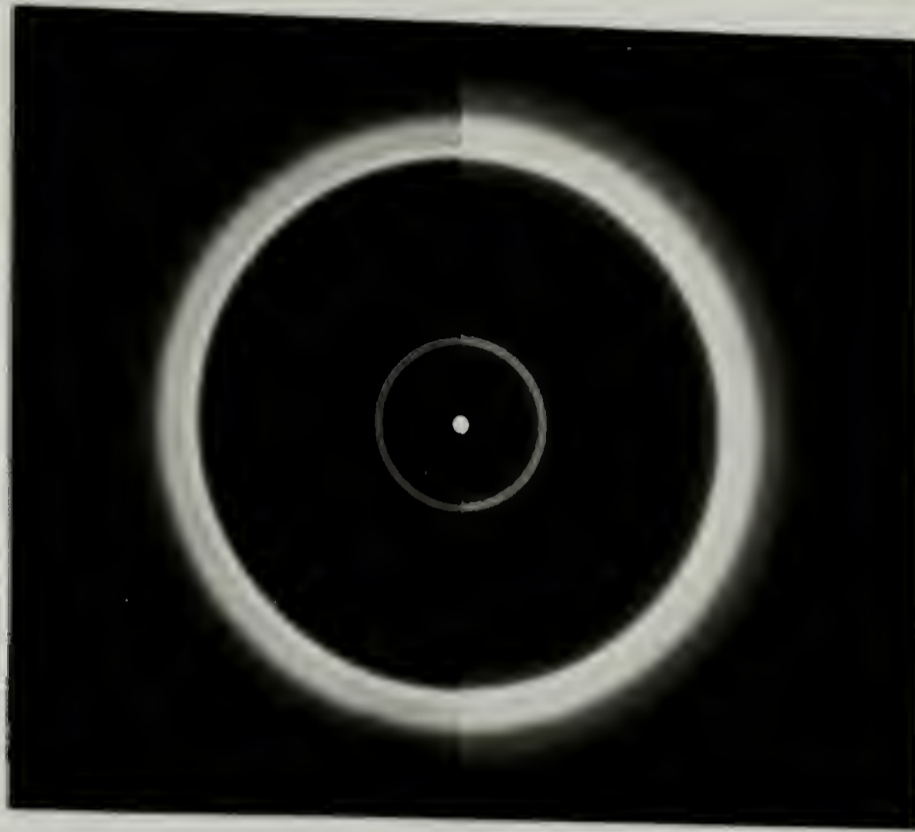
(D)
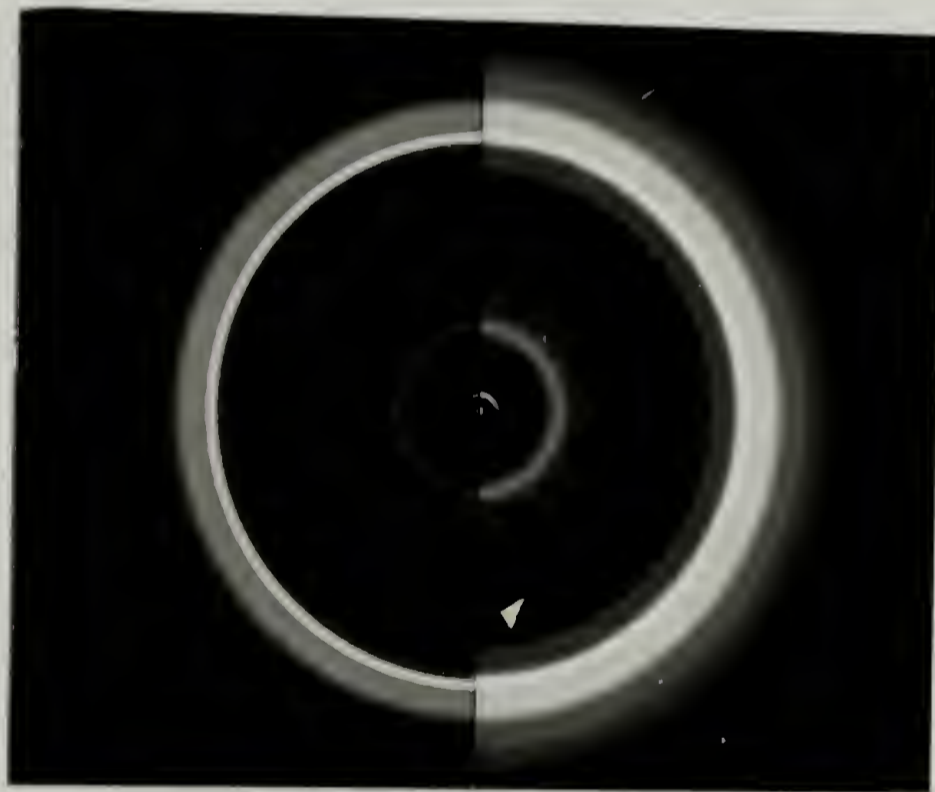
Figure 3.8   (Continued.)

91
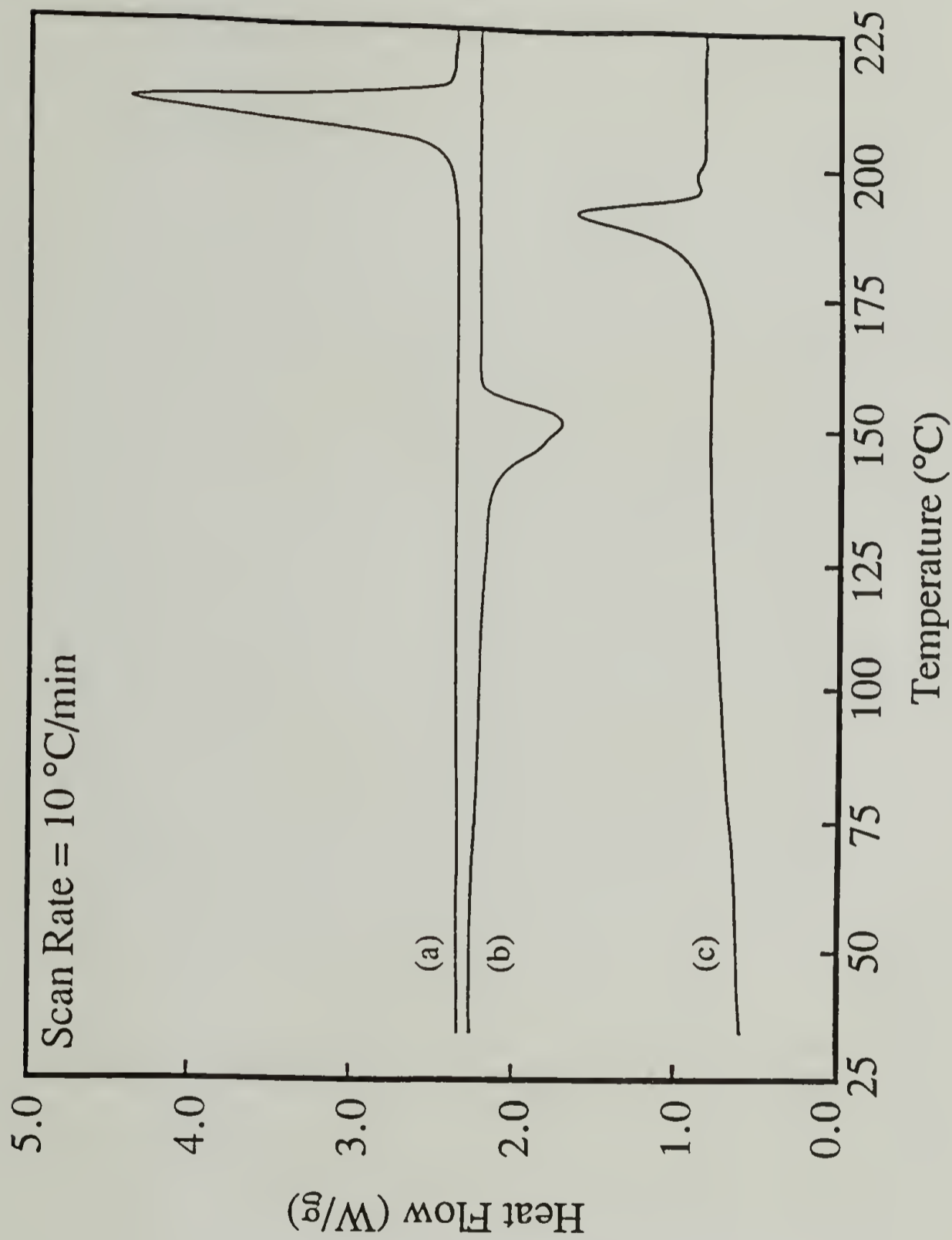
Figure 3.9 10 °C/min DSC traces of a high molecular weight 2,6-LCPU-6 sample previously annealed at 165 °C for 4 days. (a) first heating; (b) first cooling; (c) second heating.

92
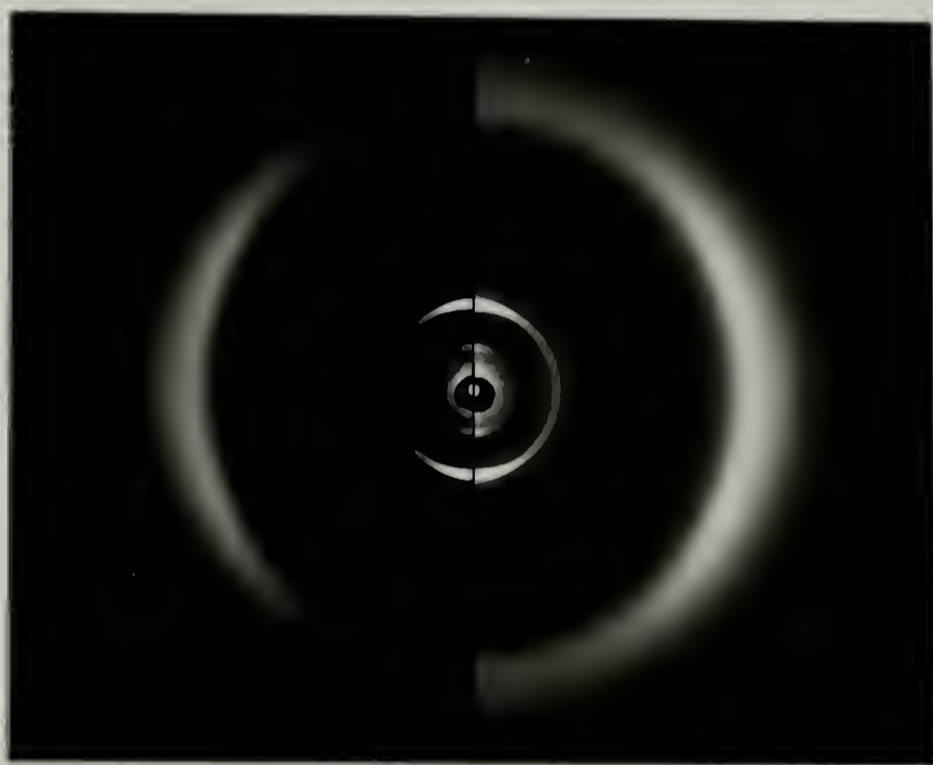
Figure 3.10 Room temperature X-ray diffraction pattern of a high molecular weight 2,6-LCPU-6 fiber drawn from the melt (underexposed, left half; overexposed, right half). Fiber axis is vertical.

94
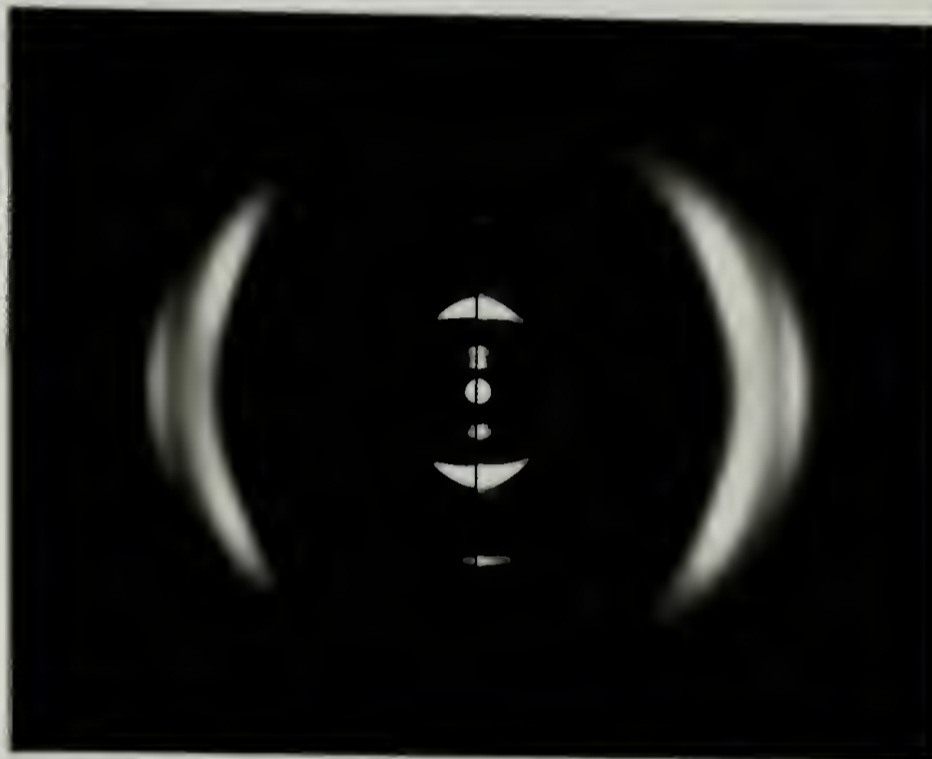
Figure 3.11   Room temperature X-ray diffraction pattern of a high
molecular weight 2,6-LCPU-6 fiber drawn from the melt,
and soxhlet extracted in MeOH for 4 days (underexposed,
left half; overexposed, right half). Fiber axis is vertical.

94
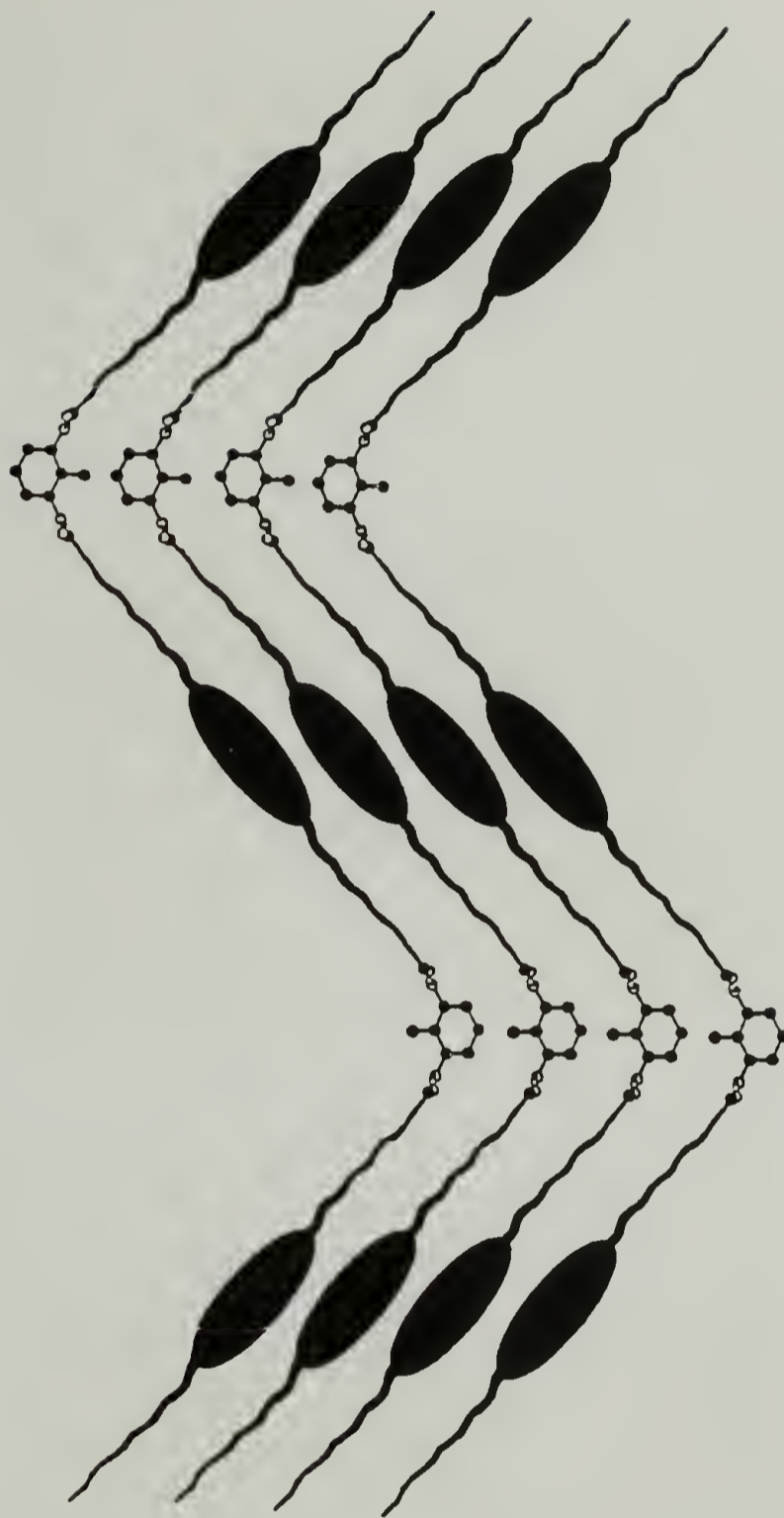
Figure 3.12 Schematic diagram to illustrate structural criteria needed to explain basic features of the mesophase oriented WAXS fiber pattern of figure 3.11. The carbon atoms (black circles) and hetero-atoms (lightly spotted white circles) portray the less mobile meta substituted 2,6-TDI moiety. The biphenyl mesogen units (ovals) along with the hexamethylene spacer (black curly string) portray the more mobile regions. All hydrogens have been removed for clarity (see text for details). Fiber axis is vertical.

Figure 3.13   Room temperature X-ray diffraction pattern of the high
molecular weight 2,6-LCPU-6 fiber of figure 3.11
subjected to 5 days annealing at 165 °C (underexposed, left
half; overexposed, right half). Fiber axis is vertical.
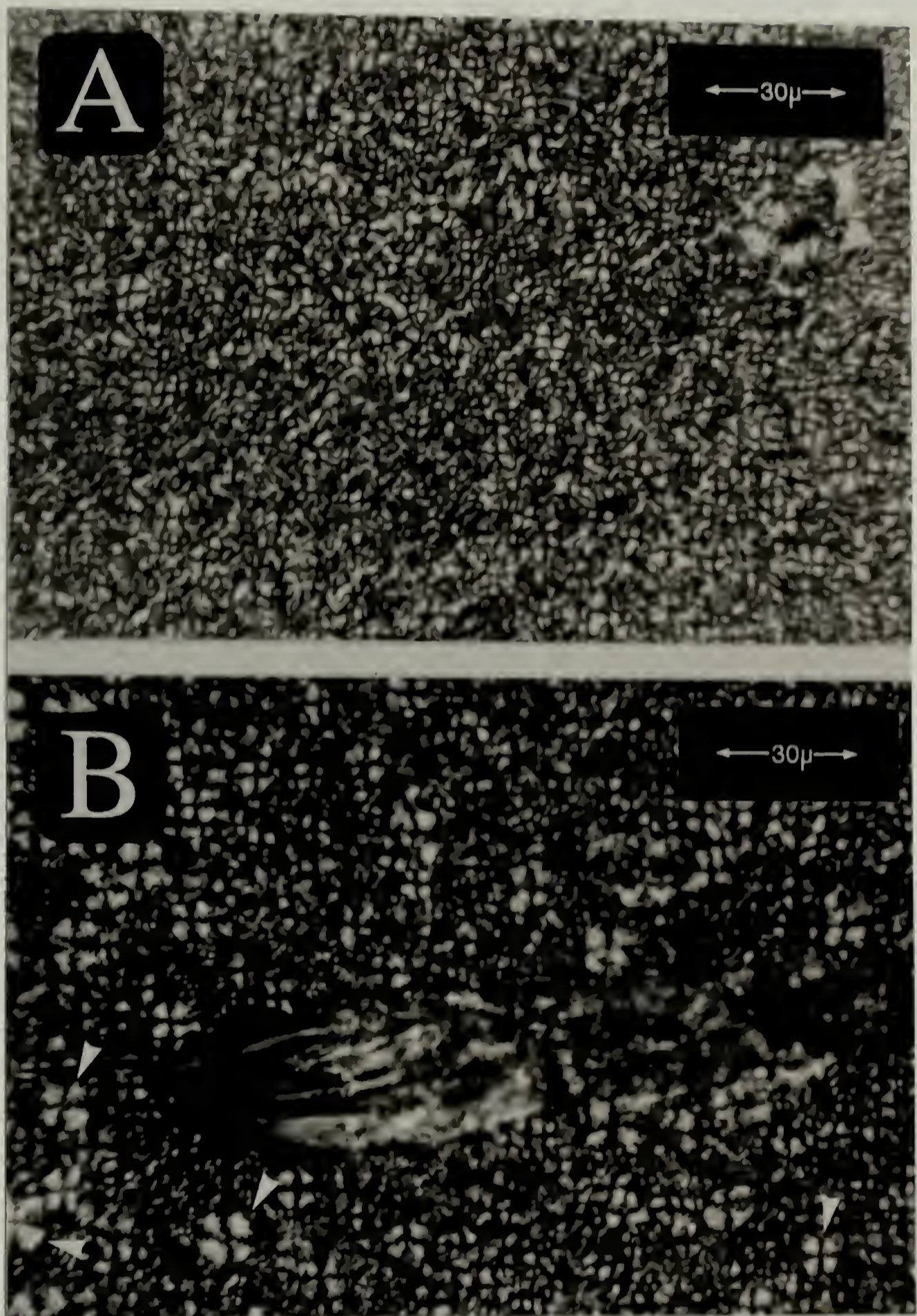
Figure 3.14   Room temperature, cross polarized optical micrographs from different regions of a 2,6-LCPU-6 sample quenched from the melt with cold air and soxhlet extracted in hot methanol for 2 days: (A, top) The *schlieren* texture of the smectic mesophase; (B, bottom) The *schlieren* texture of the smectic mesophase along with banded spherulites (indicated with the white arrows).
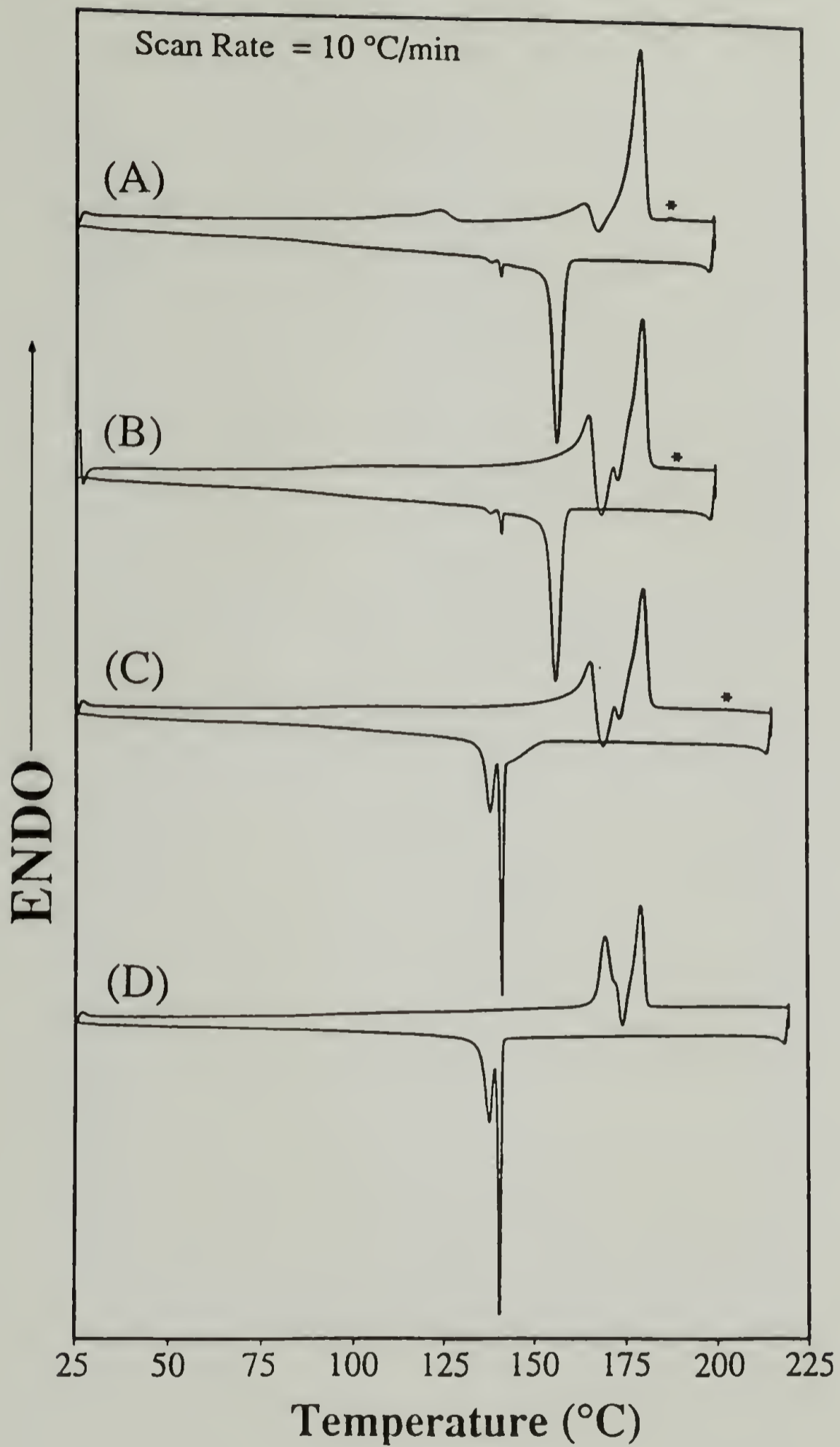
Figure 3.15 Cyclic 10 °C/min DSC heating and cooling traces of an 1,3-LCPU-6 sample. The sample was isothermally annealed at the end of each heating scan for: (A) 0.5 min at 200 °C; (B) 2 min at 200 °C; (C) 1 min at 210 °C; and 1 min at 220 °C. (See text for details.)
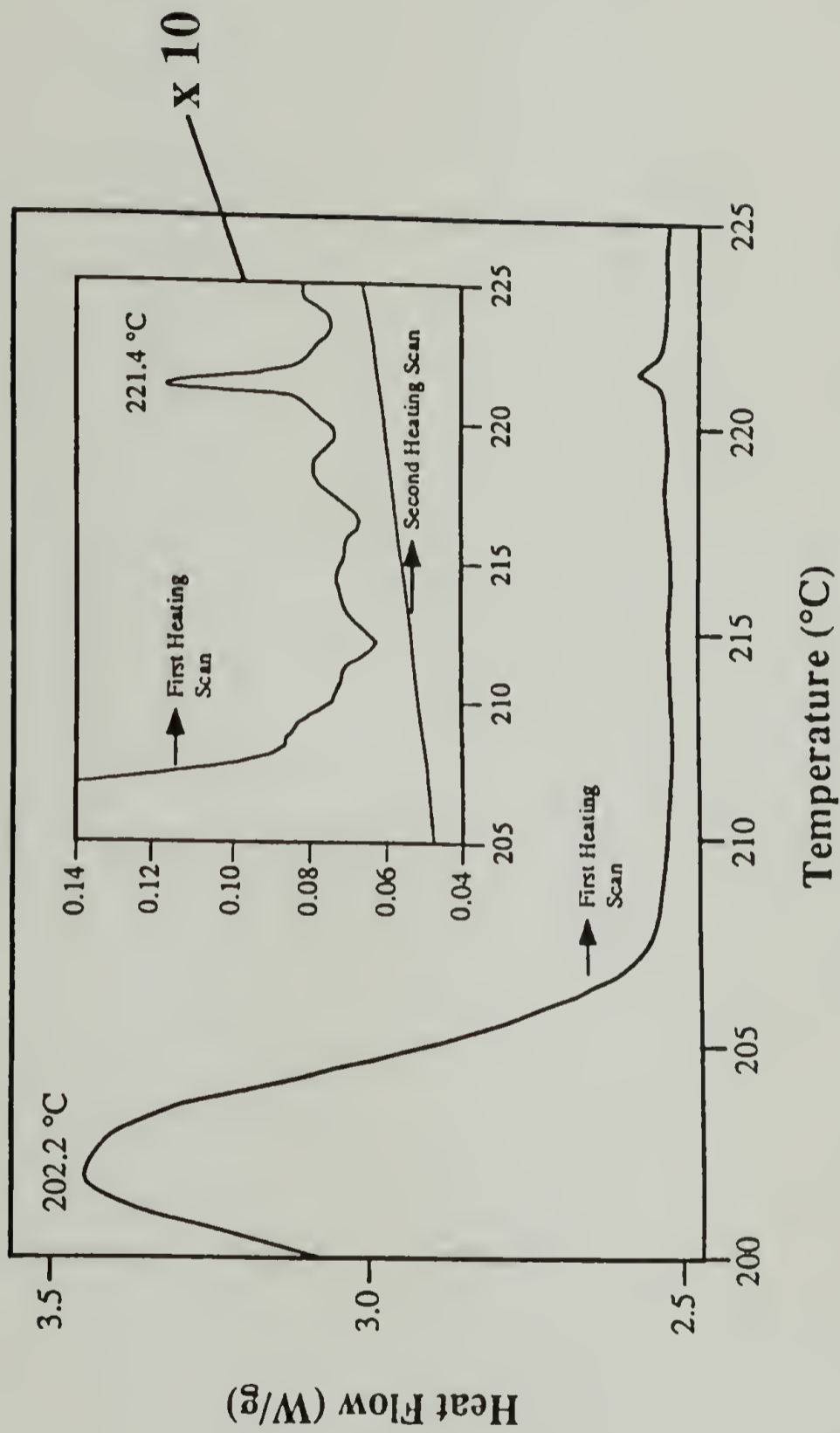
Figure 3.16 First and second 10 °C/min DSC heating traces of an 1,3-LCPU-6 fiber drawn from the melt, Soxhlet extracted in hot MeOH for 4 days, and annealed at 165 °C for 5 days. (See text for details.)
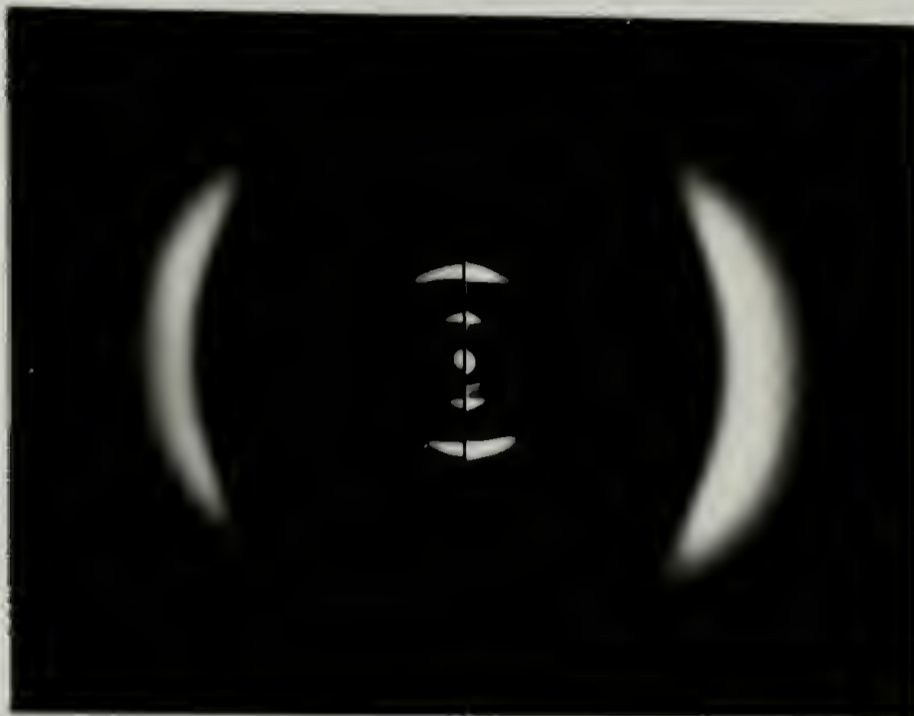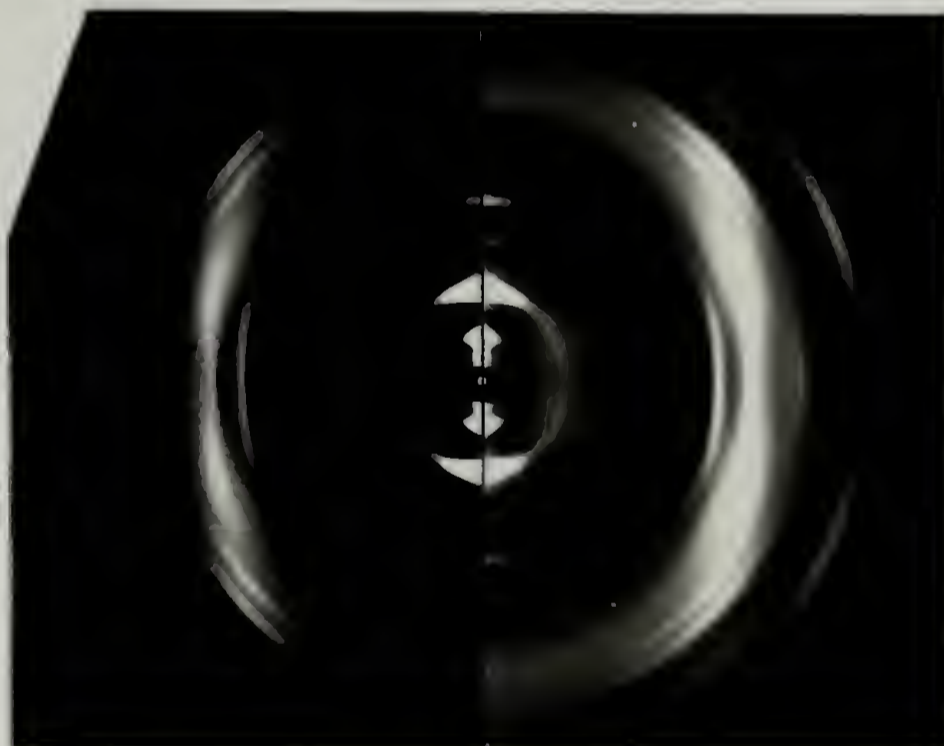
Figure 3.17 Room-temperature X-ray diffraction patterns of an 1,3-LCPU-6 fiber drawn from the melt, Soxhlet extracted in hot MeOH for 4 days (A), and annealed at 165 °C for 5 more days (B) (underexposed, left half; overexposed, right half).
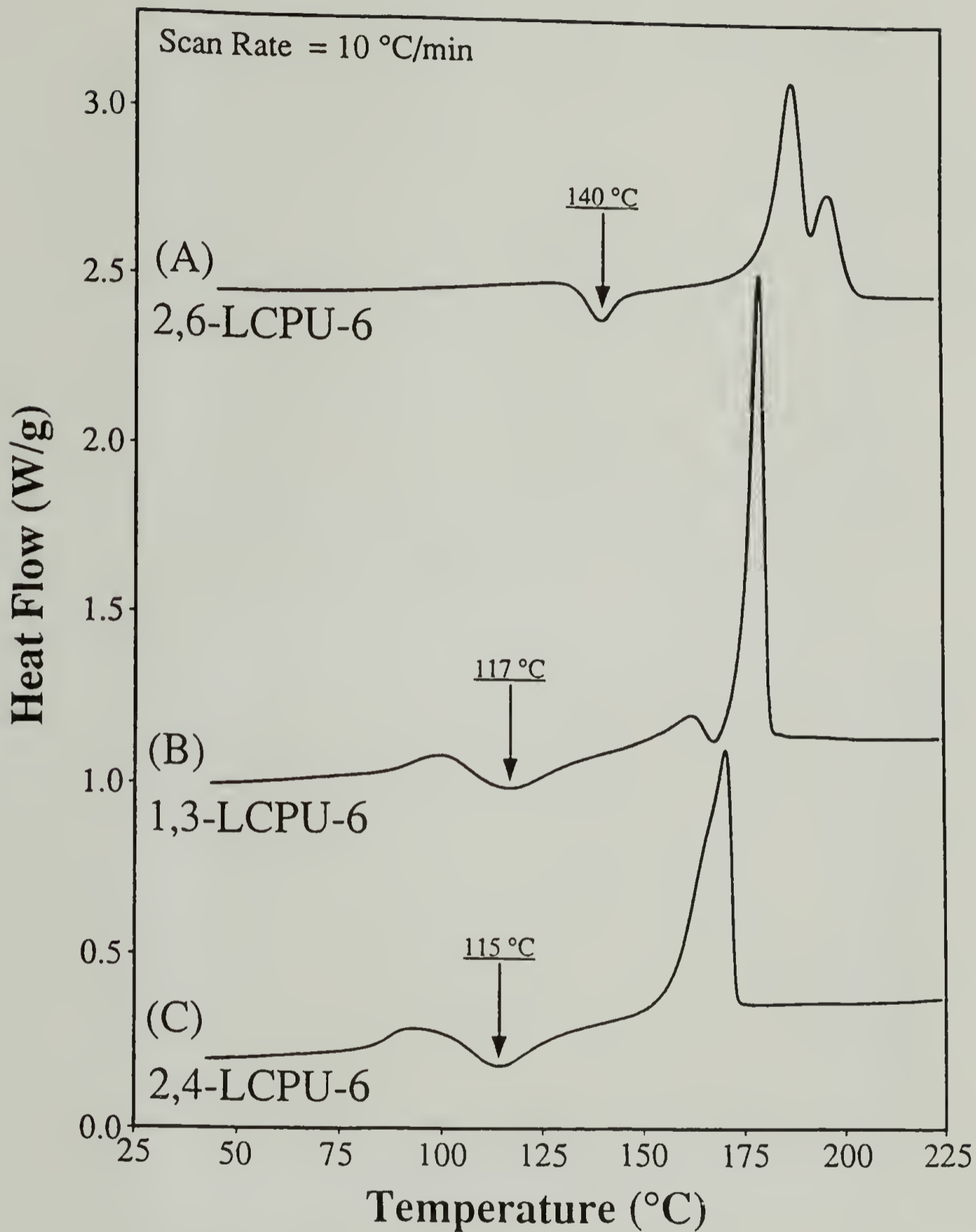
Figure 3.18 10 °C/min DSC heating traces of a 2,6-LCPU-6 [η] = 0.882 dL/g sample (A), an 1,3-LCPU-6 [η] = 0.402 dL/g sample (B), and a 2,4-LCPU-6 [η] = 0.60 dL/g sample (C), quenched into liquid N₂ from the melt.
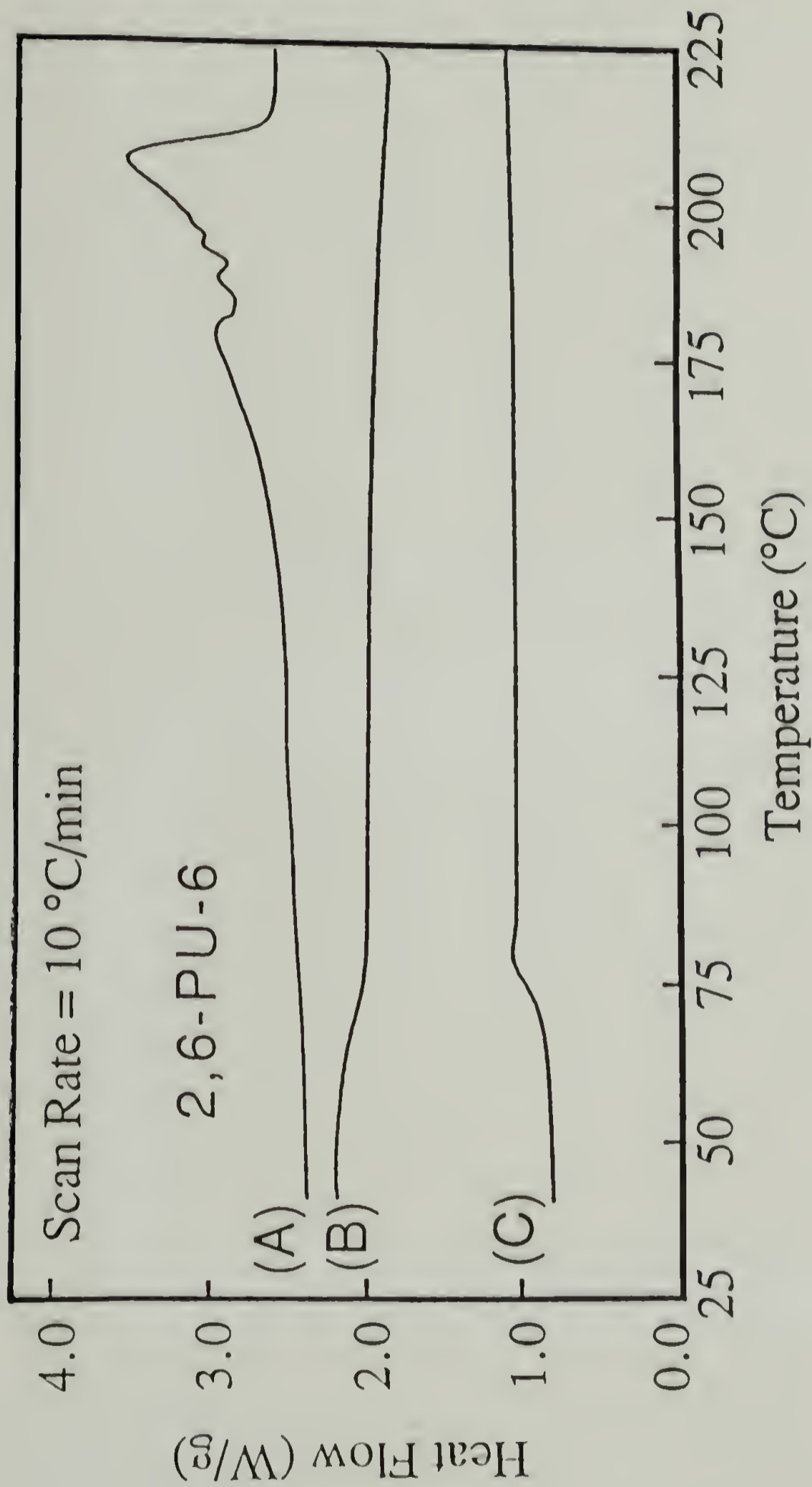
Figure 3.19 10 °C/min DSC traces of a fresh 2,6-PU-6 sample, Soxhlet-extracted in hot MeOH for 4 days: (A) first heating scan; (B) first cooling scan; (C) second heating scan.
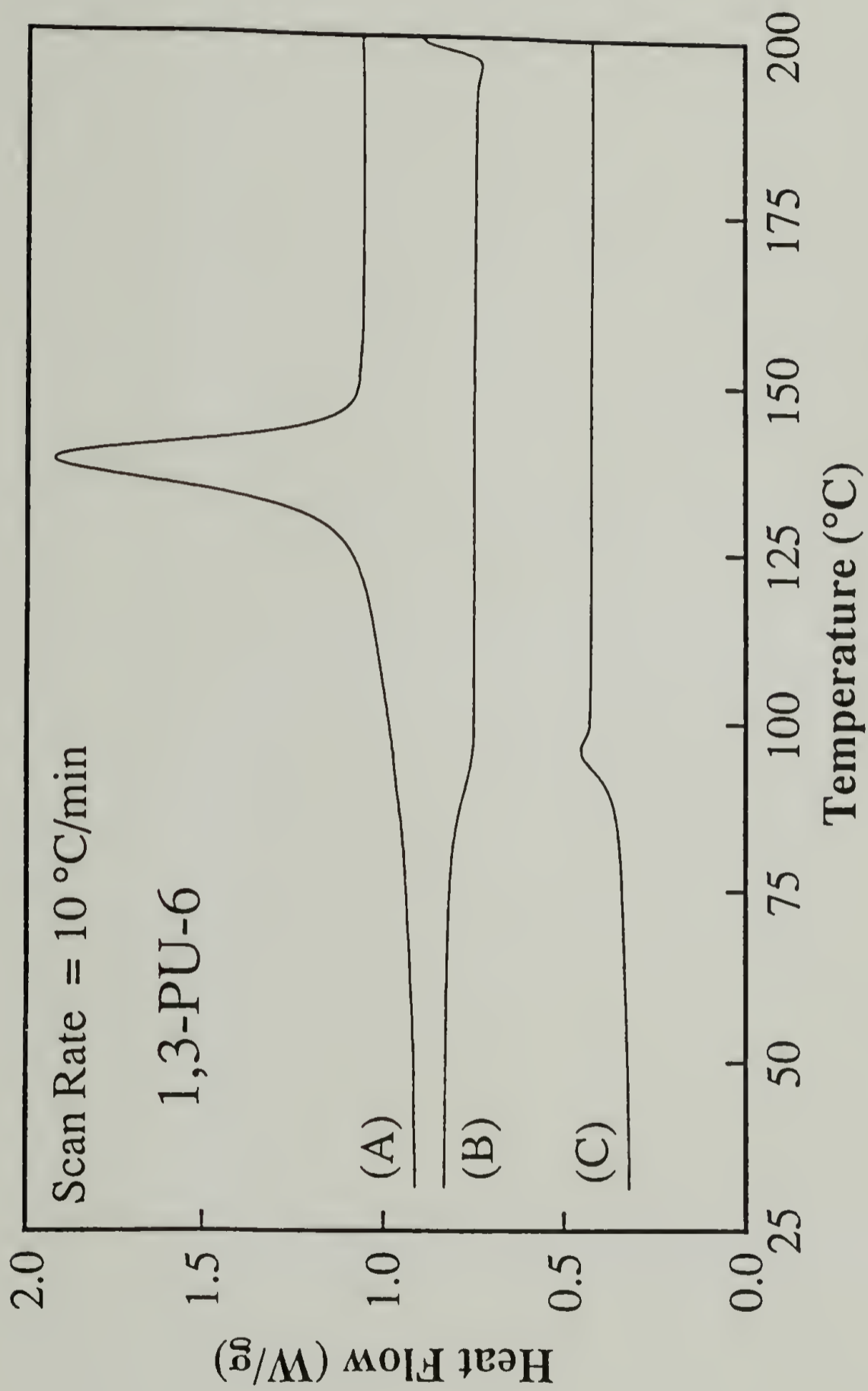
Figure 3.20. 10 °C/min DSC traces of a fresh 1,3-PU-6 sample, Soxhlet-extracted in hot MeOH for 4 days: (A) first heating scan; (B) first cooling scan; (C) second heating scan.

103
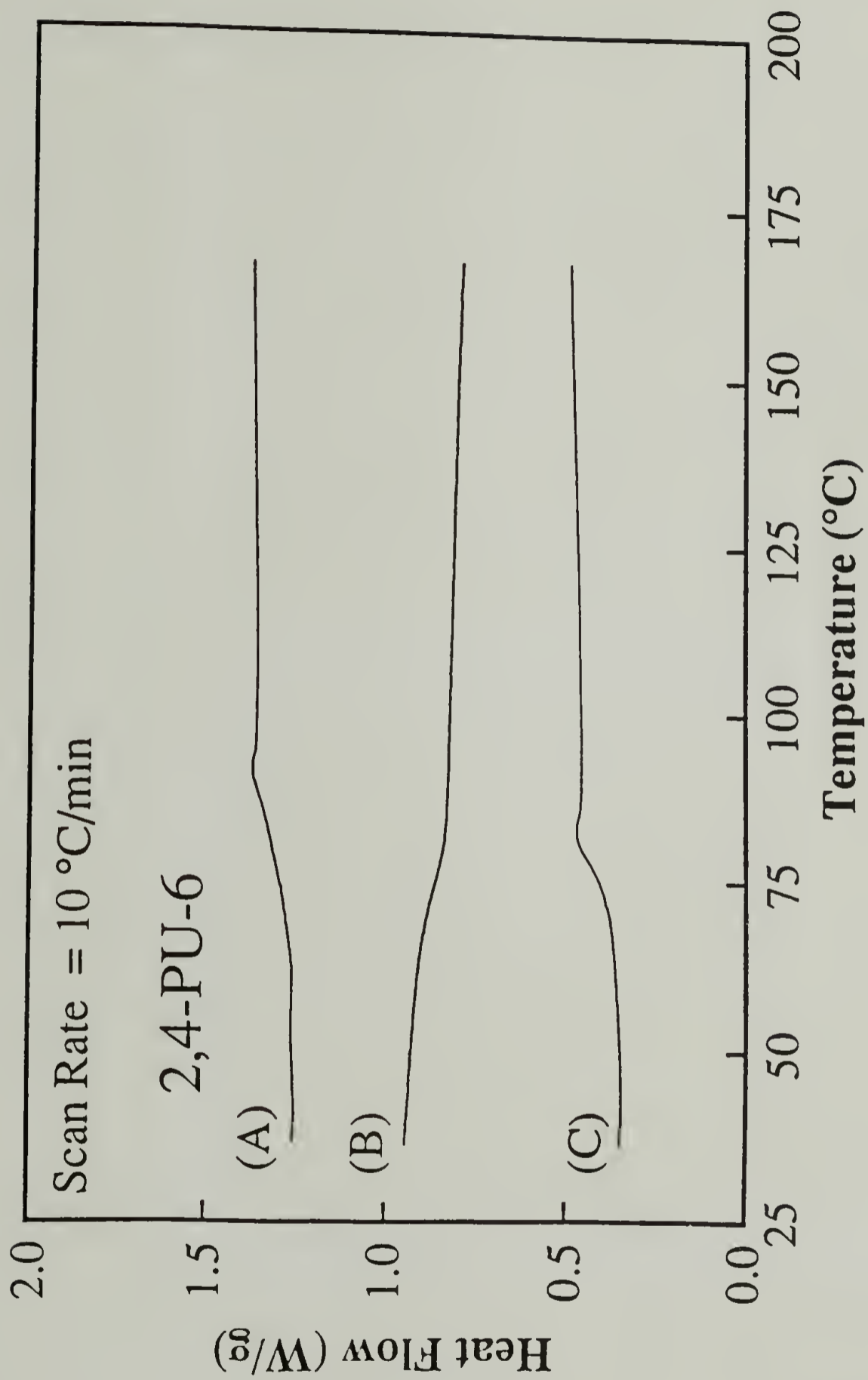
Figure 3.21. 10 °C/min DSC traces of a fresh 2,4-PU-6 sample, Soxhlet-extracted in hot MeOH for 4 days: (A) first heating scan; (B) first cooling scan; (C) second heating scan.

104

References

(1) Smyth, G.; Valles, E. M.; Pollack, S. K.; Grebowicz, J.; Stenhouse, P. J.; Hsu, S. L.; MacKnight, W. J. *Macromolecules* **1990**, *23*, 3389.

(2) Keller, A.; Ungar, G., To be published.

(3) Percec, V.; Keller, A. *Macromolecules* **1990**, *23*, 4347.

(4) Dyer, E.; Hammond, R. J. *Journal of Polymer Science: Part A* **1964**, 2, 1.

(5) Yang, W. P.; Macosko, C. W.; Wellinghoff, S. T. *Polymer* **1986**, *27*, 1235.

(6) Shriver, D. F.; Drezdzon, M. A. *The Manipulation of Air-Sensitive Compounds;* 2nd ed.; Wiley-Interscience Pub.: 1986.

(7) Wyckoff, R. W. G. *Crystal Structures;* 2nd ed.; Interscience Publishers: New York, 1963-1965; Vol. 5.

(8) Wunderlich, B. *Macromolecular Physics;* Academic Press: New York, 1973-80; Vol. (Vols. 1-3).

(9) Wunderlich, B. *Polymer Preprints* **1990**, *31 (1)*, 272.

(10) Gray, G. W.; Goodby, J. W. G. *Smectic Liquid Crystals;* Leonard Hill: Philadelphia, 1984.

(11) Stenhouse, P. J. Thesis, University of Massachusetts, 1992.

(12) Stenhouse, P. J.; Valles, E. M.; Kantor, S. W.; MacKnight, W. J. *Macromolecules* **1989**, *22*, 1467.

(13) Hong, S. K.; Blackwell, J. *Polymer* **1989**, *30*, 225.

(14) Pollack, S. K.; Shen, D. Y.; Hsu, S. L.; Wang, Q.; Stidham, H. D. *Macromolecules* **1989**, *22*, 551.

(15) Blackwell, J.; Gardner, K. H. *Polymer* **1979**, *20*, 13.

(16) Kazaryan, L. G.; Tsvankin, D. Y.; Ginzburg, B. M.; Tuichiev, S.; Korzhavin, L. N.; Frenkel, S. Y. *Vysokomol. Soyedin.* **1972**, *A14*, 1199.

(17) Conte, G.; D'Ilario, L.; Pavel, N. V.; Snamprogetti, S. A.; Giglio, E. *J. Polym. Sci., Polym. Phys. Ed.* **1976**, *14*, 1553.

(18) Pouget, J. P.; Jozefowicz, M. E.; Epstein, A. J.; Tang, X.; MacDiarmid, A. G. *Macromolecules* **1991**, *24*, 779.

(19) McCammon, J. A.; Harvey, S. C. *Dynamics of Proteins and Nucleic Acids;* Cambridge University Press: Cambridge, England, 1987.

(20) Mayo, S. L.; Olafson, B. D.; Goddarrd, W. A. *J. Phys. Chem.* **1990**, *94*, 8897.

(21) Burns, G.; Glazer, A. M. *Space Groups for Solid State Scientists;* 2nd ed.; Academic Press: New York, 1990.

(22) Henry, N. F. M.; Lonsdale, K. *International Tables for X-ray Crystallography*; Kynoch Press: Birmingham, England, 1969; Vol. 1.

(23) Leadbetter, A. J.; Norris, E. K. *Mol. Phys.* **1979**, *38*, 669.

(24) Azaroff, L. V. *Mol. Cryst. Liq. Cryst.* **1980**, *60*, 73.

(25) Doucet, J. In *The Molecular Physics of Liquid Crystals*; G. R. Luckhurst and G. W. Gray, Ed.; Academic Press: 1979; pp 317-341.

(26) Singler, R. E.; Willingham, R. A.; Noel, C.; Bosio, L.; Atkins, E. *Macromolecules* **1991**, *24*, 510.

(27) Tsukruk, V.; Shilov, V.; Lipatov, Y. *Macromolecules* **1986**, *19*, 1308.

(28) Tsukruk, V.; Shilov, V. *Polymer* **1990**, *31*, 1793.

(29) Sato, M.; Komatsu, F.; Takeno, N.; Mukaida, K. *Makromol. Chem., Rapid Commun.* **1991**, *12*, 167.

(30) MacKnight, W. J.; Yang, M. *Journal of Polymer Science, Symposium Series* **1973**, *42*, 817.

(31) Vladimirov, S. V. *Vysokomol. soyed.* **1985**, *A27*, 1757.

CHAPTER 4

INFRARED (IR) SPECTROSCOPIC PHASE CHARACTERIZATION

Introduction

In the previous Chapter of this dissertation, the phase behavior of the thermotropic liquid crystal polyurethane poly(4,4'-bis(6-hydroxyhexoxy)biphenyl-2,6-tolylene diisocyanate) (2,6-LCPU-6) was examined with emphasis on the mesophase structure
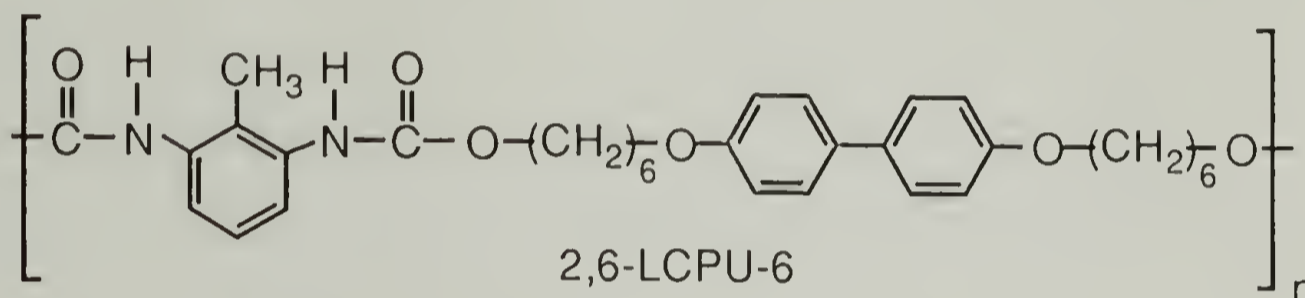
2,6-LCPU-6

characterization. Detailed thermal, wide-angle X-ray scattering (WAXS), and optical microscopy investigations have shown that 2,6-LCPU-6 is a monotropic[1,2] liquid crystalline polymer, with its isotropic to mesophase transition 60-70 °C lower than the crystal melting transition. One of the most striking characteristics of this polymer is the rapid crystallization of the vitrified mesophase upon heating, which occurs 50-60 °C lower than the crystal melting transition.

While the microstructural changes and dynamics that govern enantiotropic[1,2] liquid crystal phase behavior have been active and growing areas of study among the scientific community[3-11], comparatively little attention has been paid to monotropic liquid crystals. This arises from the absence of the traditional crystal to mesophase transition observed in enantiotropic liquid crystals, making them easily amenable to such studies. In the case of 2,6-LCPU-6, heating the vitrified mesophase above its melting point results in a well

defined mesophase to crystal transition, just the reverse of the enantiotropic case. Therefore, it can be treated in a fashion similar to the transition in enantiotropic liquid crystal polymers.

Vibrational spectroscopy is one of the principal techniques for examining chain-chain interactions and conformational order in polymers,[12-16] and their temperature dependencies. Provided that band overlapping does not occur, the various functional groups in the chemical repeat unit of 2,6-LCPU-6 can yield useful information about the degree of conformational order[16,17], the degree of self association in the urethane moieties[18-21], and other intra- and intermolecular interactions of rigid aromatic units.[12] Yang et al.[5] using specifically labeled partially-deuterium-substituted molecules were able to determine the extent to which the disordering of aliphatic chains contributes to the overall entropy of phase transitions compared to the contribution of rigid aromatic groups in discotic liquid crystalline systems. The strong and specific hydrogen-bonding interactions in polyurethane systems lead to infrared bands sensitive to chain packing. Lee et al.[22] utilized this observation to determine the degree of phase separation in segmented polyurethane elastomers.

The polyurethane used in this study (2,6-LCPU-6) as well as the isomeric 2,4-LCPU-6 and 1,3-LCPU-6(see Chapter 2,3) provides three regular alternating moieties, based on different functionalities.[23-25] The rigid biphenol units and TDI moieties may be used to probe the contribution of the intermolecular forces that lead to the ordering of the liquid crystalline and crystalline phases[12] On the other hand the hexamethylene sequence may provide a measure of the intramolecular disorder through the trans-gauche ratio[3,12,16,17] present in it. With the combination of vibrational spectroscopy which provides a measure of the localized structure, along with DSC, WAXS, and optical microscopic measurements (which examine the long-range order of the sample), we hope to provide a better understanding of the microstructural changes occurring in the different phases.

The present work is a continuation of the vibrational spectroscopic investigation of mesogen containing polyurethanes. Previous efforts by Pollack et al.[23,25] and by Shen et al.[24] on the 2,4-LCPU-6 did not address all the microstructural changes occurring in the different phases. The reason for this lies in the structure of 2,4-LCPU-6. The random placement of the methyl group along the polymer backbone results in slower crystallization of the vitrified mesophase upon thermal treatment than is the case with 2,6-LCPU-6. This leads to a coexistence of both the mesophase and crystal state, complicating the interpretation. 2,6-LCPU-6 with its highly regular structure and sharp crystallization from the vitrified mesophase does not present the above problems.

Experimental

Materials. The synthesis of 2,6-LCPU-6 has been described elsewhere in Chapter 3. In this study, all of the 2,6-LCPU-6 samples had an intrinsic viscosity of 0.400 dL/g at 30.0 °C, corresponding to the low molecular weight sample described in the previous Chapter of this dissertation.

Characterization Techniques. Thin films of 2,6-LCPU-6 were prepared by casting a 2% (w/v) solution of the polymer in 1,1,1,3,3,3-hexafluoro-2-propanol (99.8+%, Aldrich) (HFIP) onto disposable aluminum pans (for DSC and WAXS), glass slides (for optical microscopy), and potassium bromide windows (for IR), at room temperature. Following the fast evaporation of most of the solvent, in a laminar flow hood, the samples were vacuum dried at 60 °C overnight to remove residual HFIP. The complete removal of solvent was confirmed by the absence of the specific IR bands of HFIP.

Differential scanning calorimetric (DSC) measurements were conducted with a Perkin-Elmer DSC-7, employing a 20 mL/min flow of dry nitrogen as a purge gas for the sample and reference cells. The coolant was an ice-water bath. The temperature and power ordinates of the DSC were calibrated with respect to the known melting point and heat of fusion of a high-purity indium standard.

Room-temperature X-ray diffraction (XRD) patterns were recorded on flat films with a Statton X-ray camera using Ni-filtered Cu Kα radiation. The sample was contained in 1.5-mm Lindemann glass tubes and was mounted directly on the pinhole with the help of a double stick tape. The X-ray camera length was calibrated with the 2.319-Å diffraction line of NaF and 3.035-Å diffraction line of $CaCO_3$. The X-ray films were measured for interplanar spacing data with a Supper circular film measuring device. Furthermore, from the powder pattern films, the radial XRD profiles were obtained with the use of an Optronics C-4500 2D microdensitometer and the Polygraf X-ray diffraction software.[26]

Optical microscopy was described in the experimental section of Chapter 2.

Infrared spectroscopic data were obtained using an IBM model 32 Fourier transform infrared spectrometer. Spectra were collected at 2-cm^{-1} resolution. A minimum of 40 scans was signal averaged and the spectrum was stored on magnetic storage media. The films used in this study were sufficiently thin to be within an absorbance range where the Beer-Lambert law is obeyed. Elevated temperature spectra were obtained by placing thin films between potassium bromide windows, in a temperature-controlled cell. The temperature was monitored via a thermocouple placed adjacent to the KBr windows and was controlled within 1 °C. The heating rate was 20 °C/min from room temperature to 90 °C, and 5 °C/min from 90 to 220 °C. Before each spectral acquisition the temperature was kept constant for 10 min to ensure complete temperature equilibration along the sample cell. At the end of the first heating scan (up to 220 °C), the sample was cooled slowly to room temperature, followed by a second, third, and fourth heating scan in a similar fashion.

Results and Discussion

As has been discussed in Chapter 3, the 2,6-LCPU-6 requires cooling rates much faster than 100 °C/min in order to avoid homogeneous nucleation and crystallization and to bring the sample into the mesophase. It is easily understood that this kind of behavior makes difficult the preparation of thin films with mesophase morphology appropriate for

spectroscopic analysis. The need for a quick and versatile way of producing such films led to a study of the casting behavior of 2,6-LCPU-6 from a variety of solvents, such as dioxane, THF, DMSO, DMAC, DMF, and HFIP. The solubility of 2,6-LCPU-6 in the above solvents increases in the order listed, and for the low boiling point ethers such as dioxane and THF, elevated temperatures need to be employed. Casting a 2% (w/v) solution of the polymer in the above solvents (except HFIP), at room temperature, resulted mainly in films with crystalline morphology* due to crystallization prior to solvent removal. On the other hand, the great solubility power of HFIP,[27] along with its low boiling point (b.p. = 59 °C), produced a thin film with the desired mesophase morphology. Before we proceed with the vibrational analysis of these thin films, it is essential to understand their structure and morphology in more detail.

Differential Scanning Calorimetry: Typical 10 °C/min heating and cooling traces of 2,6-LCPU-6 thin films cast from HFIP are illustrated in Figure 4.1. Upon the first heating scan (a), the familiar step in heat capacity, corresponding to the glass transition (T_g), is observed at approximately 72 °C, along with a small enthalpy relaxation[28] endotherm peaking at 76 °C. This rather distinct glass transition behavior compared to the broad step in heat capacity generally obtained from melted samples (Figure 4.4) was the first indication of the amount of disorder present in the cast films due to the rapid solvent evaporation. The exotherm peaking at 133 °C ($\Delta H = 6.6$ J/g; $\Delta S = 1.6 \times 10^{-2}$ J/g·K) is the most important feature in this DSC heating scan. In Chapter 3 the nature of this exotherm was discussed extensively and it has been attributed to the mesophase-crystal transition. Cheng et al.[29] observed similar behavior with a thermotropic polyether, and they characterized it accordingly as arising from the monotropic nature of the liquid crystal. This exothermic transition upon heating is the characteristic signature of the monotropic liquid crystalline state. It arises primarily from the greater thermodynamic stability of the crystalline phase versus the mesophase, which defines the thermodynamic potential for this

---

* DSC and WAXS analyses were used to characterize the sample morphology.

transition. A schematic plot of the temperature dependence of the Gibbs free energy (Figure 4.2) is a convenient way to express the relative thermodynamic stability of the crystalline, liquid crystalline, and liquid phases. The solid lines in Figure 4.2 represent the equilibrium temperature dependences of each phase.** Additionally, kinetic factors such as sample mobility (which is a function of chain flexibility, mesophase structure, molecular weight, impurities, etc.) and chemical repeat regularity influence the overall process. According to Figure 4.2 (first heating scan), the mesophase-crystal transition must be located immediately above the mesophase-liquid "intersection", due to the limited mobility of the highly ordered (higher than smectic C) mesophase.

Following the 133 °C exotherm in Figure 4.1a we observe two endotherms with maxima at 186 and 197 °C. The overall ΔH_m from 116 to 204 °C is 40.1 J/g. These two peaks have been assigned to the crystalline melting transitions of two macroscopically distinct morphologies - a spherulitic morphology produced from slow cooling and a threaded crystalline morphology produced upon heating from the quenched mesophase. Similar behavior has been observed for the 2,4-LCPU-6, as well as other monotropic liquid crystalline polymers.[29] Upon cooling, a sharp exotherm around 157 °C followed by a 25 °C exothermic "tail" is observed. The overall ΔH_c from 121 to 165 °C is 40.6 J/g. This exotherm was discussed in the previous Chapter of this dissertation and attributed to a combined mesophase-crystallization process. The slow cooling rate (10 °C/min) of the first cooling scan resulted in a crystalline sample, as proven by the absence of the 133 °C exotherm in Figure 4.1c. Therefore, the second heating scan is expected to follow a different route on the temperature dependent Gibbs free energy diagram of Figure 4.2, indicated by the thick broken curve, showing only a crystal melting transition. This in fact occurs, with the two familiar melting endotherms at 188 °C and 197 °C. The overall ΔH_m from 133 to 202 °C is 40.3 J/g, almost identical with its counterpart from Figure 4.1a (40.1 J/g).

** Note that each sample can be a composite of many individual phases.

X-ray Diffraction and Optical microscopy: Figure 4.3 illustrates the radial X-ray diffraction (XRD) profiles of these thin films as a function of thermal history. The temperatures noted on Figure 4.3 represent the maximum temperatures to which these films were exposed during a 10 °C/min heating scan, followed by a quick quench to room temperature. The room temperature (35 °C) radial XRD profile verifies the low degree of order of these films upon casting, previously inferred from the DSC T_g behavior. The poorly resolved 002, 004, and 008 smectic layer reflections at 27.3 Å ($2\theta = 3.24°$), 13.7 Å ($2\theta = 6.45°$), and 6.8 Å ($2\theta = 13°$), respectively, correspond to a 54.9-Å repeat, much shorter than the 57.6 Å of the melt-quenched sample. The broad and diffuse wide angle reflection with a maximum at 4.5 Å ($2\theta = 19.8°$) is a product of the convolution of the 4.5 Å ($2\theta = 19.8°$), 4.0 Å ($2\theta = 22°$), and 3.3 Å ($2\theta = 27°$) reflections. The strongest 4.5-Å reflection arises from lateral stacking of the biphenyls, while the other two wide-angle reflections arise from the dimensional correlation of the TDI moieties. Evidently the rapid solvent evaporation results in a less ordered smectic structure with a repeat distance almost 3 Å shorter than the "equilibrium", higher than smectic C, mesophase structure. Further proof of the mesophasic character of these thin films comes from the *schlieren* textures observed under the polarizing optical microscope. These *schlieren* textures are similar to those discussed in Chapter 3.

Upon temperature increase this poorly ordered smectic structure transforms slowly into a more highly ordered one, as shown by the (125 °C) radial XRD profile of Figure 4.3. The highly resolved 002, 004, and 008 smectic layer reflections correspond to a 58.1-Å repeat, almost identical to the 58.2-Å repeat from the melt-quenched sample heated at 125 °C. The strong correlation of the smectic layers imposes a better lateral stacking of the chains which results in stronger and sharper wide-angle reflections (4.5, 4.0, and 3.3 Å). Upon further temperature increase the mesophase to crystal transition takes place, clearly indicated by the (160 °C) radial XRD profile of Figure 4.3. The 002 and 004 reflections of

the (160 °C) curve correspond to a 58.5-Å repeat which is in complete agreement with the bulk 2,6-LCPU-6 crystal sructure.

A careful observation of the two crystal melting endotherms of Figure 4.1a shows that they are separated by a small exotherm, indicative of a melting-recrystallization[30] process. This process occurs faster in the solvent cast films than in the samples quenched from the melt. However, samples previously annealed at 165 °C, show little melting-recrystallization between the higher and the lower peak, as indicated at Chapter 3. Apparently, the method of sample preparation controls the degree of chain entanglement as well as the free volume, affecting drastically the behavior of this strongly intermolecularly interacting system. Further demonstration of the effect of sample preparation upon the underlying transitions is presented in Figure 4.4. A rapid examination of the four scans (Figures 4.4a-c and 4.1a) indicates that all of them look very much alike, except that of Figure 4.4c which possesses an additional endotherm at 113 °C, 20 °C below the mesophase-crystal transition. As a result of MeOH soxhlet extraction the sample of Figure 4.4c has been shown in Chapter 3 to exhibit a perfected mesophase structure and macroscopic morphology. In addition, the enthalpy associated with the 113 °C endotherm is almost the same as that of the 133 °C exotherm (Table 4.1). This sort of behavior suggests a mesophase melting prior to crystallization. For the rest of the quenched samples, mesophase imperfections result in melting over a broad temperature range, and make this transition diffuse and difficult to observe. The fact that this peak occurs 30-40 °C higher than the T_g, rules out the possibility that it is an enthalpy relaxation peak from a more ordered "mesophase glass" (see Chapter 2).

Table 4.1 lists the transition temperatures and enthalpies observed for the four different techniques of freezing the sample into the mesophase (Figures 4.4 and 4.1a). Moving from left to right, the mesophase-crystal transition temperatures show an apparent trend toward lower temperatures. The same trend, only much weaker, can be noted for the threaded morphology crystal melting temperatures, indicating that these crystals developed

from the mesophase. In contrast to the above, the spherulitic morphology crystal melting temperature remains constant at 197 °C. The explanation of these phenomena lies in the method of sample preparation. Solvent treatment results in greater sample free volume and fewer chain entanglements, which yields greater mobility and lower transitions. On the other hand, the spherulitic morphology crystalline regions preexisted before the mesophase to crystal transition, making their melting temperatures insensitive to sample preparation.

Infrared Spectroscopy: The room-temperature infrared spectrum of a HFIP-cast 2,6-LCPU-6 thin film is illustrated in Figure 4.5. A total of 19 out of the 31 observable peaks and peak shoulders have been assigned (Table 4.2) from spectral comparisons of 2,6-LCPU-6, similar polymers and model compounds in the literature,[3,14,15,23,25] as well as of our own. Specifically the mesogenic polyurethanes 2,4-LCPU-6 and 1,3-LCPU-6 aid in the vibrational peak assignments of the meta-substituted phenylene ring (TDI moiety). On the other hand, normal polyurethanes like the 2,6-PU-6, 2,4-PU-6, and 1,3-PU-6, which are polycondensation products of hexanediol with 2,6-TDI, 2,4-TDI, and 1,3-PDI, respectively, aid in the peak assignments of the biphenol moiety. Last but not least, the low molecular weight diurethanes from the reactions of 2,6-TDI, 2,4-TDI, and 1,3-PDI with MeOH assist in the hexamethylene moiety peak assignments.

There are distinct differences between the spectra measured at room temperature and those at high temperatures, mainly due to peak shifts (Table 4.2) and intensity changes. Major differences can be identified between 3200-3500 cm^{-1} (N-H stretch region), 1690-1735 cm^{-1} (carbonyl stretch, amide I region), 1500-1550 cm^{-1} (amide II region), 1590-1600 cm^{-1} (TDI benzene ring C=C stretch region), 1600-1620 cm^{-1} (biphenyl C=C stretch region), and 810-830 cm^{-1} (biphenyl out-of-plane C-H wag region). The changes occurring in these regions in intensities, peak sharpness, and peak shifts, will be discussed in detail in order to understand the 2,6-LCPU-6 phase behavior better.

Figure 4.6 displays the amide I region recorded as a function of increasing temperature for the first and the second heating scan of a freshly cast thin film of 2,6-

LCPU-6 on a KBr window. The spectra in Figure 4.6 have not been arbitrarily scaled and are shown on an equal absorbance scale. It is well-known that the infrared absorbance of H-bonded urethane carbonyl appears at lower wavenumbers than that of free urethane carbonyl.[20,31,32] The amide I infrared spectra of semicrystalline samples such as nylons[33,34] and polyurethanes[23,35] have been reported to comprise distinct spectral features due to the degree of carbonyl H-bonding. It has been proposed that there are three overlapping peaks in the amide I region.[33] In order of increasing wavenumbers, these are H-bonded carbonyl groups in ordered ("crystalline") domains, H-bonded carbonyl groups in disordered ("amorphous") conformations, and non-H-bonded (free) carbonyl groups. Accordingly, the well-resolved peak in the vicinity of 1699 cm^{-1} in Figure 4.6 is assigned to the ordered hydrogen-bonded (crystalline) carbonyl stretch. Possible multiple peaks similar to those observed from the asymmetrically substituted 2,4-LCPU-6[23,35] are less likely to occur in 2,6-LCPU-6 due to the single type of urethane linkage (ortho to the methyl group of the TDI moiety) versus the dual type (ortho and para) in 2,4-LCPU-6.

It is apparent from Figure 4.6 that two distinct transitions occur in the spectral shape. The spectra for the first heating scan (Figure 4.6A) have been separated to facilitate visualization of a transition that involves the sudden appearance of the well defined ordered H-bonded carbonyl stretch above 120 °C. The second transition (isotropization) is easily observable in both first and second heating scans (Figure 4.6A,B) as an abrupt decrease in H-bonding at the melting point (above 180 °C). The fact that the third and fourth scans are identical to the second one excludes any possibility of sample decomposition. The freshly cast film has a mesophase structure as shown on the basis of DSC and X-ray scattering. The cooling rate in the IR experiments was less than 10 °C/min, so that any subsequent scans after the first one involve a crystalline sample.

To make these features clearer, we plotted the peak absorbance of each band as a function of temperature. There are a variety of methods to extract the peak absorbance from an IR spectrum. Some of them, such as the pseudo-base-line method, the subtraction

method, and the curve fitting method have been applied[15] to the present system. However, the pseudo-base-line method was used mainly, accompanied with curve fitting which will be discussed later.

Figure 4.7 illustrates the peak absorbance of the first and second heating scans as a function of temperature for the 1699 cm^{-1} ordered H-bonded carbonyl band (A) and the 2941 cm^{-1} CH$_2$ out-of-phase stretching band (B). The CH$_2$ out-of-phase stretching band has been used in the past as an internal standard for infrared thermal analysis of polyurethanes.[22,23,25] With that in mind, Figure 4.7B was included to prove that the changes in the peak absorbance of the ordered H-bonded carbonyl groups reflect intermolecular changes, rather than changes arising from sample thickness. In addition, there is no significant difference observed between the first and second heating scan. Furthermore, Figure 4.7(B) demonstrates the lack of sensitivity of the CH$_2$ out-of-phase stretching vibration to the phase transitions occurring within the temperature range of interest. The same is not true for the first and second heating scans of Figure 4.7(A). Apart from the melting transition above 180-200 °C, accompanied by a drastic decrease in the ordered H-bonded amide I absorbance in both scans, there is another transition around 130 °C in the first heating scan only. This corresponds to the mesophase-crystal transition, which is accompanied by a dramatic increase in the ordered H-bonded peak intensity during crystallization between 120 and 140 °C. This is in agreement with the results of Chapter 2, where it was established through H-bonding elimination that the mesophase arises primarily from the biphenol alignment, and the presence or absence of H-bonding is not important. Although this transition has been observed previously from DSC and X-ray diffraction, IR spectroscopy provides a technique to probe the localized microstructural changes taking place during this phase transition. In order to analyze the data quantitatively, it is necessary to resolve the amide I mode into its constituents.

As has been pointed out extensively,[33,34,36,37] deconvolution of overlapping peaks leading to a unique solution is generally not possible. Without previous knowledge of the

band shape, the number, position and breadth of the bands, base-line position, etc., one can arrive at almost any desired solution. Even with a knowledge of the number of bands, good prior estimates of the above-mentioned factors are necessary prerequisites for obtaining valid solutions. For this reason we followed step by step the well-established amide I deconvolution technique of Painter and Coleman.[33,34,37] In particular, the essential starting parameters were extracted from the analysis of semicrystalline nylon 11 of Skrovanek et al.[33].

In summary, each spectrum recorded at different temperatures was resolved into three components (two above the crystalline melting point), using the following procedure.

(1) The band shape of all three peaks was assumed to be Gaussian. Curve-fitting attempts allowing band shape to vary proved to favor the pure Gaussian band shape by a least squares criterion. Imposing Lorentzian band shape on the ordered H-bonded amide I peak changes substantially the relative values of the deconvoluted peak area but does not change the temperature dependence.

(2) A linear base-line was assumed from 1800 to 1630 cm^{-1} and minimized as well, during curve fitting. Although the "correct" base-line is rather subjective, the base-line choice again affects mostly the absolute values of the deconvoluted peak area but does not change the temperature dependence.

(3) Curve fitting was limited to the spectral data of the amide I region between 1800 cm^{-1} (left end) and 1630 - 1643 cm^{-1} (right end). The low-wavenumber end was determined as the minimum between the 1699 and 1608 cm^{-1} peak. Although the two peaks are well separated and the low-wavenumber end lies on a fairly shallow minimum, one can anticipate a certain degree of interference from the wing of the 1608 cm^{-1} peak with the base line. This deviation is just about visible at the right wing of each spectrum of Figure 4.8. This does not lead to significant error but is certainly the weakest point of the curve-fitting procedure.

Figure 4.8 presents the least-squares fitting results of the amide I region of a HFIP-cast, 2,6-LCPU-6 thin film from the first heating scan at 120, 140, and 220 °C. Each spectrum is representative of the series of spectra in between the two phase transitions mentioned above. The main component of the 120 °C spectra is the disordered H-bonded amide I band. This is consistent with the DSC and X-ray diffraction data showing that the sample exhibits smectic mesophase morphology. The higher than smectic C mesophase of 2,6-LCPU-6 has the required chain conformation to place both carbonyls of the TDI moiety in close proximity with the N-H groups of the neighboring TDI moiety. The variation in distance and angle between the neighboring N-H and C=O groups generates the large width at half-height ($W_{1/2,d}$) (55-60 cm^{-1}) of the disordered H-bonded amide I peak with respect to the 18-25 cm^{-1} and 14-15 cm^{-1} for the "free" and ordered H-bonded amide I peaks. Above the mesophase to crystal transition (140 °C) the ordered H-bonded amide I peak increases by more than a factor of 2 compared to the disordered one, as would be expected for this transition. Upon further heating, sample isotropization occurs, manifested by the disapearance of the ordered H-bonded amide I peak in the 220 °C spectrum.

The detailed results of the curve fitting of the amide I region throughout the temperature range 25-220 °C are given in Tables 4.3 and 4.4 for the first and second heating scans, respectively. The curve-fitting data summarized in Tables 4.3 and 4.4 are plotted in Figures 4.9 - 4.11 to facilitate better visualization of the underlying transitions. The changes in the areas of the ordered (A_o) and disordered (A_d) H-bonded amide I peaks (Figure 4.9) show unequivocally that the 130 °C transition is associated with the mesophase to crystal transition. It is characteristic that the entire fraction of carbonyl groups which transform to the crystal (ordered) phase originates from the mesophase (disordered H-bonded carbonyl groups), while the "free" carbonyl content shows a monotonic increase. The same transition is also visible from the peak position and width at half-height of the ordered and disordered H-bonded amide I peaks in Figures 4.10 and 4.11, respectively. The 130 °C transition is reflected by a sudden decrease in the peak

frequencies of both H-bonded carbonyl groups (Figure 4.10). This is indicative of a substantial lateral ordering taking place in both phases. On the other hand, while the width at half-height of the ordered H-bonded amide I peak continues to shift to lower values as anticipated, the disordered one shows a different behavior. Below 130 °C this peak arises from the mesophase which perfects itself and narrows its width at half-height. Above 130 °C the nature of this peak changes. An assembly of imperfect crystalline domains (portion of the mesophase which did not manage to achieve crystalline order) along with the remaining amorphous fraction contributes to the width increase observed.

Although the main goal of the curve-fitting analysis was to analyze the mesophase to crystal transition, it also proved useful in the analysis of the melting transitions. In the DSC section we observed the melting behavior of crystalline regions with different macroscopic morphologies. The first heating scan resulted (through a melting-recrystallization process) in the higher melting point spherulitic rich sample (Figure 4.1a). On the other hand, the slow cooling rate of the first cooling scan resulted in a threaded texture rich sample which melts at a lower temperature (Figure 4.1c). Figure 4.9 reflects these features. Characteristically, the lower value of the A_0 at 180 °C versus the 160 and 200 °C values reinforces the evidence for a melting-recrystallization process taking place during the first heating scan. Figures 4.10 and 4.11 indicate substantial changes in the disordered H-bonded carbonyl portion above 180 °C. It is worth noting that these changes occur prior to the melting of the crystalline domains (188 and 197 °C from DSC). This suggests that above 180 °C imperfect crystalline domains cannot exist. Therefore, the disordered H-bonded amide I peak changes in this temperature region are identified with a molten, quite mobile H-bonded carbonyl groups shifting its frequency 10 cm^{-1} higher and its width at half-height 7 cm^{-1} lower. On the other hand, the changes in the "free" amide I peak are much smaller upon melting and mostly occur also above 180 °C.

As pointed out previously,[33,37] unlike the N-H stretching region, the total area of the amide I region (A_I) does not vary appreciably with temperature, and the absorptivity

coefficients can be assumed the same for the three different bands. Skrovanek et al.[33] in their study of nylon 6 reported the total area of the amide I region to vary approximately 7%. Tables 4.3 and 4.4 as well as Figure 4.9 indicate a 5 and 7% variation for the first and second heating scan respectively. The values of A_t for the first heating scans, were found to be 5 - 6% lower than those for the second heating scan. We believe that this arises primarily from the quick solvent evaporation that produces a slightly opaque thin film which contributes to scattering. The same values of A_t above the melting point provide adequate proof of the validity of the above argument. Figure 4.10 indicates that all three peaks of the first scan exhibit peak positions (ν) at higher wavenumbers than those of the second scan, below the melting point. This is a clear manifestation of the effect of fast solvent evaporation on the average hydrogen bonding that affects the strength of the intermolecular interactions as well as the sample free volume.

A measure of the inaccuracy of our curve-fitting analysis is indicated from the ν_f curves of Figure 4.10. Theoretically the two lines should coincide. By taking the average of the two n_f and not allowing the computer to vary it, we derive less than 1% error in the area values of A_f and A_d and much less for the A_o. In the same study of nylon 11, referenced above, Skrovanek et al. reported that the fraction of ordered H-bonded amide groups in nylon 11 provides a good estimate of the sample crystallinity. On the basis of a similar argument, we can estimate our sample crystallinity to be between 18 and 19% (Tables 4.3 and 4.4).

In the N-H stretching region (3500 - 3200 cm-1) of 2,6-LCPU-6 the peak observed at 3290 cm-1 is assigned to the ordered H-bonded N-H stretch,[32,38] while the shoulder at 3430 cm-1 is typically assigned to the "free" N-H stretch. Infrared spectroscopic data of polyamides and polyurethanes in the N-H stretching region have been used in the past to calculate some thermodynamic parameters.[39,40] However, Coleman et al.[20,33,37,41] pointed out the strong dependence of the extinction coefficient upon frequency, which is highly affected by the H-bond strength. Unlike the amide I vibration which is sensitive to

conformation through dipole-dipole interactions, the N-H stretching mode is more or less conformationally insensitive. Therefore, we did not attempt to extract information similar to that obtainable from the amide I mode but systematically monitored the temperature dependence of the peak absorbance of the ordered H-bonded N-H stretch (Figure 4.12A). Features similar to those observed in the carbonyl stretching region can be seen here. Molecular simulations of the 2,6-LCPU-6 indicate complete H-bonding formation between the N-H and C=O groups in the crystal lattice. Therefore, it is expected for the N-H stretching region to behave similarly to that of the carbonyl. Figure 4.12B shows the peak absorbance of the amide II region (1526 cm^{-1}) as a function of temperature. Its features are almost identical to those of the H-bonded C=O and N-H stretch mentioned previously.

Figures 4.7 - 4.12 described the changes in H-bonding during the mesophase-crystal transition. It is also of interest to monitor the behavior of the mesogenic moiety during this process. Figure 4.13A depicts the temperature dependence of the peak absorbances for two different vibrational modes of the biphenyl benzene ring. The peak at 823 cm^{-1} is assigned to the out-of-plane C-H wag of the biphenyl, while the 1608 cm^{-1} peak is assigned to the biphenyl C=C stretch, and their peak absorbances are displayed on the upper and lower parts of Figure 4.13A, respectively. Although the exact influence of the intermolecular interactions on these vibration modes is not fully established, it is noteworthy to mention the following features. These peaks, associated with the biphenyl moiety, exhibit relatively small changes in the vicinity of the mesophase-crystal transition and somewhat greater changes at the melting transition (Figure 4.13A). In Figure 4.13B the temperature dependence of the 1594 cm^{-1} C=C stretch in the TDI moiety is displayed. This band exhibits behavior similar to that of the bands associated with H-bonding (Figures 4.7A and 4.12A,B). The direct bonding of the tolylene ring (C=C stretch) to the urethane groups that undergo extensive H-bonding must be largely responsible for this result. An explanation can be proposed either on the basis of the presence of a coupled vibration mode between the benzene ring C=C stretch and the adjacent urethane groups, which undergo

extensive H-bonding, or upon changes of the spatial arrangement of the bulky tolylene ring during crystallization. Molecular simulations integrated with crystallographic analysis of 2,6-LCPU-6, presented in Chapter 5, reveal considerable changes in the spatial arrangement of the TDI rings upon crystallization in order to accommodate their bulky methyl group, but this argument alone is not sufficient to discriminate between the two alternative explanations.

Specific methylene bands, such as CH_2 rocking and CH_2 wagging, have been used extensively to analyze alkyl chain conformations from the infrared spectra of low and high molecular weight compounds.[12,13,16,17] The intense CH_2 rocking bands in the vicinity of 730 cm-1 from trans sequences, as well as some specific bands such as gtg', gg, and gtt (end gauche), and (gtg and gtg') in the 1300-1400 cm-1 region, have been heavily utilized for this purpose. Unfortunately, we were unable to assign these peaks definitively, because they were overlapped by other rather intense vibration peaks of 2,6-LCPU-6.

Conclusions

(1)   DSC, WAXS, polarized optical microscopy, and infrared spectroscopy indicate that fast solvent evaporation from HFIP solutions results in 2,6-LCPU-6 thin films with a glassy mesophase morphology.

(2)   The mesophase to crystal exothermic transition (monotropic liquid crystal) has been observed by DSC between 130 and 140 °C, depending on sample preparation. At 10 - 20 °C below this transition, the mesophase melting occurs, which provides adequate mobility for crystallization.

(3)   Curve fitting analysis of the conformationally sensitive amide I region resulted in a quantitative assessment of the temperature depedence of H-bonding. The behavior of the H-bonds correlated well with that expected from the results of calorimetric and WAXS studies.

(4)   The mesophase to crystal transition has been observed by infrared spectroscopy to be between 120 and 140 °C, primarily on the basis of the substantial increase of the ordered H-bonded amide I peak and the decrease of the disordered H-bonded amide I peak in this temperature ramp. The crystal melting transition occurs between 180 and 210 °C and is accompanied by the complete disappearance of the ordered H-bonded amide I peak along with substantial changes in the frequency and width at half-height of the disordered H-bonded amide I peak.

Table 4.1

DSC transition temperatures and enthalpies from Figure 4.4 and 4.1a. (10 °C/min heating scans.)

Transition element	Melt, quenched in liquid N_2 (Figure 4a)	Fiber drawn from the melt (Figure 4b)	Fiber, soxhlet extracted in hot MeOH (Figure 4c)	Thin film, cast from HFIP (Figure 1a)
Mesophase melting temp.*	- -	- -	113 °C	- -
Mesophase - crystal transition temp.	140 °C	136 / 141 °C	133.1 °C	133.0 °C
Threaded morphology crystal melting temp.	189.0 °C	188.2 °C	187.8 °C	186.4 °C
Spherulitic morphology crystal melting temp.	197 °C	197 °C	197 °C	197 °C
Mesophase melting enthalpy.*	- -	- -	7.0 J/g	- -
Mesophase - crystal transition enthalpy	- 5.8 J/g	- 4.2 J/g	- 6.6 J/g	- 6.6 J/g
Overall crystal melting enthalpy	47.2 J/g	39.4 J/g	40.8 J/g	46.7 J/g

* see text for details.

125

Table 4.2

Infrared band assignments for 2,6-LCPU-6.

Peak frequency (cm⁻¹) at		Assignment
25 °C	200 °C	
3430‡	3430‡	free N-H stretch
3290	3307	H-bonded N-H stretch
3039	3034	aromatic C-H stretch
2941	2940	CH_2 stretch (out-of phase stretch)
2866	2865	CH_2 stretch (in-phase stretch)
1734‡†	1740‡†	"free" amide I mode ("free" C=O stretch)
1702‡†	1720‡†	disordered H-bonded amide I mode
1697‡†	1696‡†	ordered H-bonded amide I mode
1608	1604	benzene ring C=C stretch (biphenyl > TDI)*
1594	1593	benzene ring C=C stretch (TDI)
1526	1521	amide II
1501	1498	benzene ring semicircle stretch
1464	1464‡	CH_2 deformation
1271	1266	aromatic ether C-O **
1241	1237	aromatic ether C-O **
823	821	out-of-plane C-H wag of biphenyl
713	709	out-of-plane N-H wag
652	652	out-of-plane C=O wag
518	522	out-of-plane quadrant benzene ring bend (biphenyl)

‡ estimated from peak deconvolution.
† The present value corresponds to the second heating scan (see text for details).
* The biphenyl moiety contributes mostly to the absorbance of this peak, with a smaller contribution from the TDI moiety as well.
** The present assignment bears a small degree of uncertainty because of a great deal of peak overlapping in this spectral region.

Table 4.3

Deconvolution results for the amide I region of a HFIP-cast, 2,6-LCPU-6 thin film.* (First heating scan.)

| temp, °C | Hydrogen Bonded | | | | | | "Free" | | | A_t | A_o/A_t | A_d/A_t |
| | Ordered | | | Disordered | | | | | | | | |
	ν, cm^{-1}	$W_{1/2}$ cm^{-1}	A_o	ν, cm^{-1}	$W_{1/2}$ cm^{-1}	A_d	ν, cm^{-1}	$W_{1/2}$ cm^{-1}	A_f			
25	1697.3	15.6	0.520	1704.5	61.6	9.22	1736.2	17.6	0.289	10.0	0.0519	0.919
100	1698.7	14.7	0.597	1709.7	56.8	8.06	1737.0	21.3	0.739	9.40	0.0635	0.858
120	1698.8	14.6	0.681	1711.2	55.9	7.70	1737.6	21.6	0.806	9.18	0.0742	0.838
140	1696.9	13.9	1.52	1709.9	56.8	6.65	1738.0	23.1	0.868	9.04	0.169	0.735
160	1697.0	13.8	1.72	1710.2	59.2	6.60	1738.5	23.0	0.823	9.15	0.188	0.722
180	1697.3	13.6	1.65	1711.0	59.5	6.49	1738.9	23.0	0.940	9.08	0.182	0.714
200	1696.1	14.1	1.71	1719.8	52.0	6.15	1740.2	24.6	1.12	8.99	0.191	0.685
220				1721.6	51.5	7.20	1740.8	25.2	1.88	9.08		0.793

* A_o = area (arbitrary units) of band attributed to ordered domains, A_d = area (arbitrary units) of band attributed to mesophase and amorphous domains, A_f = area (arbitrary units) attributed to "free" carbonyl groups, and A_t = total area = $A_o + A_d + A_f$. $W_{1/2}$ = width at half-height of Gaussian curve.

Table 4.4

Deconvolution results for the amide I region of a HFIP-cast, 2,6-LCPU-6 thin film.* (Second heating scan.)

| temp, °C | Hydrogen Bonded | | | | | | "Free" | | | | | |
| | Ordered | | | Disordered | | | | | | | | |
	ν, cm^{-1}	$W_{1/2}$ cm^{-1}	A_o	ν, cm^{-1}	$W_{1/2}$ cm^{-1}	A_d	ν, cm^{-1}	$W_{1/2}$ cm^{-1}	A_f	A_t	A_o/A_t	A_d/A_t
30	1693.7	11.8	1.90	1702.0	50.4	7.09	1734.4	26.3	1.33	10.3	0.185	0.687
100	1694.3	12.4	1.84	1704.0	52.0	6.75	1735.8	26.9	1.39	9.98	0.184	0.677
120	1694.5	12.7	1.84	1705.4	54.1	6.73	1736.6	26.9	1.41	9.98	0.184	0.675
140	1694.8	12.9	1.83	1706.7	56.0	6.68	1737.2	26.9	1.44	9.94	0.184	0.671
160	1695.2	13.3	1.84	1707.7	57.3	6.58	1737.7	27.1	1.47	9.89	0.186	0.665
180	1695.5	13.5	1.83	1708.6	59.2	6.63	1738.2	27.2	1.45	9.91	0.184	0.669
200	1695.9	13.9	0.889	1719.8	52.1	6.78	1740.2	26.0	1.65	9.32	0.0954	0.727
220				1721.6	51.7	7.09	1740.8	25.7	1.89	8.98		0.790

* A_o = area (arbitrary units) of band attributed to ordered domains, A_d = area (arbitrary units) of band attributed to mesophase and amorphous domains, A_f = area (arbitrary units) attributed to "free" carbonyl groups, and A_t = total area = $A_o + A_d + A_f$. $W_{1/2}$ = width at half-height of Gaussian curve.

128
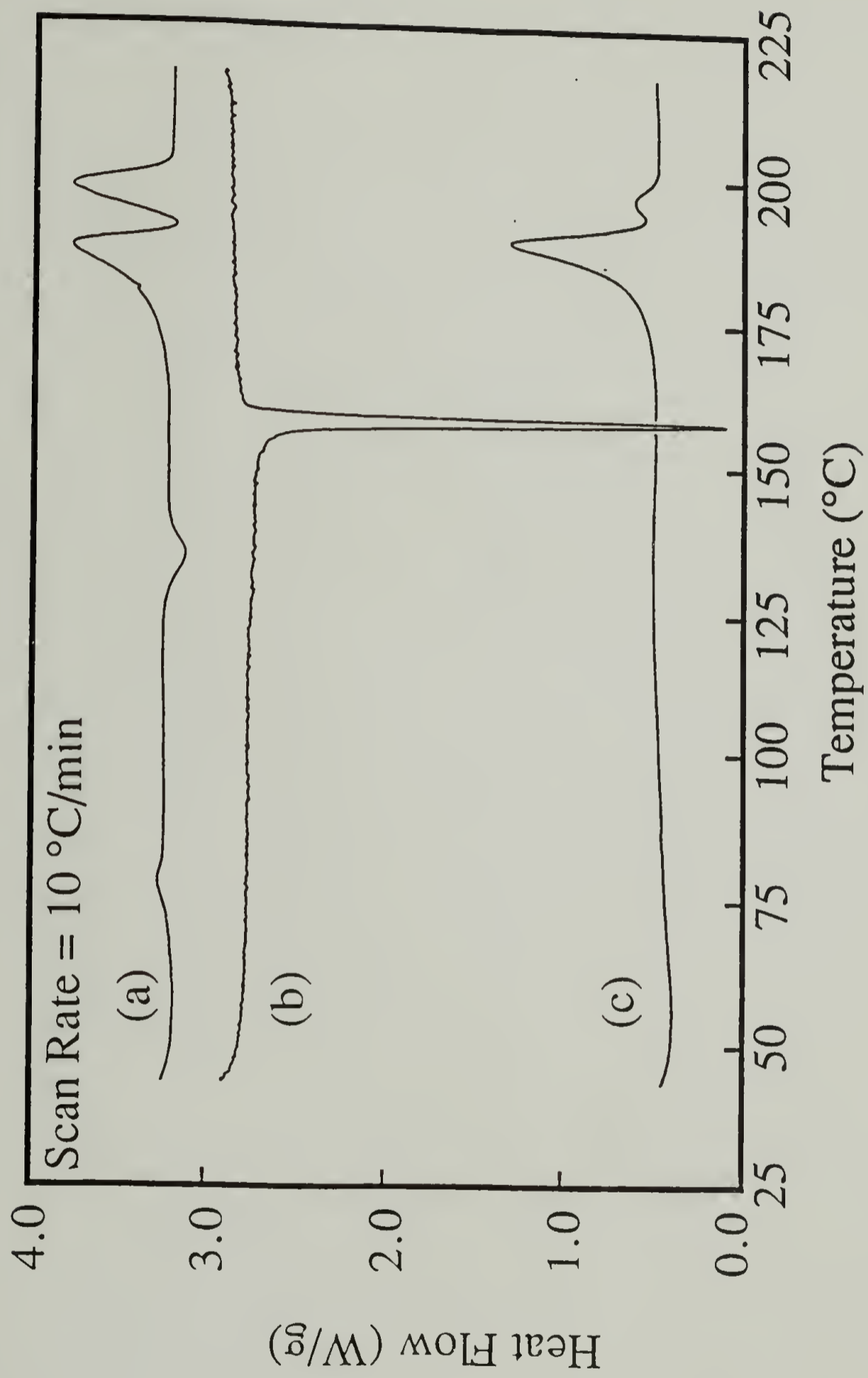
Figure 4.1 10 °C/min DSC traces of HFIP-cast, 2,6-LCPU-6 thin film: (a) first heating scan; (b) first cooling scan; (c) second heating scan.
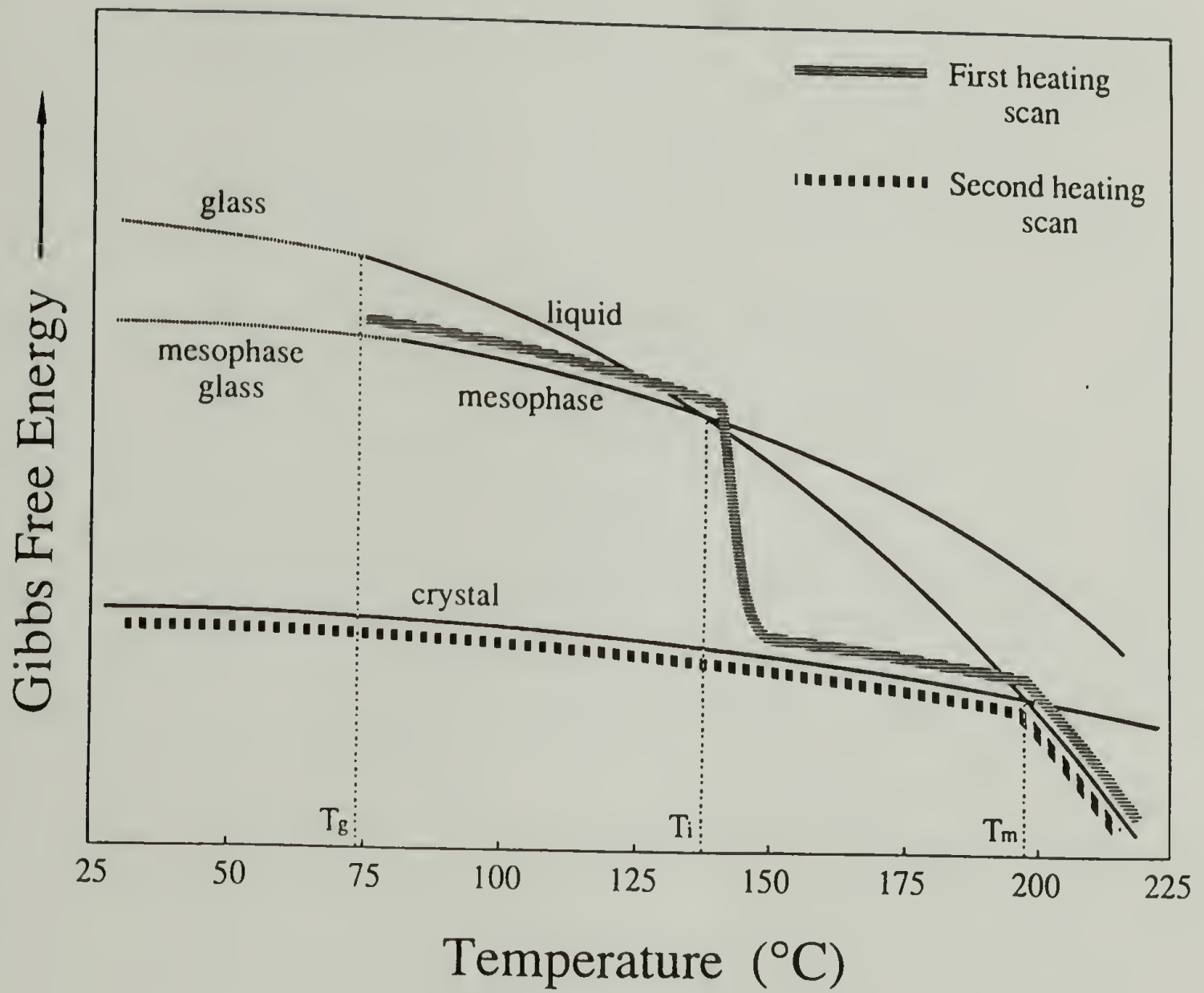
Figure 4.2 Schematic plot of temperature dependence of Gibbs free energy for 2,6-LCPU-6 (see text for details).
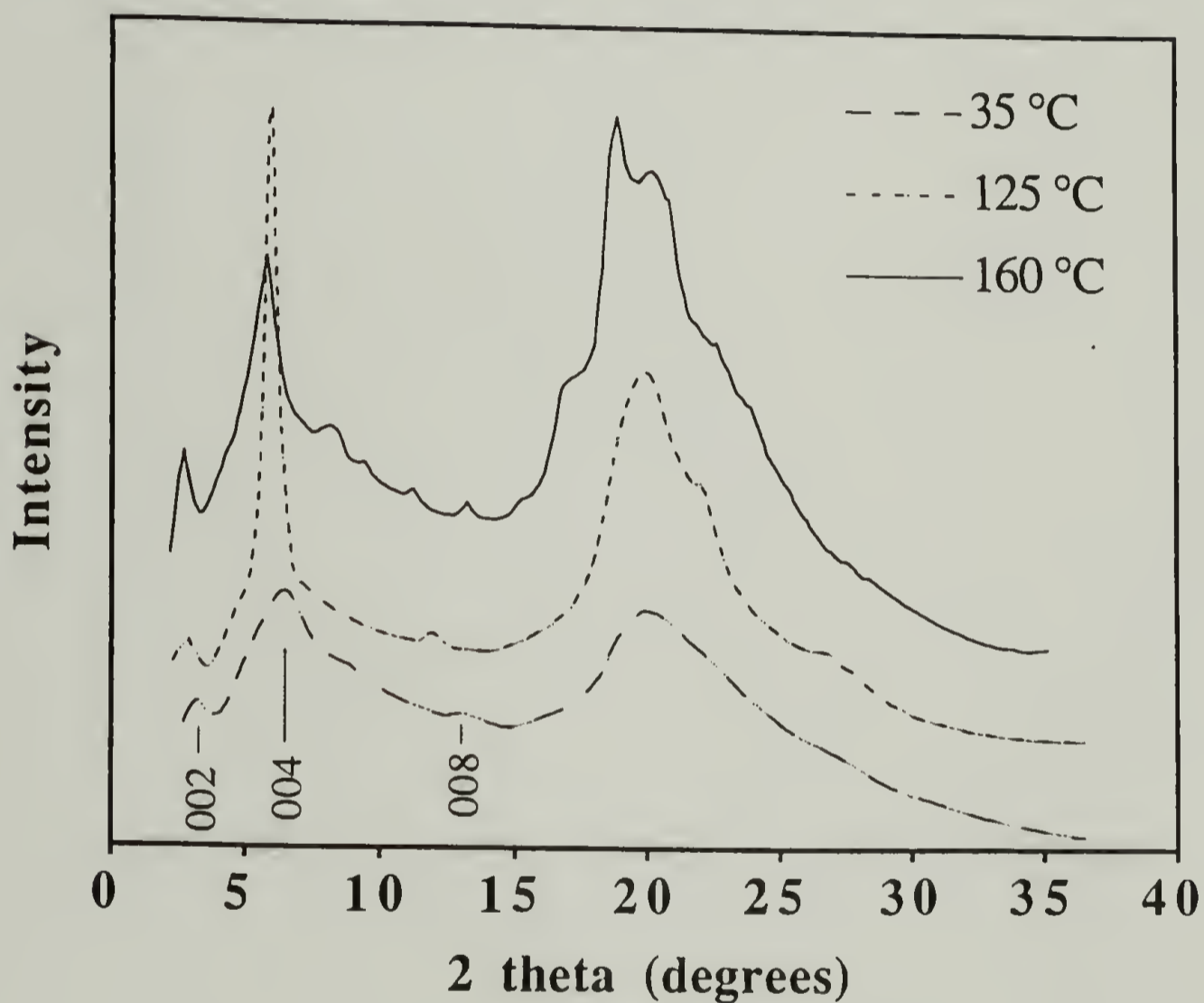
Figure 4.3 Room-temperature radial X-ray diffraction (XRD) profiles of HFIP-cast, 2,6-LCPU-6 thin films as a function of thermal history. The noted temperature corresponds to the maximum temperature to which these films were exposed during a 10 °C/min heating scan, followed by a quick quench to room temperature.

131
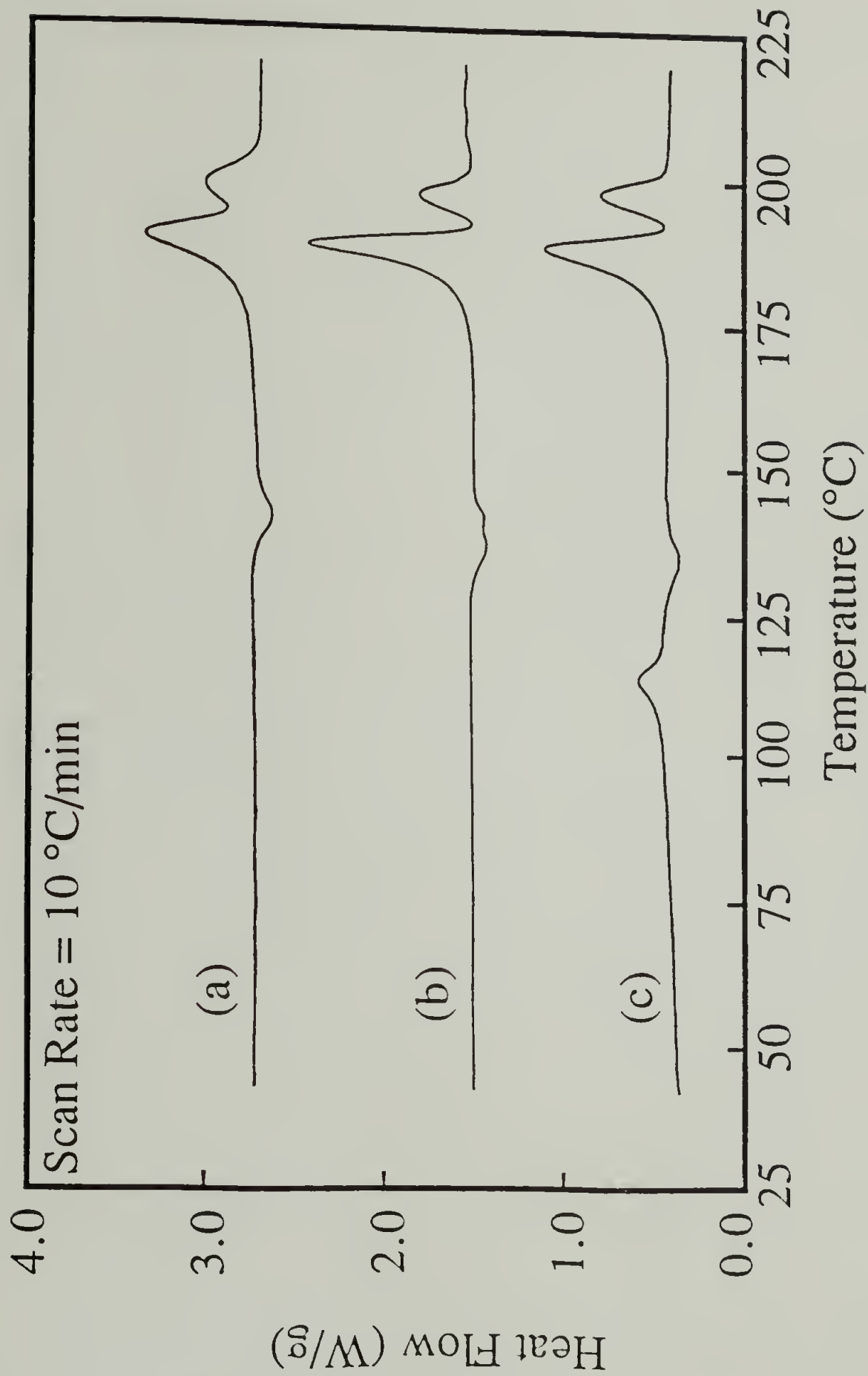
Figure 4.4 10 °C/min DSC heating traces of 2,6-LCPU-6: (a) sample quenched into liquid N_2 from the melt; (b) fiber drawn from the melt; (c) fiber drawn from the melt, Soxhlet-extracted in hot MeOH for 4 days, and vacuum dried at 60 °C overnight. (See Table 4.1 for transition temperatures and enthalpies.)
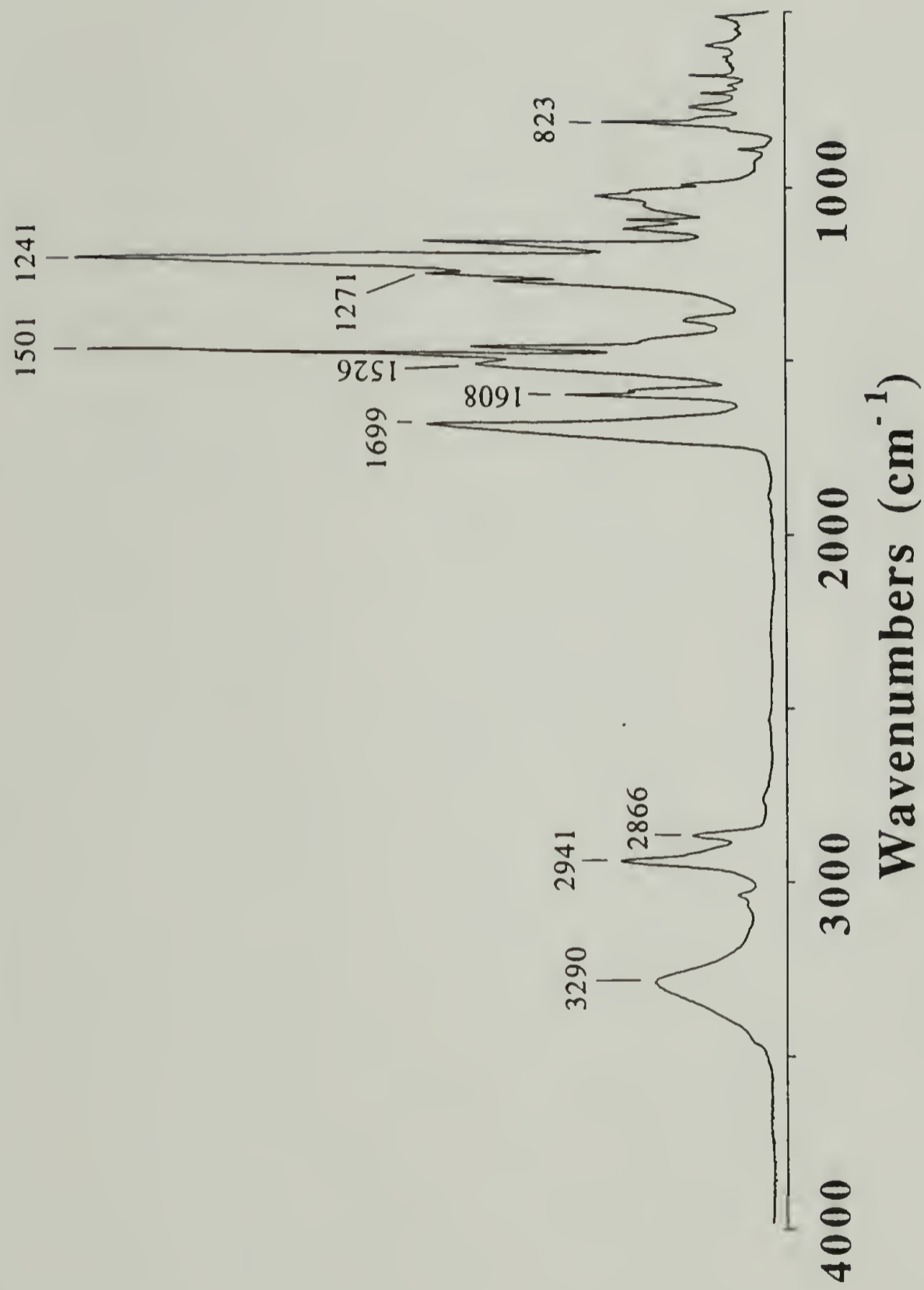
Figure 4.5 Survey FTIR spectrum of a HFIP-cast, 2,6-LCPU-6 thin film, taken at room temperature.
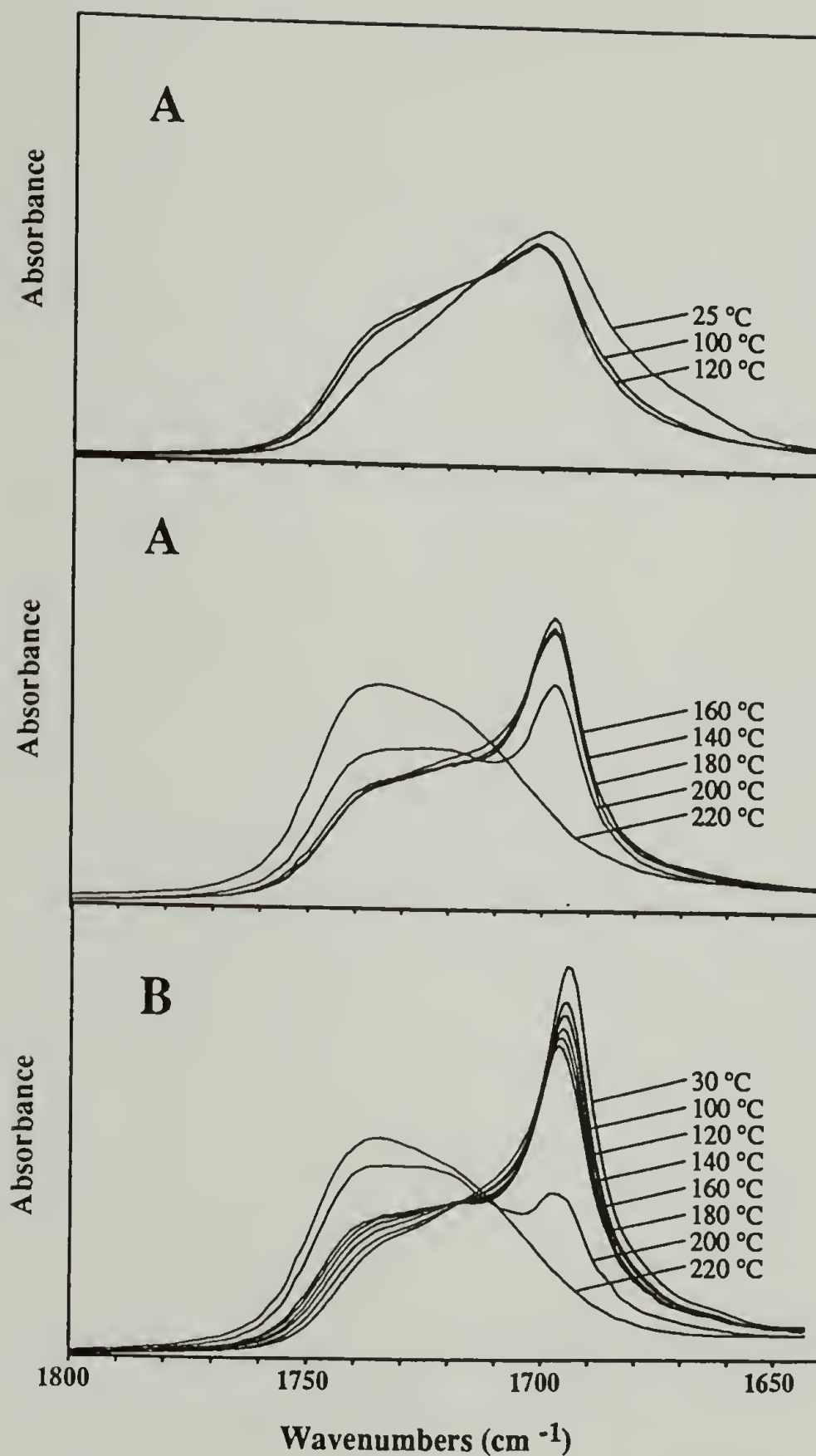
Figure 4.6 FTIR spectra of the amide I region (1640-1800 cm^{-1}), of a HFIP-cast, 2,6-LCPU-6 thin film as a function of increasing temperature: (A) spectra recorded on the first heating scan; (B) spectra recorded on the second heating scan.
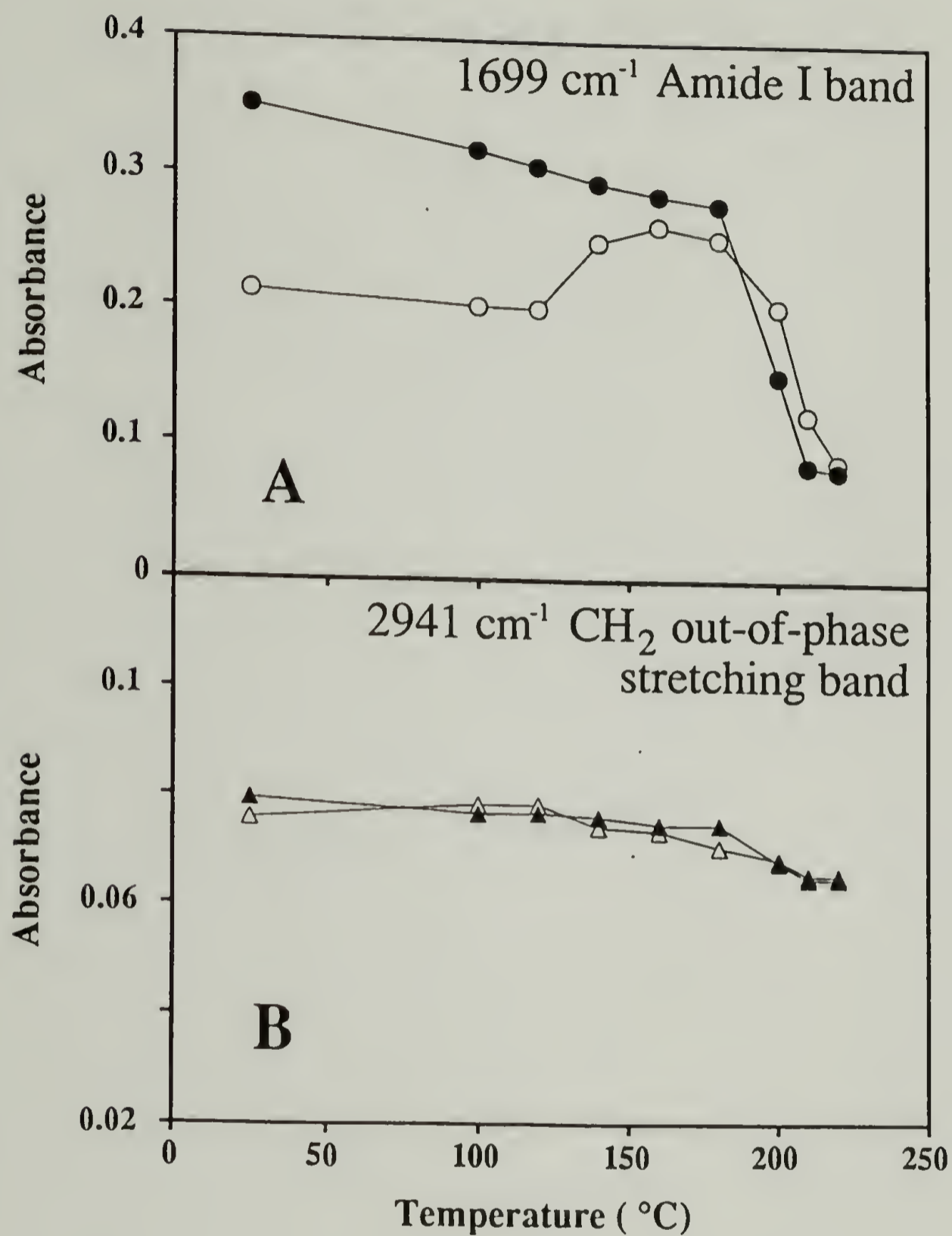
Figure 4.7 Peak absorbance as a function of temperature for the 1699 cm^{-1} ordered H-bonded amide I band (A) and the 2941 cm^{-1} CH$_2$ out-of-phase stretching band (B). First heating scan data are indicated with unfilled symbols and second heating scan data with filled symbols.
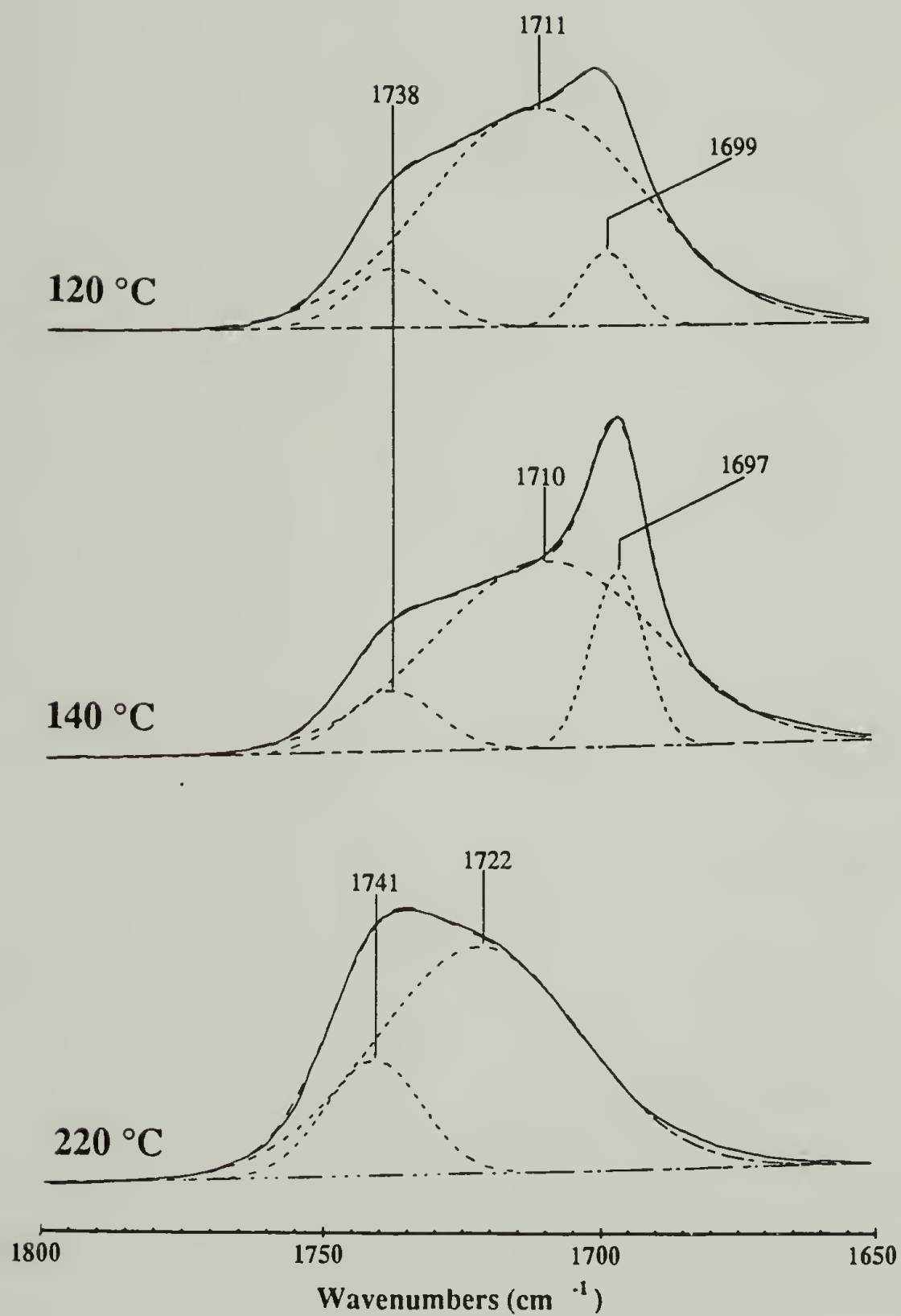
Figure 4.8 Least-squares deconvolution of the amide I region of a HFIP-cast, 2,6-LCPU-6 thin film from the first heating scan at 120, 140, and 220 °C.
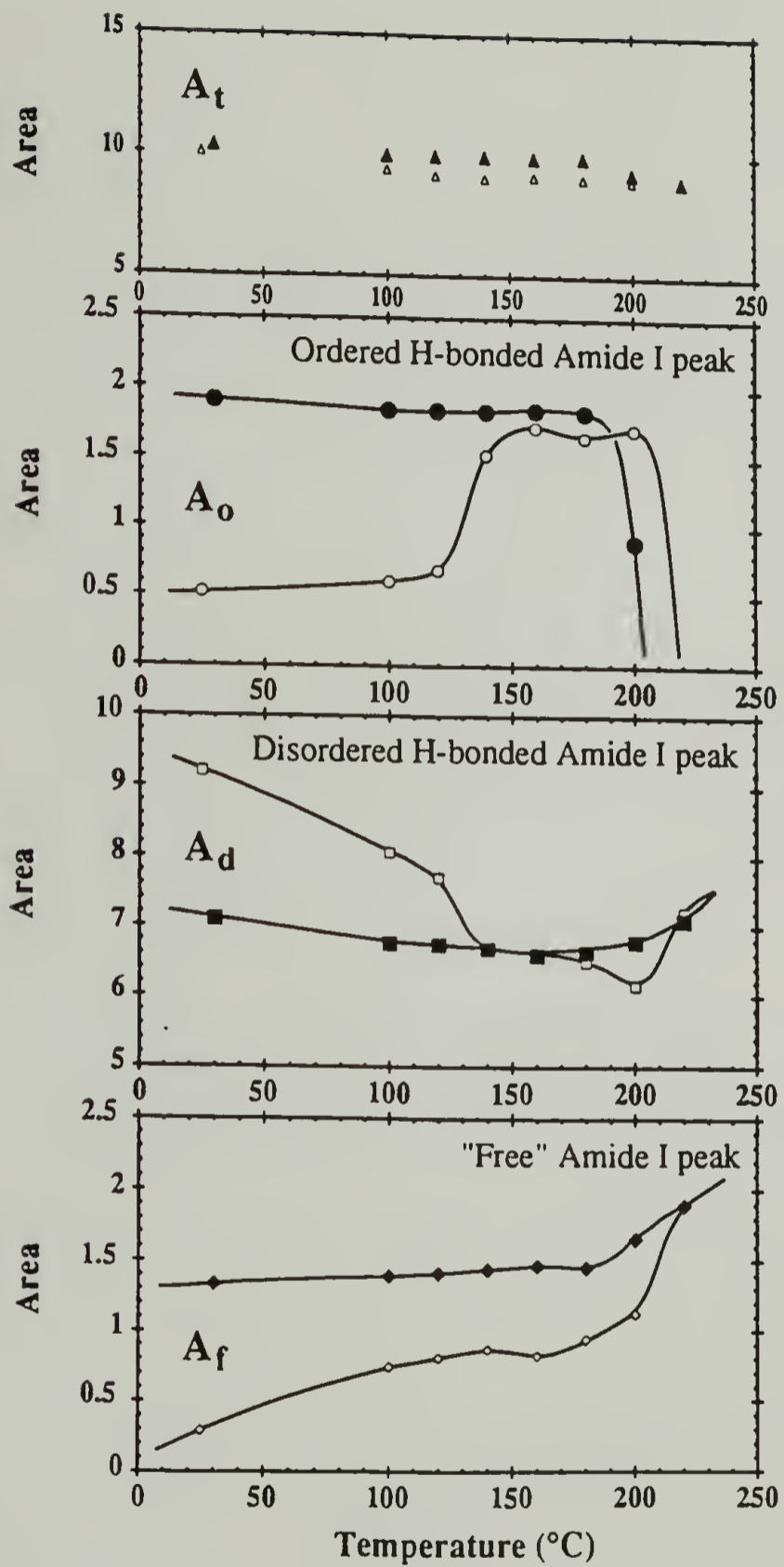
Figure 4.9 Plots of the areas of the "free" (A_f), disordered (A_d), and ordered (A_o) H-bonded peaks as well as the total (A_t) carbonyl groups obtained from the amide I region as a function of temperature. First heating scan data are indicated with unfilled symbols and second heating scan data with filled symbols.
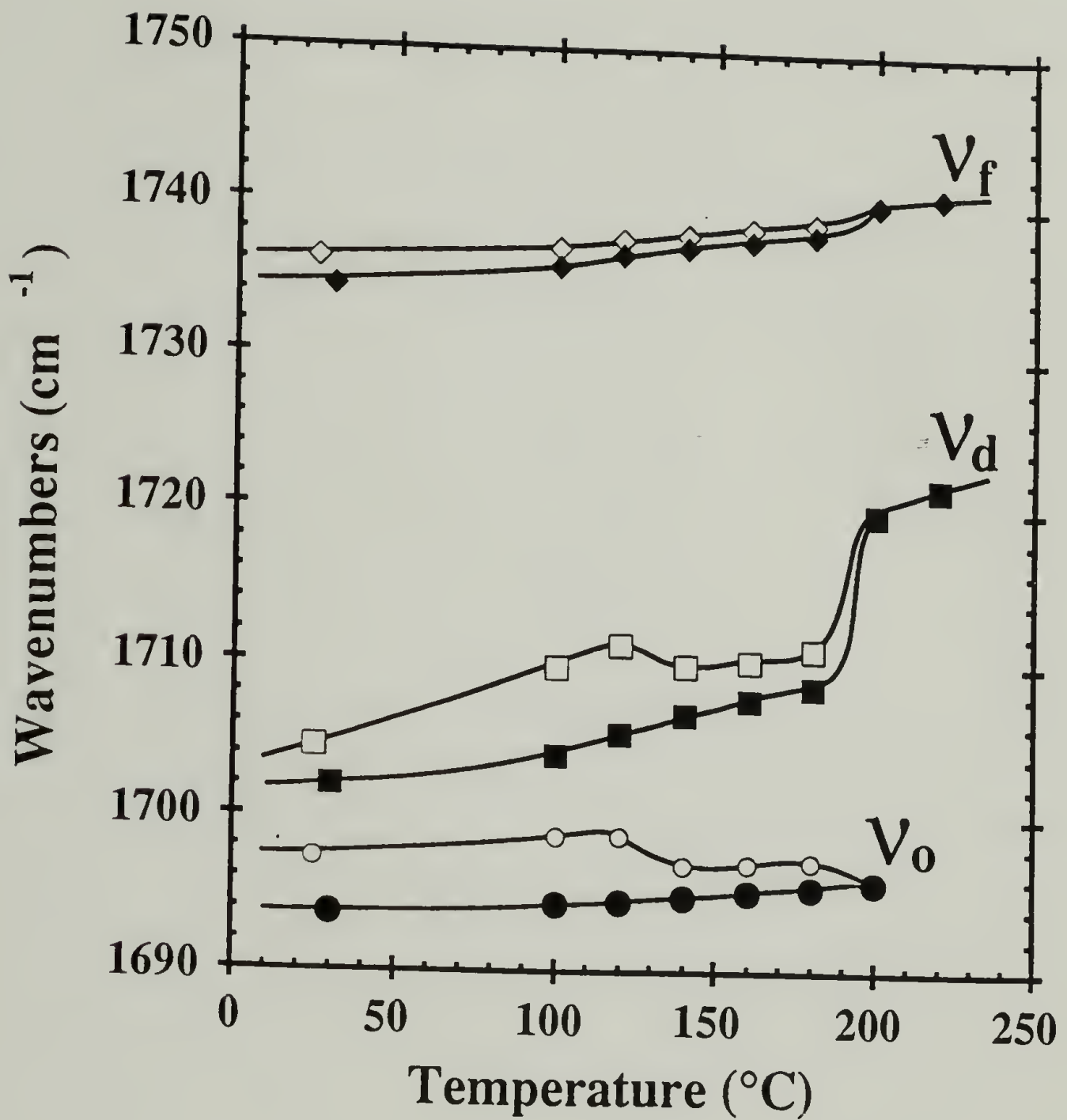
Figure 4.10 Plots of the peak frequency of the "free" (ν_f), disordered (ν_d), and ordered (ν_o) H-bonded carbonyl peaks from the amide I region as a function of temperature. First heating scan data are indicated with unfilled symbols and second heating scan data with filled symbols.
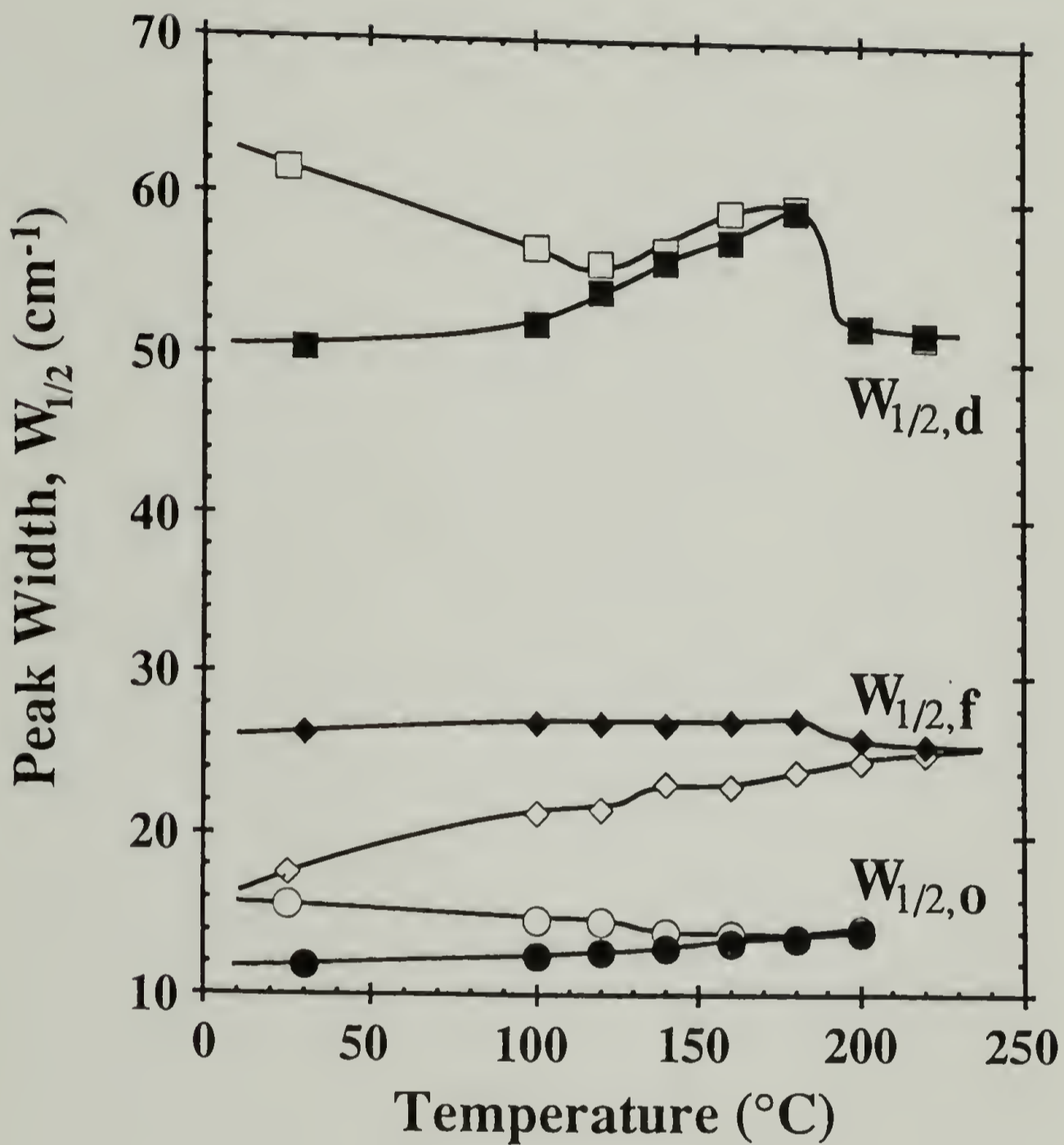
Figure 4.11 Plots of the width at half-height of the "free" ($W_{1/2,f}$), disordered ($W_{1/2,d}$), and ordered ($W_{1/2,o}$) H-bonded carbonyl peaks from the amide I region as a function of temperature. First heating scan data are indicated with unfilled symbols and second heating scan data with filled symbols.
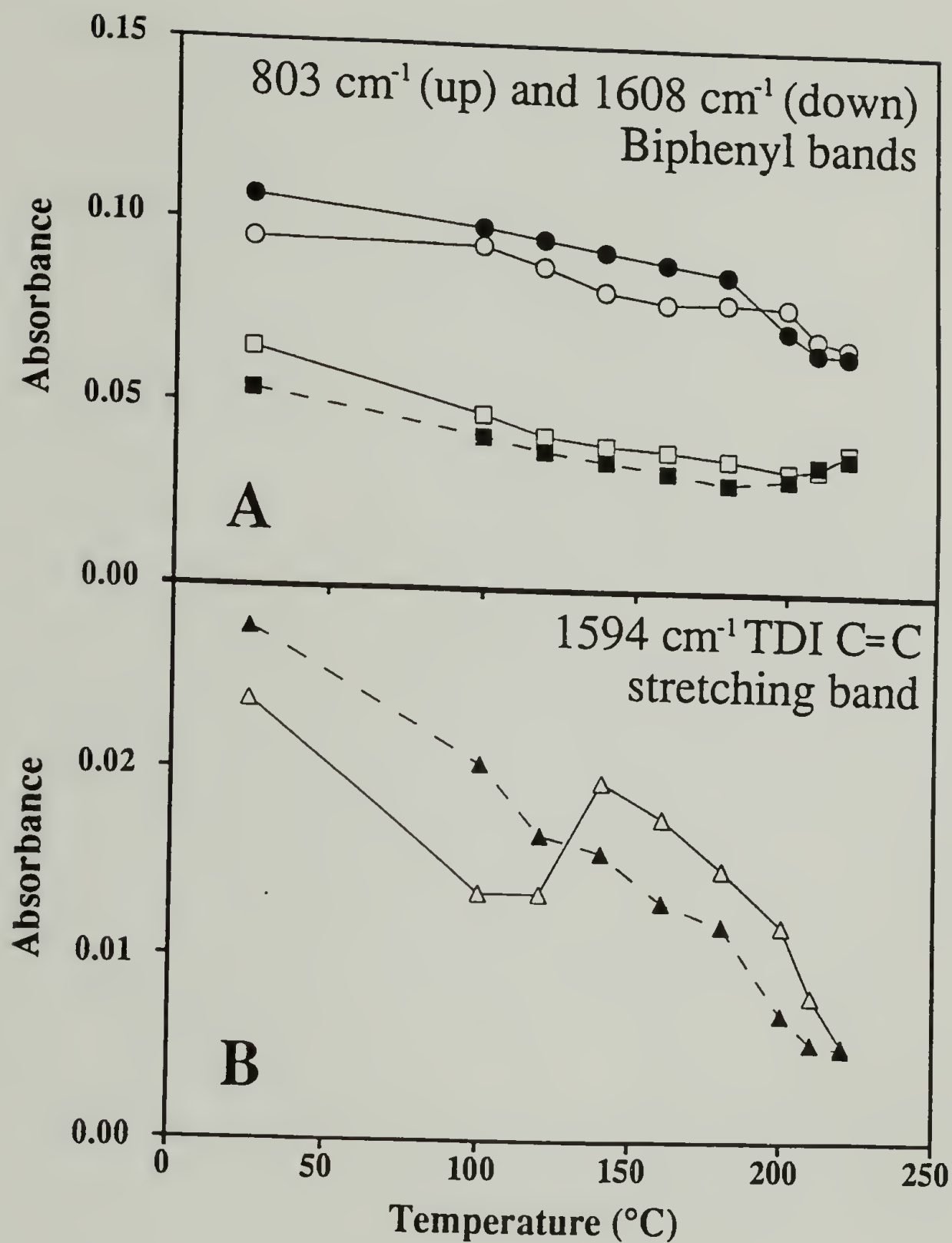
Figure 4.12 Peak absorbance as a function of temperature for the H-bonded N-H stretching band (A) and the amide II band (1526 cm^{-1}) (B). First heating scan data are indicated with unfilled symbols and second heating scan data with filled symbols.
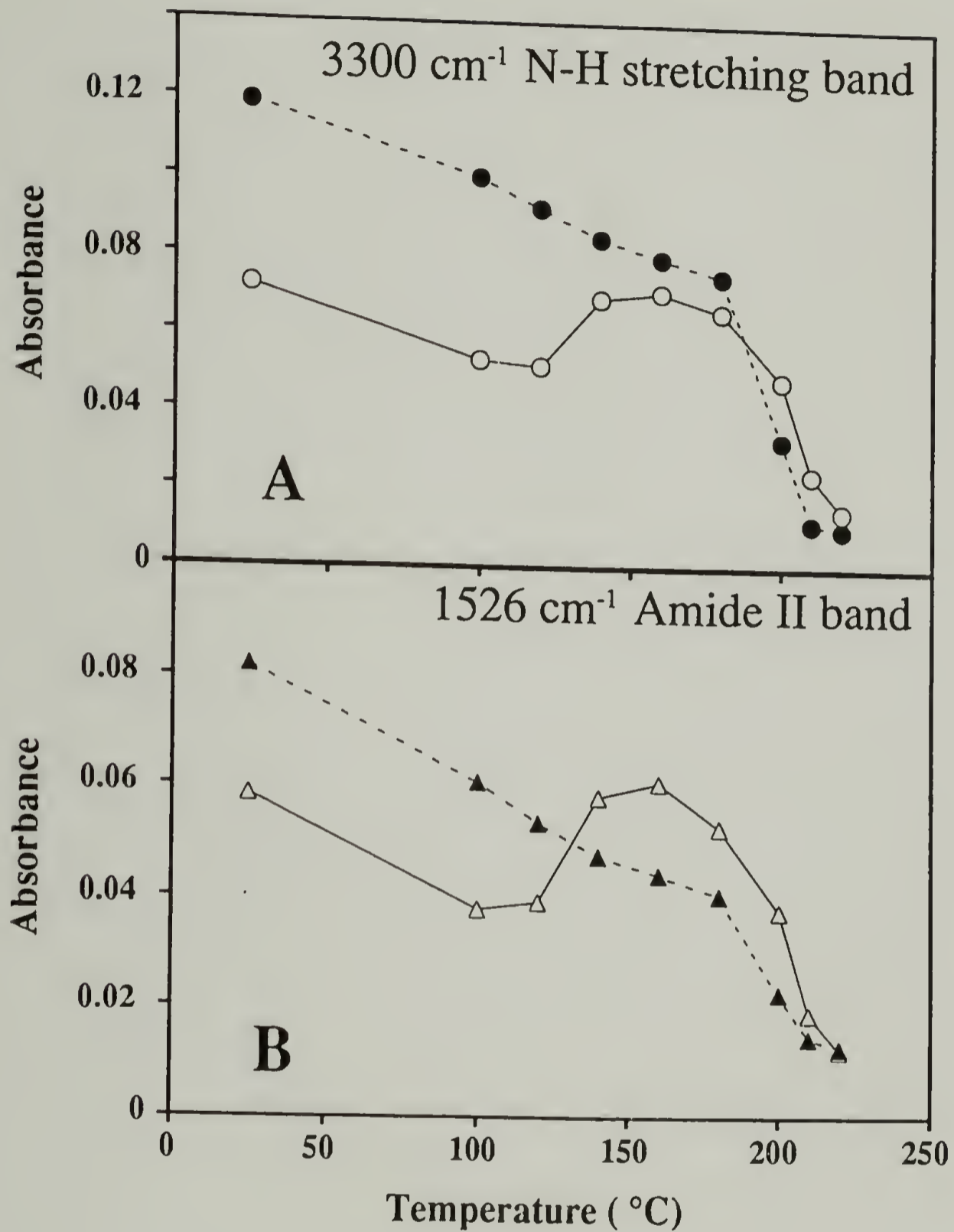
Figure 4.13 Peak absorbance as a function of temperature for the biphenyl out-of-plane C-H wagging band (803 cm⁻¹) (upper pair of curves in (A)); the biphenyl C=C stretching band (1608 cm⁻¹) (lower pair of curves in (A)); and the TDI C=C stretching band (1594 cm⁻¹) (B). First heating scan data are indicated with unfilled symbols and second heating scan data with filled symbols.

References

(1)   Keller, A.; Ungar, G., To be published.

(2)   Percec, V.; Keller, A. *Macromolecules* **1990**, *23*, 4347.

(3)   Smyth, G.; Pollack, S. K.; MacKnight, W. J.; Hsu, S. L. *Liquid Crystals* **1990**, *7*, 839.

(4)   Yang, X.; Waldman, D. A.; Hsu, S. L.; Nitzsche, S. A.; Thakur, R.; Collard, D. M.; Lillya, C. P.; Stidham, H. D. *Journal of Chemical Physics* **1989**, *89*, 5950.

(5)   Yang, X.; Kardan, M.; Hsu, S. L.; Collard, D.; Heath, R. B.; Lillya, C. P. *Journal of Physical Chemistry* **1988**, *92*, 196.

(6)   Kardan, M.; Kaito, A.; Hsu, S. L.; Takur, R.; Lillya, C. P. *Journal of Physical Chemistry* **1987**, *91*, 1809.

(7)   Kardan, M.; Reinhold, B. B.; Hsu, S. L.; Thakur, R.; Lillya, C. P. *Macromolecules* **1986**, *19*, 616.

(8)   Lee, W. K.; Heiney, P. A.; J. P., J. M.; Smith, A. B. I. *Molecular Crystals and Liquid Crystals* **1991**, *198*, 273.

(9)   Gregoriou, V. G.; Chao, J. L.; Toriumi, H.; Palmer, R. A. *Chemical Physics Letters* **1991**, *179*, 491.

(10) Boeffel, C.; Spiess, H. W. *Macromolecules* **1988**, *21*, 1626.

(11) Goldfarb, D.; Luz, Z.; Zimmermann, H. *Journal of chemical Physics* **1983**, *78*, 7065.

(12) Tashiro, K.; Ono, K.; Minagawa, Y.; Kobayashi, M.; Kawai, T.; Yoshino, K. *Journal of Polymer Science: Part B: Polymer Physics* **1991**, *29*,

(13) Koenig, J. L. In *Advances in Polymer Science*; E. D. v. Meerwall, C. W. Frank, S. N. Semerak and J. L. Koenig, Ed.; Springer-Verlag: New York, 1984; Vol. 54; pp 87-154.

(14) Colthup, N. B.; Daly, L. H.; Wiberley, S. E. *Introduction to Infrared and Raman Spectroscopy*; Academic Press: New York, 1990.

(15) Bower, D. I.; Maddams, W. F. *The Vibration Spectroscopy of Polymers*; Cambridge University Press: New York, 1989.

(16) Snyder, R. G. *The Journal of Chemical Physics* **1967**, *47*, 1316.

(17) Hagemann, H.; Strauss, H. L.; Snyder, R. G. *Macromolecules* **1987**, *20*, 2810.

(18) West, J. C.; Cooper, S. L. *Journal of Polymer Science* **1977**, *Polymer Symposium 60*, 127.

(19) Srichatrapimuk, V. W.; Cooper, S. L. *Journal of Macromolecular Science & Physics* **1978**, *B15*, 267.

(20) Coleman, M. M.; Lee, K. H.; Skrovanek, D. J.; Painter, P. C. *Macromolecules* **1986**, *19*, 2149.

(21) Bummer, P. M.; Knutson, K. *Macromolecules* **1990**, *23*, 4357.

(22) Lee, H. S.; Wang, Y. K.; MacKnight, W. J.; Hsu, S. L. *Macromolecures* **1988**, *21*, 270.

(23) Pollack, S. K.; Shen, D. Y.; Hsu, S. L.; Wang, Q.; Stidham, H. D. *Macromolecules* **1989**, *22*, 551.

(24) Shen, D. Y.; Pollack, S. K.; Hsu, S. L. *Macromolecules* **1989**, *22*, 2564.

(25) Pollack, S. K.; Smyth, G.; Papadimitrakopoulos, F.; Stenhouse, P.; Hsu, S. L.; MacKnight, W. J. *Macromolecules* **1992**, *25*, 2381.

(26) Gromek, J. M. In Institute of Material Science, University of Connecticut, Storrs, CT 06269.

(27) Yoon, S. C.; Sung, Y. K.; Ratner, B. D. *Macromolecules* **1990**, *23*, 4351.

(28) Struick, L. C. E. *Physical Aging in Amorphous Polymers and Others Materials*; Elsevier Science Publishing. Co.: New York, 1978.

(29) Cheng, S. Z. D.; Yandrasits, M. A.; Percec, V. *Polymer* **1991**, *32*, 1284.

(30) Wunderlich, B. *Macromolecular Physics*; Academic Press: New York, 1973-80; (Vols. 1-3).

(31) Seymour, R. W.; Estes, G. M.; Cooper, S. L. *Macromolecules* **1970**, *3*, 579.

(32) MacKnight, W. J.; Yang, M. *Journal of Polymer Science, Symposium Series* **1973**, *42*, 817.

(33) Skrovanek, D. J.; Painter, P. C.; Coleman, M. M. *Macromolecules* **1986**, *19*, 699.

(34) Coleman, M. M.; Graf, J. F.; Painter, P. C. *Specific Interactions and the Miscibility of Polymer Blends*; Technomic Publishing Co., Inc.: Lancaster, PA 17604, USA, 1991.

(35) Wang, Q. Master Thesis, University of Massachusetts at Amherst, 1989.

(36) Maddams, W. F. *Applied Spectroscopy* **1980**, *34*, 245.

(37) Skrovanek, D. J.; Howe, S. E.; Painter, P. C.; Coleman, M. M. *Macromolecules* **1985**, *18*, 1676.

(38) Brunette, C. M.; Hsu, S. L.; MacKnight, W. J. *Macromolecules* **1982**, *15*, 71.

(39) Senich, G. A.; MacKnight, W. J. *Macromolecules* **1980**, *13*, 106.

(40) Schroeder, L. R.; Cooper, S. L. *Journal of Applied Physics* **1976**, *47*, 4310.

(41) Coleman, M. M.; Skrovanek, D. J.; Howe, S. E.; Painter, P. C. *Macromolecules* **1985**, *18*, 299.

CHAPTER 5

CONFORMATION CHARACTERISTICS AND CRYSTAL PACKING
OF TDI BASED
"REGULAR" AND LIQUID CRYSTAL POLYURETHANES

Introduction

The solid-state structure of liquid crystalline polymers has been the subject of considerable interest and research in recent years.[1,2] Liquid crystal polyesters[3-5] and polyamides[6,7] have attracted most of the attention of the scientific community. Although a fair number of publications have indicated the strong tendency of liquid crystalline polyurethanes to crystallize,[8-16] there is very little known about their solid-state structure.[11] In general, the poor quality of the X-ray diffraction patterns of polyurethanes has been the major obstacle towards a thorough crystallographic analysis.[17] This is usually attributed to the low degree of polymerization and strong H-bonding which result in poor orientation and small domain size.

The chain conformation and packing of the diphenylmethane 4,4'-diisocyanate (MDI) – butane diol (BDO) polyurethane [17-20] presents the most complete crystallographic analysis in the field of polyurethanes and in particular, polyurethane thermoplastic elastomers. Its structure was deduced from well oriented fiber diffraction patterns of a slowly stretched (ca. 700%) and annealed (at 130 °C for 24 hours) elastomer,[18] as well as from the single crystal X-ray analysis of two low molecular weight model compounds.[17,19] Subsequent publications[21-23] utilized conformational analysis, based on empirical and semi-empirical (CNDO/2) calculations, in order to investigate the intramolecular interactions of the various groups in the molecular repeat. The subject of

145

interest was the torsional angles between phenyl-CH$_2$-phenyl, phenyl-urethane, and urethane-butanediol. Although good values were achieved for the phenyl-CH$_2$-phenyl and urethane-butanediol torsions, the phenyl-urethane torsion angle ϕ was in disagreement

where: X = O for urethanes
X = CH$_2$ for amides
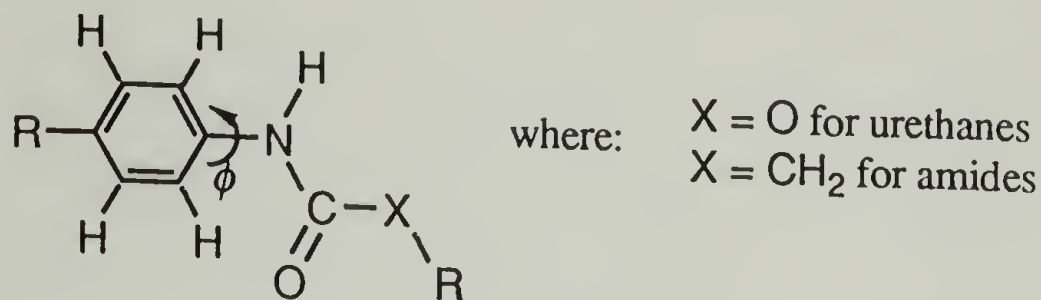
with the crystallographic data from the model compounds (90° versus 25° ± 10°). In order to explain the above discrepancy, Blackwell et al. attributed on the following parameters that were not taken into account by their calculation; 1) the strong intermolecular interaction of the H-bond, 2) the packing of the bulky phenyl group, and 3) the π-interactions between the phenyl and urethane groups. Hummel et al.[24] as well as Tashiro et al.[25] have applied a potential function to model the effect of electron delocalization in their studies of p-phenylene polyamides and polyesters. This potential function has the form

$$V_\pi = -V_\pi{}^0 \cos^2\phi = V_\pi{}^0 (1+ \cos 2\phi)/2$$

and tends to produce planar ($\phi = 0°$) phenyl-amide conformations depending of the magnitude of the constant $V_\pi{}^0$. According to Hummel et al.,[24] without taking into account H-bonding, a 7 kcal mol^{-1} value for $V_\pi{}^0$ can yield a minima for polyamides near 30°, with a corresponding barrier of ca 2.6 Kcal mol^{-1} at 90°. On the other hand, Tashiro et al.[25] estimate the $V_\pi{}^0$ to be around 16 Kcal mol^{-1} with a corresponding barrier of ca 11 Kcal mol^{-1}. Evidently, the value of $V_\pi{}^0$ has been a subject of debate, while the contribution of H-bonding, which averages strengths between 6 - 10 Kcal mol^{-1}, has not been seriously considered.

Recent computer software and hardware developments have shortened drastically the computation time needed to perform these types of calculations.[26,27] Utilizing

146

periodical boundary conditions,[27] non bonding interactions such as H-bonding can be easily incorporated, even for quite complicated polymers such as proteins. The primary focus of this chapter is to elucidate the conformational characteristics and crystal packing of meta substituted phenylene polyurethanes via molecular simulations and crystallographic analysis. A direct correlation between the structure, H-bonding and torsional angle ϕ has been established for the 2,6-TDI and 1,3-PDI based polyurethanes. In addition to that, it is our intention to demonstrate the effect of the TDI's methyl group on the crystalline structure, and correlate it with the following experimental results.

Polymer	T_m (°C)	Density (g/cm^3)
2,6-LCPU-6	209	1.22$_8$
1,3-LCPU-6	202	1.24$_1$
2,6-PU-6	215	1.27$_4$
1,3-PU-6	145	1.26$_5$

The above table indicates that the melting point (T_m) of the 2,6-LCPU-6 is 7 °C higher than 1,3-LCPU-6, despite its lower density. On the other hand, a 70 °C difference in the melting points of 2,6-PU-6 and 1,3-PU-6 has been observed, although their densities are comparable. The strong differences in the wide-angle WAXS patterns of 2,6-TDI and 1,3-PDI based "regular" and liquid crystal polyurethanes, indicate a distinctively different packing arrangement. While the crystallographic analysis of liquid crystal polyurethanes (LCPUs) was based on well oriented WAXS fiber patterns, in order to extend the same analysis to the "regular" 2,6-PU-6 and 1,3-PU-6 polyurethanes as well, we had to rely solely on their WAXS powder patterns. Although this seems to limit substantially this comparison, the close structural similarity of the "regular" polyurethanes (PUs) to those of LCPUs has proven to assist greatly in establishing their packing characteristics.

Experimental

Materials. The synthesis and characterization of 2,6-LCPU-6, 1,3-LCPU-6, 2,4-LCPU-6, 2,6-PU-6, 1,3-PU-6 and 2,4-PU-6 were detailed in Chapter 3. Both the high ([η] = 0.882 dL/g) and low ([η] = 0.400 dL/g) molecular weight samples of 2,6-LCPU-6 were studied in terms of their structure, density, and ultimate melting temperature. They were found to behave similarly, although the higher molecular weight sample resulted in better oriented WAXS fiber patterns.

Characterization Techniques. The density of each sample was determined by flotation in a toluene-carbon tetrachloride density gradient column at 21.0 °C. Samples of each polymer were compressed in vacuum, above their melting points, into a 0.5 mm thick disk-like specimen and cooled slowly to room temperature. Soxhlet extraction in hot MeOH and annealing at various temperatures was utilized in order to maximize the crystallinity of each specimen (see Table 5.1).

Room-temperature X-ray diffraction patterns were recorded on flat films with a Statton X-ray camera using Ni filtered Cu Kα radiation. The samples, free-standing fibers, or 0.5 mm thick films, were mounted directly on the pinhole with the help of a double-stick tape. The X-ray camera length was calibrated with the 2.319-Å diffraction line of NaF and 3.035-Å diffraction line of $CaCO_3$ for the wide-angle range, while for the intermediate angle range, the layer diffraction lines of the monoclinic form of n-hexatriacontane, n-$C_{36}H_{74}$[28] was used. The X-ray films were measured for interplanar spacing data with a Supper circular film measuring device. For the liquid crystalline polyurethanes, well-oriented samples were produced by drawing fibers from melt. Free-standing fibers were exposed to thermal and Soxhlet treatment in MeOH, while a weight of 0.5—3 g was attached to their ends in order to prevent shrinkage. No significant elongation was observed after the end of each treatment. WAXS powder patterns for the "regular" polyurethanes were obtained from the Soxhlet extracted and annealed samples utilized in the density determination (see Table 5.1).

148

Differential scanning calorimetric (DSC) measurements were conducted with a Perkin-Elmer DSC-7, employing a 20 mL/min flow of dry nitrogen as a purge gas for the sample and reference cells. The temperature and power ordinates of the DSC were calibrated with respect to the known melting point and heat of fusion of a high-purity indium standard. The melting point of the samples employed in X-ray and density determination were determined by a 10 °C/min preheating up to 120 °C in order to maximize the sample-pan contact, followed by a slow cooling and a subsequent heating scan, 50 °C past their major endotherm.

Molecular simulations were conducted using the commercially available software package, POLYGRAF, provided by Molecular Simulations, Inc. The force field utilized in order to perform molecular mechanics and molecular dynamics calculations was the Dreiding II, previously described elsewhere.[26] Long-range interactions were taking into account through periodic boundary conditions. Charges were assigned to individual atoms according to a method described by Gasteiger.[29] X-ray diffraction data and patterns were calculated by the commercially available software package, CERIUS, provided also by Molecular Simulations, Inc..

Results and Discussion

Despite the extensive structural analysis of MDI based polyurethanes ,[17,18,21-23] meta-substituted phenylene (PDI) or tolylene (TDI) diisocyanate polyurethanes have attracted much less interest, primarily in the areas of infrared analysis.[11,30] In order to proceed with a detailed crystallographic analysis, an in depth understanding of the conformation and packing characteristics of the TDI or PDI moiety has to be obtained first. Blackwell et al.[17] used single crystal X-ray analysis to determine the structure of MDI based model compounds, such as the methanol-capped MDI diurethane. Similar model compounds have been prepared and studied extensively in our laboratory[11,31,32] as well as other laboratories.[30,33-35] On the basis of the structure of the ethanol-capped-2,4-TDI

model compound,[36] which crystallizes in a none extended form (unable to accommodate the propagation of a polymer-like chain), as well as the partially H-bonded methanol-capped-1,3-PDI in its crystalline form,[32] the model compound approach appeared to be not as straight forward as in the case of MDI based polyurethanes.

Molecular simulations proved to be much more effective. The accuracy of this technique is determined from each one of the interatomic interactions that are taken into account. In these simulations we considered intramolecular as well as intermolecular degrees of freedom. The intramolecular or covalent interactions have been described in terms of bond stretching, bond angle bending, bond angle torsion and hybridization motion. The intermolecular interactions take into account van der Waals, electrostatic, and Hydrogen-bonding (H-bonding) terms. On the basis of the infrared analysis presented in Chapter 4 (which suggests the complete H-bonding of both urethane groups in the crystal phase), and the crystalline structure of meta-substituted aromatic polyamides,[25] Figure 5.1 illustrates the most favorable conformation in order to achieve complete H-bonding for this class of materials. Both urethane groups are tilted 50 - 60° towards the same direction with respect to the tolylene ring in order to facilitate the approach of the H-bonding sites N-H and O=C respectively. This tilt is energetically expensive due to the partial double bond character of the phenyl-urethane bond. The equilibrium value of the phenyl-urethane torsional angle ϕ is affected by the strength of π-interactions between phenyl and urethane groups, H-bonding, and packing considerations.

This problem is conventionally dealt with in two stages.[37] The first is to understand the conformational behavior of isolated polymer chains or even smaller key elements of each chain. The second is to understand how individual chains interact with their neighbors. On the basis of this simple scheme, much emphasis was given to the rotational potential of the phenyl-urethane bond. Figure 5.2 illustrates the conformational energy as a function of torsional angle ϕ for the phenyl-methyl-carbamate and o-tolyl-methyl carbamate, based on the Dreiding II empirical force field.[26] These calculations were

carried out with full relaxation of bond lengths, bond angles, torsions, inversions, and non bonding interactions in each conformation angle ϕ. The default parameters of the Dreiding II force field were utilized throughout these calculations. In reference to the introductory remarks concerning the magnitude of the constant default $V_\pi{}^0$, Dreiding II employs a value of 15 Kcal mol^{-1} for every exocyclic sp^2-sp^2 torsion, slightly smaller than the 16 Kcalmol^{-1} used by Tashiro et al.[25]

For the phenyl-methyl-carbamate (Figure 5.2, filled diamonds), a very shallow energy minima is observed between $0°$ and $30°$ followed by a maximum of 4.2 Kcal mol^{-1} at $\phi = 90°$. These results arise from the fact that bond lengths and angles are able to relax in order to alleviate the stress between the N–H and ortho C–H hydrogens. In a similar calculation, with a fixed set of bond lengths and bond angles ($V_\pi{}^0 = 17$ Kcal mol^{-1}), Khranovskii et al.[30] reported a much more pronounced minimum at $25°$, with 5 and 10 Kcal mol^{-1} barriers at $0°$ and $90°$ respectively. In the case of o-tolyl-methyl carbamate (Figure 5.2, open squares), two minima were observed at $145°$ and $55°$, with the $145°$ minimum 2.0 Kcal lower than the $55°$ one. The energy differences between the maxima and the $145°$ minimum are 7.1, 2.8, and 1.1 Kcal mol^{-1} for $0°$, $90°$, and $180°$ respectively. The corresponding minima from Khranovskii et al.[30] were located at $155°$ and $70°$ with much larger energy differences due to the fixed bond lengths and bond angles.

The 4.2 Kcal mol^{-1} barrier for the phenyl–methyl–carbamate at $\phi = 90°$ has been verified by the *ab initio* calculations conducted by Stidham et al.[32]. Figure 5.3 illustrates the results of the conformational energy map for the phenyl–methyl–carbamate at the STO-3G ($\phi = 0°$, $30°$, $60°$, and $90°$) and 3-21G ($\phi = 0°$ and $90°$) level. In both levels of calculation the minimum was found to be at $0°$ which indicated that the bond lengths and angles are slightly softer that those of the Dreiding force field. On the other hand, the 3.7 and 3.34 Kcal mol^{-1} barrier for the STO-3G and 3-21G level respectively indicate that the Dreiding II empirical force field represents the phenyl-urethane torsion adequately.

Evidently, the urethane group prefers to be planar with respect to the phenyl group, providing it can alleviate the Van der Waals repulsion of the nearest neighbors (H--H or H--CH3 for the two cases presented above). Based on the conformational energy map of Figure 5.2, a torsional angle* ϕ of ca. 30° can be considered more or less a minimum for both cases. An additional tilt of 20 - 30° will result in up to 1.5 Kcal mol^{-1} higher energy for each torsional angle. This is the energy that a hydrogen bond has to overcome in order to bring the urethane group into its most favorable conformation to hydrogen bond (see Figure 5.1).

<u>Molecular Architecture of meta-substituted polyurethanes.</u> Assuming a more or less extended BHHBP segment (see Chapter 3) a rough model of an isolated 2,6-LCPU-6 chain (or in the same manner 1,3-LCPU-6 chain) has been constructed and placed in periodic boundary conditions in order to provide more understanding of how individual chains interact with their neighbors. For reasons that will become apparent during the course of this discussion, main emphasis was given to the 2,6-LCPU-6 polymer, which turned out to be the simplest case. For reasons discussed extensively in Chapter 3 of this dissertation, the unit cell of each meta-substituted phenylene polyurethane is composed of at least a single dimer repeat. Energy minimizations based on molecular mechanics and molecular dynamics[27] resulted always in the c-axis length of a fully relaxed dimer repeat to be 57.8 ± 0.2 Å (see Figure 5.4). This is in excellent agreement with the 57.6 — 58.2 Å observed WAXS d spacing of the layer distance for the 2,6-LCPU-6 mesophase structure. Attempts to either extend or compress the c-axis length of the dimer repeatedly failed when the unit cell was minimized with no external constrains.

In order to elucidate the nature of this strongly preferred c-axis length, the focus of attention was drawn on the TDI moiety which acts as a "scissors" swivel. For this purpose, a fully relaxed 2,6-LCPU-6 dimer repeat was stretched out in the c direction with a large external force, while the rest of the unit cell parameters (a, b, α, β, γ, and ρ) were

---

* From this point on the torsional angle ϕ for the o-tolyl-methyl carbamate and consequently for the 2,6-LCPU-6 will be defined as the complementary angle of that used in Figure 5.2.

minimized simultaneously. After one day of slow computational stretching, a value of 73.2 Å was reached for the c-axis. Figure 5.4 (top) illustrates the conformation of the minimized dimer repeat at fixed c-axis of 73.2 Å In addition to that, Figure 5.4 (bottom) portrays a view along the b-axis of the H-bonded TDI moieties. The parameters of interest are the phenyl-urethane torsional angle ϕ, the H-bond angle ω, and the H-bond distance H···O and N···O distance respectively. The 73.2 Å repeat exhibits $\phi = 44°$, $\omega = 164°$, H···O distance =1.96 Å, and N···O distance = 2.89 Å. On the other hand, the fully relaxed 57.8 Å conformation exhibits $\phi = 54°$, $\omega = 176°$, H···O distance =1.93 Å, and N···O distance = 2.88 Å respectively. The profound differences between these two conformations motivated a detailed mapping at the intermediate extensions. This was accomplished by the following two step procedure. Using the 73.2 Å unit cell as a starting point, the unit cell is minimized (using molecular mechanics) at first to a lower c-axis length, by having all axes and angles unconstrained. When the desired c-axis length was reached, the minimization was aborted, the c-axis was constrained at the present value, and the unit cell was minimized again using a combination of molecular mechanics and dynamics.

Figure 5.5 illustrates the results of the above investigation. Evidently, the driving force for this unit cell contraction is not the H-bonding distance, which remains more or less constant, but the H-bonding angle ω. This is due to the increase of the ω towards linearity (180°) during contraction, which also increases ϕ as well. These two angles affect the overall energy of the system in opposite senses. The H-bond angle ω decreases the energy while the phenyl-urethane angle ϕ increases the energy of the system. The equilibrium length of the unit cell (minimum total energy) is controlled by the competition between these two angles. According to Figure 5.2, the 2,6-LCPU-6 equilibrium angle ϕ of 54° stands only 0.9 Kcal mol^{-1} higher than the equilibrium ϕ of 35°for the non H-bonded o-tolyl-methyl carbamate. Therefore, the strong intermolecular force of the H-bond with

average strengths between 6 - 10 Kcal mol^{-1}, can easily compensate for the 0.9 Kcal mol^{-1} increase in energy due to the dihedral angle ϕ.

Crystalline structure of 2,6-LCPU-6. Figure 5.6 displays a highly oriented WAXS fiber pattern of 2,6-LCPU-6 along with a sketch of the observed reflections and hkl assigned indices. Table 5.2 lists the observed and calculated d spacings from Figure 5.6. These reflections correspond to a monoclinic unit cell with a = 4.783 Å, b = 10.66 Å, c = 58.6 Å, and γ = 103° which obeys a P2$_1$/b space group symmetry. The density of this unit cell is 1.282 g/cm^3, while the experimentally observed density is 1.228 g/cm^3 (see Table 5.1). The WAXS pattern of Figure 5.6 displays a series of 00l, 01l, 02l, 10l, and $1\bar{2}l$, reflections with the 004, 028, and 101 as the most prominent ones. Figure 5.7 presents the intensity-refined results for the computer-simulated 2,6-LCPU-6 structure of Figure 5.8. The two chains in the unit cell are displaced relative to each other in order to accommodate the bulky methyl group of the TDI moiety. The H-bonds lie on the ac-plane, forming two dimensional H-bonded sheets, while the TDI rings are stacked parallel to each other (face to face) (see view along the $1\bar{2}0$ plane of Figure 5.8). Similar stacking exists for the biphenyls as well. This arrangement leads to 1.93 Å H-bond distance, 1.282 g/cm^3 density and a very strong 101 reflection.

The BHHBP's hexamethylene portions lie on the 028 plane, which give rise to the intense 028 reflection as well as the 004 reflection. In fact, if all the atoms in this unit cell were placed on the 028 plane, the meridional 00l reflections should obey the l = 4n extinction rule. Apparently, this is not completely true with the 2,6-LCPU-6 unit cell, but it is quite close. A very good intensity agreement has been achieved for the meridional reflections (001, 002, 004, and 006) of the simulated and experimental WAXS fiber patterns of Figure 5.7B and 5.7C respectively. On the other hand, with the current software package, we were unable to restrict the hexamethylene chains precisely to the 028 plane due to their great flexibility. Therefore, planes such as the 027 and 029 share substantial intensity with the 028 reflection (see Figure 5.7A and B). Realizing the

software limitations as well as the sizable unit cell of 2,6-LCPU-6 with its 264 atoms, forced us to do only a qualitative X-ray intensity refinement rather than a more rigorous calculation which would be prohibitive with respect to time limitations.

The face to face stacked arrangement of the biphenyl moieties creates an internal stress in the unit cell which causes the biphenyls to lie on the *104* plane (see view along the *b*-axis of Figure 5.8). This manifests a stepwise translation from one side of the unit cell to the other and explains the strong *101* reflection (Figure 5.7A), as well as the medium *104* reflection (Figure 5.7B and C). The displacement of the two chains relative to each other is manifested by the *011* set of reflections. The greater the displacement, the stronger the intensities of the *011* reflections, and in particular the *011* reflection. The schematic diagram for the mesophase of 2,6-LCPU-6 proposed in Figure 3.12, where the chains are not displaced relative to each other, is based on the absence of these reflections in the WAXS fiber pattern of Figure 3.11. Additional proof of this observation will be presented in the structure of 1,3-LCPU-6. Figure 5.7 indicates that the intensity of the *101* reflection has been slightly overestimated, where as for the rest of the *101* reflections (*103, 105, 107,* and *109*) the intensity agreement is poor. In terms of the rest of the reflections in the WAXS pattern of 2,6-LCPU-6, relatively good agreement has been reached for the *1 $\overline{2}$ 1* reflections (*1 $\overline{2}$ 0, 1 $\overline{2}$ 2, 1 $\overline{2}$ 6,* and *1 $\overline{2}$ 8*) and *1 $\overline{3}$ 1* reflection as shown in Figure 5.7B and C.

Figure 5.8 illustrates additional information on the key elements of the 2,6-LCPU-6 structure. As can be seen from the view along the *a*-axis, there are two distinct positions for the urethane moieties. The A position, which is more or less linear with the hexamethylene moiety, shows a 53° ± 2° phenyl-urethane torsional angle ϕ, while the B position has a $\phi = 58° ± 1°$. The greater ϕ for the B position is due to the neighboring methyl group of the TDI moiety, which causes it to rotate further in order to facilitate better packing. The H-bond distance H···O is 1.93 Å (N···O is 2.87 Å) while the H-bond angle is 171° ± 4°. The dihedral angle γ between the planes that contain the urethane and

hexamethylene groups is $3° \pm 1°$ for the A position and $56° \pm 1°$ for the B position. The biphenyl moiety on the other hand is planar and its plane is tilted relative to the hexamethylene plane by $69° \pm 3°$ and $81° \pm 5°$ for the A and B position respectively.

<u>Crystalline structure of 1,3-LCPU-6.</u> Similar analysis has been performed for the 1,3-LCPU-6 liquid crystalline polyurethane. Figure 5.9 displays a highly oriented WAXS fiber pattern of 1,3-LCPU-6 along with a sketch of the observed reflections and *hkl* assigned indices. The reflections indicated with asterisks do not belong in the unit cell discussed in this section, but in another unit cell which will be addressed under the 1,3-LCPU-6 polymorphism section . Table 5.3 lists the observed and calculated *d* spacings from Figure 5.9. These reflections correspond to an orthorhombic unit cell with $a = 5.01_0$ Å, $b = 10.2_8$ Å, $c = 54.6$ Å which belongs to a $Pbn2_1$ space group symmetry. The density of this unit cell is 1.291 g/cm^3, while the experimentally observed density is 1.24_1 g/cm^3 (see Table 5.1). The WAXS pattern of Figure 5.9 displays a series of *00l*, *02l*, *11l*, and *12l* reflections with the *002*, *004*, *028*, *029*, and *114* as the most prominent ones. Figure 5.10 presents the intensity-refined results for the computer-simulated 1,3-LCPU-6 structure of Figure 5.11. The lack of the bulky methyl group in the PDI moiety results in a regular zigzag structure with no chain displacement, like the one observed in 2,6-LCPU-6 unit cell. The H-bonds still lie on the *ac*-plane, forming two dimensional H-bonded sheets. The phenylene as well as the biphenyl groups are stacked almost perpendicularly with respect to each other, in a herringbone type of arrangement (face to edge) (see view along the 120 plane of Figure 5.11). This arrangement leads to a 1.99 Å H-bond distance, 1.29_1 g/cm^3 density and the absence of a strong equatorial reflection like the *101* of 2,6-LCPU-6.

The distinctly different packing of the 1,3-LCPU-6 relative to that of 2,6-LCPU-6 can be attributed mostly to the absence of the bulky methyl group on the PDI moiety. Although this appears to be true in general, there is still the question why the herringbone structure is more stable rather than the face to face stacked one. Molecular mechanics calculations indicate that the herringbone is the most stable structure. The herringbone

arrangement is the most common motif found in the crystal structures of benzene, naphthalene, and other lower aromatics.[38] As a result of the herringbone packing the unit cell density increases by 0.01 g/cm^3 relative to that of 2,6-LCPU-6. On the other hand, this arrangement results in a 0.06 Å longer H-bond than that of 2,6-LCPU-6 which explains the 7 °C difference in their melting points. The great difference in the wide angles of the two fiber patterns is caused by the existence of a 2_1 screw axis along the a-axis of the 1,3-LCPU-6 structure. This causes only the even $h00$ reflections to be observed, and results in the extinction of the otherwise strong 100 equatorial reflection.

The hexamethylene portions of BHHBP do not lie only on the 028 plane, but they are rather distributed between the 028 and 029 plane. This gives rise to the intense 028 and 029 reflection, but also causes the 002 reflection to be quite intense along with the most intense 004 reflection. The lack of chain displacement relative to each other, contributes to the lack of the 011 set of reflections. The 111 reflections correspond directly to the herringbone structure. For example, the hexamethylene moieties lie between the 114 and 116 plane, while the biphenyls lie between the 112 and 114 plane. Good X-ray intensity agreement has been reached between the simulated and experimental fiber patterns of Figure 5.10B and C respectively. As it will be discussed in the polymorphism section of 1,3-LCPU-6, the fiber pattern of Figure 5.9 and 5.10C arises from the scattering of more than one unit cell. Additional concern has also been raised by DSC experiments about how much of the mesophase is still present in this WAXS fiber pattern. The presence of the mesophase greatly alters the intensities of the meridional reflections, and causes them to be far more intense than the simulated ones. In addition to this, software limitation causes similar problems in restricting the hexamethylene chains between the 028 and 029 plane, and the final product indicates that they are distributed between the 029 and 0210 plane. In terms of the rest of the reflections in the WAXS pattern of 1,3-LCPU-6, a moderate agreement has been achieved for the 121 reflections (120, 122, 124, 126, 128, and 1210) as shown in Figure 5.7.

157

Figure 5.11 illustrates addition information on the key elements of the 1,3-LCPU-6 structure. The phenyl-urethane torsional angle ϕ is $55° \pm 9°$. The relatively large error in this measurement arises from the urethane moiety which is not perfectly planar . The H-bond distance H···O is 1.99 Å (N···O is 2.94 Å) while the H-bond angle is $175.2°$. The dihedral angle γ between the planes of the urethane and hexamethylene groups is $9° \pm 1°$. The biphenyl moiety on the other hand is planar and its plane is tilted relative to the hexamethylene plane by $76° \pm 1°$.

Crystalline structure of 2,6-PU-6. For the 2,6-PU-6 and 1,3-PU-6 "regular" polyurethanes, although fibers were drawn from the melt, X-ray diffraction indicated their complete lack of orientation. On the basis of structural similarity, and with the help of well resolved X-ray powder patterns, we were able to deduce the crystalline chain conformation of the "regular" polyurethanes as well. Table 5.4 lists the observed and calculated reflections from the 2,6-PU-6 WAXS powder pattern of Figure 5.12C. These reflections correspond to a monoclinic unit cell with $a = 4.722$ Å, $b = 10.47$ Å, $c = 31.5$ Å, and $\gamma = 103°$ which belongs to a $P2_1/b$ space group symmetry. The density of this unit cell is 1.279 g/cm^3, while the experimentally observed density is 1.274 g/cm^3 (see Table 5.1). Figure 5.12 presents the intensity-refined results for the computer-simulated 2,6-PU-6 structure of Figure 5.13. Similar to the 2,6-LCPU-6 structure, the two chains in the unit cell are displaced relative to each other to accommodate the bulky methyl group of the TDI moiety. The H-bonds lie on the ac-plane, forming two dimensional H-bonded sheets, while the TDI rings are stacked parallel to each other (face to face). This arrangement leads to 1.92 Å H-bond distance, 1.279 g/cm^3 density and a very strong 100 reflection. The H-bond distance is 0.01 Å shorter than the 2,6-LCPU-6.

According to the simulated WAXS fiber pattern of 2,6-PU-6 (see Figure 5.12A and B), the $00l$, $01l$, $02l$, $10l$, and $\overline{1}\,\overline{2}\,l$ set of reflections can be observed. The medium-broad inner scattering ring of Figure 5.12C corresponds to the 002 meridional reflection. The broad character of this reflection suggests a relatively large variation of c-axis lengths or

158

comparable small crystalline sizes in the c-dimension. The medium sharp *011* reflection along with the weaker *013* reflection establishes the fact that the chains are displaced relative to each other in order to accommodate the bulky methyl group. The very strong and sharp ring at 4.60 Å corresponds primarily to the *100* reflection, reminiscent of the *101* reflection of the 2,6-LCPU-6. The strong and broad 4.18 Å reflection corresponds to the *024* and *025* planes that arise from the stacking of the hexamethylene moieties. On the other hand the medium, well distinguished 3.88 Å reflection is due to the *1 $\overline{2}$ 1* plane where the TDI moieties are located. Considering the difficulty to interpret a WAXS powder pattern, relatively good X-ray intensity agreement has been reached, as indicated from Figure 5.12.

Figure 5.13 illustrates addition information on the key elements of the 2,6-PU-6. As can be seen from the view along the a-axis, there are two positions for the urethane moieties. Similar to the 2,6-LCPU-6, the A position which is more or less linear with the hexamethylene moiety, shows a $53° \pm 1°$ phenyl-urethane torsional angle ϕ, while the B position a $\phi = 56° \pm 2°$. The H-bond distance H$\cdots$O is 1.92 Å (N$\cdots$O is 2.86 Å) while the H-bond angle is $168° \pm 3°$. The dihedral angle γ between the planes that contain the urethane and hexamethylene groups is $4° \pm 1°$ for the A position and $63° \pm 3°$ for the B position.

<u>Crystalline structure of 1,3-PU-6.</u> Table 5.5 lists the observed and calculated reflections from the 1,3-PU-6 WAXS powder pattern of Figure 5.14C. These reflections correspond to an orthorhombic unit cell with $a = 5.28_0$ Å, $b = 10.16$ Å, $c = 25.83$ Å which belongs to a Pbn2_1 space group symmetry. The density of this unit cell is 1.33_4 g/cm^3, while the experimentally observed density is 1.26_5 g/cm^3 (see Table 5.1). Figure 5.14 presents the intensity-refined results for the computer-simulated 1,3-PU-6 structure of Figure 5.15. Similar to the 1,3-LCPU-6 structure, the lack of the bulky methyl group on the PDI moiety results in a regular zigzag structure with no chain displacement, like the one observed in 2,6-LCPU-6 and 2,6-PU-6 unit cell. The H-bonds still lie on the ac-plane

159

forming two dimensional H-bonded sheets, while the phenylene and biphenyl groups are stacked in a herringbone type of arrangement (face to edge). This arrangement leads to a 2.22 Å H-bond distance, 1.334 g/cm³ density and the absence of a strong equatorial reflection. Although this organization densifies the unit cell considerably, it results in a 0.3 Å longer H-bond than the 2,6-PU-6 which explains the 70 °C melting point difference.

According to the simulated WAXS fiber pattern of 1,3-PU-6 (see Figure 5.14A and B), the *001, 021, 111*, and *121* set of reflections can be observed. The strong and broad inner scattering ring as well as a faint ring at twice the radius of the first one correspond to the *002* and *004* meridional reflections (see Figure 5.14C) Similar to the 2,6-PU-6 the broad character of this reflection suggest a relatively large variation of *c*-axis lengths or comparable small crystalline sizes in the *c*-dimension. The medium-strong, well-distinguished 4.73 Å reflection corresponds mainly to the *110* plane, which is quite prominent due to the herringbone stacking. Similar to the 1,3-LCPU-6, the *021* and *111* reflections dominate those causing the greater intensity. The *113* is the most intense of the *111* reflections, while the *025* and *026* are among the strongest *021* reflections because the hexamethylene chains lie on these planes. Considering the strong overlap of equally spaced reflections and the limited resolution of the present WAXS powder pattern, relatively good X-ray intensity agreement has been reached, as indicated from Figure 5.14.

Figure 5.15 illustrates additional information on the key elements of the 1,3-PU-6 structure. The phenyl-urethane torsional angle ϕ is 53° ± 7°. Similarly to the 1,3-LCPU-6, the relatively large error in this measurement arises from the fact that the urethane moiety is not perfectly planar. The H-bond distance H⋯O is 2.22 Å (N⋯O is 3.18 Å) while the H-bond angle is 172° ± 1°. On the other hand the dihedral angle γ between the planes of the urethane and hexamethylene groups is 22° ± 5°.

Polymorphism of 1,3-LCPU-6. As has been mentioned previously, the 1,3-LCPU-6 fiber pattern of Figure 5.9 and 5.10C is a result of more than one structure. In particular, the reflections indicated with asterisks have not been addressed by the

160

crystallographic analysis of the herringbone structure of 1,3-LCPU-6. Specifically, the equatorial reflection at 4.0 Å is located where there are no other nearby reflections from the calculated WAXS fiber pattern of the herringbone structure (see and compare Figure 5.10B and C). According to extensive molecular simulations performed for the face to face stacked 1,3-LCPU-6 (see Figure 5.16), this structure possesses a strong $1\bar{1}0$ reflection that can explain the 4.0 Å reflection. In addition to that, its very strong 101 reflection that can also address the inner equatorial reflection of Figure 5.9, marked by one asterisk. According to these reflections, the structure of Figure 5.16 is expected to melt at higher than 202 °C (melting point of the herringbone structure), because of its shorter H-bond distance (H···O distance of about 1.89 to 1.91 Å). Indeed, a number of small endotherms over 202 °C have been observed for highly crystalline fibers of the 1,3-LCPU-6, with the 221 °C endotherm as the most prominent one (see Figure 3.16).

Correlation of melting points and H-bond distances. Figure 5.17 plots the H-bond distances versus the melting point temperatures of the crystallographically investigated 2,6-PU-6, 2,6-LCPU-6, 1,3-LCPU-6 and 1,3-PU-6 samples. On the basis of the good correlation between the H-bond distance[**] and the melting temperature, it is suggested that melting is primarily controlled by the dissociation of H-bonds in the ordered domains. This result is in agreement with the dramatic depression of the transition temperatures of the N-methyl substituted polyurethanes presented in Chapter 2 of this dissertation. In addition to that, preliminary studies on the increase of the melting point upon perfection of the 2,6-LCPU-6's unit cell (which causes the H-bond distance to become shorter) suggests a similar effect of the H-bond strength on the melting point temperature for this class of materials.

[**]   The comparable (near 180°) H-bonding angle (ω) for the four polymers allows $\cos^2\omega$ to be taken as a constant.

Conclusions

1) The competition between the phenyl-urethane torsional angle ϕ and the H-bonding angle ω controls the c-axis length of the meta substituted phenylene or tolylene diisocyanate based polyurethanes.

2) The steric hindrance of the TDI's methyl group makes the herringbone arrangement of the TDI rings unfavorable. The final stacked arrangement decreases the density and strengthens H-bonding by decreasing the H-bond distance.

3) The good correlation between the H-bond distance and the melting temperature suggests that melting is primarily controlled by the dissociation of H-bonds in the ordered domains.

Table 5.1

Observed[‡] and calculated[*] densities for "regular" and mesogenic polyurethanes.

Polyurethane sample	Compressed, and slowly cooled at 25 °C. Density (g/cm^3)	Annealed at 160 °C for 3 days. Density (g/cm^3)	Soxhlet extracted in hot MeOH and annealed [**] Density (g/cm^3)	Calculated, unit cell density. Density (g/cm^3)
2,6-LCPU-6	1.22$_3$	1.22$_8$	- -	1.28$_2$
1,3-LCPU-6	1.23$_3$	1.24$_1$	- -	1.29$_1$
2,4-LCPU-6	1.21$_1$	1.21$_1$	- -	#
2,6-PU-6	1.26$_3$	- -	1.274	1.27$_9$
1,3-PU-6	1.25$_5$	- -	1.26$_5$	1.33$_4$
2,4-PU-6	1.23$_2$	- -	1.226	##

‡ Measured in a toluene-carbon tetrachloride density gradient column at 21.0 °C.

* On the basis of crystallographic analysis.

** Samples were soxhlet extracted in hot MeOH, vacuum dried at 60 °C, compressed at 110 °C (20 °C above their glass transition temperature) to minimize the void contribution to density due to solvent evaporation, and annealed 20-30 °C below their melting point in order to maximize the degree of crystallinity.

The crystallographic analysis of 2,4-LCPU-6 is not available at the present.

2,4-PU-6 is an amorphous polymer.

Table 5.2

Observed and calculated d spacings from Figure 5.6, 2,6-LCPU-6 WAXS fiber pattern.

unit cell params	scattering condtns, obsd	scattering condtns, P2$_1$/b
$a = 4.783$ Å		
$b = 10.66$ Å	$00l$: $l = 2n$	hkl: No conditions
$c = 58.6$ Å	$hk0$: $k = 2n$	$00l$: $l = 2n$
$\gamma = 103°$		$hk0$: $k = 2n$

$\rho_{calcd} = 1.282$ g/cm^3 $\rho_{obsd} = 1.228$ g/cm^3

h	k	l	d_{calcd} Å	d_{obsd} Å	Intensity
0	0	2	29.30	29.06	medium, sharp
0	0	4	14.65	14.67	strong, sharp
0	0	6	9.77	9.76	weak w.d.‡
0	1	1	10.23	10.23	medium, sharp
0	1	3	9.17	9.12	weak, w.d.‡
0	1	5	7.77	7.85	weak, w.d.
0	1	7	6.52	6.62	weak, w.d.
0	1	9	5.52	5.61	faint, w.d.
0	2	0	5.19	} 5.15	medium, sharp
0	2	2	5.11		
0	2	8	4.24	4.24	med. strong, w.d.‡
0	2	10	3.89	3.90	weak, w.d.
1	0	1	4.66	4.66	very strong, sharp
1	0	4	4.44	4.44	medium, sharp
1	-2	0	3.94	3.94	medium, diffuse
1	-2	2	3.90	3.90	medium, diffuse
1	-2	6	3.65	3.68	medium, w.d.‡
1	-2	8	3.47	3.48	weak, w.d.
1	-3	1	3.13	3.13	weak, w.d.

‡ Well distinguished.

Table 5.3

Observed and calculated d spacings from Figure 5.9, 1,3-LCPU-6 WAXS fiber pattern.

unit cell params	scattering condtns, obsd	scattering condtns, Pbn2₁
$a = 5.010$ Å	$h0l$: $h + l = 2n$	hkl: No conditions
$b = 10.28$ Å	$0kl$: $k = 2n$	$h0l$: $h + l = 2n$
$c = 54.6$ Å	$h00$: $k = 2n$	$0kl$: $k = 2n$
	$0k0$: $k = 2n$	$hk0$: No conditions
$\alpha = \beta = \gamma = 90°$	$00l$: $l = 2n$	$h00$: $k = 2n$
		$0k0$: $k = 2n$
$\rho_{calcd} = 1.291$ g/cm³	$\rho_{obsd} = 1.241$ g/cm³	$00l$: $l = 2n$

h	k	l		d_{calcd} Å	d_{obsd} Å	Intensity
0	0	2		27.30	27.38	strong, sharp
0	0	4		13.65	13.64	very strong, sharp
0	0	6		9.10	9.02	weak w.d.‡
0	0	8		6.83	6.84	medium w.d.
0	0	12		4.55	4.55	faint, broad
0	2	0		5.14	5.14	medium, sharp
0	2	2		5.05	5.03	weak, w.d.‡
0	2	4		4.81	4.83	weak, w.d.
0	2	7		4.29	4.27	weak, w.d.
0	2	8		4.11	4.08	med. strong, sharp
0	2	9		3.92	3.87	med. strong, sharp
0	2	11		3.57	3.53	medium, w.d.‡
1	0	5		4.55	4.53	weak, w.d.
1	1	0	*	4.50	4.60	medium, sharp*
1	1	2		4.44	4.45	medium, broad
1	1	4		4.28	4.23	med. strong, diffuse
1	1	6		4.04	4.08	medium, diffuse
1	1	7		3.90	3.87	weak, broad
1	2	0		3.59	3.63	weak, diffuse
1	2	2		3.56	3.58	weak, diffuse
1	2	4		3.47	3.51	medium, diffuse
1	2	6		3.34	3.34	med. strong, sharp
1	2	8		3.18	3.17	weak, diffuse
1	2	10		3.00	2.98	weak, diffuse

‡ Well distinguished.

* This reflection might not belong in this unit cell and be a result of polymorphism. See text for details.

Table 5.4

Observed and calculated d spacings from Figure 5.12C,
2,6-PU-6 WAXS powder pattern.

unit cell params	scattering condtns, obsd	scattering condtns, P2$_1$/b
$a = 4.72_2$ Å		
$b = 10.47$ Å	$00l$: $l = 2n$	hkl: No conditions
$c = 31.5$ Å	$hk0$: $k = 2n$	$00l$: $l = 2n$
$\gamma = 103°$		$hk0$: $k = 2n$

$\rho_{calcd} = 1.279$ g/cm^3 $\rho_{obsd} = 1.274$ g/cm^3

h	k	l	d_{calcd} Å	d_{obsd} Å	Intensity
0	0	2	15.75	15.75	medium, broad
0	1	1	9.71	9.71	medium, sharp
0	1	3	7.32	7.30	weak, broad
0	2	0	5.10	} 5.09	strong, w.d.[‡]
0	2	1	5.04		
1	0	0	4.60	} 4.60	very strong, sharp
0	2	3	4.59		
0	2	4	4.28	} 4.18	strong, broad
0	2	5	3.96		
1	-2	1	3.85	3.88	medium, w.d.[‡]
1	-2	2	3.76	3.72	very weak, w.d.
1	-2	3	3.64	} 3.55	medium, broad
1	-2	4	3.48		
1	-2	5	3.30	3.35	faint, broad
1	-3	1	3.07	3.06	weak, diffuse

[‡] Well distinguished.

Table 5.5

Observed and calculated d spacings from Figure 5.14C,
1,3-PU-6 WAXS powder pattern.

unit cell params	scattering condtns, obsd	scattering condtns, $Pbn2_1$
$a = 5.280$ Å	$h0l$: $h + l = 2n$	hkl: No conditions
$b = 10.16$ Å	$0kl$: $k = 2n$	$h0l$: $h + l = 2n$
$c = 25.83$ Å	$h00$: $k = 2n$	$0kl$: $k = 2n$
$\alpha = \beta = \gamma = 90\,°$	$0k0$: $k = 2n$	$hk0$: No conditions
	$00l$: $l = 2n$	$h00$: $k = 2n$
		$0k0$: $k = 2n$
$\rho_{calcd} = 1.334$ g/cm^3	$\rho_{obsd} = 1.265$ g/cm^3	$00l$: $l = 2n$

h	k	l	d_{calcd} Å	d_{obsd} Å	Intensity
0	0	2	12.92	12.92	strong, broad
0	0	4	6.46	6.60	faint, diffuse
1	0	1	5.17	5.04	weak, broad
0	2	0	5.08		
1	1	0	4.69	4.75	med. strong, w.d.[‡]
0	2	2	4.73		
0	2	3	4.66	4.40	weak, broad
1	1	2	4.38		
1	1	3	4.12	4.08	med. strong, broad
0	2	4	3.99		
1	1	4	3.79	3.72	strong, broad
1	2	1	3.62		
0	2	5	3.62		
1	2	3	3.37	3.41	weak, broad
0	2	6	3.28	3.21	medium, w.d.[‡]

[‡] Well distinguished.

167
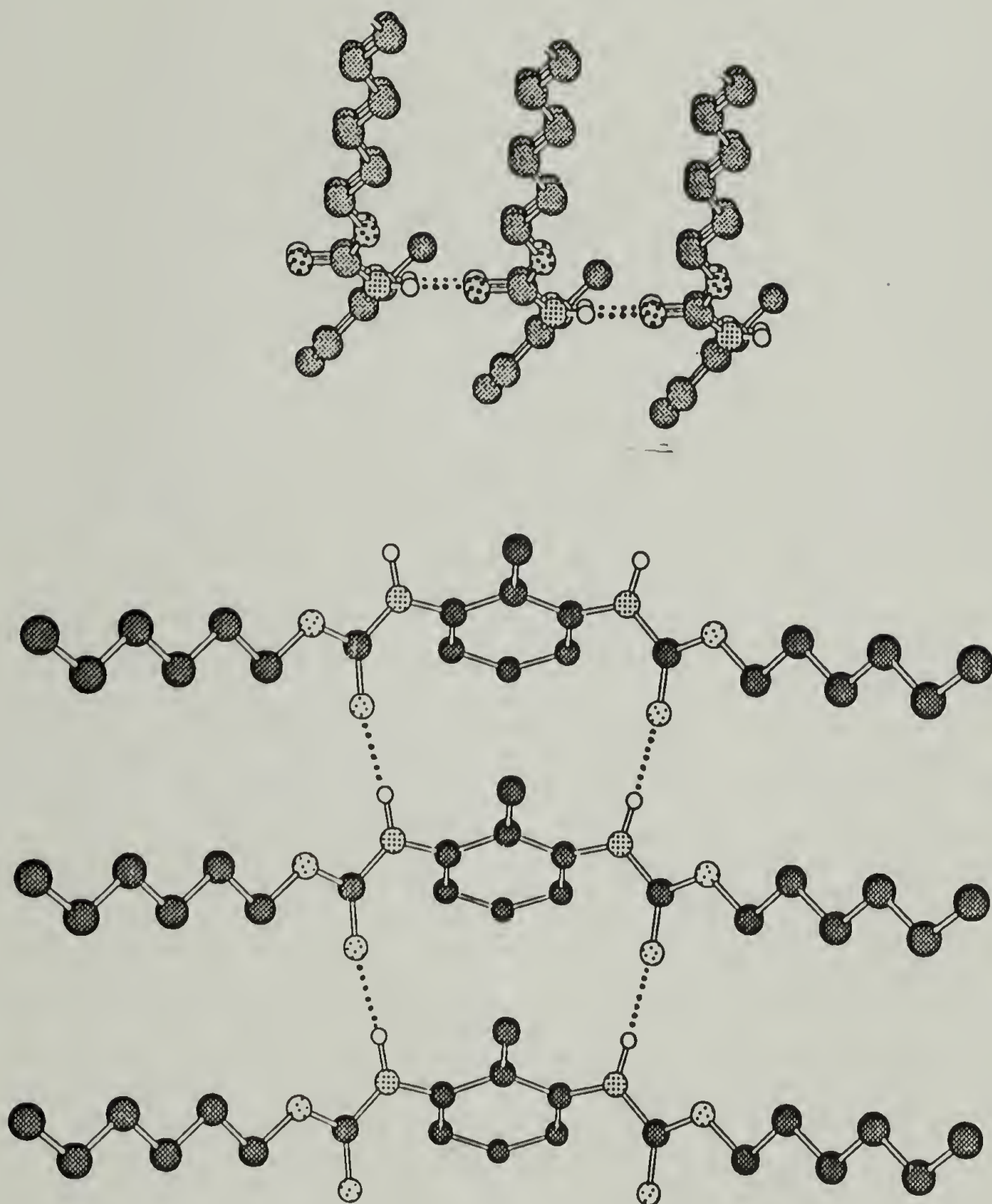
Figure 5.1 Favorable conformation of meta-substituted phenylene diurethanes in order to achieve complete H-bonding.
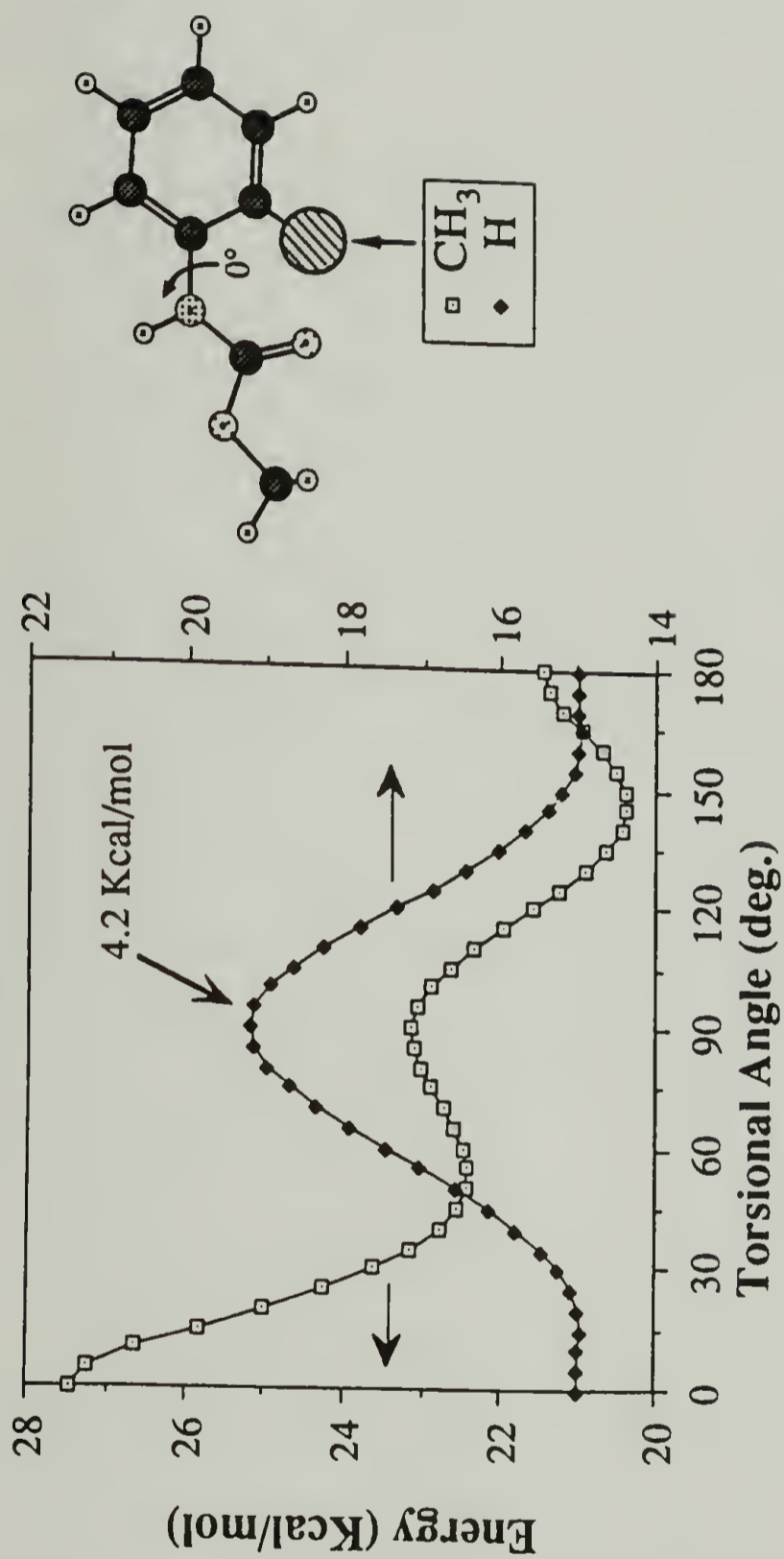
Figure 5.2 Conformational energy as a function of the phenyl-urethane torsional angle (ϕ), for the phenyl-methyl-carbamate and o-tolyl-methyl-carbamate, based on Dreiding II empirical force-field (energy minimization was applied at each individual angle).
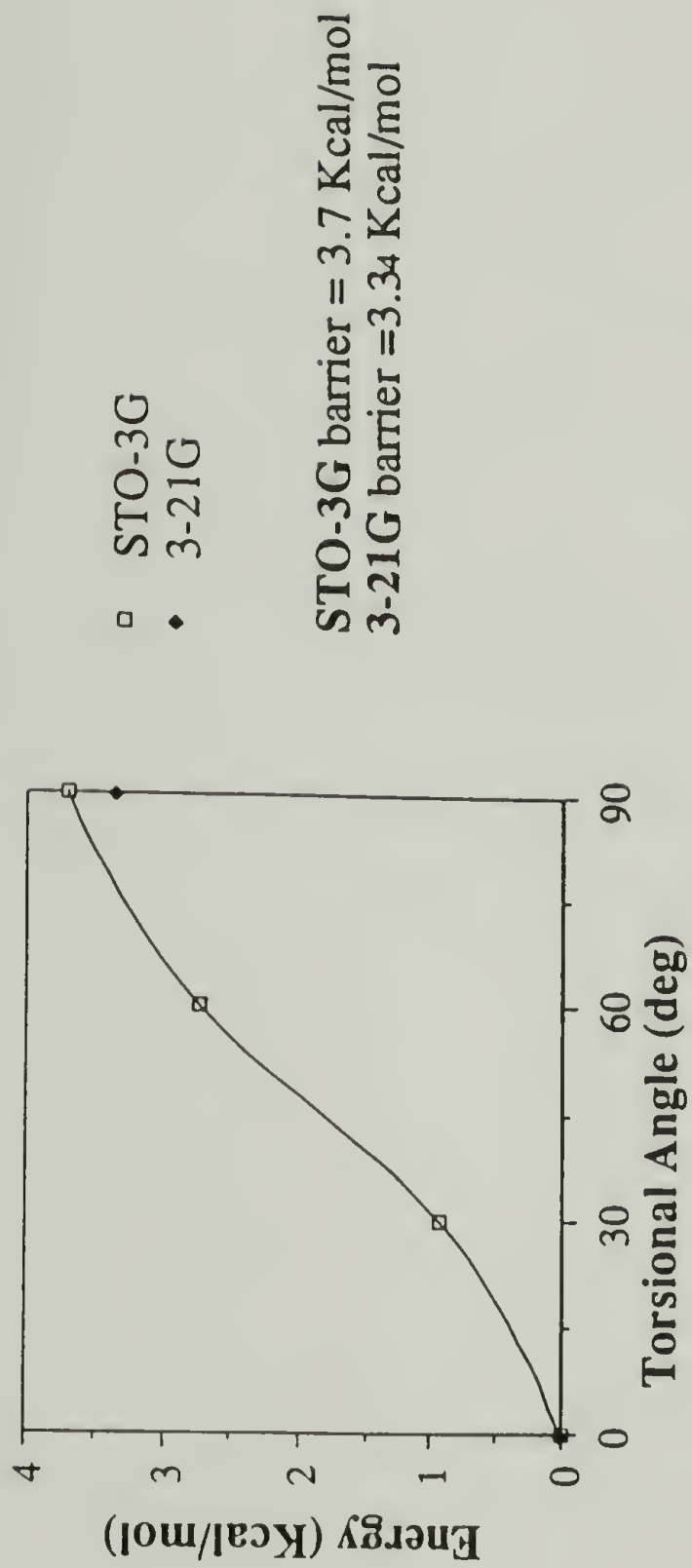
Figure 5.3 *Ab initio conformational search of the phenyl-urethane torsional angle (φ), for the phenyl–methyl–carbamate, at the STO-3G (0°, 30°, 60°, and 90°) and 3-21G (0° and 90°) level.*
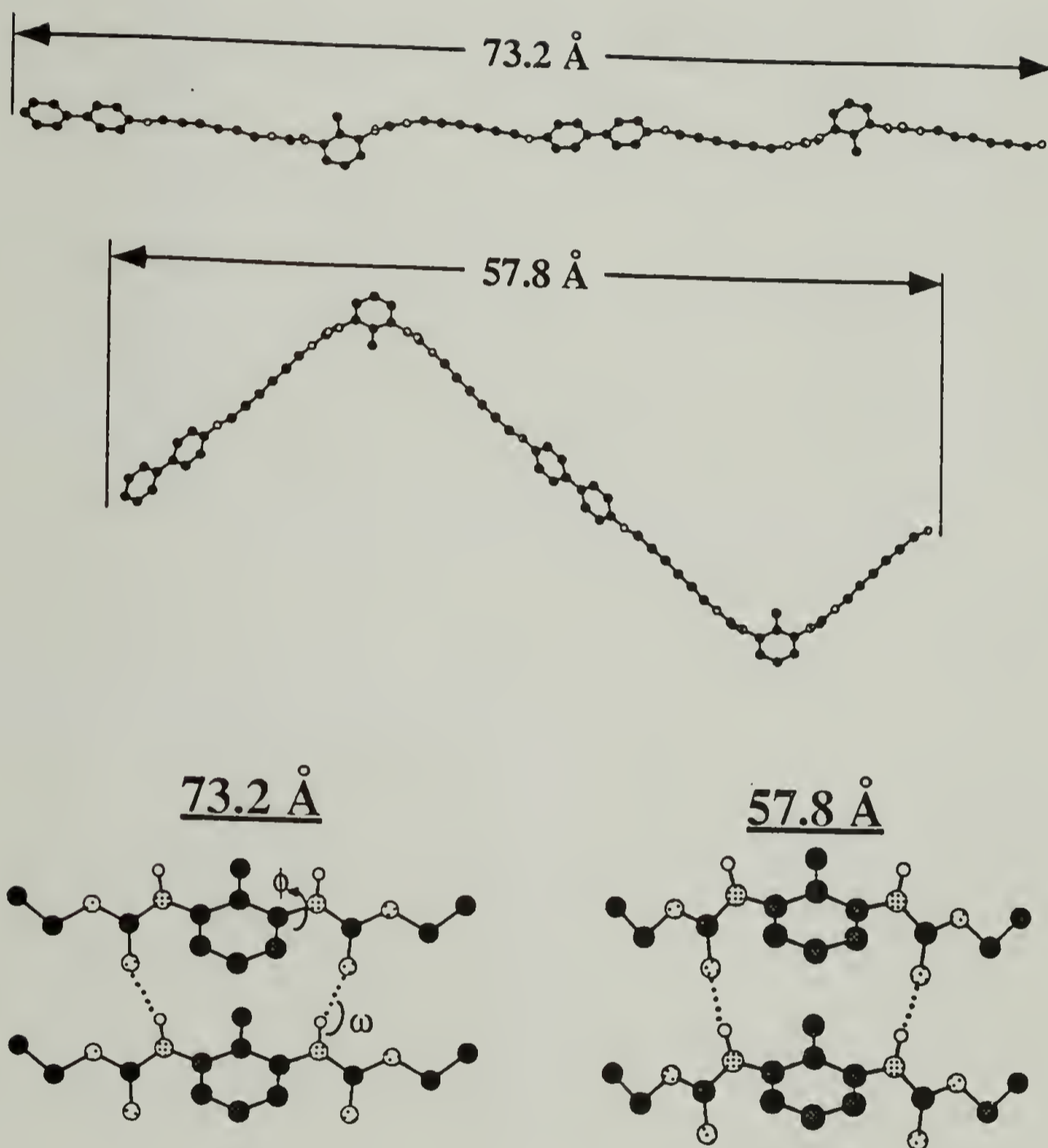
Figure 5.4 Conformational characteristics of 2,6-LCPU-6 molecular repeat at maximum c-axis extension (73.2 Å) and in a fully relaxed unit cell (57.8 Å). See text for details.
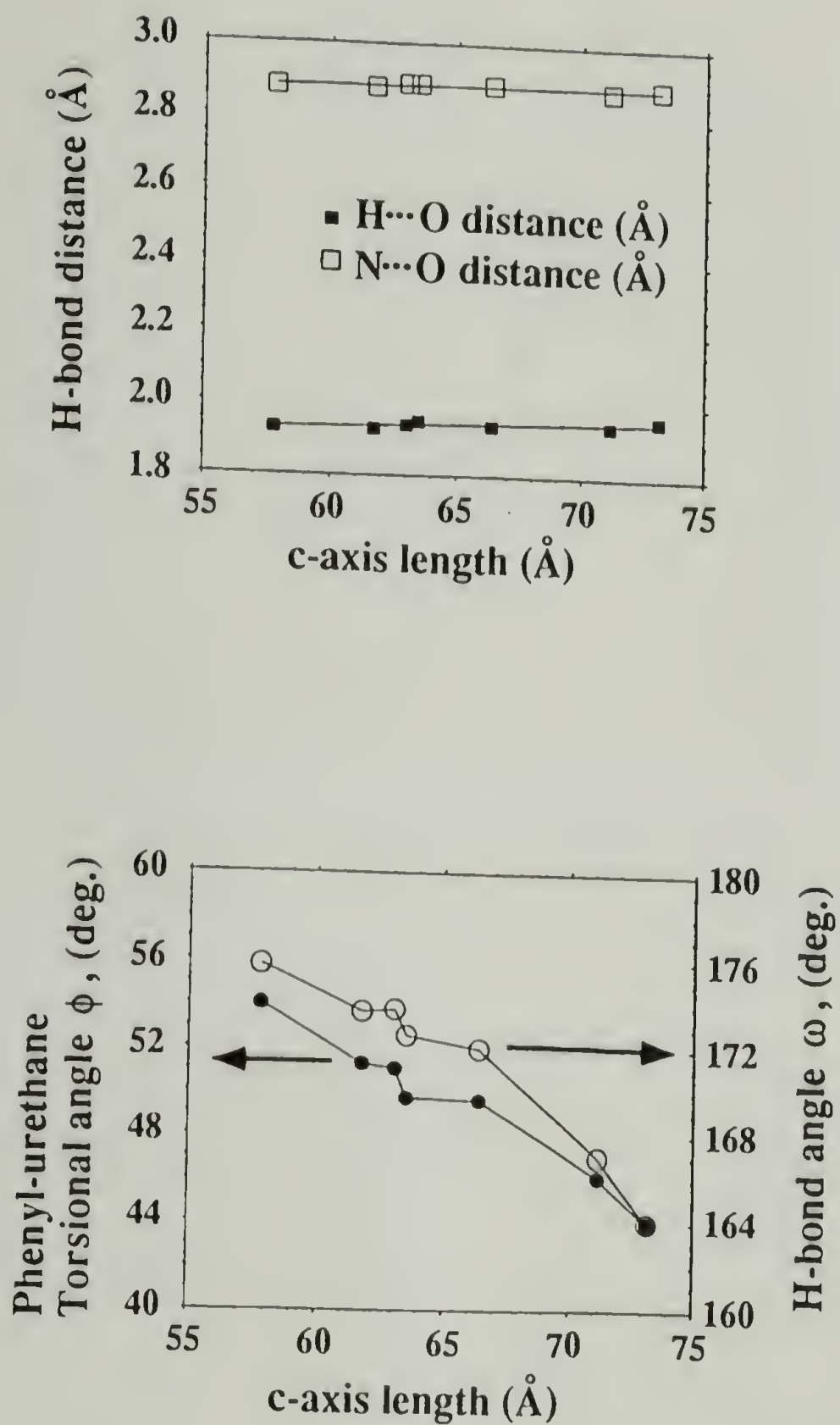
Figure 5.5 Dependence of H-bond distance, phenyl-urethane torsional angle (φ), and H-bond angle (ω), as a function of the c-axis length for the 2,6-LCPU-6 dimer repeat.
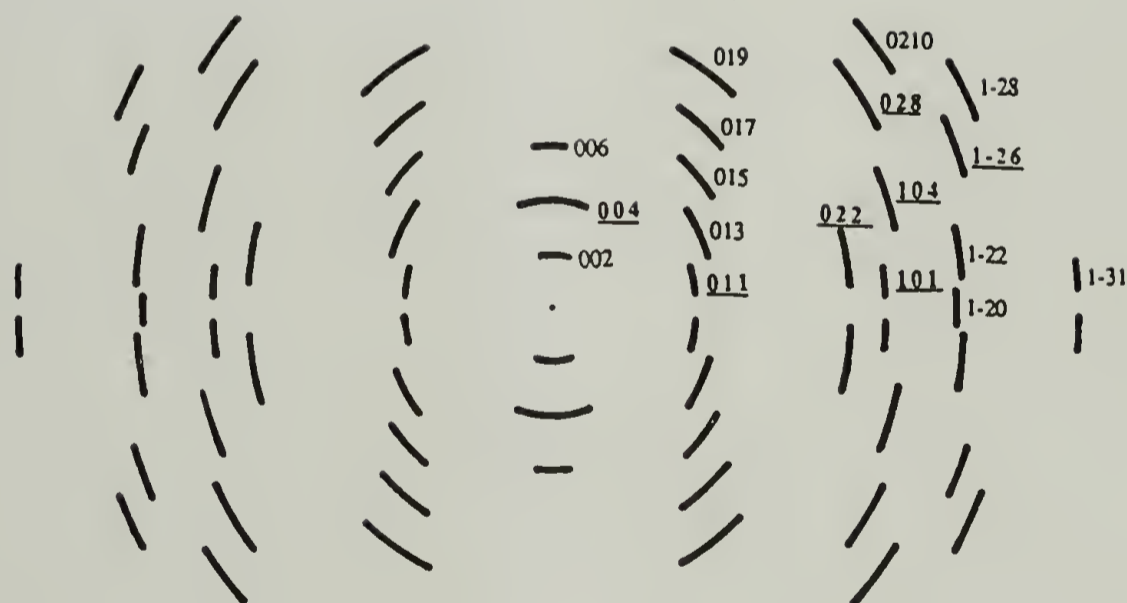
Figure 5.6 Room temperature X-ray diffraction pattern of a high molecular weight 2,6-LCPU-6 fiber drawn from the melt, soxhlet extracted in hot MeOH for four days, and subjected to 5-days annealing at 165 °C (upper part). Sketch of the observed reflections along with their assigned *hkl* indices (lower part).

Figure 5.7 Computer simulated (A and B) and experimental (C) WAXS fiber patterns for the 2,6-LCPU-6.

(A) CMD-Cerius® simulated X-ray fiber pattern in ideal orientation.

(B) CMD-Cerius® "realistic" fiber pattern with the following parameters:

Camera type:	Flat
Film scale:	Linear
Fiber tilt angle:	0°
Orientation distribution half-width:	7.5°
Crystallite size (a, b, c):	400, 350, 750 Å
Lattice distortion factors:	0, 0.5, 0.2

174
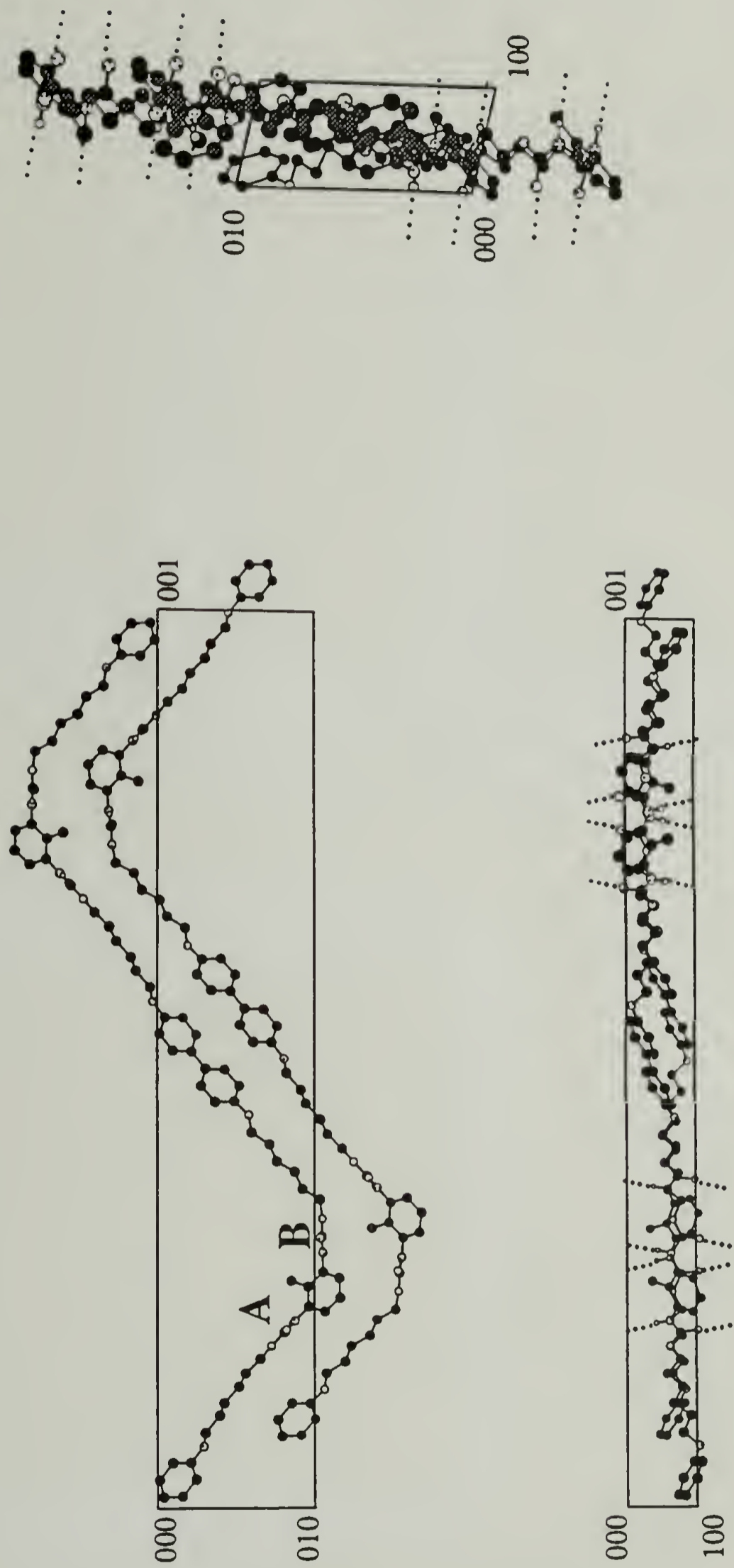
Views along a-axis (top), b-axis (bottom) and c-axis (right) of 2,6-LCPU-6 unit cell.

Figure 5.8 Crystal structure of 2,6-LCPU-6 showing the phase to phase stacking of TDI and biphenyl rings.

175
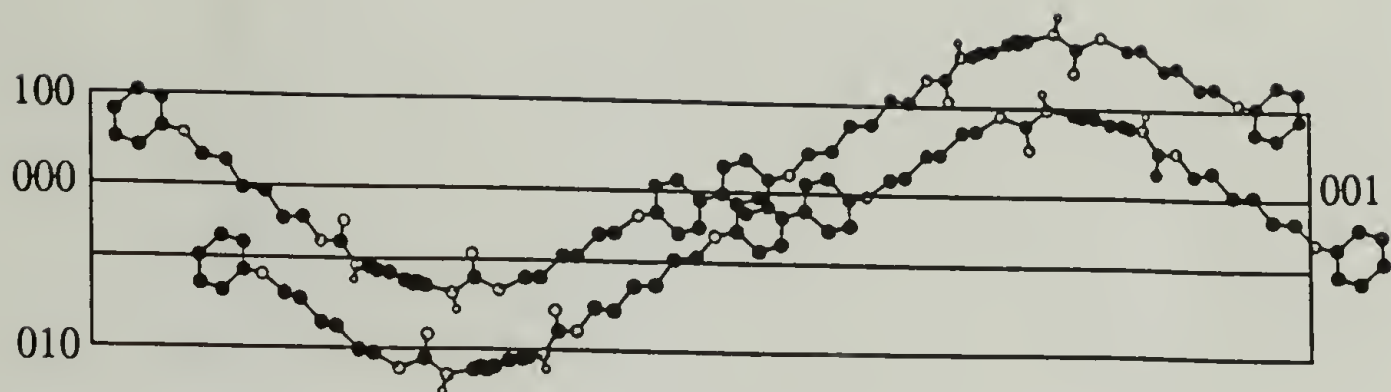
2,6-LCPU-6 unit cell
view along the 1$\bar{2}$0 plane

Unit cell, (monoclinic)
$a = 4.783$ Å
$b = 10.66$ Å
$c = 58.6$ Å
$\gamma = 103°$

Space Group:

$P2_1/b$ C_{2h}^5

Density:
calc: 1.282 g/ml
exp: 1.228 g/ml

H-bond Distance:
$H \cdots O = 1.93$ Å
$N \cdots O = 2.87$ Å

H-bond Angle:
$\stackrel{\frown}{N\text{-}H\text{-}O} = 171° \pm 4°$

Phenyl-Urethane Torsional Angle:

Position A: $53° \pm 2°$
Position B: $58° \pm 1°$

Figure 5.8   (Continued.)
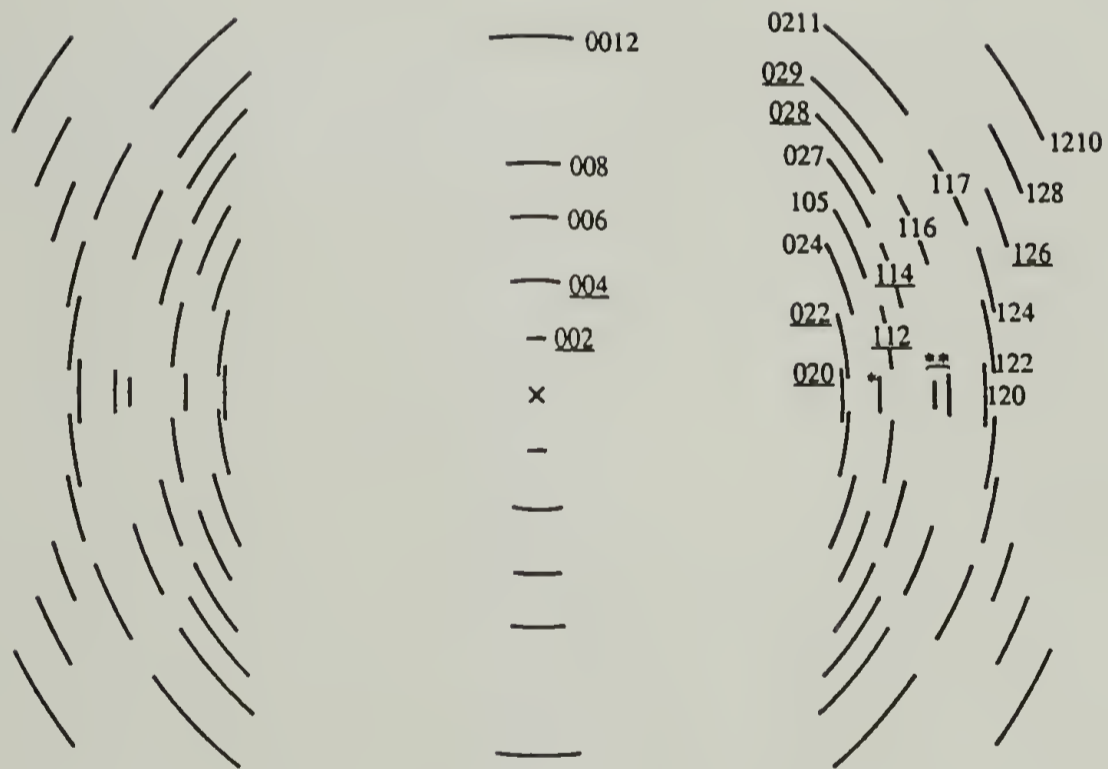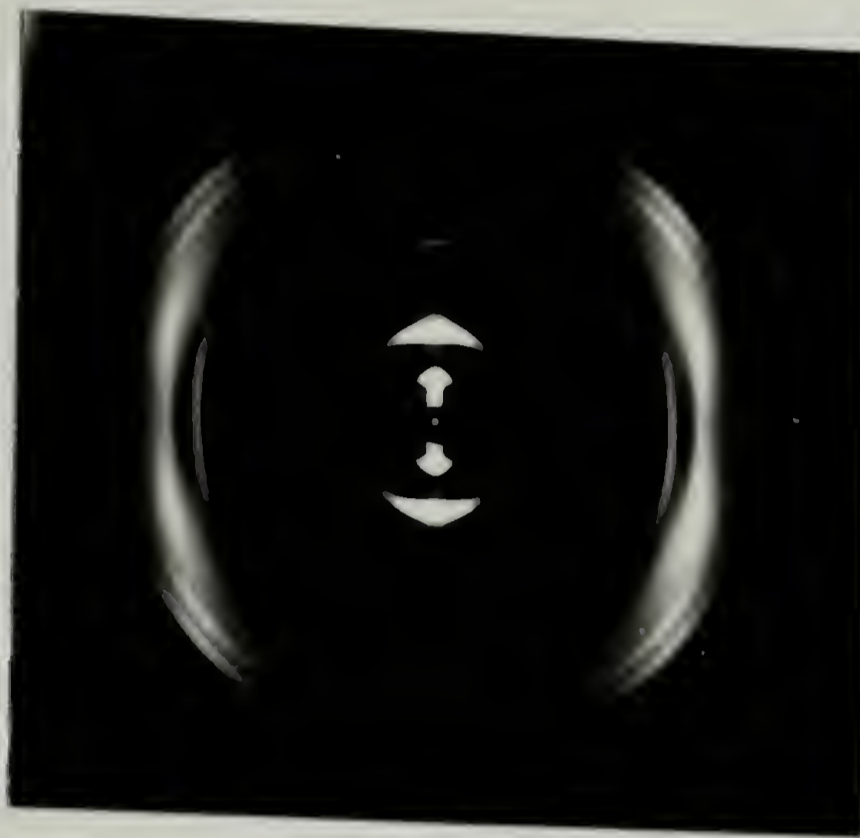
Figure 5.9 Room temperature X-ray diffraction pattern of a 1,3-LCPU-6 fiber drawn from the melt, soxhlet extracted in hot MeOH for 4-days, and subjected to 5-days annealing at 165 °C (upper part). Sketch of the observed reflections along with their assigned *hkl* indices (lower part).
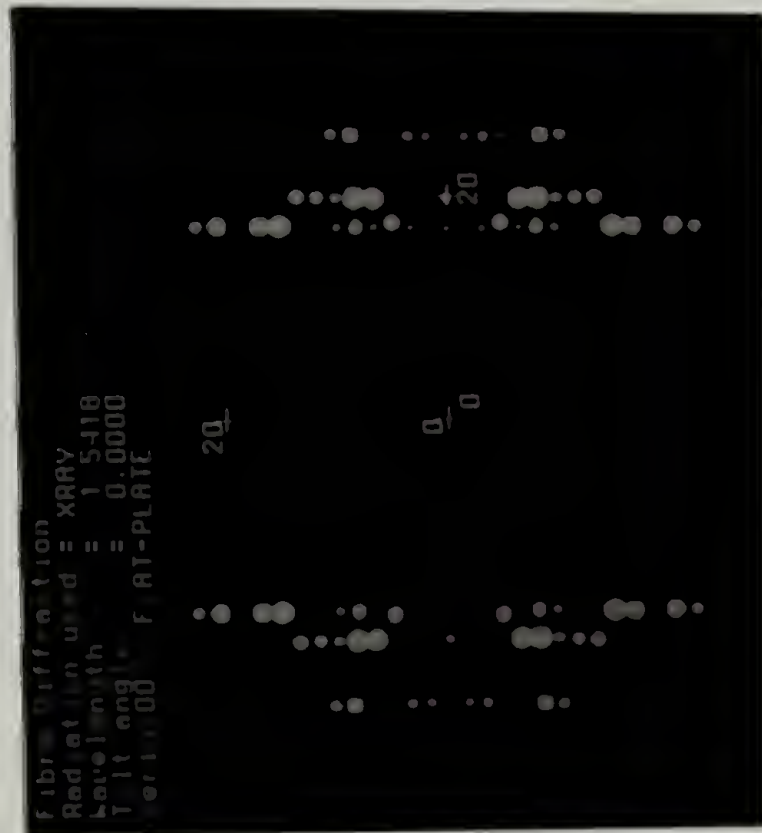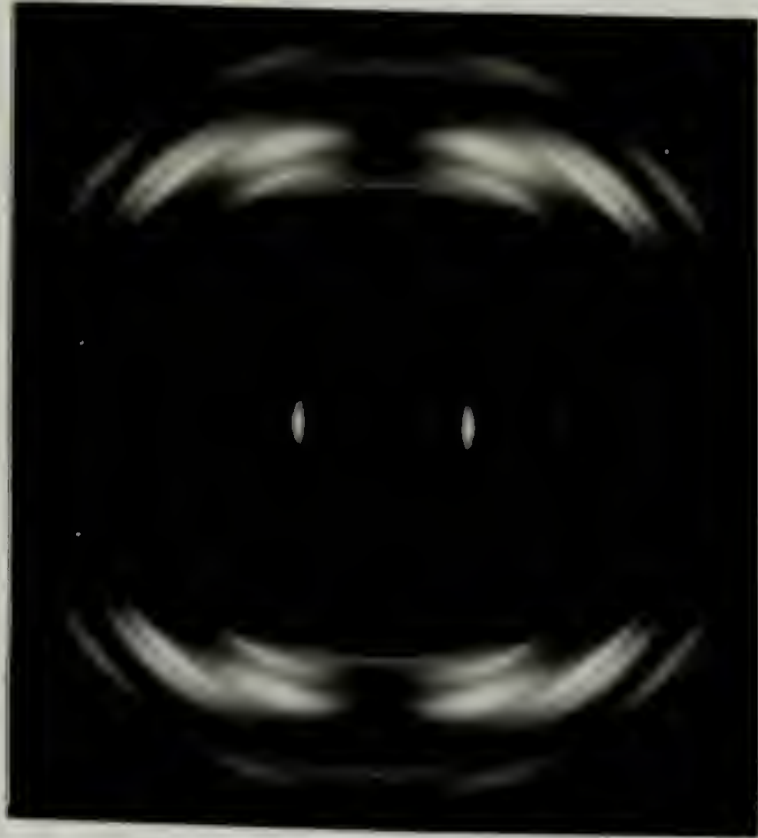
Figure 5.10 Computer simulated (A and B) and experimental (C) WAXS fiber patterns for the 1,3-LCPU-6.

(A) CMD-Cerius® simulated X-ray fiber pattern in ideal orientation.

(B) CMD-Cerius® "realistic" fiber pattern with the following parameters:

Camera type:	Flat
Film scale:	Linear
Fiber tilt angle:	0°
Orientation distribution half-width:	8.5°
Crystallite size (a, b, c):	500, 750, 650 Å
Lattice distortion factors:	2, 0, 0.75
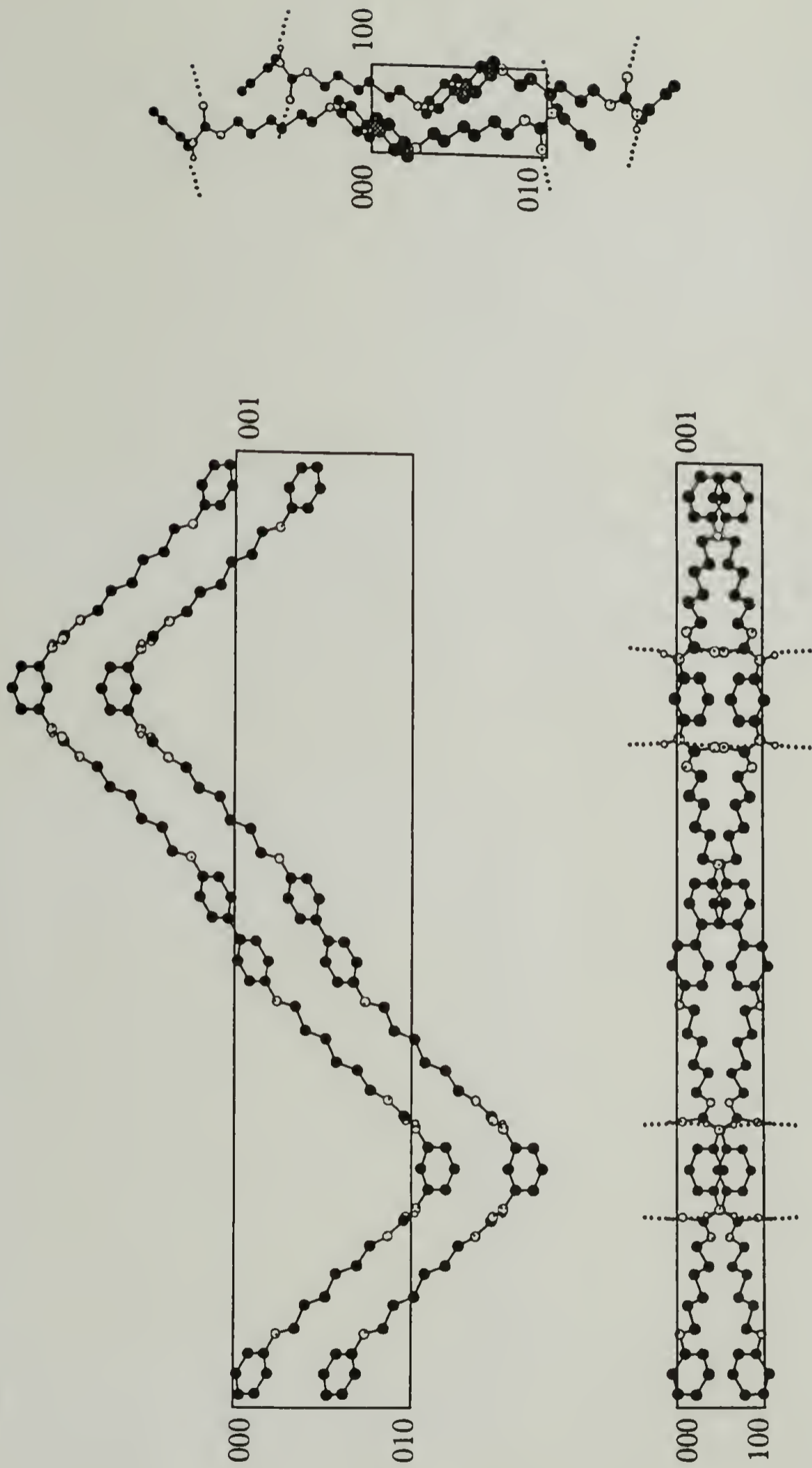
Views along a-axis (top), b-axis (bottom) and c-axis (right) of 1,3-LCPU-6 unit cell.

Figure 5.11 Crystal structure of 1,3-LCPU-6 showing the phase to edge (herringbone) packing of PDI and biphenyl rings.

179
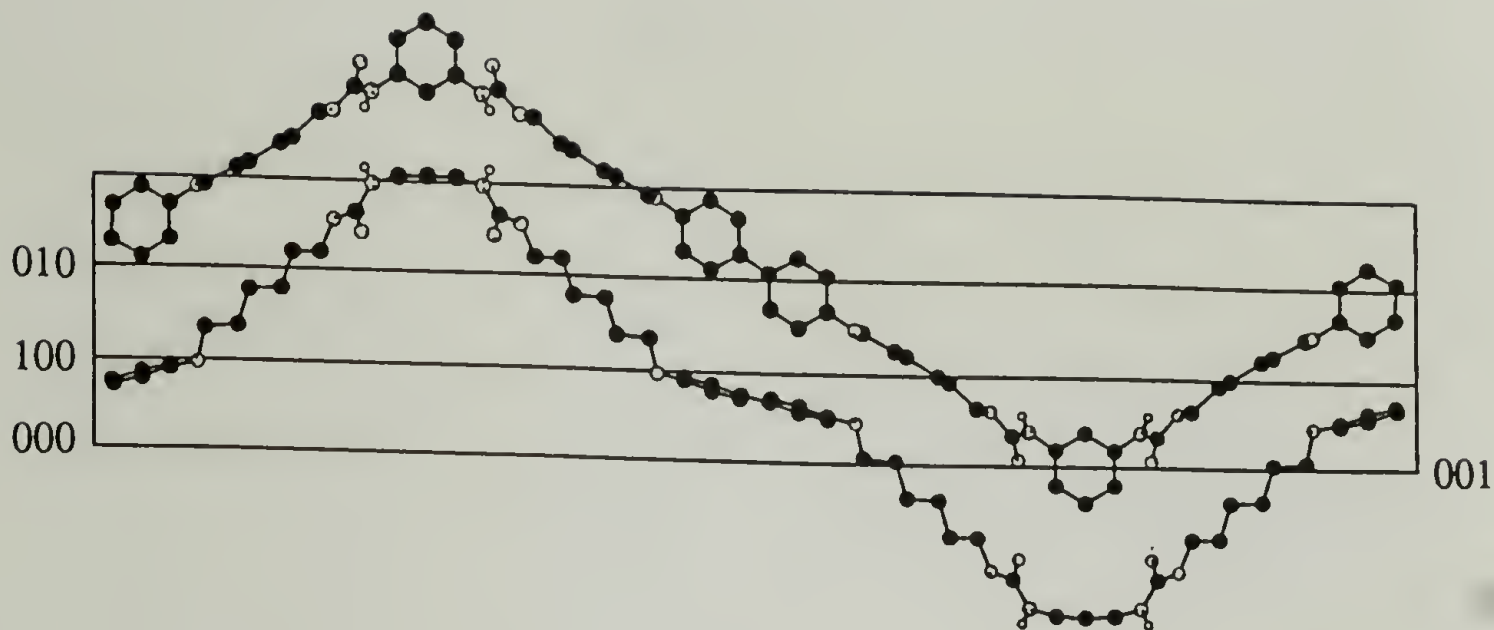
1,3-LCPU-6 unit cell
view along the 120 plane

Unit cell, (orthorombic)
$a = 5.010$ Å
$b = 10.28$ Å
$c = 54.6$ Å

Space Group:

$Pbn2_1 \quad C_{2v}^9$

Density:

calc: 1.291 g/ml
exp: 1.241 g/ml

H-bond Distance:
H···O = 1.99 Å
N···O = 2.94 Å

Phenyl-Urethane
Torsional Angle:

$55° \pm 9°$

H-bond Angle:

$\widehat{\text{N-H-O}} = 175.2°$

Figure 5.11   (Continued.)

(B)

(C)

(A)

Figure 5.12 Computer simulated WAXS fiber patterns (A and B) and experimental powder pattern (C) for the 2,6-PU-6.

(A) CMD-Cerius® simulated X-ray fiber pattern in ideal orientation.

(B) CMD-Cerius® "realistic" fiber pattern with the following parameters:

Camera type:	Flat
Film scale:	Linear
Fiber tilt angle:	0°
Orientation distribution half-width:	8.5°
Crystallite size (a, b, c):	400, 350, 200 Å
Lattice distortion factors:	0, 0.5, 1

181
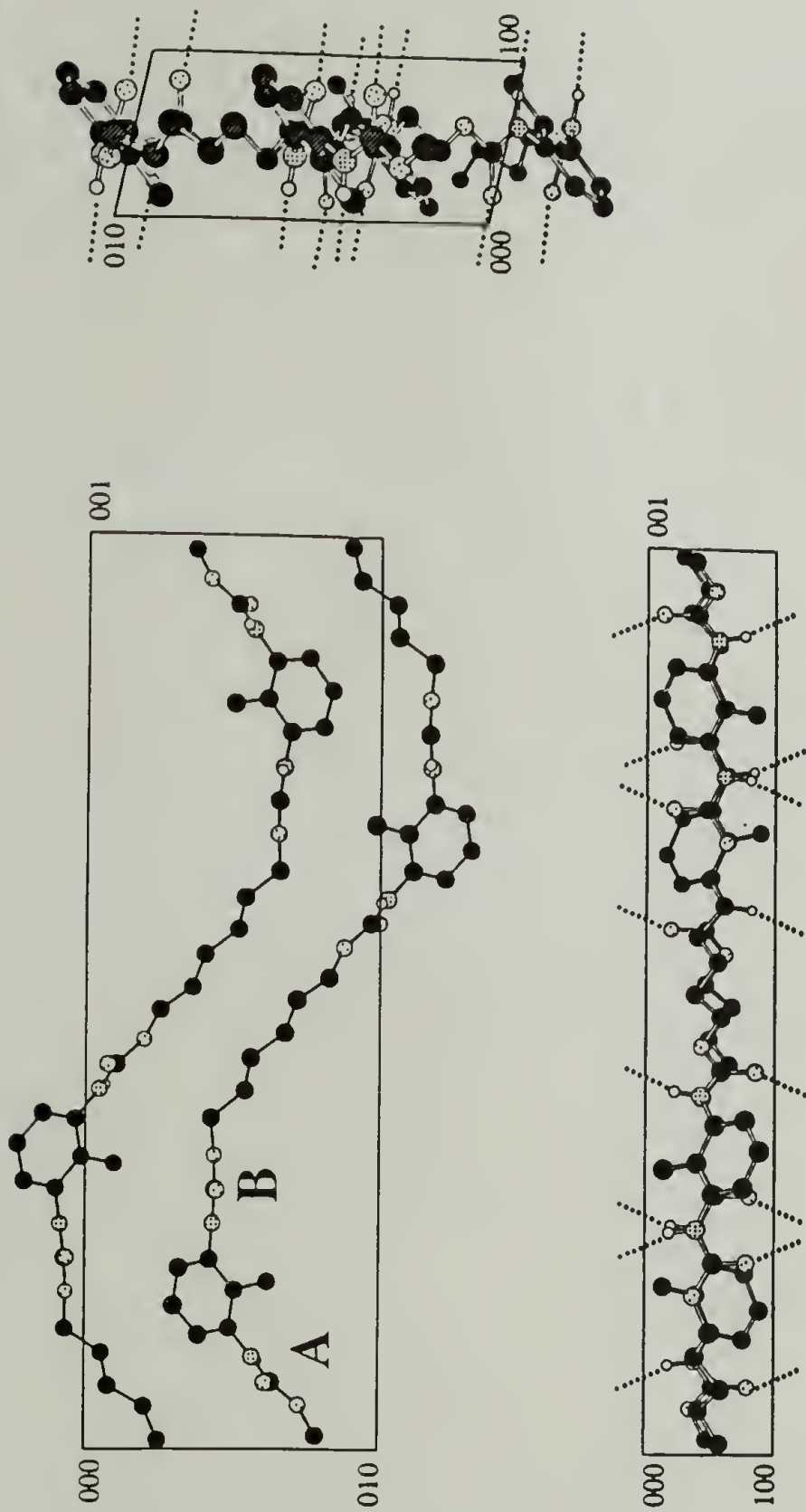
Views along a-axis (top), b-axis (bottom) and c-axis (right) of 2,6-PU-6 unit cell.

Unit cell (monoclinic)
a = 4.722 Å
b = 10.47 Å
c = 31.5 Å
γ = 103°

Space Group:
P2₁/b   C²ₕ⁵

Density:
calc: 1.279 g/ml
exp: 1.274 g/ml

H-bond Distance:
H···O = 1.92 Å
N···O = 2.86 Å

H-bond Angle:
N-H-O = 168° ± 3°

Phenyl-Urethane Torsional Angle:
Position A: 53° ± 1°
Position B: 56° ± 2°

Figure 5.13 Crystal structure of 2,6-PU-6 showing the phase to phase stacked nature of TDI rings.

182
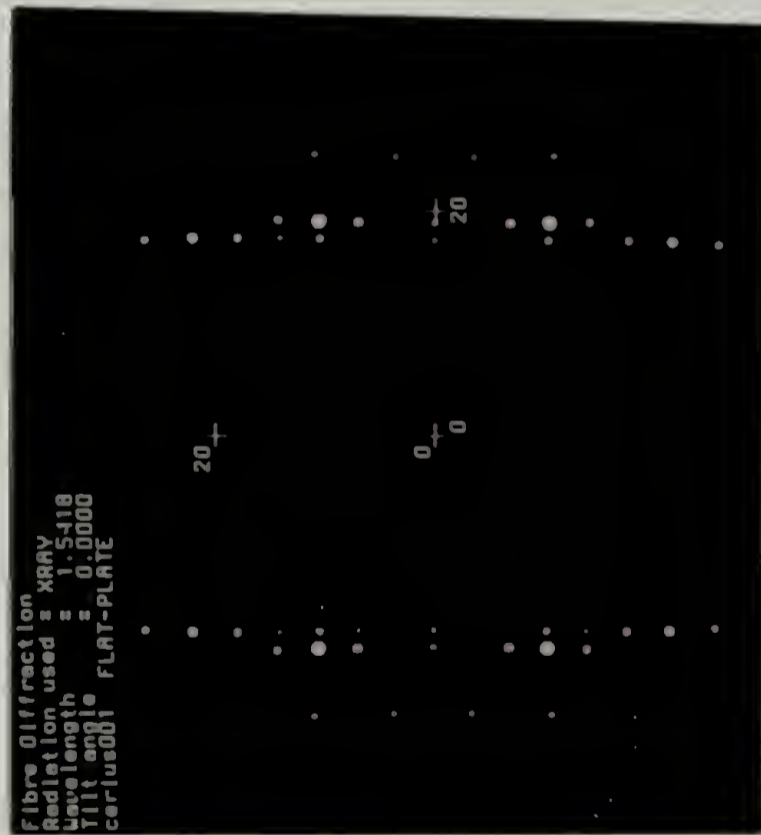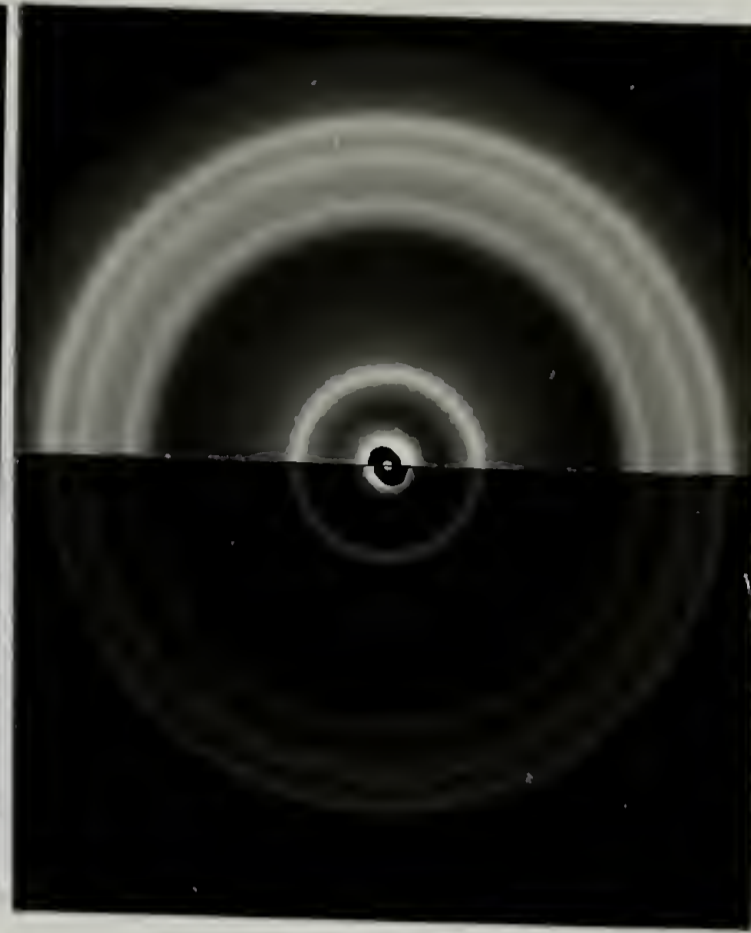
Figure 5.14 Computer simulated WAXS fiber patterns (A and B) and experimental powder pattern (C) for the 1,3-PU-6.

(A) CMD-Cerius® simulated X-ray fiber pattern in ideal orientation.

(B) CMD-Cerius® "realistic" fiber pattern with the following parameters:

Camera type:	Flat
Film scale:	Linear
Fiber tilt angle:	0°
Orientation distribution half-width:	8.5°
Crystallite size (a, b, c):	500, 500, 200 Å
Lattice distortion factors:	2, 0.2, 1.2

183
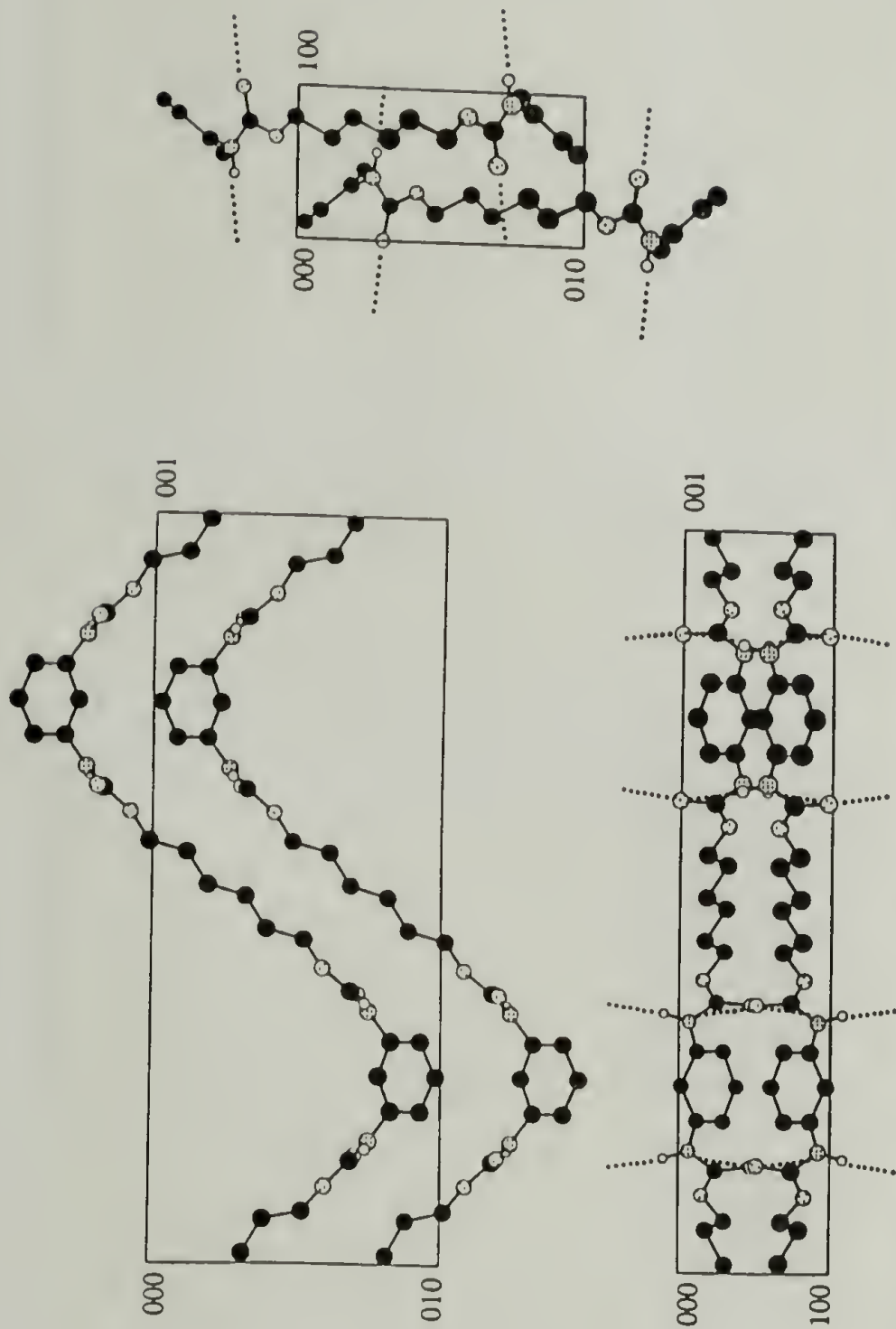
Views along a-axis (top), b-axis (bottom) and c-axis (right) of 1,3-PU-6 unit cell.

Unit cell (orthorombic)	Space Group:	H-bond Distance:	Phenyl-Urethane

Unit cell (orthorombic)
$a = 5.280$ Å
$b = 10.16$ Å
$c = 25.8$ Å

Space Group:
Pbn2$_1$ C$_{2v}^9$

Density:
calc: 1.334 g/ml
exp: 1.265 g/ml

H-bond Distance:
H···O = 2.22 Å
N···O = 3.18 Å

H-bond Angle:
$\widehat{\text{N-H-O}}$ = 172° ± 1°

Phenyl-Urethane Torsional Angle:
53° ± 7°

Figure 5.15 Crystal structure of 1,3-PU-6 showing the phase to edge (herringbone) stacking of PDI rings.

184
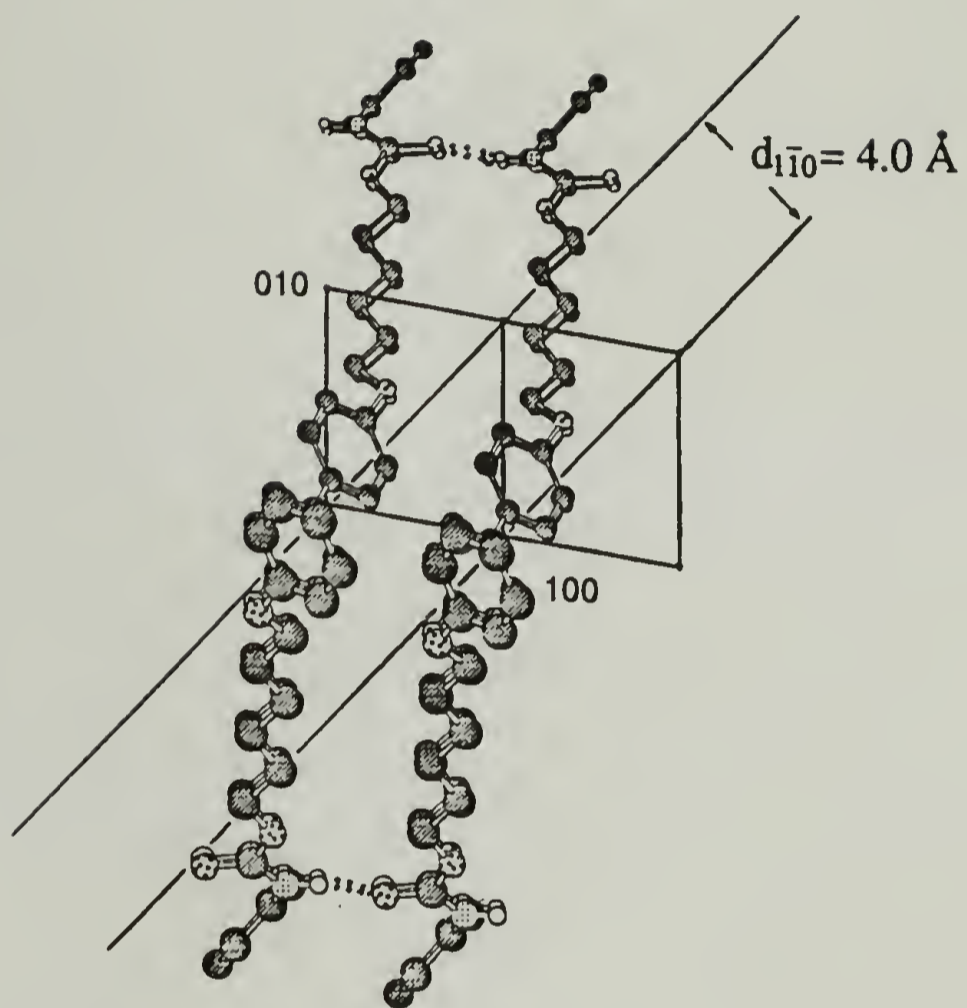
Figure 5.16 Proposed polymorphic structure of 1,3-LCPU-6 with phase to phase stacked PDI and biphenyl rings. This structure exhibits a strong $1\bar{1}0$ equatorial reflection at ~4.0 Å. See text for details.
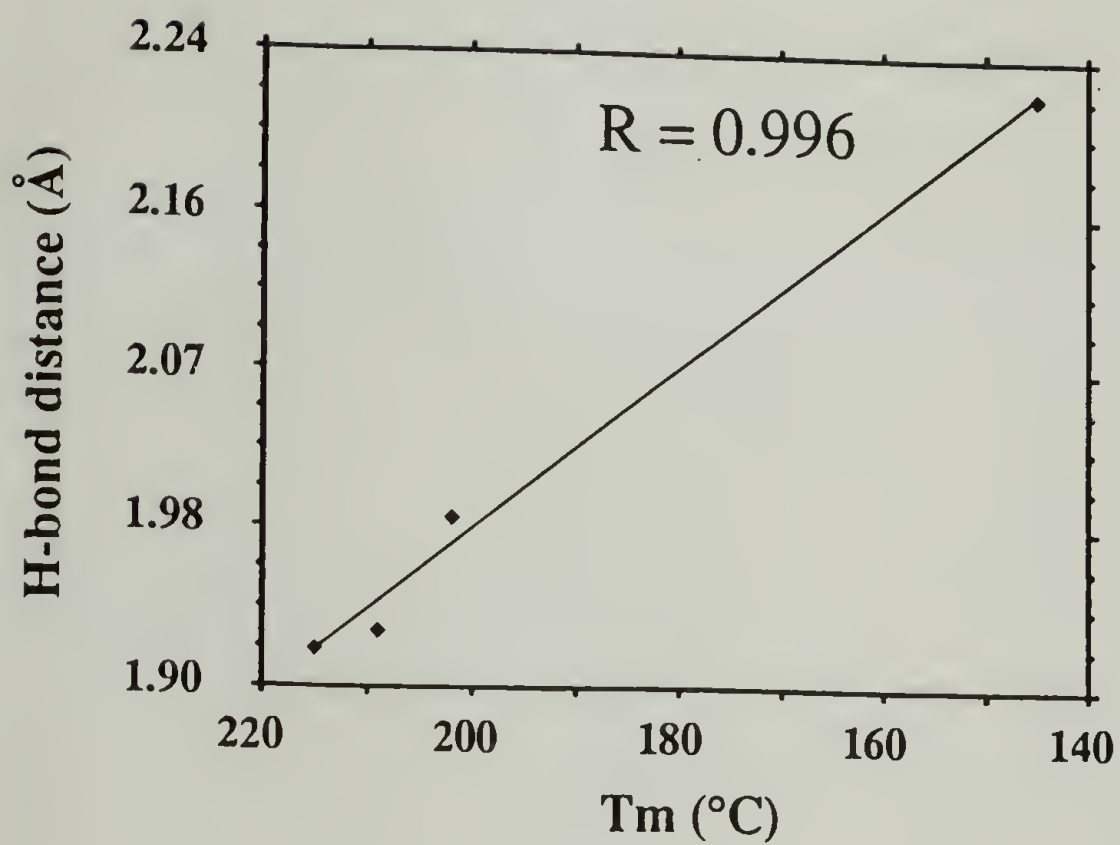
Figure 5.17 Plot of the H-bond distances versus the melting point temperatures of the crystallographically investigated 2,6-PU-6, 2,6-LCPU-6, 1,3-LCPU-6 and 1,3-PU-6 polyurethanes. See text for details.

References

1. Dobb, M. G.; McIntyre, J. E. In *Liquid Crystal Polymers II/III*; M. Gordon and N. A. Plate, Ed.; Springer-Verlag: New York, 1984; Vol. 60/61; pp 61.

2. Biswas, A.; Blackwell, J. *Macromolecules* **1988**, *21*, 3146.

3. Gutierrez, G. A.; Chivers, R. A.; Blackwell, J.; Stamatoff, J. B.; Yoon, H. *Polymer* **1983**, *24*, 937.

4. Blackwell, J.; Gutierrez, G. A.; Chivers, R. A. *Macromolecules* **1984**, *17*, 1219.

5. Hong, S. K.; Blackwell, J. *Polymer* **1989**, *30*, 225.

6. Okuyama, K.; Hidaka, H.; Ichige, H.; Osawa, M. *Macromolecules* **1989**, *22*, 3776.

7. Aharoni, S. M.; Correale, S. T.; Hammond, W. B.; Hatfield, G. R.; Murthy, N. S. *Macromolecules* **1989**, *22*, 1137.

8. Smyth, G.; Valles, E. M.; Pollack, S. K.; Grebowicz, J.; Stenhouse, P. J.; Hsu, S. L.; MacKnight, W. J. *Macromolecules* **1990**, *23*, 3389.

9. Smyth, G.; Pollack, S. K.; MacKnight, W. J.; Hsu, S. L. *Liquid Crystals* **1990**, *7*, 839.

10. Stenhouse, P. J.; Valles, E. M.; Kantor, S. W.; MacKnight, W. J. *Macromolecules* **1989**, *22*, 1467.

11. Pollack, S. K.; Shen, D. Y.; Hsu, S. L.; Wang, Q.; Stidham, H. D. *Macromolecules* **1989**, *22*, 551.

12. Pollack, S. K.; Smyth, G.; Papadimitrakopoulos, F.; Stenhouse, P.; Hsu, S. L.; MacKnight, W. J. *Macromolecules* **1992**, *25*, 2381.

13. Mormann, W.; Brahm, M. *Makromol. Chem.* **1989**, *190*, 631.

14. Mormann, W.; Brahm, M. *Macromolecules* **1991**, *24*, 1096.

15. Tanaka, M.; Nakaya, T. *J. Macromol. Sci. - Chem.,* **1987**, *A24*, 777.

16. Tanaka, M.; Nakaya, T. *Makromol. Chem.* **1986**, *187*, 2345.

17. Blackwell, J.; Gardner, K. H. *Polymer* **1979**, *20*, 13.

18. Blackwell, J.; Ross, M. *Journal of Polymer Science: Polymer Letters Edition* **1979**, *17*, 447.

19. Born, L.; Crone, J.; Hespe, H.; Muller, E. H.; Wolf, K. H. *J. Polym. Sci.: Polym. Phys.* **1984**, *22*, 163.

20. Briber, R. M.; Thomas, E. L. *J. Macromol. Sci.-Phys.* **1983**, *B22*, 509.

21. Blackwell, J.; Nagarajan, M. R. *Polymer* **1981**, *22*, 202.

22. Blackwell, J.; Nagarajan, M. R.; Hoitink, T. *Polymer* **1981**, *22*, 1534.

23. Blackwell, J.; Nagarajan, M. R.; Hoitink, T. *Polymer* **1982**, *23*, 950.

24. Hummel, J. P.; Flory, P. J. *Macromolecules* **1980**, *13*, 479.

25. Tashiro, K.; Kobayashi, M.; Tadokoro, H. *Macromolecules* **1977**, *10*, 413.

26. Mayo, S. L.; Olafson, B. D.; Goddarrd, W. A. *J. Phys. Chem.* **1990**, *94*, 8897.

27. McCammon, J. A.; Harvey, S. C. *Dynamics of Proteins and Nucleic Acids*; Cambridge University Press: Cambridge, England, 1987.

28. Wyckoff, R. W. G. *Crystal Structures*; 2nd ed.; Interscience Publishers: New York, 1963-1965; Vol. 5.

29. Gasteiger, J. *Tetrahedron* **1980**, *36*, 3219.

30. Khranovskii, V. A.; Kutsenko, O. M.; Giritsenko, T. M.; Stepanenko, L. V.; Nedashkovskaya, N. S. *Zh. Prikl. Spektroskopii* **1981**, *33*, 474.

31. Wang, Q. Master Thesis, University of Massachusetts at Amherst, 1989.

32. Wang, Q.; Stidham, H. D.; Papadimitrakopoulos, F. *Spectrochimica Acta* **1992**, in press.

33. Maklakov, L. I.; Dement'eva, I. N. *Vysokomol. soyed.* **1987**, *A29*, 1981.

34. Vladimirov, S. V.; Arifullin, F. R.; Grasinskaya, S. B.; Maklakov, L. I.; Sinaiskii, A. G. *Vysokomol. soyed.* **1977**, *A19*, 1713.

35. Vladimirov, S. V. *Vysokomol. soyed.* **1985**, *A27*, 1757.

36. Zhou, Z. Y.; Chen, G. S.; Shi, J. Q. *Acta Chim. Sin.* **1984**, *42*, 367.

37. Coulter, P.; Windle, A. H. *Macromolecules* **1989**, *22*, 1129.

38. Desiraju, G. R. *Crystal Enginnering*; Elsevier: New York, 1989; Vol. 54.

CHAPTER 6

CONCLUSIONS AND FUTURE WORK

Conclusions

This dissertation presents a comprehensive study of pure hard-phase "regular" (α,ω-hexane diol) and mesogenic (BHHBP) based polyurethanes. The inherent complexities of these systems, such as H-bonding, biphenol moiety, and asymmetric position of the methyl group in the TDI moiety, have been addressed in a systematic fashion throughout this dissertation. Conclusions of the individual chapters have already been presented with respect to their individual accomplishments. The overall conclusions of this thesis are presented here in the context of the three general questions set forth in Chapter 1.

The effect of H-bonding upon the structure and phase behavior of liquid crystal polyurethanes is the main theme of the first question. Previous investigations have shown that the mesogenic polyurethane (2,4-LCPU-6) is a monotropic liquid crystal. In order to investigate the effect of H-bonding in this system, we synthesized the N-methyl analog of 2,4-LCPU-6 (NM-2,4-LCPU-6), which possesses a similar structure to 2,4-LCPU-6 but without the H-bonding. Thermal and morphological characterization of the NM-2,4-LCPU-6 provided the necessary data to perform a close and valid comparison of these two polymers. The main result of this investigation is that the presence or absence of H-bonding is not important in determining the mesophase morphology, even though the isotropic to mesophase transition of the NM-2,4-LCPU-6 is ~90 °C lower than for the 2,4-LCPU-6. Careful DSC annealing experiments indicate that H-bonding affects the temperatures of the various transitions, primarily through an enthalpic effect. Since H-

189

bonding contributes considerably greater to the stability of the more ordered crystalline-phase than the more disordered mesophase, it results in the enantiotropic liquid-crystalline nature of the NM-2,4-LCPU-6 versus the monotropic one of the 2,4-LCPU-6.

The extent and perfection of H-bonding in the individual phases of liquid crystal polyurethanes is the last part of the first question. In order to address that, we chose to study the well documented (Chapter 3 and 5) mesophase to crystal transition of the 2,6-LCPU-6 by infrared spectroscopy. Curve fitting analysis of the conformational sensitive amide I region resulted in a quantitative assessment of the temperature dependence of H-bonding. The substantial increase of the ordered H-bonded amide I peak, accompanied by the comparable decrease in the disordered H-bonded amide I peak, during the mesophase to crystal transition indicate the disordered nature of H-bonding in the mesophase. This behavior correlates well with the calorimetric and WAXS data obtained for this polymer.

The subject of the second question is the contribution of the BHHBP mesogenic diol in the crystallization of liquid crystal polyurethanes (LCPUs). We have seen in Chapters 2 and 3 that all three LCPUs crystallize readily from the melt, versus the α,ω-hexane diol based "regular" polyurethanes which do not. This sort of behavior is due to a mesophase assisted crystallization. The relative rigidity and excellent packing characteristics of BHHBP mesogen result in a smectic-type mesomorphic state that exhibits considerable positional and orientational order. This state, frequently called mesophase, arranges the molecular repeats in close proximity with each other. At this stage, the specific intermolecular interactions along the polymer chains initiate a secondary process which increases the density and results in crystallization. All three LCPUs demonstrate a remarkable capability to nucleate crystallization from the mesophase. Upon 10 °C/min cooling, the mesophase–crystal transition trails the isotropic–mesophase transition from 0 to 5 °C for the 2,6-LCPU-6 and 2,4-LCPU-6 respectively, while the 1,3-LCPU-6 is somewhere in between. Surprisingly enough, their frozen mesophases can also nucleate crystallization upon heating. This usually occurs at the temperature range where the

mesophase gets adequate mobility and is about to melt. This is manifested between 115—140 °C and is determined on the basis of the underlying mesophase order (see Table 3.6).

The third and last question involves the molecular architecture and packing characteristics of meta-substituted phenylene-diisocyanates. These type of diisocyanates introduce a "kink" in the polymer backbone and result in a zigzag-type structure. Atomistic molecular simulations indicate that the phenyl-urethane torsional angle, which controls the c-axis length of the polymer, controls also H-bonding through the N–H⋯O angle. The competition between these two angles governs the length of the repeat and the perfection of H-bonding. The intramolecular architecture of this repeat remains more or less the same with the introduction of a methyl group ortho to both urethane groups (2,6-tolylene-diisocyanate, 2,6-TDI). The same is not true for their intermolecular arrangement into the crystalline lattice. The steric hindrance between the methyl group and the TDI's benzene ring makes the herringbone arrangement of the TDI moieties unfavorable and results into a different crystalline packing than for the 1,3-phenylene-diisocyanate (1,3-PDI) based polyurethanes. Although the resulting stacked arrangement decreases the unit cell density, surprisingly enough, it increases H-bonding by decreasing the H⋯O distance. Based on the mesophase WAXS fiber patterns of 2,6-LCPU-6 we can claim that the mesophase exhibits similar stacking of the TDI moieties to the crystal one. Unfortunately, the lower order of the 1,3-LCPU-6 mesophase does not provide adequate WAXS evidence to infer the stacking of the PDI moieties at this state.

The contribution of H-bonding in the formation and disruption of the ordered phase has been a subject of great interest throughout this thesis. The good correlation between the H-bonding distance[‡] and melting temperatures for the 2,6-LCPU-6, 1,3-LCPU-6, 2,6-PU-6, and 1,3-PU-6, suggests that melting is primarily controlled by the dissociation of H-bonds in the ordered domains. With regards to the participation of H-bonding in the formation of the ordered phase, things are not so straight forward. On the basis of the

---

[‡] The comparable (near 180°) H-bonding angle (ω) for the four polymers allows $\cos^2\omega$ to be taken as a constant.

polymorphism observed with the 1,3-LCPU-6, we can infer the secondary role of H-bonding upon crystal formation. Apparently, packing consideration is the primary force that dictates the crystal packing although H-bonding contributes to a somewhat lower extent.

Future Work

The continuation and expansion of this research promises to be fruitful and challenging. The suggested investigations listed below include the extension of this work towards the field of thermoplastic elastomers, as well as individual investigations in order to clarify certain aspects of LCPUs.

1) The potential applicability of LCPUs as a hard phase in thermoplastic elastomers has been a matter of great interest for our laboratory since the beginning of this project. It is worth mentioning the prime advantages and disadvantages of LCPUs versus the regular PUs currently used in the production of thermoplastic elastomers. Starting from their advantages, one has to mention their inherent ability to form easily elongated superstructures under shear fields. This can be utilized to obtain anisotropic hard domains that can lead to anisotropic elastomers as well. In addition to that, they possess the capability to crystallize readily from the melt, versus the regular polyurethanes which do not. The crystalline nature of the hard domains holds a great potential towards increasing the useful temperature window of operation from ~90 °C to ~160 °C without sacrificing processability or recyclability. As an outcome of this thesis, a number of disadvantages have also surfaced, besides the significant manufacturing cost of BHHBP. The relative amount of H-bonding per unit volume for LCPUs is about one half less than that of the regular polyurethanes. Since the mesophase glass-transition temperature (T_g) is not much higher that the Tg of the disordered glass (see Chapter 1), we can expect a rather small loss[1] of the ultimate elastic properties of a LCPU based elastomer compared to the regular

192

one (see T_gs and density measurements in Chapters 3 and 5 respectively). In order to utilize the full potential of LCPUs, it is essential to increase as much as possible the hard domain crystallinity. This can be accomplished in a two stage process described below. At the first stage the elastomer is extruded at relatively high speed in order to achieve considerable orientation of the hard domains. While under strain, treatment in hot methanol will additionally perfect the orientation and annihilation of the hard domains, although this is not that vital. The second stage involves careful heat treatment under strain around 100–140 °C, where the mesophase–crystal transformation occurs. If everything goes as planned, we should have a thermoplastic elastomer with anisotropic, highly crystalline hard domains.

2) The lower melt viscosity of nematic mesophases has attracted considerable attention in the field of liquid crystals.[2] Processing of thermoplastic elastomers with their polyurethane hard-phase in the nematic state holds a great potential in order to acheive complex-shaped elastomeric objects. Biphenol mesogens have been shown to exhibit mainly smectic mesophases as a result of their rigid and highly regular shape. In addition to that, the periodic backbone "kink" introduced by the TDI moiety reduces even more the longitudinal degree of freedom, and assists in the formation of smectic mesophases. Reduction of the mesogen regularity along with a relatively linear backbone has shown to lead to nematic mesophases, where there is complete loss of lateral order.[3,4] Mesogens based on substituted stilbenes and azo- or azoxybenzenes, incorporated in main chain polyesters and polyethers, have been shown to exhibit stable nematic mesophases as well as a crystalline order at lower temperatures.[5-8] On the other hand, the use of linear diisocyanates (e.g. hexamethylene-diisocyanate), will provide the desired backbone linearity discussed above. The limited polyurethane stability[9,10] (~200 °C) poses an additional restriction to the choice of mesogen, spacer and diisocyanate. Evidently, this research requires a fair amount of fine tuning in order to attain a nematic mesophase with behavior comparable to the present LCPUs.

3) The determination of the crystalline structure of 2,4-LCPU-6 can be also quite challenging. Figure 3.11.C illustrates a highly oriented 2,4-LCPU-6 WAXS crystalline fiber pattern capable of supporting a detailed crystallographic analysis. This sort of analysis holds the potential of addressing the packing of the randomly substituted TDI's methyl group alone the stacking of the backbone "kinks". One way to approach this problem is to apply an aperiodic array of methyl substitutions, according to the well defined aperiodic X-ray analysis of Blackwell et al.[5,11-13]

4) Although the local structure of the TDI, PDI, and biphenol have been rigorously addressed in this thesis, their mesophase and crystal mobility remains largely unclear. Smith et al.[14] utilized solid-state ^{13}C-NMR to study the microstructure and dynamics of the crystalline phase of 2,4-LCPU-6. The frozen mesophase to crystal transition presented in this dissertation provides a unique opportunity to study the local structure and the dynamics of this reorganization. Recent developments in deuterium solid-state NMR spectroscopy[15] have made these kinds of studies feasible, providing that the sample contains a well-defined deuterium label. The exchange of the four ortho to the hydroxy-groups biphenol protons, with deuterons can be accomplished easily, by treating biphenol in a D_2O/EtOD/NaOD solution. Incorporating this deuterated biphenol into the 2,6-LCPU-6 and 1,3-LCPU-6 can provide enough signal to noise to study the local environment and dynamics of the biphenol mesogen. Utilizing more elaborate chemistry, it is possible to deuterium-label the urethane and hexamethylene spacer,[16] and integrate the contribution of the individual moieties in the phase behavior of LCPUs.

References

(1) Haak, C. A. Ph.D. Thesis, University of Massachusetts, 1992.

(2) Finkelmann, H. *Angew. Chem. Int. Ed. Engl.* **1987**, *26*, 816.

(3) Capasso, R.; Roviello, A.; Sirigu, A. *J. Polym. Sci., Polym. Phys.* **1987**, *25*, 2431.

(4) Gray, G. W.; Goodby, J. W. G. *Smectic Liquid Crystals*; Leonard Hill: Philadelphia, 1984.

(5) Babad, H.; Zeiler, A. G. *Chemical Reviews* **1973**, *73*, 75.

(6) Blumstein, R. B.; Blumstein, A. *Mol. Cryst. Liq. Cryst.* **1988**, *165*, 361.

(7) Percec, V.; Tomazos, D.; Pugh, C. *Macromolecules* **1989**, *22*, 3259.

(8) Percec, V.; Yourd, R. *Macromolecules* **1989**, *22*, 3229.

(9) Yang, W. P.; Macosko, C. W.; Wellinghoff, S. T. *Polymer* **1986**, *27*, 1235.

(10) Dyer, E.; Hammond, R. J. *Journal of Polymer Science: Part A* **1964**, *2*, 1.

(11) Blackwell, J.; Gutierrez, G. A.; Chivers, R. A. *Macromolecules* **1984**, *17*, 1219.

(12) Biswas, A.; Blackwell, J. *Macromolecules* **1988**, *21*, 3146, 3152, 3158.

(13) Gutierrez, G. A.; Chivers, R. A.; Blackwell, J.; Stamatoff, J. B.; Yoon, H. *Polymer* **1983**, *24*, 937.

(14) Pollack, S. K.; Smyth, G.; Papadimitrakopoulos, F.; Stenhouse, P.; Hsu, S. L.; MacKnight, W. J. *Macromolecules* **1992**, *25*, 2381.

(15) Spiess, H. W. *Colloid Polym. Sci.* **1983**, *261*,

(16) Yang, X.; Kardan, M.; Hsu, S. L.; Collard, D.; Heath, R. B.; Lillya, C. P. *Journal of Physical Chemistry* **1988**, *92*, 196.

BIBLIOGRAPHY

Adibi, K., M. H. George, and J.A. Barrie, "Anionic synthesis of poly(urethane-g-acrylonitrile)." *Polymer*, **20**, 483, (1979).

Aharoni, S. M., S. T. Correale, W. B. Hammond, G. R. Hatfield, and N. S. Murthy, "Conformation of alkylene segments of poly(ester amides) in their crystalline and mesomorphic states." *Macromolecules*, **22**, 1137, (1989).

Azaroff, L. V., "X-ray diffraction by liquid crystals." *Mol. Cryst. Liq. Cryst.*, **60**, 73, (1980).

Azaroff, L. V. and C. A. Schuman, "X-ray diffraction by cybotactic nematics." *Mol. Cryst. Liq. Cryst.*, **122**, 309, (1985).

Babad, H. and A. G. Zeiler, "The chemistry of phosgene." *Chemical Reviews*, **73**(1), 75, (1973).

Bechtoldt, H., J. H. Wendorff, and H. J. Zimmermann, "Studies on the nature of order in a rigid random copolymer." *Makromol. Chem.*, **188**, 651, (1987).

Bilibin, A. Yu., E. E. Pashkovsky, A. V. Tenkovtsev, and S. S. Skorokhodov, "Thermotropic polyesters, 3. Synthesis and study of thermal properties of quasi-regular mesomorphic copolyesters." *Makromol. Chem., Rapid Commun.*, **6**, 545, (1985).

Bilibin, A. Yu., A. V. Ten'kovtsev, O. N. Piraner, and S. S. Skorokhodov, "Synthesis of high molecular weight liquid crystal polyesters based on a polycondensation mesogenic monomer." *Polymer Science U.S.S.R.*, **26**, 2882, (1984).

Bilibin, A. Yu., V. V. Zuev, and S. S. Skorokhodov, "Thermotropic polyesters, 4. Synthesis of liquid crystalline poly(oxyfumaroyloxy-1,4-phenylenecarbonyloxy-alkyleneoxycarbonyl-1,4-phenylene)s." *Makromol. Chem., Rapid Commun.*, **6**, 601, (1985).

Biswas, A. and J. Blackwell, "Three-dimentional structure of main-chain liquid-crystalline copolymers. 1. 2. 3." *Macromolecules*, **21**, 3146, 3152, 3158, (1988).

Blackwell, J. and K. H. Gardner, "Stucture of the hard segments in polyurethane elastomers." *Polymer*, **20**, 13, (1979).

Blackwell, J., G. A. Gutierrez, and R. A. Chivers, "Diffraction by aperiodic polymer chains: The structure of liquid-crystalline copolyesters." *Macromolecules*, **17**, 1219, (1984).

Blackwell, J. and M. R. Nagarajan, "Conformation analysis of poly(MDI-butandiol) hard segment in polyurethane elastomers." *Polymer*, **22**, 202, (1981).

Blackwell, J., M. R. Nagarajan, and T. Hoitink, "Structure of polyurethane elastomers. X-ray diffraction and conformational analysis of MDI-propandiol and MDI-ethylene glycol hard segments." *Polymer*, 22, 1534, (1981).

Blackwell, J., M. R. Nagarajan, and T. Hoitink, "Structure of polyurethane elastomers: Effect of chain extender length on the structure of MDI/diol hard segments." *Polymer*, 23, 950, (1982).

Blackwell, J. and M. Ross, "X-ray studies of the stucture of polyurethane hard segments." *Journal of Polymer Science: Polymer Letters Edition*, 17, 447, (1979).

Blumstein, A. Liquid crystalline order in polymers. N.Y.: Academic Press, (1978).

Blumstein, R. B. and A. Blumstein, "Inherently flexible thermotropic main chain polymer liquid crystals." *Mol. Cryst. Liq. Cryst.*, 165, 361, (1988).

Blumstein, R. B., E. M. Stickles, M. M. Gauthier, A. Blumstein, and F. Volino, "Influence of molecular weight on phase transitions and alignment of a thermotropic nematic polyester." *Macromolecules*, 17, 177, (1984).

Boeffel, C. and H. W. Spiess, "Highly ordered main chain in a liquid crystalline side-group polymer." *Macromolecules*, 21, 1626, (1988).

Born, L., J. Crone, H. Hespe, E. H. Muller, and K. H. Wolf, "On the structure of polyurethane hard segments based on MDI and butanediol-1,4: X-ray diffraction analysis of the oriented elastomers and of single crystals of a model compound." *J. Polym. Sci.: Polym. Phys.*, 22, 163, (1984).

Bosma, M., G. T. Brinke, and T. S. Ellis, "Polymer-polymer miscibility and enthalpy relaxations." *Macromolecules*, 21, 1465, (1988).

Bower, D. I. and W. F. Maddams. The vibration spectroscopy of polymers. Cambridge Solid State Science Series, ed. R. W. Cahn, E. A. Davis, and I. M. Ward. New York: Cambridge University Press, (1989).

Briber, R. M. and E. L. Thomas, "Investigation of two crystal forms in MDI/BDO- based polyurethanes." *J. Macromol. Sci.-Phys.*, B22(4), 509, (1983).

Brunette, C. M., S. L. Hsu, and W. J. MacKnight, *Macromolecules*, 15, 71, (1982).

Bualek, S. and R. Zentel, "Crosslinkable liquid-crustalline combined main-chain/side-chain polymers with low glass transition temperatures." *Makromol. Chem.*, 189, 791, (1988).

Bummer, P. M. and K. Knutson, "Infrared spectroscopic examination of the surfaces of hydrated copoly(ether-urethane-ureas)." *Macromolecules*, 23, 4357, (1990).

Burns, G. and A. M. Glazer. Space groups for solid state scientists. 2nd ed., New York: Academic Press, (1990).

Capasso, R., A. Roviello, and A. Sirigu, "Molecular orientation in liquid fibers of nematic polymers." *J. Polym. Sci., Polym. Phys.*, 25, 2431, (1987).

197

Chapoy, L. L. Recent advances in liquid crystalline polymers. Elsevier Appl. Sci. Publ., (1985).

Chen, D. and H. G. Zachmann, "Glass transition temperature of copolyesters of PET, PEN and PHB asdetermined by dynamic mechanical analysis." To be published.

Cheng, S. Z. D., "Kinetics of mesophase transitions in thermotropic copolyesters. 1. Calorimetric study." *Macromolecules*, **21**, 2475, (1988).

Cheng, S. Z. D., M. A. Yandrasits, and V. Percec, "Phase behavior in a thermotropic polyester involving rod-like mesogenic groups based on conformational isomerism." *Polymer*, **32**(7), 1284, (1991).

Christenson, C. P., M. A. Harthcock, M. D. Meadows, H. L. Spell, W. L. Hpward, M. W. Crestwick, R. E. Guerra, and R. B. Turner, *J. Polym. Sci., Polym. Phys.*, **24**, 1401, (1986).

Cifferri, A., W. R. Krigbaum, and R. B. Meyer. Polymer liquid crystals. N.Y.: Academic Press, (1982).

Coleman, M. M., J. F. Graf, and P. C. Painter. Specific interactions and the miscibility of polymer blends. Lancaster, PA 17604, USA: Technomic Publishing Co., Inc., (1991).

Coleman, M. M., K. H. Lee, D. J. Skrovanek, and P. C. Painter, "Hydrogen bonding in polymers. 4. Infrared temperature studies of a simple polyurethane." *Macromolecules*, **19**, 2149, (1986).

Coleman, M. M., D. J. Skrovanek, S. E. Howe, and P. C. Painter, *Macromolecules*, **18**, 299, (1985).

Colthup, N. B., L. H. Daly, and S. E. Wiberley. Introduction to infrared and raman spectroscopy. New York: Academic Press, (1990).

Conte, G., L. D'Ilario, N. V. Pavel, S. A. Snamprogetti, and E. Giglio, "An X-ray and conformational study of kapton-H." *J. Polym. Sci., Polym. Phys. Ed.*, **14**, 1553, (1976).

Coulter, P. and A. H. Windle, "Geometric and rotation parameters for the conformational modeling of liquid crystalline polyesters." *Macromolecules*, **22**, 1129, (1989).

Demus, D. and L. Richter. Textures of liquid crystals. Weihheim: Verlag Chemie, (1978).

Desiraju, G. R. Crystal enginnering. Vol. 54. Material Science Monographs, New York: Elsevier, (1989).

Devinsky, F., I. Lacko, and L. Krasnec, "A convenient synthesis of secondary N,N'-Dimethylalkanediamines." *Synthesis*, **4**, 303, (1980).

Dobb, M. G. and J. E. McIntyre. "Properties and applications of liquid-crystalline main-chain polymers." In Liquid Crystal Polymers II/III, ed. M. Gordon and N. A. Plate. 61. 60/61. New York: Springer-Verlag, (1984).

Doucet, J. "X-ray studies of ordered smectic phases." In The Molecular Physics of Liquid Crystals, ed. G. R. Luckhurst and G. W. Gray. 317-341. Academic Press, (1979).

Dyer, E. and R. J. Hammond, "Thermal degradation of N-substituted polycarbamates." Journal of Polymer Science: Part A, 2, 1, (1964).

Eckert, H. and B. Forster, "Triphosgene, a crystalline phosgene substitute." Angew. Chem. Int. Ed. Engl., 26(9), 894, (1987).

Edwards, K. N. Urethane chemistry and applications. Vol. 172. ACS Symposium Series, ed. M. J. Comstock. Washington, D.C: ACS, (1981).

Ellzey, Jr., S. E. and C. H. Mack, "Interaction of phenyl isocyanate and related compounds with sodium borohydride." J. Org. Chem., 28, 1600, (1962).

Finholt, A. E., C. D. Anderson, and C. L. Agre, "The reduction of isocyanates and isothiocyanates with lithium aluminum hydride." J. Org. Chem., 18, 1338, (1953).

Finkelmann, H., "Liquid crystalline polymers." Angew. Chem. Int. Ed. Engl., 26, 816, (1987).

Fisher, H., F. E. Karasz, and W. J. MacKnight. To be published.

Galli, G., E. Chiellini, C. K. Ober, and R. W. Lenz, "Liquid crystalline polymers, 8. Structurally ordered thermotropic polyesters of glycol ethers." Makromol. Chem., 183, 2693, (1982).

Gasteiger, J., Tetrahedron, 36, 3219, (1980).

Goldfarb, D., Z. Luz, and H. Zimmermann, "Deuterium magnetic resonance in the discotic columnar mesophases of Hexaalkyloxytriphenylenes: The conformation of the aliphatic side chains." J. Chem. Phys., 78(12), 7065, (1983).

Gray, G. W. and J. W. G. Goodby. Smectic liquid crystals. Philadelphia: Leonard Hill, (1984).

Grebowicz, J. and B. Wunderlich, J. Polym. Sci., Polym. Phys., 21, 141, (1983).

Gregoriou, V. G., J. L. Chao, H. Toriumi, and R. A. Palmer, "Time-resolved vibrational spectroscopy of an electric field-induced transiton in a nematic liquid crystal by use of step-scan 2D FT-IR." Chemical Physics Letters, 179(5-6), 491, (1991).

Gromek, J. M. "Polygraf, Beta version 9.0." Institute of Material Science, University of Connecticut, Storrs, CT 06269:

Gutierrez, G. A., R. A. Chivers, J. Blackwell, J. B. Stamatoff, and H. Yoon, "The structure of liquid crystalline aromatic copolyester prepared from 4-hydroxybenzoic acid and 2-hydroxy-6-napthoic acid." Polymer, 24, 937, (1983).

Haak, C. A. "Energy, orientation, and deformation of urethane thermoplastic elastomers." Ph.D., University of Massachusetts, (1992).

Hagemann, H., H. L. Strauss, and R. G. Snyder, "Structure and crystallization of n-$C_{21}H_{44}$, n-$C_{36}H_{74}$ and low molecular weight polyethylene glasses." *Macromolecules*, **20**, 2810, (1987).

Hager, S. L., T. B. Mac Rury, R. M. Gerkin, and F. E. Gritchfield. "Urethane block polymers. Kinetics of formation and phase development." In <u>Urethane Chemistry and Applications</u>, ed. K. N. Edwards. 149-166. 172. Washington, D.C: ACS, (1981).

Harrell, L. L. Jr., "Segmented polyurethanes. Properties as a function of segment size and distribution." *Macromolecules*, **2**, 607, (1969).

Henry, N. F. M. and K. Lonsdale. <u>International tables for X-ray crystallography</u>. Vol. 1. Birmingham, England: Kynoch Press, (1969).

Hong, S. K. and J Blackwell, "X-ray analysis of the structure of the thermotropic copolyester poly(phenyl-p-phenylene terephthalate)." *Polymer*, **30**, 225, (1989).

Hummel, J. P. and P. J. Flory, "Structural geometry and torsional potentials in p-phenylene polyamides and polyesters." *Macromolecules*, **13**, 479, (1980).

Hwang, K. K. S., T. A. Speckhard, and S. L. Cooper, "Properties of polyurethane anionomers: Ionization via bimolecular nucleophilic displacement of the urethane hydrogen." *J. Macromol. Sci.-Phys.*, **B 23**(2), 153, (1984).

Iimura, K., N. Koide, H. Tanabe, and M. Takeda, "Synthesis of thermotropic liquid crystalline polymers, 2. Polyurethanes." *Makromol. Chem.*, **182**, 2569, (1981).

Jashav, J. Y. and S. W. Kantor. 1986. Personal Communication.

Kardan, M., A. Kaito, S. L. Hsu, R. Takur, and C. P. Lillya, "Infrared spectroscopic characterization of ultra thin films of disklike molecules on metallic substrates." *Journal of Physical Chemistry*, **91**(7), 1809, (1987).

Kardan, M., B. B. Reinhold, S. L. Hsu, R. Thakur, and C. P. Lillya, "Spectroscopic characterization of the microstructures in disklike liquid crystalline molecules: Model compounds for polymers." *Macromolecules*, **19**, 616, (1986).

Kazaryan, L. G., D. Ya. Tsvankin, B. M. Ginzburg, Sh. Tuichiev, L. N. Korzhavin, and S. Ya. Frenkel, "X-ray diffraction study of the crystalline structure of aromatic polyimides." *Vysokomol. Soyedin.*, **A14**, 1199, (1972).

Keller, A. and G. Ungar. "Liquid crystal polymers; A unifying thermodynamics based scheme." To be published.

Khranovskii, V. A., O. M. Kutsenko, T. M. Giritsenko, L. V. Stepanenko, and N. S. Nedashkovskaya, "Hydrogen bond and IR spectra of polyurethanes." *Zh. Prikl. Spektroskopii*, **33**, 474, (1981).

Kim, D. Y. and R. B. Blumstein, "Glass transition in main chain polyesters formed by alternating mesogens and spacers." *Polymer Preprints*, **30**(2), 472, (1990).

Koberstein, J. T., I. Gancarz, and T. C. Clark, *J. Polym. Sci., Polym. Phys.*, **24**, 2487, (1986).

Koenig, J. L. "Fourier transform infrared spectroscopy of polymers." In <u>Advances in Polymer Science</u>, ed. E. D. v. Meerwall, C. W. Frank, S. N. Semerak, and J. L. Koenig. 87-154. 54. New York: Springer-Verlag, (1984).

Leadbetter, A. J. and E. K. Norris, "Distribution function in three liquid crystals from X-ray diffraction measurements." *Mol. Phys.*, **38**, 669, (1979).

Lee, D., R. A. Register, C. Yang, and S L. Cooper, "Methylenebis(p-phenyl isocyanate)-based polyurethane ionomers. 1. New small-angle X-ray scattering model." *Macromolecules*, **21**, 998, (1988a).

Lee, H. S., Y. K. Wang, W. J. MacKnight, and S. L. Hsu, "Spectroscopic analysis of phase-separation kinetics in model polyurethanes." *Macromolecures*, **21**, 270, (1988b).

Lee, W. K., P. A. Heiney, Jr McCauley J. P., and A. B. III Smith, "Fourier transform infrared absorption study of Hexa(hexylthio)triphenylene: A discotic liquid crystal." *Molecular Crystals and Liquid Crystals*, **198**, 273, (1991).

Leis, D. G. "Automotive uses for polyurethanes." In <u>Urethane Chemistry and Applications</u>, ed. K. N. Edwards. 33-48. 172. Washington, D.C: ACS, (1981).

Lorenz, R., M. Els, F. Haulena, A. Schmitz, and O. Lorenz, "Thermische und mechanische eigenschaften von polyurethanen mit mesogenen diolkomponenten." *Angewandte Makromoleculare Chemie*, **180**, 51, (1990).

Loufakis, K. and B. Wunderlich, "Computation of heat capacity of liquid macromolecules based on a statistical mechanical approximation." *J. Phys. Chem.*, **92**, 4205, (1988).

MacKnight, W. J. and M. Yang, "Property-structure relationships in polyurethanes: Infrared studies." *Journal of Polymer Science, Symposium Series*, **42**, 817, (1973).

Maddams, W. F., "The scope and limitations of curve fitting." *Applied Spectroscopy*, **34**(3), 245, (1980).

Maklakov, L. I. and I. N. Dement'eva, "Crystallization of oligomeric systems based on polutetramethyleneoxide." *Vysokomol. soyed.*, **A29**, 1981, (1987).

Mayo, S. L., B. D. Olafson, and W. A. Goddarrd, "DREIDING: A generic force field for molecular simulations." *J. Phys. Chem.*, **94**, 8897, (1990).

McCammon, J. A. and S. C. Harvey. <u>Dynamics of proteins and nucleic acids</u>. Cambridge, England: Cambridge University Press, (1987).

McGowan, C. B., D. Y. Kim, and R. B. Blumstein, "Glass transition in main chain polyesters: DSC investigation of physical aging below Tg." *Polymer Preprints*, **31**(1), 261, (1990).

McMillan, W. L., "Measurement of smectic-phase order parameter fluctuations in the nematic phase of heptyloxyazoxybenzene." *Phys. Rev. A*, **8**(1), 328, (1973).

201

Melendez, E., F. Navarro, M. Pinol, J. L. Rodriguez, and J. L. Serrano, "Synthesis and study of polymers using complex monomers." *Mol. Cryst. Liq. Cryst.*, **155**, 83, (1988).

Melzger, S. H. and Jr. "Metal replacement opportunities for urethane systems." In Urethane Chemistry and Applications, ed. K. N. Edwards. 69-86. 172. Washington, D.C: ACS, (1981).

Merrill, S. H., "Block copolymers based on 2,2-bis(4-Hydroxyphenyl)-propane polycarbonate. I. Preparation and properties of copolymers from a variety of homopolymers." *Journal of Polumer Science*, **55**, 343, (1961).

Mormann, W. and M. Brahm, "Polymers from multifunctional isocyanates, 3. Synthesis and polyaddition reaction of (liquid-crystalline) fully aromatic diisocyanatoesters." *Makromol. Chem.*, **190**, 631, (1989).

Mormann, W. and M. Brahm, "Polymers from multifunctional isocyanates. 5. Synthesis of liquid-crystalline polyurethanes from methyl-substituted diisocyanato-substituted benzoates." *Macromolecules*, **24**, 1096, (1991).

Murno, M. S., R. C. Eberhart, N. J. Maki, B. E. Brink, and W. J. Fry, "Thromboresistant alkyl derivatized polyurethanes." *American Society for Artificial Internal Organs*, **6**, 65, (1983).

Odian, G. Principles of polymerization. Wiley-Intersience Pub., (1981).

Ogata, N., K. Sanui, and S. Kitayama, "Molecular-weight distribution of poly(p-phenylene terephthalamide)." *Journal of Polymer Science: Polymer Chemistry Edition*, **22**, 865, (1984).

Oishi, Y., M. Kakimoto, and Y. Imai, "Synthesis of aromatic polyamides from N,N'-bis(trimethylsilyl)-substituted aromatic diamines and aromatic diacid chlorides." *Macromolecules*, **21**, 547, (1988).

Oishi, Y., M. Padmanaban, M. Kakimoto, and Y. Imai, "Synthesis and characterization of N-phenylated aromatic polyureas from N,N'-dichloroformyl-p-dianilinobenzene and N-N'-bistrimethylsil-diamines." *Journal of Polymer Science: Part A: Polymer Chemistry*, **25**, 3387, (1987).

Okuyama, K., H. Hidaka, H. Ichige, and M. Osawa, "Crystal structure of poly(4-methyl-m-phenylene terephalamide)." *Macromolecules*, **22**, 3776, (1989).

O'shea, F. X. "Thermoplastic polyurethanes based on poly(oxyethylene-oxypropylene) glycols. The dependence of properties and injection moldability on molecular structure." In Urethane Chemistry and Applications, ed. K. N. Edwards. 243-257. 172. Washington, D.C: ACS, (1981).

Percec, V. and A. Keller, "A thermodynamic interpretation of polymer molecular weight effect on the phase transitions of main-chain and side-chain liquid-crystal polymers." *Macromolecules*, **23**, 4347, (1990).

Percec, V., D. Tomazos, and C. Pugh, "Influence of molecular weight on the thermotropic mesophases of poly[6-[4-(4-methoxy-β-methylstyryl)phenoxy]hexyl methacrylate]." *Macromolecules*, **22**, 3259, (1989).

Percec, V. and R. Yourd, "Liquid crystalline polyethers and copolyethers based on conformational isomerism. 3." *Macromolecules*, **22**, 3229, (1989).

Pollack, S. K., D. Y. Shen, S. L. Hsu, Q. Wang, and H. D. Stidham, "Infrared and X-ray diffraction studies of a semirigid polyurethane." *Macromolecules*, **22**, 551, (1989).

Pollack, S. K., G. Smyth, F. Papadimitrakopoulos, P. Stenhouse, S. L. Hsu, and W. J. MacKnight, "Development of crystallinity in a semiflexible thermotropic polyurethane. 2. Structure and dynamics." *Macromolecules*, **25**, 2381, (1992).

Pottick, L. A. "Reinforced elastomers." Polymer Alloys & Blends, Elastomers Business Center, Shell Chemical Company, 1991.

Pouget, J. P., M. E. Jozefowicz, A. J. Epstein, X. Tang, and A. G. MacDiarmid, "X-ray structure of polyaniline." *Macromolecules*, **24**, 779, (1991).

Raiford, L. C. and K. J. Alexander, "Migration of the carbamyl radical in 2-aminophenol derivatives." *J. Org. Chem.*, **5**, 300, (1940).

Reck, B. and H. Ringsdorf, "Combined liquid crystalline polymers: Mesogens in the main chain and as side groups." *Makromol. Chem., Rapid Commun.*, **6**, 291, (1985).

Richards, J. W., *Chem. News*, **75**, 278, (1987).

Rojstaczer, S. R. and R. S. Stein, "Effect of thermal history on the nematic state of a thermotropic liquid crystal polymer." *Macromolecules*, **23**, 4863, (1990).

Safinya, C. R., L. J. Martinez-Miranda, M. Kaplan, J. D. Litster, and R. J. Birgeneau, "High-resolution X-ray scattering study of the nematic-to-smectic-C transitions in 8S5-7S5 mixtures." *Phys. Rev. Lett.*, **50**(1), 56, (1983).

Saotome, K. and H. Komoto, "N-alkyl-substituted polyamides and copolyamides having long methylene chain units." *Journal of Polymer Science: Part A-1*, **5**, 107, (1967).

Sato, M., F. Komatsu, N. Takeno, and K. Mukaida, "Synthesis and liquid-crystalline properties of novel homo- and copolyurethanes from a diol with a mesogenic unit and dicarbamates." *Makromol. Chem., Rapid Commun.*, **12**, 167, (1991).

Sato, M., K. Kurosawa, K. Nakatsuchi, and Y. Ohkatsu, "Synthesis and liquid crystalline properties of thermotropic homo- and copolycarbonates." *Journal of Polymer Science: Part A: Polymer Chemistry*, **26**, 3077, (1988).

Sato, M., K. Nakatsuchi, and Y. Ohatatsu, "New liquid-crystalline polycarbonates from diols containing a biphenyl ring sequence as central core." *Makromol. Chem., Rapid Commun.*, **7**, 231, (1986).

Sato, M., K. Nakatsuchi, and Y. Ohatatsu, "Liquid-crystalline behavior of central core-type model compounds of thermotropic polycarbonates." *Makromol. Chem., Rapid Commun.*, **8**, 383, (1987).

Schroeder, L. R. and S. L. Cooper, "Hydrogen bonding in polyamides." *Journal of Applied Physics*, **47**(10), 4310, (1976).

Senich, G. A. and W. J. MacKnight, "Fourier transform infrared thermal analysis of a segmented polyurethane." *Macromolecules*, **13**, 106, (1980).

Seymour, R. W., G. M. Estes, and S. L. Cooper, *Macromolecules*, **3**, 579, (1970).

Shen, D. Y., S. K. Pollack, and S. L. Hsu, "Far-infrared study of hydrogen bonding in a semicrystalline polyurethane." *Macromolecules*, **22**, 2564, (1989).

Shriver, D. F. and M. A. Drezdzon. The manipulation of air-sensitive compounds. 2nd ed., Wiley-Interscience Pub., (1986).

Singler, R. E., R. A. Willingham, C. Noel, L. Bosio, and E. Atkins, "Thermotropic liquid crystalline poly(organophosphazene)." *Macromolecules*, **24**, 510, (1991).

Skorokhodov, S. S. and A. Yu. Bilibin, "Rational path of the synthesis of liquid-crystalline high-molecular-weight polyesters and their properties in solution." *Makromol. Chem., Makromol. Chem.*, **26**, 9, (1989).

Skrovanek, D. J., S. E. Howe, P. C. Painter, and M. M. Coleman, "Hydrogen bonding in polymers; Infrared Temperature studies of an amorphous polyamide." *Macromolecules*, **18**, 1676, (1985).

Skrovanek, D. J., P. C. Painter, and M. M. Coleman, "Hydrogen bonding in polymers. 2. Infrared temperature studies of Nylon 11." *Macromolecules*, **19**, 699, (1986).

Smith, P. A. S. The chemistry of open-chain organic nitrogen compounds. Vol. 1. New York: W. A. Benjamin Inc., (1965).

Smyth, G., S. K. Pollack, W. J. MacKnight, and S. L. Hsu, "Microstructure and dynamics of a mesogenic diol." *Liquid Crystals*, **7**(6), 839, (1990a).

Smyth, G., E. M. Valles, S. K. Pollack, J. Grebowicz, P. J. Stenhouse, S. L. Hsu, and W. J. MacKnight, "Development of crystallinity in a polyurethane containing mesogenic units. 1. Morphology and mechanism." *Macromolecules*, **23**, 3389, (1990b).

Snyder, R. G., "Vibrational stydy of the chain conformation of the liquid n-paraffins and molten polyethylene." *The Journal of Chemical Physics*, **47**(4), 1316, (1967).

Sorenson, W. R. and T. W. Campbell. Preparative methods in polymer chemistry. 2 ed., New York Interscience Pub.,

Spiess, H. W., *Colloid Polym. Sci.*, **261**, 193, (1983).

Srichatrapimuk, V. W. and S. L. Cooper, "Infrared thermal analysis of polyurethane block polymers." *J. Macromol. Sci., Phys.*, **B15**(2), 267, (1978).

Stenhouse, P. J. "Liquid-crystalline polyurethanes." Ph.D. Thesis, University of Massachusetts, (1992).

Stenhouse, P. J., E. M. Valles, S. W. Kantor, and W. J. MacKnight, "Thermal and rheological properties of a liquid-crystalline polyurethane." *Macromolecules*, 22, 1467, (1989).

Struick, L. C. E. Physical aging in amorphous polymers and others materials. New York: Elsevier Science Publishing. Co., (1978).

Tadokoro, H. Structure of crystalline polymers. Malabar, FL: Robert E. Krieger Publ. Co., (1990).

Takayanagi, M. and T. Katayose, "N-substituted poly(p-phenylene terephthalamide)." *J. Pol. Sci., Pol. Chem. Ed.*, 19, 1133, (1981).

Tanaka, M. and T. Nakaya, "Liquid crystalline polyurethanes, 1 Polyurethanes based on 4,4'-[1,4-phenylenebis(methylidynenitrilo)]diphenylethanol." *Makromol. Chem.*, 187, 2345, (1986).

Tanaka, M. and T. Nakaya, "Liquid crystalline polyurethane. Polyurethanes containing bis-(p-oxymethylphenyl) terephthalate." *J. Macromol. Sci. - Chem.*, A24(7), 777, (1987).

Tashiro, K., M. Kobayashi, and H. Tadokoro, "Elastic moduli and molecular structures of several crystalline polymers, including aromatic polyamides." *Macromolecules*, 10, 413, (1977).

Tashiro, K., K. Ono, Y. Minagawa, M. Kobayashi, T. Kawai, and K. Yoshino, "Structure and thermodynamic solid-state phase transition of poly(3-alkylthiophene)." *J. Polym. Sci., Part B: Polym. Phys.*, 29, (1991).

Tsitsilianis, C. and G. Staikos, "Phase behavior in PS-b-PMMA block copolymer by enthalpy relaxation." *Macromolecules*, 25, 910, (1992).

Tsukruk, V. and V. Shilov, "One-dimentional correlation in ordered smectic phases of comb-like polymers." *Polymer*, 31, 1793, (1990).

Tsukruk, V., V. Shilov, and Y. Lipatov, "Changes of liquid crystalline polymer structure with temperature. 6. Distortion of one-dimentional order in smectic B polymer." *Macromolecules*, 19, 1308, (1986).

Ungar, G., J. L. Feijoo, V. Percec, and R. Yourd, "Liquid crystalline polyethers and copolyethers based on conformational isomerism. 3." *Macromolecules*, 24, 1168, (1991).

Van Krevelen, D. W. and P. J. Hoftyzer. Properties of polymers, their estimation and correlation with chemical structure. Netherlands: Elsevier Scientific Pub. Co., (1976).

Vladimirov, S. V., "Cryoscopy of crystalline formations in oligomer systems." *Vysokomol. soyed.*, A27(8), 1757, (1985).

Vladimirov, S. V., F. R. Arifullin, S. B. Grasinskaya, L. I. Maklakov, and A. G. Sinaiskii, "A study of structure formation in systems based on oligo-dienemethylurethanes." *Vysokomol. soyed.*, **A19**(8), 1713, (1977).

Vries, A. D., "The use of X-ray diffraction in the study of thermotropic liquid crystals with rod-like molecules." *Mol. Cryst. Liq. Cryst.*, **131**, 131, (1985).

Vries, A. D., "X-ray diffraction studies of the structure of the skewed cybotactic nematic phase: A review of the literature." *Journal of Molecular Liquids*, **31**, 193, (1986).

Walden, P., Z. *Electrochem.*, **14**, 713, (1908).

Wang, Q. "Infrared spectroscopic investigation of semi-rigid polyurethane." Master Thesis, University of Massachusetts at Amherst, (1989).

Wang, Q., H. D. Stidham, and F. Papadimitrakopoulos. "A Spectroscopic Study of Model Urethanes." *Spectrochimica Acta*, (1992)

Wendorff, J. H., G. Frick, and H. Zimmerman, *Mol. Cryst. Liq. Cryst.*, **157**, 455, (1988).

West, J. C. and S. L. Cooper, "Infrared studies of block copolymers." *J. Polymer Sci.*, Polymer Symposium **60**, 127, (1977).

Weygand, F. and R. B. Mitgau, "Aromatische aldehyde aus kohlenwasserstoffen uberdie cabonsaure-N-methylanilide. Aldehyde aus carbonsauren." *Beilstein*, **88**, 301, (1955).

Wunderlich, B. Macromolecular physics. Vol. (Vols. 1-3). New York: Academic Press, (1973-80).

Wunderlich, B., "The heat capacity of rigid crystal and amorphous phase macromolecules." *Polymer Preprints*, **31**(1), 272, (1990).

Wyckoff, R. W. G. Crystal structures. 2nd ed., Vol. 5. New York: Interscience Publishers, (1963-1965).

Yang, W. P., C. W. Macosko, and S. T. Wellinghoff, "Themal degradation of urethanes based on 4,4'-diphenylmethane diisocyanate and 1,4-butanediol (MDI/BDO)." *Polymer*, **27**, 1235, (1986).

Yang, X., M. Kardan, S. L. Hsu, D. Collard, R. B. Heath, and C. P. Lillya, "Spectroscopic characterization of side-chain disordering process in disklike liquid crystals." *Journal of Physical Chemistry*, **92**(1), 196, (1988).

Yang, X., D. A. Waldman, S. L. Hsu, S. A. Nitzsche, R. Thakur, D. M. Collard, C. P. Lillya, and H. D. Stidham, "Spectroscopic characterization of mesogen order in discotic liquid crystal." *Journal of Chemical Physics*, **89**(9), 5950, (1989).

Yoon, S. C., Y. K. Sung, and B. D. Ratner, "Surface and bulk structure of segmented poly(ether urethanes) with perfluoro chain extenders. 4. Role of hydrogen bonding on thermal transitions." *Macromolecules*, **23**, 4351, (1990).

Zachmann, H. G., D. Chen, J. Nowacki, E. Olbrich, and C. Schulze. "Molecular order, morphology and phase separation in blends of isotropic and liquid-crystalline polymers." In <u>Integration of Fundamental Polymer Science and Technology</u>, ed. L. A. Kleintjents and P. J. Lemstra. Elsevier, (1990).

Zentel, R. and G. Reckert, "Liquid crystalline elastomers based on liquid crystalline side group, main chain and combined polymers." *Makromol. Chem.*, **187**, 1915, (1986).

Zhou, Z. Y., G. S. Chen, and J. Q. Shi, *Acta Chim. Sin.*, **42**, 367, (1984).